GEORGIA INSTITUTE OF TECHNOLOGY
OFFICE OF CONTRACT ADMINISTRATION
SPONSORED PROJECT INITIATION

Date: 9/24/80

Project Title: Collision Induced Optical and Auger Spectra of Solids

Project No: G-41-607

Project Director: Dr. E.W. Thomas

Sponsor: National Science Foundation

Agreement Period: From July 1, 1980 Until ~~December 31, 1983~~ 12/31/84 (includes 6-month flexibility period)

Type Agreement: Grant No. DMR-8000671, dtd. 6/10/80

Amount: $37,400 NSF(G-41-607)
$ 9,818 GIT(G-41-337)
$47,218 TOTAL

Reports Required: Annual Progress Report(s); Final Project Report - 3/31/85

Sponsor Contact Person (s):

Technical Matters

NSF Program Official

Fred E. Stafford
Program Director
Solid State Chemistry Program
Condensed Matter Sciences Section
Division of Materials Research
Directorate for Mathematical and Physical Sciences
National Science Foundation
Washington, D.C. 20550
(202) 357-9787

Contractual Matters
(thru OCA)

NSF Grants Official

Myra B. Galinn
MPS/STIA Branch, Section II
Division of Grants and Contracts
Directorate for Administration
National Science Foundation
Washington, D.C. 20550
(202) 357-9671

Defense Priority Rating: N/A

Assigned to: Physics (School/Laboratory)

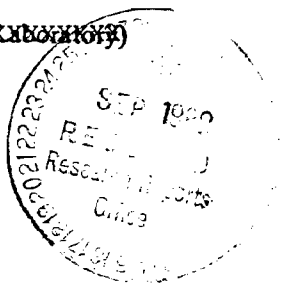

COPIES TO:

Project Director
Division Chief (EES)
School/Laboratory Director
Dean/Director--EES
Accounting Office
Procurement Office
Security Coordinator (OCA)
Reports Coordinator (OCA)

Library, Technical Reports Section
EES Information Office
EES Reports & Procedures
Project File (OCA)
Project Code (GTRI)
Other C.E. Smith

CA-3 (3/76)

GEORGIA INSTITUTE OF TECHNOLOGY OFFICE OF CONTRACT ADMINISTRATION

SPONSORED PROJECT TERMINATION/CLOSEOUT SHEET

Date 8/9/85

Project No. G-41-607 School/~~XXX~~ PHY

Includes Subproject No.(s)

Project Director(s) E. W. Thomas GTRC / ~~GIT~~ XXXX

Sponsor National Science Foundation

Title Collision Induced Optical and Auger Spectra of Solids

Effective Completion Date: 12/31/84 (Performance) 3/31/85 (Reports)

Grant/Contract Closeout Actions Remaining:

- [ ] None
- [ ] Final Invoice or Final Fiscal Report
- [ ] Closing Documents
- [X] ~~XXXXXXXXXXXXXXXXXXXXXXXX~~ Patent Questionnaire
- [ ] Govt. Property Inventory & Related Certificate
- [ ] Classified Material Certificate
- [ ] Other

Continues Project No. Continued by Project No.

COPIES TO:

Project Director
Research Administrative Network
Research Property Management
Accounting
Procurement/GTRI Supply Services
Research Security Services
Reports Coordinator (OCA)
Legal Services

Library
GTRC
Research Communications (2)
Project File
Other A. Jones; M. Heyser

FORM OCA 69.285

G-41-607

GEORGIA TECH RESEARCH INSTITUTE
ADMINISTRATION BUILDING
GEORGIA INSTITUTE OF TECHNOLOGY
ATLANTA, GEORGIA 30332

Telex: 542507 GTRIOCAATL
Fax: (404) 894-3120

Phone: (404) 894-4814

23 January 1981

Dr. Fred E. Stafford
Program Director
Solid State Chemistry Program
Condensed Matter Sciences Section
Division of Materials Research
National Science Foundation
Washington, DC 20550

Subject: Research Proposal Entitled, "Collision Induced Optical and Auger Spectra of Solids"
(Continuation of NSF Grant No. DMR 8000671)

Dear Dr. Stafford:

Enclosed herewith are two copies of the subject continuation proposal and three copies of the proposed budget, in accordance with NSF requirements. Please note that no funds are expected to remain in the current grant period.

Please contact Dr. Edward Thomas, the Principal Investigator, or this office, if you should desire additional information.

Thank you for your attention in this matter.

Very truly yours,

Phyllis R. Oliver
GEORGIA TECH RESEARCH INSTITUTE

PRO/gem

Addressee: In duplicate
Enclosures: Proposal - in duplicate
Budget - in triplicate

PROPOSAL TO THE NATIONAL SCIENCE FOUNDATION
Cover Page

FOR CONSIDERATION BY NSF ORGANIZATIONAL UNIT (Indicate the most specific unit known, i.e. program, division, etc.)	IS THIS PROPOSAL BEING SUBMITTED TO ANOTHER FEDERAL AGENCY? Yes ___ No X ; IF YES, LIST ACRONYM(S):
Solid State Chemistry;	

PROGRAM ANNOUNCEMENT/SOLICITATION NO.:	CLOSING DATE (IF ANY):
NONE	N/A

NAME OF SUBMITTING ORGANIZATION TO WHICH AWARD SHOULD BE MADE (INCLUDE BRANCH/CAMPUS/OTHER COMPONENTS)
GEORGIA TECH RESEARCH INSTITUTE
Georgia Institute of Technology

ADDRESS OF ORGANIZATION (INCLUDE ZIP CODE)
225 North Avenue, N. W., Atlanta, Georgia 30332

TITLE OF PROPOSED PROJECT
Collision Induced Optical and Auger Spectra of Solids.

REQUESTED AMOUNT	PROPOSED DURATION	DESIRED STARTING DATE
$39,978	12 Months	July 1981

PI/PD DEPARTMENT	PI/PD ORGANIZATION	PI/PD PHONE NO.
Physics	Georgia Institute of Technology	(404)894-5215

PI/PD NAME	SOCIAL SECURITY NO.*	DATE OF HIGHEST DEGREE ACHIEVED	MALE*	FEMALE*
Edward W. Thomas	255-78-4048	1964	X	
ADDITIONAL PI/PD				
ADDITIONAL PI/PD				
ADDITIONAL PI/PD				
ADDITIONAL PI/PD				

FOR RENEWAL OR CONTINUING AWARD REQUEST, LIST PREVIOUS AWARD NO.: 8000671	IF SUBMITTING ORGANIZATION IS A SMALL BUSINESS CONCERN, CHECK HERE ☐ (See CFR Title 13, Part 121 for Definitions)

* Submission of SSN and other personal data is voluntary and will not affect the organization's eligibility for an award. However, they are an integral part of the NSF information system and assist in processing proposals. SSN solicited under NSF Act of 1950, as amended.

CHECK APPROPRIATE BOX(ES) IF THIS PROPOSAL INCLUDES ANY OF THE ITEMS LISTED BELOW:

☐ Animal Welfare ☐ Human Subjects ☐ National Environmental Policy Act
☐ Endangered Species ☐ Marine Mammal Protection ☐ Research Involving Recombinant DNA Molecules
☐ Historical Sites ☐ Pollution Control ☐ Proprietary and Privileged Information

PRINCIPAL INVESTIGATOR/ PROJECT DIRECTOR	AUTHORIZED ORGANIZATIONAL REP.	OTHER ENDORSEMENT (optional)
NAME: Edward W. Thomas	NAME: *Phyllis R. Oliver*	NAME:
SIGNATURE:	SIGNATURE:	SIGNATURE:
TITLE: Professor	TITLE: *Contracting Officer*	TITLE:
DATE: 20 January 1981	DATE: 1/23/81	DATE:

Continuation Proposal for NSF Grant No. DMR 8000671

Collision Induced Optical and Auger Spectra of Solids

I. Administrative Details.

This project was initiated by a letter from NSF dated June 10, 1980 and commenced on July 1, 1980 as a continuing grant with support envisaged for a three year period. This present document is the continuation request for the second year. The Project Director-and Principal Investigator is Professor E. W. Thomas.

II. Summary of Scientific Progress.

(a) Introduction

It is our general objective to study inelastic collision events resulting from energetic (5 to 200 keV) ion impact on surfaces where target atoms are ejected in excited or ionized states. In the long term we seek a comprehensive understanding of these inelastic mechanisms in terms of processes already well known in bi-particle (gas phase) collision studies. As an example of progress in developing this understanding we would point to our[1] recent studies of ion-induced Auger electron spectra from solid targets. We have shown (as have others) that the initial inner shell excitation mechanism is due to L-shell electron promotion and curve crossings in quasi-molecules formed temporarily during a collision; such process are well known in bi-particle collisions and the mechanism was first detailed by Barat and Lichten.[2] Our work, and that of Wittmaack[3] has shown that the Auger elecrons (representing inner shell excitation) and the multiply charged ejected target ions exhibit similar fluxes. Thus it appears an atom (or ion) ejected with an inner shell vacancy undergoes first an Auger decay (giving the detected Auger electron) leaving the ejected particle multiply ionized and contributing then to the spectrum of secondary ions. For the limited group of cases considered so far there would seem to be no significant flux of multiply charged ions produced by any other mechanism. Thus we have the beginings of a comprehensive understanding with the hitherto unrelated phenomena of Auger and secondary ion emission connected to the same (well understood) bi-particle collision mechanism.

While some understanding of inelastic excitation of pure targets has been achieved, it is clear that any comprehensive model must also explain behaviour when a species of interest is bound in some different chemical environment. Thus much of our effor is devoted to inelastic processes in compounds and alloys.

---

1. W. A. Metz et al., J. Appl. Phys. 51, 2888 (1980).
2. M. Barat and W. Lichten, Phys. Rev. A. 6, 211 (1972).
3. K. Wittmaack, Nucl. Instrum. Meth. 170, 565 (1980).

The program makes use of two general experimental facilities, connected to an accelerator. One facility allows us to study the optical spectrum induced by ion impact on a surface, the other permits study of the ejected electron energy spectrum which is related to Auger transitions excited by particle impact. In both arrangements ions, from the accelerator, at 5 to 200 keV energy are incident on a solid target housed in a ultra-high-vacuum environment. The targets are generally high purity metals or their compounds prepared by mechanical polishing and preliminary argon ion sputter cleaning. Surface cleanliness can be monitored by routine electron induced Auger spectra. By backfilling with various gases we can produce adsorbate layers. Details of the basic arrangements are to be found in our earlier publication.[1,4]

In general the photon spectrum consists of sharp lines, readily identifiable from standard tables, whose intensity can be related to the probability for excited state formation. Auger electron lines, coming from atoms with inner shell vacancies, are often difficult to identify precisely and represent very fast decays that may occur while an atom still interacts with the solid target. Thus in any work with Auger spectra one must inevitably devote some effort to understanding what the Auger line represents.

Our work has progressed as envisaged in our original program and can be usefully divided into studies of ion induced Auger spectra and ion induced optical spectra representing the two different detection arrangements.

(ii) Ion Induced Auger Spectroscopy

Under previous NSF support we have initiated studies of the Auger spectra induced by ion impact on solids. Of particular interest are the spectra of Al and Si induced by Ar^+ ions. These both show one major line plus three subsidiary features. The lines are sharp and atomic like, differing in both shape and energy from those induced by electron impact on solids. We have argued[1] that the lines are primarily from ejected (neutral) target atoms with L - shell vacancies and that they decay in free space. We have attempted to calculate line energy and can generally explain the form of the spectra from Al and Si as being due to unresolved groups of lines.

A disturbing feature about the spectra and our interpretation of them is that we cannot resolve all the lines we predict to be present. We believe this may be due to Doppler broadening related to the energy of the sputtered particles. Our major effort since the initiation of the present grant has been to construct a better electron spectrometer following the pattern of Allyn et al.,[5]. This will have an improved resolution compared with the present device and has a unidirectional acceptance geometry (rather than an annular cone of the equipment used previously) permitting a precise definition of direction and therefore allowing a prediction of Doppler broadening. With this we can not only provide a better resolution but also we will be able to de-convolute overlapped lines using a predicted Doppler broadening function. The instrument can also be rotated about the target to arrive at an angular distribution of electrons. Using single crystal targets we can search for directional effects related to crystal orientation.

---

4. W. E. Baird et al., Phys. Rev. A 10, 2063 (1974).
5. C. L. Allyn, T. Gustafsson and W. E. Plummer, Rev. Sci. Instrum. 49, 1197 (1978).

If (as we have proposed for Al) the Auger decay occurs in free space there will be no directional effects. If (as others have argued) the excited atoms lie in the target matrix then there will be strong directional effects. We anticipate that as one goes to targets of higher Z (e.g. P or S) in single crystal compounds, directional effects should become more apparent because lifetime decreases and decay inevitably must occur while the ejected atom still interacts with the target.

Within the six month period since the initiation of the present grant we have devoted our efforts entirely to development of the equipment and the computer control necessary for handling the complicated focusing sequence of the spectrometer. Both hardware and software are complete and now under test. No problems are apparent.

During the remaining six months of the present grant period we anticipate recording high resolution spectra induced by Ar^+ impact on Al and Si for detailed comparison with our predicted line positions. We would hope to detect an increasing Doppler breadth with incident energy indicating increased average energy of ejected species. We intend to perform high resolution studies of the Si LMM Auger spectra from various silicon compounds to explore why the relative intensities of features change with target chemical composition. It is possible that these changes reflect simply alteration of M shell populations (i.e. excited outer shells) with chemical species. We would then anticipate corresponding changes to the optical spectra and these also will be monitored.

(iii) Ion Induced Optical Spectra of the Target

We continue to perform quantitative optical spectroscopy of the emissions induced by ion impact on the target. Of particular interest are emissions from molecules. The rotational and vibrational state population of the molecule should reveal the underlying characteristics of the excitation and ejection process. For example if excitation and ionization occurs in some local plasma situation (as suggested by the Anderson-Hinthorne[6] model) then populations should show a Boltzman distribution related to an effective plasma temperature; these temperatures are estimated[7] to be 4000-7000°K. If the molecule exists on the surface and is ejected as a single entity the populations should be a Boltzman distribution appropriate to surface temperature which would normally be about 300°K. A third possibility, invoked in the formation of dimer ions,[8] is that the constituents of the molecule are ejected as separate atoms but with kinetic energies, in their center of mass frame, less than the molecular binding energy so that they appear at a distance from the surface as a molecule; in this case a high degree of rotational excitation is expected due to the variety of initial trajectories.

Our major objective is to study long lived transition metal oxide molecules which give continuous emission spectra. We believe these continua occur because transitions are to a repulsive state. Others argue that the apparent continua simply represent high degrees of rotational excitation. There is some question as to what excited states are involved in these cases. Consequently we are performing some

---

6. C. A. Andersen and J. R. Hinthorne, Anal. Chem. 45, 1421 (1973).
7. C. J. Good-Zamin et al., Radiat. Effects. 35, 139 (1978).
8. G. P. Können, A. Tip and A. E. deVries, Radiat. Effects. 21, 269 (1974); and 26, 23 (1975).

preliminary studies on ejection of excited molecules where the molecular configurations are well known.

We have studied the spectra of N_2 induced by Ar^+ impact on Si with implanted N_2 and the N_2 spectrum induced when N^+ is incident on Si. In both cases the predominant features are from the v=0 level of N_2 in the $C^3\pi u$ state. The rotational distribution is appropriate to a temperature of around 300^oK and population of the v=1 vibrational level is small or negligible. Both observations indicate that N_2 is formed on the surface and ejected as a single entity. The observations are inexplicably different from similar experiments of Snowdon et al.,[9] which claim that the emission spectrum is of N_2^+ and that there are high rotational and vibrational populations. We do however note that earlier experiments of Battacharya et al.[10] on this situation show spectra of N_2 agreeing with our work. The present data indicates that the nitrogen atoms implanted into the solid do not migrate but are simply revealed as the surface is sputter eroded down to the implantation depth. When two separate atoms are revealed at the surface they presumably recombine to N_2 and are ejected.

We have recently shown that the CN radical may be formed in an alkali halide crystal by sequentially implanting C^+ and N^+ ions so that their range distributions overlap. They are detected by their optical emission spectrum which may be induced by any projectile (ions, or electrons) having a range greater than the implant depth. We are developing a detailed model which suggests that formation of CN is simply related to the statistical probability that both a C and an N projectile come to rest on the same lattice site. There is no evidence that C and N thermally migrate to recombine. The existence and behaviour of CN^- ions in alkali halides is of course well known. The CN molecule exhibits directional disorder until temperatures are lowered below an 83^oK phase transition.[11] That CN forms in the target is an interesting curiosity but not surprising in view of the stability of the CN bond and the strong binding of CN^- to anion sites. We have no evidence that molecules form in the lattice for other implant situations and believe molecular systems observed during sputtering are formed at the surface.

We are now undertaking a brief study of the BH spectrum induced by Ar^+ impact on a B target with adsorbed H. This has a particularly well separated rotational structure. We have also returned to the study of the Mo O^* spectrum [12] observed during Ar^+ impact on Mo with adsorbed oxygen. We are seeking first to confirm that the intensity of this emission increases with oxygen coverage in the manner predicted by our earlier model.[12]

---

9. K. J. Snowdon, E. Taglauer and W. Heiland, Proc. of the Symposium on Sputtering, (Pechtolsdorf/Wien, Austria). Pub., Technische Universität Wien, Austria, June 1980. Page 294.
10. R. S. Battacharya et al., Radiat. Effects. 33, 57 (1977).
11. M. Rossinelli and M. A. Bösch, J. Phys. C, 13, 2671 (1980).
12. E. O. Rausch, A. I. Bazhin and E. W. Thomas, J. Chem. Phys. 65, 4447 (1976).

III. Re-iteration of the Program for the Next Grant Year

Our overall objectives and program remain the same as in our original proposal. We intend to develop an understanding of inelastic collision processes leading to changes in the quantum state of target atoms. Taking relatively simple target systems such as Al and Si we shall record excitation of inner and outer shells and compare these with secondary ion spectra (generated by other groups or if necessary by ourselves). We have shown already similarities between Auger and secondary ion fluxes suggesting that atoms or singly charged ions are ejected with inner shell vacancies, decay to give the detected Auger electrons and thereby produce highly charged ions. Since the Auger decays leave the outer shells in an excited configuration it is possible that at least part of the optical photon spectrum results also from inner shell excitation. We must explore these concepts with further measurements. Of particular importance is the effect of chemical environment which should alter all these signals in a similar manner.

We shall continue to study also the ejection of excited molecules to determine whether they are ejected as separate atoms or as a molecular entity. Of ultimate interest is to understand the molecular structure which gives rise to continuous spectra when the transition metal oxides are bombarded. The ultimate test of a proposed structure is to diagnose directly the nature of the sputtered species by a technique such as laser induced fluoresence.

IV. Personnel

Prof. E. W. Thomas remains Principal Investigator on the project assisted by graduate students W. A. Metz, L. Efstathiou and R. Whaley, Mr. Metz will finish his Ph.D during the next six months but no other personnel changes are forseen.

V. Publications

Manuscripts appearing in print or being accepted for publication during the first six months of this grant were follows:

"Identification of Auger Spectra Induced by Ar^+ and Kr^+ Impact on Transition Metals", K. O. Legg, W. A. Metz and E. W. Thomas, J. Appl. Phys. 51, 4437 (1980).

"Electron and Ion Impact Phenomena: Sputtering," E. W. Thomas, Encyclopedia of Physics (Ed., R. Lerner, G. Trigg, Pub, Addison-Wesley Pub. Co. MA) (to be published).

"Formation of Excited States by Ion Impact on Surfaces", Progress in Surface Science 10, #4 (to be published).

"Inelastic Surface Collisions," Chapter in "Applications of Atomic Collision Physics, Volume IV, Condensed Matter" (Academic Press, N. Y., 1981, H. S. W. Massey, B. Bederson, E. W. McDaniel and S. Datz, Editors).

VI. Current Support

Prof. Thomas has an R & D subcontract with Union Carbide Corp for work in support of the Fusion Program at Oak Ridge. This amounts to $53,000 for the period 1 March 1981 through 28 February 1982. This work is independent of the NSF grant using separate facilities and graduate students. No further research support is pending or being sought.

VII. Statement of Remaining Funds.

The present grant year commenced on 1 August 1980 with an award of $37,400. Accounts as of November 30, 1980 (after 33% of grant year has passed) showed an unencumbered balance of $10,376.51 (ie 73% of grant expended).

We anticipate no significant unobligated funds at the end of the present grant period (31 July 1981).

VIII. Budget

Attached separately is the proposed budget in NSF format. The requested total is essentially that envisaged in the award letter of June 10, 1980.

Continuation Proposal for NSF Grant No. DMR 8000671

Collision Induced Optical and Auger Spectra of Solids

I. Administrative Details

This project was initiated by a letter from NSF dated June 10, 1980 and commenced on July 1, 1980 as a continuing grant with support envisaged for a three year period. This present document is the continuation request for the third year. The Project Director and Principal Investigator is Professor E. W. Thomas.

II. Summary of Scientific Progress

(a) Introduction

It is our general objective to study inelastic collision events resulting from energetic (5 to 200 keV) ion impact on surfaces where target atoms are ejected in excited or ionized states. The basic ejection process involving transfer of kinetic energy to the target atoms, described broadly by the term sputtering, is largely understood. One may refer particularly to the extended reviews edited by Behrisch[1]. The problem can generally be handled by a model treating the kinematics of collision events generated by the impact of the projectile. Largely intractable, however, is the description of the quantum state of the ejected species, the state of excitation and ionization. The quantum state of the ejected particle is governed by processes occuring as it progresses from its position in the matrix, where its condition may be described by solid state theory, to its final position in vacuum where it is described by the well known characteristics of atomic structure. Thus, study of the quantum state distribution of ejected species provides information on the evolution of electronic structure as a particle moves away from the solid and into free space.

We are studying the quantum states of ejected species by performing optical and Auger spectroscopy of atoms and molecules ejected out of solids by impact of energetic particles. The optical spectroscopy provides information concerning the outer shells of the ejected species and in turn is related to the valence band structure of the solid. The Auger spectroscopy probes the inner shell populations and in turn is related to the relatively unperturbed inner shells of atoms in the solid. Considerable world-wide activity exists in both areas and we have recently summarized the situation in two major review articles[2,3]. Innumerable theoretical approaches exist for the description of the excitation processes but, in general, each is specific to a limited class of observations and does not describe other phenomena that should intrinsically be related.

---

1. R. Behrisch, "Topics in Sputtering", Springer Verlag, Berlin, 1981.
2. E. W. Thomas, "Formation of Excited States by Ion Impact on Surfaces", Progress in Surface Science 10, #4, 1982 (in course of publication).
3. E. W. Thomas, "Inelastic Surface Collisions", in "Applications of Atomic Collision Physics, Vol. IV, Condensed Matter", Academic Press, N.Y., 1981, H. S. W. Massey, Ed., (in course of publication).

For example, a description of excited outer shell formation will often be inconsistent with observations of (ground state) populations of particles with differing charge states. Our overall objective is to move towards a unified description of quantum state population or at least to delineate the reasons why no single description applies. As an example, it has been shown by ourselves[4] and by Wittmaack[5] that for Ar^+ on Aℓ and Si the flux of Auger electrons from ejected Aℓ and Si particles is essentially the same as the flux of ions in all charge states, leading to the conclusion that charged ejected particles result from Auger decay of atoms ejected with inner shell vacancies. Thus only a single mechanism is responsible for these two apparently different types of observations. We would further note that the Auger decay will generally leave some atoms with excited outer shells so that part of the optical emission spectrum must also have atoms with inner shell vacancies as a precursor state.

Since a major aspect of our work is the study of outer shell excitation we are vitally concerned with the influence of surface chemistry on the observed processes. It is well known[2] that oxidation changes the excited state population of ejected atoms, and we have shown that even Auger spectra coming from ejected atoms are sensitive to the nature of the chemical environment from which they were ejected. Indeed, a fraction of the ejected particles are in fact molecules representing the chemical composition of the solid. Any detailed understanding of ejection must include consideration of these chemical effects. We have recently completed an extensive study of whether molecules can be created by atomic collision events in the solid. As a vehicle we have considered sequential implantation of C and N into alkali halides and shown (see section b) that CN^- radicals are created by a process involving localized melting followed by recombination. Our work includes also a continuing study of excited molecules ejected from solids which reveals interesting rotational excitation populations that relate to the ejection mechanism (see section c).

This experimental research program employs two major facilities. A high resolution optical spectrometer monitors, quantitatively, the population distribution of ejected particles with excited outer shells. A high resolution Auger spectrometer monitors the shape and intensity of Auger spectra. Both systems are little changed from descriptions given earlier in the literature[6,7] and need not be described further here. Both are at present mounted on an ion implanter that provides projectile beams of energy 20 to 200 keV. Both may also be connected to a separate lower energy accelerator if desired.

In general, the work has progressed as envisaged in our proposals and we expect to follow the proposed program for the third year of this continuing grant. There follows a detailed description of recent progress, subdivided

---

4. W. A. Metz, K. O. Legg and E. W. Thomas, J. Appl. Phys. 51, 2888 (1980).
5. K. Wittmaack, Nucl. Instrum. and Meth. 170, 565 (1980).
6. W. E. Baird et al., Phys. Rev. A 10, 2063 (1974).

according to the objectives of the various program segments.

(b) Formation of CN^- Radicals by Ion Implantation

We have been concerned for some time with the question of whether molecules can be created by ion implantation and the general question as to how an incident ion comes to rest and forms chemical bonds with its neighbors. We have now completed a study of CN^- formation by sequential implantation of C and N into alkali halide crystals. The work is described in two papers submitted for publication[7,8] and we reproduce the abstract of the major work[7] here; copies are included with this proposal.

Formation of CN^- Radicals by Sequential Implantation of Carbon and Nitrogen Ions into KCl

It is shown that the sequential implantation of 20 to 200 keV C^+ and N^+ ions into a KCl crystal gives rise to formation of the CN^- molecular configuration. Detection of the CN^- is by the characteristic luminescence spectrum induced when He^+ ions are incident on the implanted target, a technique which represents a direct in-situ determination of their presence. It is shown how the ion induced optical emission may be used to provide a routine relative measurement of the quantity of CN^- present. We describe a phenomenological model of the formation process which leads to the conclusion that each incoming ion searches a volume of the target approximately 3.4 x 10^{-21} cm^3 in extent and has a unit probability of combining with an atom of the other species lying in this region. This model explains why saturation of the CN^- density occurs at an N^+ dose independent of the quantity of C^+ implanted previously.

The most valuable result of the work comes from the information it provides on the mechanism whereby the molecule is formed. With a small preliminary dose of C^+ one can follow the formation of CN^- as a function of the following N^+ dose. Saturation of the CN^- density occurs at a dose corresponding to only one N^+ ion implanted for (approximately) every 100 cation lattice sites. Thus each N^+ ion has "searched" a substantial region of the solid to find the C atom with which it combines. To explain this we utilize the results of an (unpublished) molecular dynamics calculation of Landman which shows that a foreign atom introduced into a crystal cause a localized melting over a region of some four or five lattice constants in radius. We propose that the implanting N^+ causes such a localized melt as it comes to rest, and that if a C ion lies in this region there is a conventional atom-atom recombination. The necessary recombination coefficients are consistent with recent calculations for high density situations. Subsequently (in about 10^{-14} seconds) the melt recrystallizes and the newly formed CN^- occupies a cation site.

---

7. W. A. Metz and E. W. Thomas, J. Appl. Phys. (submitted).
8. W. A. Metz and E. W. Thomas, Nucl. Instrum. Meth. (accepted).

This model provides considerable insight into the process whereby an implanted atom arrives at a lattice site. While we propose no further work on this particular system we are seeking a similar case for study where the theoretical model can be quantitatively linked to experiment.

(c) Excitation of Sputtered Molecules

Molecules possess rotational and vibrational degrees of freedom and the population of such states in sputtered particles will provide clues as to the dynamics whereby the molecule is formed and ejected. To capitalize on this opportunity we have been studying the excited state populations of N_2 molecules sputtered from nitrogen implanted Si. The N_2 molecule is an attractive candidate having well understood energy levels and exhibiting relatively simple rotational and vibrational structures. The nitrogen is first implanted into Si and then the sample bombarded with either Ar^+ or further N^+ to produce a spectrum dominated by N_2^* lines from the C $^3\Pi_u$ v = 1 state. There is significant rotational broadening that can be modelled by an effective rotational temperature of 1100°K. Vibrational excitation is negligible.

It is often argued that sputtered molecules are created by simultaneous ejection of two separate atoms (here N) with kinetic energies in the center of mass frame less than the binding energy of the molecule. Such a situation can be shown to result in significant rotational and vibrational excitation, features that we do not observe. Our approach is to consider that the impact causes the molecular formation on the surface. An incident particle causes an N atom to recoil transversely across the surface to arrive at a site already occupied by an N atom. A temporary molecule forms, stabilizes by collision with surrounding atoms, and emerges because the residual interaction with the surface is repulsive. Sample trajectory calculations show that the maximum rotational energy of the molecule will be appropriate to a state of rotational quantum number J = 11. This is approximately what we observe. Stabilization of the molecule is by conversion of vibrational energy into kinetic energy in the manner described by Willis and Fitton[9] in a study of H_2 desorption from interstellar dust. The model remains under development and now requires a detailed Monte-Carlo calculation of trajectories leading to a distribution of rotational population that can be compared with observations.

A brief interim report on this work has been accepted for publication[10] and is attached as an appendix.

(d) Ion Induced Auger Spectra

A typical lifetime for a 2p inner shell vacancy in a third row element is around 10^{-14} sec. Thus atoms (or ions) ejected with only a few eV of energy will frequently undergo the Auger decay process while still significantly influenced by the potential of the surface. A mechanism that both excites such inner shell vacancies as well as providing the kinetic energy for ejection, is inner shell promotion in the quasi molecule formed as two heavy particles approach each

---

9. R. F. Willis and B. Fitton, At. and Space Sci. 34, 57 (1975).
10. L. Efstathiou and E. W. Thomas, Nucl. Instrum. Meth. (accepted for publication).

other. The promotion produces the vacancy and the necessary close distance of approach ensures that substantial kinetic energy is transferred to the target atom. Such promotions can be instigated by projectile-target collisions as well as target-target collisions in the collision cascade. These matters are well described in the literature and require no further comment here[2,4].

An Auger spectrum induced by, say, Ar^+ impact on Aℓ or Si is expected to be of target atoms recoiling from the solid with an energy appropriate to a collision event of sufficiently small impact parameter that molecular orbitals may become degenerate and promotion occur. We have recently performed model calculations for such events which show that 70% of the Auger decays in sputtered Si occur within 5 Å of the surface. Thus the majority of decay processes occur while the emerging atom is still interacting with the target. The fraction increases as one proceeds to sulphur and phosphorus where lifetimes are yet shorter.

The Auger spectrum is then emitted by particles either in free space or suffering some limited interaction with the surface they are leaving. Since the Auger decay occurs from atoms no longer in the matrix one expects no plasmon spectra, and sharp atomic like lines; these characteristics we have documented[4].

We have calculated[4] the line spectrum for aluminum assuming that the principal source of Auger electrons is ejected Aℓ atoms in a $2p^5\ 3s^2\ 3p^2$ configuration. For Si we propose[4] that the source is Si in a $2p^5\ 3s^2\ 3p^3$ state. Again we have predicted the line spectrum and have an excellent opportunity to check in detail the predictions since for Si the separation of individual lines is comparable with the resolution of our detection system.

We have shown in the case of Si that the relative intensity of different features in the Si spectrum change with the chemical nature of the surface. A change of line intensity without change of line position implies either change to level population or to decay probability. If only a single state is the precursor to the transition and line structure reflects only different final states we are forced to conclude that the change to the structure of the Auger spectrum relates to altered transition probabilities. Auger matrix elements expressed in terms of the vector separation of ion cores $\vec{R}$ vary as R^{-3} so that probabilities of interatomic transitions (involving two atoms) are small. Hence the Auger line is characteristic of the atom where the original core hole was created[11]. Changes to transition probability are then due to perturbations of outer shell wavefunctions by the adjacent solid.

We are proceeding by accumulating high resolution ion induced Auger spectra of Si from various chemical compounds (Si, SiO_2, SiC, Si_3N_4, etc.) in an attempt to relate details of the Auger spectra to perturbations by the other atom present (O, C or N). It appears that a typical spectrum from a compound has two groups of components. One group is common to all cases and may represent Si interacting with Si. The other varies with compound and may represent interaction of Si with the other atom.

---

11. T. Kunnjunny and D. K. Ferry, Phys. Rev. B. 24, 4606 (1981).

Continuation of this work will represent approximately 60% of the effort in the 12 month period covered by this continuation request.

NSF Project
DMR-8000671

COLLISION INDUCED OPTICAL AND AUGER SPECTRA OF SOLIDS

PROGRESS REPORT

Covering the Period

Dec. 31, 1982 to Jan. 1, 1983

by

E. W. Thomas

Report Prepared by

The Georgia Institute of Technology

School of Physics

Atlanta, Georgia 30332

Under Grant DMR-8000671

from the National Science Foundation

Division of Materials Research

Solid State Chemistry Program

1 January 1983

TABLE OF CONTENTS

I. TITLE

Collision Induced Optical and Auger Spectra of Solids.

II. ADMINISTRATIVE INTRODUCTION

This report covers work performed under NSF Grant DMR-8000671 during the period 12/31/82 through 1/1/83. The Principal Investigator is Edward W. Thomas, Professor of Physics and Director of the School of Physics. This report is sent as an accompanyment to a proposal for continued support.

III. ABSTRACT

Impact of ions on surfaces gives rise to excited ejected particles and excitation of the solid itself. This report covers three rather distinct investigations of such phenomena.

We show that CN^- radicals are formed by sequential implantation of C and N into KCℓ crystals; the formation is detected by ion induced luminescence of the radical. The process of formation appears to be conventional recombination occurring in a region of localized disorder at the end of the projectile track.

Molecules of N_2 sputtered from Si are shown to be rotationally excited with a non-Boltzman population distribution. This is evidence that the molecule on the surface is in a hindered rotational state and we are able to estimate the angle in which the hindered rotor moves. Data from other sources for rotationally excited sputtered molecules and rotationally excited scattered molecules is also consistent with the model.

Auger spectra induced by ion impact (Ne^+, Ar^+) on solids (Na, Mg, Al, Si) show evidence of decays occurring while the emerging atom is still within the potential field of the solid.

IV. DISCUSSION OF PROGRESS

This project is designed to study the interaction of atomic and molecular species with surfaces. The experimental techniques involve detection of optical spectra and Auger electron spectra when heavy ions are incident on various surfaces. The optical spectra are from ejected atoms and molecules with excited outer shell electrons. With the long lifetime against radiative decay (typically 10^{-8} sec) the ejected species is distant from the surface before decay occurs. Thus the quantitative measure of line intensity provides the asymptotic quantum state distribution of the ejected species. Auger spectra are from atoms with excited inner shells. Due to the short lifetime against Auger decay (typically 10^{-14} sec) ejected atoms may undergo their decay while still interacting with the surface. In this case the spectrum may be perturbed by surface interactions and analysis may in principle provide information on the energy levels and transition probabilities of atomic structures perturbed by the field of the surface.

The two distinct experimental techniques provide different types of information and it is most convenient to discuss them separately. The report is

organized along the following lines. We discuss first in general terms the experimental facilities used for the work. There follows a series of reports on the results of studies of optical emissions then a report on the study of Auger emissions; finally the understanding gained is summarized. In some cases the work has been largely published in the open literature and we shall reporduce the publications as Appendixes for detailed reference.

(i) Experimental Facilities

The work has involved study of optical and Auger spectra induced by ion impact on solid targets. In simplistic terms the equipment consists of an optical or Auger spectrometer viewing the point of beam impact on a surface. Ion beams for all experiments have been provided by a 20 to 200 keV ion implanter. The work on Auger spectra has generally involved Ne^+ and Ar^+ ions. The optical spectroscopy has involved work with He^+, Ne^+, N^+, N_2^+ and Ar^+. The ion beam is mass analyzed, collimated and directed into a uhv chamber (base pressure $< 10^{-9}$ torr) to impact on the selected target surface. An Auger electron spectrometer is available to monitor surface composition and a sputter ion gun can be used for in-situ cleaning. The targets themselves are high purity materials (generally, Na, Mg, Al, Si, KCl) and in some cases (Si and KCl) single crystals are used. Targets are either cleaved (Si and KCl) or polished before mounting on a precision manipulator and insertion into the vacuum chamber. The uhv system is baked to 200°C before use and background pressures are below 10^{-8} torr even when the ion accelerator is operative.

A Jarrel Ash 1/2 meter (or Oriel 1/4 meter) scanning optical monochromator views the point of beam impact and signals from the low noise photomultiplier recorded on a multi-channel scalar as a function of wavelength. The Auger spectrometer, with its integral electron gun is used to record the Auger spectrum, again onto the multi-channel-scalar. The Auger spectrum may be recorded in either the derivative or integral modes. Data records may be transmitted to a computer for analysis.

(ii) Formation of Radicals in the Solid by Ion Implantation

One matter that has concerned us for some time is the ultimate fate of an atom implanted into a solid. There is of course substantial information on the crystallographic location of implanted non reactive species such as rare gases. However, what occurs when the implanted species can react with the matrix? To study this matter we implanted C and N separately into KCl and other alkali halide crystals then subsequently monitored the formation of CN^-. Detection of CN^- was by exciting it to fluorescence with energetic He^+ and detecting the characteristic CN spectrum. We sought to study first whether the separately implanted C and N chemically combined at all and secondly what was the rate at which this occurred. This particular combination of species was chosen because there is substantial information on CN^- in alkali halides where it substitutes for the halide atom.

The results have all been published and the reader is referred to Appendix I for an extensive report and Appendix II for a less extensive publication. Briefly the conclusions were as follows.

Firstly the radical CN^- was in fact formed by sequential implant of C and N into KCl and the fluorescence spectrum was in fact identical to that of

CN^- in a KCN crystal. We showed in some detail how the density of CN^- varied with implant energy and dose showing it to be directly related to the local density of implanted C and of implanted N. There is no evidence that either species migrates to form the radical. For a given dose of C the formation of CN^- by the subsequent implantation of N should of course show a saturation when all the available C is reacted. If a reaction were to occur only when an N atom came to rest on the lattice position as already occupied by a C then saturation would occur at an N dose that placed one N on every lattice site in its range. Only then could one ensure that every previously implanted C had an opportunity to react with an N atom. In practise the N density for saturation was two orders of magnitude lower. Prof. U. Landman suggested that when an atom comes to rest in a lattice it causes a localized melting. This he demonstrated by molecular dynamic simulations. The thermal energy spreads out by conduction, local energy decreases and eventually recrystallization occurs. With this model we have a disordered or molten region existing for a short period. All atoms will be mobile and can undergo chemical reaction as appropriate. If an incoming N creates such a region and a previously implanted C is located in its boundary then the reaction could occur and after recrystallization the CN^- could be found in the halide lattice site. Interpreting our data on this basis we conclude that the disordered region is about three lattice constants in radius and lasts for about 10^{-13} seconds. This is completely consistent with Landman's molecular dynamic simulation.

In conclusion, implanted species do react chemically with their surroundings in the disordered region created by the change in local potentials as the projectile comes to rest. This may be the basic explanation of how implanted species enter lattice sites at the end of their range.

Full details are to be found in Appendixes I and II. We regard this project as completed and no further work is planned.

(iii) Rotational States of Ejected Molecules

We turn now to the question of what happens to a molecule when it is ejected (sputtered) into free space and concentrate particularly on the question of rotational state populations. Detailed optical spectroscopy of the rotational state structure of an electronic decay can give us the rotational population of molecular states that have departed a macroscopic distance from the surface. These populations should in turn be related to the rotational states of the molecule when it was bound to the surface. The excitation process itself might be thought to cause changes to rotational population but it is generally expected that excitation would be by Franck-Condon transitions and that rotational configurations will not be altered. We have in fact shown this ourselves many years ago in gas phase collisions[1] and there is a substantial body of supporting evidence in the literature. Let us then assume that the rotational state population in free space is related to the earlier rotational state population of the molecule when bound on the surface. Two possible population distributions come to mind. First if the molecule is in rotational equilibrium with a surface at temperature T ^oK then the rotational state population of the ejected species should be the same. Alternatively if

[1] E. W. Thomas, G. D. Bent, J. L. Edwards, Phys. Rev. 165, 32 (1980).

ejection was by a collision cascade and this has some effective equilibrium temperature T_c associated with it then rotational state population should be a Boltzman distribution appropriate to that temperature. In studies of electronic excitation and charge state populations the value of T_c must be taken as 3000 to 7000 °K to fit the available observations.[2] We set out to decide which temperature was appropriate and found that the data fitted neither.

As a test case we considered excited N_2 sputtered from N^+ implanted Si. Implantation was with 50 keV N^+. As implant density builds up we observe a rise in the N_2 (3371 Å Band Head, $^3\pi \rightarrow {}^3\pi$ $v = 0 \rightarrow v = 0$) emission to a saturation value. This emission we have shown (see Appendix III) is due to previously implanted nitrogen atoms being revealed by sputtering, recombining to form N_2 and subsequently being ejected. The general understanding of this was formulated by Battacharya et al.[3] Plotting rotational state population as a function of J we found that for lower states we had a roughly thermal population with an effective rotational temperature of 1100 °K. Since the target was at room temperature this is not appropriate to a thermally accomodated molecule. Moreover, they do not agree either with the normally expected temperatures from the LTE collision cascade approach.[2] Our results to this point have been published and are reproduced as Appendix III.

We subsequently studied in more detail the rotational population out to high rotational quantum numbers J. We show that at $J \geq 30$ there are high populations and the total distribution can in no way be represented by a thermal population.

Almost simultaneously with our discovery there was a publication by Kleyn et al.,[4] describing rotational populations of NO observed when rotationally cold NO molecules at less than 1 eV kinetic energy are scattered from an Ag surface. Here again low J states showed a roughly thermal population but at high J states ($J \gtrsim 30$) there were high populations that are not consistent with a thermal equilibrium situation.

These two parallel observations, NO scattered from Ag[4] and N_2 sputtered from Si[4] are of rotational populations of molecules that reside (albeit temporarily for the scattering problem) on a surface before emergence into free space. U. Landman,[5] working with us at Georgia Tech, suggested that one might explain the non-thermal distribution by examining the quantum mechanics of a hindered rotor molecular state. Here the molecule is described as a rigid dumbbell executing free rotations within a conical domain bounded at some critical polar angle $\beta \leq \pi/2$ by an infinitely repulsive wall. In effect this is the spherical-coordinate-system analog of the standard textbook infinite square well potential problem. Fig. 1 illustrates the hindered rotor configuration analyzed by Gadzuk, Landman and co-workers[5] although other orientations are also possible. The angular part of the Schrodinger equation is solved to give eigenstates that are associated Legendre functions of arbitrary order.

---

[2] C. J. Good-Zamin, M. T. Chehata, D. B. Squires and R. Kelly, Rad. Effects 35, 139 (1978).

[3] R. B. Battacharya, C. B. Kerkdijk, J. F. Van der Veen and F. W. Saris, Rad. Effects 33, 57 (1977).

[4] A. W. Kleyn, A. C. Luntz and D. J. Auerbach, Phys. Rev. Lett. 47, 1169 (1981).

[5] J. W. Gadzuk, U. Landman, E. J. Kuster, C. L. Cleveland and R. N. Barnett, Phys. Rev. Lett. 49, 426 (1982).

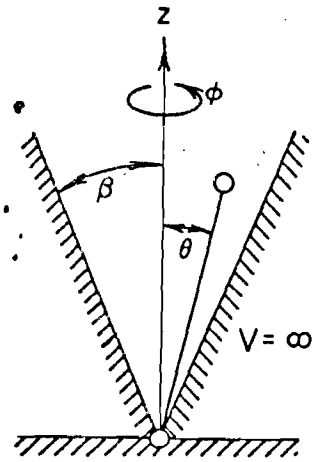

Fig. 1. Hindered rotor configuration considered in the analysis by Gadzuk, Landman and co-workers.[5] One atom is taken as stationary on the surface. The molecular axis rotates about the z direction in a potential $V = 0 \quad \theta \leq \beta$ and $V = \infty \quad \theta > \beta$.

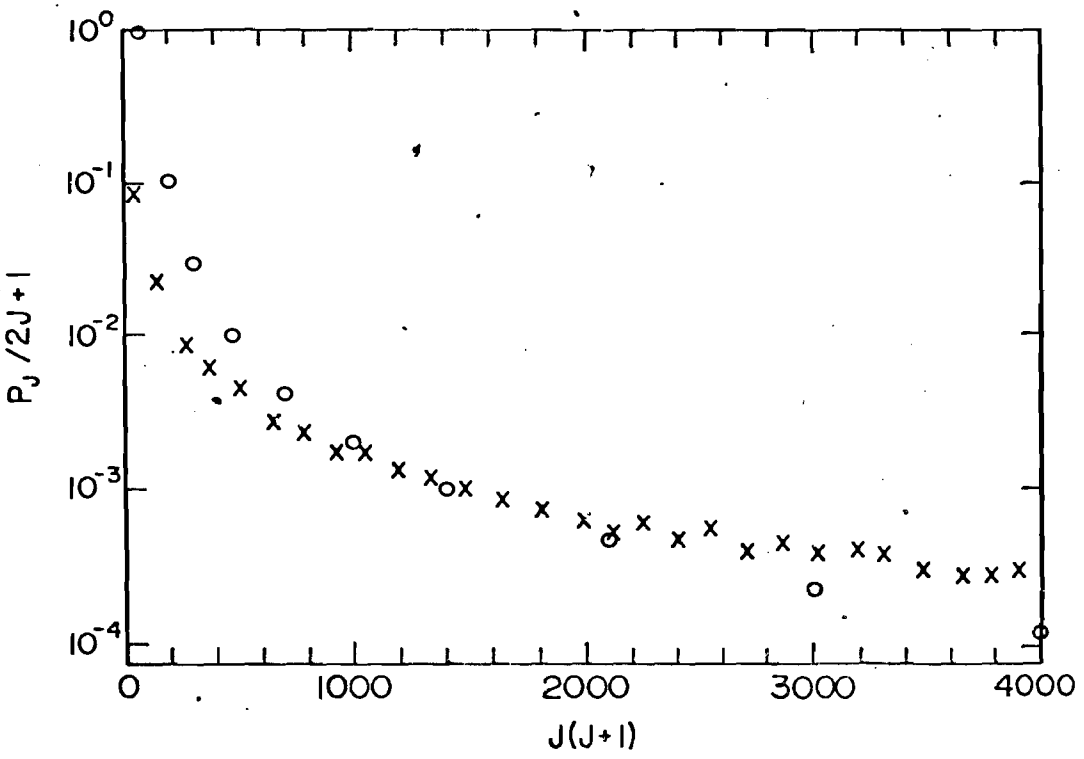

Fig. 2. Crosses show the population of the rotational states P_J as a function of rotational quantum number J from our measurements. Circles show the results of the hindered rotor model[5] for $\beta = 90^{\circ}$.

$$\psi_{\nu m}^{rot}(\theta,\phi) = \begin{cases} A_{\nu m}(2\pi)^{-1/2} P_\nu^{|m|}(\cos\theta)\, \exp(im\phi), & 0 < \theta < \beta, \\ 0, & \beta \lesssim \theta \lesssim \pi, \end{cases} \tag{1}$$

with $m^2 < \nu(\nu+1)$ and $A_{\nu m}{}^{o}$ a normalized constant. The eigenvalues are numerically determined by the condition

$$P_\nu^{m}(\cos\beta) = 0$$

and the normalization by

$$|A_{\nu m}|^{-2} = \int_{\cos\beta}^{1} dx |P_\nu^{|m|}(x)|^2 = \frac{-(\nu+m)}{(2\nu+1)} P_{\nu-1}^{m}(\cos\beta) \left[\frac{dP_\nu^{m}(\cos\beta)}{d\nu}\right] \tag{2}$$

When the hindering potential is removed the molecule becomes a free rotor described by the well known eigenfunctions:

$$Y_{\ell m}(\theta,\phi) = [A_{\ell m}'/(2\pi)^{1/2}] P_\ell^{m}(\cos\theta)\, e^{im\phi} \quad (\ell = \text{integer}) \tag{3}$$

Population of the free state rotor is evaluated by the overlap of the two wavefunctions 1 and 2.

$$\langle Y_{\ell m'} | \psi_{\nu m} \rangle = \frac{\delta_{m,m'} A_{\nu m} A_{\ell m'}'}{\nu + \ell + 1} \left(\frac{\nu+m}{\nu-\ell}\right) P_\ell^{m}(\cos\beta)\, P_{\nu-1}^{m}(\cos\beta)$$

A full explanation is to be found in the published work. One can postulate that the hindered rotor exhibited a thermal population of its rotational states appropriate to the surface temperature and calculate therefrom the population distribution one should observe in the free molecule. The calculated rotational state distributions are shown in Fig. 2 to be in substantial agreement with our observations provided the angle β of the rotor (see Fig. 1) is taken to be 90^{o} in the calculation. The principal discrepancy between theory and experiment lies at the low rotational states where the computation produces a higher population than we measure. We acknowledge that the large angle β is at first sight unrealistic but this simply indicates the molecule lies parallel to the surface. This case is now being considered theoretically.

At this point we should mention that we have also compared results of the hindered rotor calculation with the published data on rotational states of NO scattered from Ag[4]. The analysis is detailed in Appendix IV. There is acceptable agreement similar to what we show for our own data on sputtered N_2. We have also examined published spectra of rotationally excited sputtered BH published by Kelly[6] which appear to show state populations oscillating with increasing J. Again this is consistent with the hindered rotor model.[8] The oscillations should be apparent in low mass molecules (such as BH). Thus there is substantial evidence from our own work and that of others,[4,6] that the hindered rotor model may be the explanation of non-thermal rotational populations exhibited by molecules ejected from surfaces.

---

[6] R. Kelly, S. Dzioba, N. Tolk and J. C. Tully, Surf. Sci. 102, 486 (1981).

A significant piece of information readily extracted from the experimental data is the conical angle of the rotor. Indeed for simple light systems where oscillatory populations are evident the angle is simply 180° divided by the separation (measured in rotational quanta J) of the minima in state populations. Such oscillations should be evident for light molecules. Our analysis of spectra published by Kelly[6] show that BH molecules on a B surface must be in a conical well of half angle 26°. In principal one can now go forward to measure the half angles for any molecular species that may be desorbed by simply analyzing the rotational state distribution in free space. One may also vary the details of the potential function so that complete correspondence between theory and experiment is achieved and thereby confirm the potential. Of particular interest is the variation of potential with azimuthal angle. For example, a molecule located at the center of a four atom face of a cubic structure should be quite tractable. Such calculations, with realistic potentials are now being performed for us by Landman and his group.

It must be admitted that the work performed to date includes some complexities that should be removed in future experiments. Our work has been on electronically excited sputtered molecules. The electronic excitation occurs in the ejection process. Numerous gas phase experiments suggest that collisional excitation does not change rotational state populations but nevertheless this represents a source of ambiguity. It is necessary now to perform experiments on the rotational population of ground electronic states. This is quite feasible using detection techniques of laser induced fluorescence (as done by Kleyn et al. in their study of NO scattering[4]) or perhaps electron induced fluorescence (as used by Thorman et al.,[7] in the study of vibrational excitation of thermally desorbed N_2). It is also desireable to concentrate on low mass molecules of small rotational constant B where not only are the rotational states better separated but where oscillatory populations have been predicted.[4] Sputtered BH molecules apparently show the anticipated features. One should also seek to perform the experiments as a function of ejection angle from simple single crystals since this will provide information on how potential varies with azimuth. Finally one must move away from the sputtering ejection mechanism since this involves transfer of kinetic energy from the collision cascade providing an additional degree of freedom and of complexity. Bond breaking mechanisms such as photon or electron induced desorption will be far more satisfactory.

Our renewal proposal involves taking the steps outlined above and working closely with Landman's theoretical effort to provide detailed comparisons between experiment and theory that permit elucidation of detailed potentials and bond angles to describe molecules bound to surfaces in hindered rotational configurations.

Some of this work is discussed in greater detail in the Appendixes. Appendixes III and IV are interim publications, Appendix V is an analysis of Kleyn's scattering data.

---

[7] R. P. Thorman, D. Anderson and S. L. Bernasek, Phys. Rev. Lett. 44, 743 (1980).

(iv) Inner Shell Excitation

Impact of Ar^+ ions on the elements Na, Mg, Al, Si creates an Auger spectrum characteristic of the solid. We have previously reported the general features of the spectrum.[8] In Fig. 3 we show a typical integral spectrum for the case of Al. There is an underlying continuum that bears a general resemblance to an electron induced spectrum with three sharp peaks that are certainly not from a solid matrix and are often referred to as "atomic like". These sharp features are not, however, dur to isolated atomic particles with an inner shell vacancy. Such a species would be an ion, and the same spectra should be produced in gas phase collisions like $Al^+ + Si$; the observed spectra are in fact not like those seen in gas phase collisions.[9] There has been a continuing controversy regarding the precise nature and location of the emitting particle. A substantial body of opinion has argued that a sputtering process involves a collision cascade with many atoms displaced from their normal lattice position. There is, however, no direct evidence at all that such a cascade exists. It was argued by Vrakking and Kroes[10] that in the disturbed area of a collision cascade the particles should be largely neutral atoms in the nature of a high density gas. If an atom were to acquire an inner shell vacancy then the Auger spectrum would be atomic like but perturbed by its close neighbors. If this could be confirmed then one would have for the first time direct evidence of the collision cascade and also a means of assessing the atomic configurations of particles in the region. Such a result would be of great significance for the collision cascade theory. Our objectives were to examine this proposition and ascertain whether the sharp line spectra were from atoms in the solid or atoms outside the solid; further we wished to confirm that the underlying continuum was due to a normal $L_{23}VV$ transition of the matrix.

We believe that proper analysis of these spectra must be based on the use of integral rather than derivative spectra. Most authors present derivative spectra since these are most readily obtained with commercial instrumentation. While valuable in indicating locations of structures they can be quite misleading when it comes to identification or to determining the relative importance of features. We work always with integral spectra and attempt to model the observations with a series of reasonable contributions. Fig. 3, for example, suggests an underlying continuum similar to that for electron impact. An electron induced curve can be readily obtained in our apparatus and adjusted to fit the low and high energy (shoulder) regions. This fits very well and in certain cases (notably Mg) we can even unambiguously identify plasmon loss peaks. One must now tackle the sharp features. We proposed[8] earlier that these are due to sputtered atoms and our further analysis confirms that viewpoint. We argue that they are from sputtered atoms with an inner shell vacancy and an extra outer shell electron; for example, for Al the

---

[8] W. A. Metz, K. O. Legg and E. W. Thomas, J. Appl. Phys. 51, 2888 (1980).

[9] P. Dahl, M. Rodbro, G. Hermann, B. Fastrup and M. E. Rudd, J. Phys. B 9, 1581 (1976).

[10] J. J. Vrakking and A. Kroes, Surf. Sci. 84, 153 (1979).

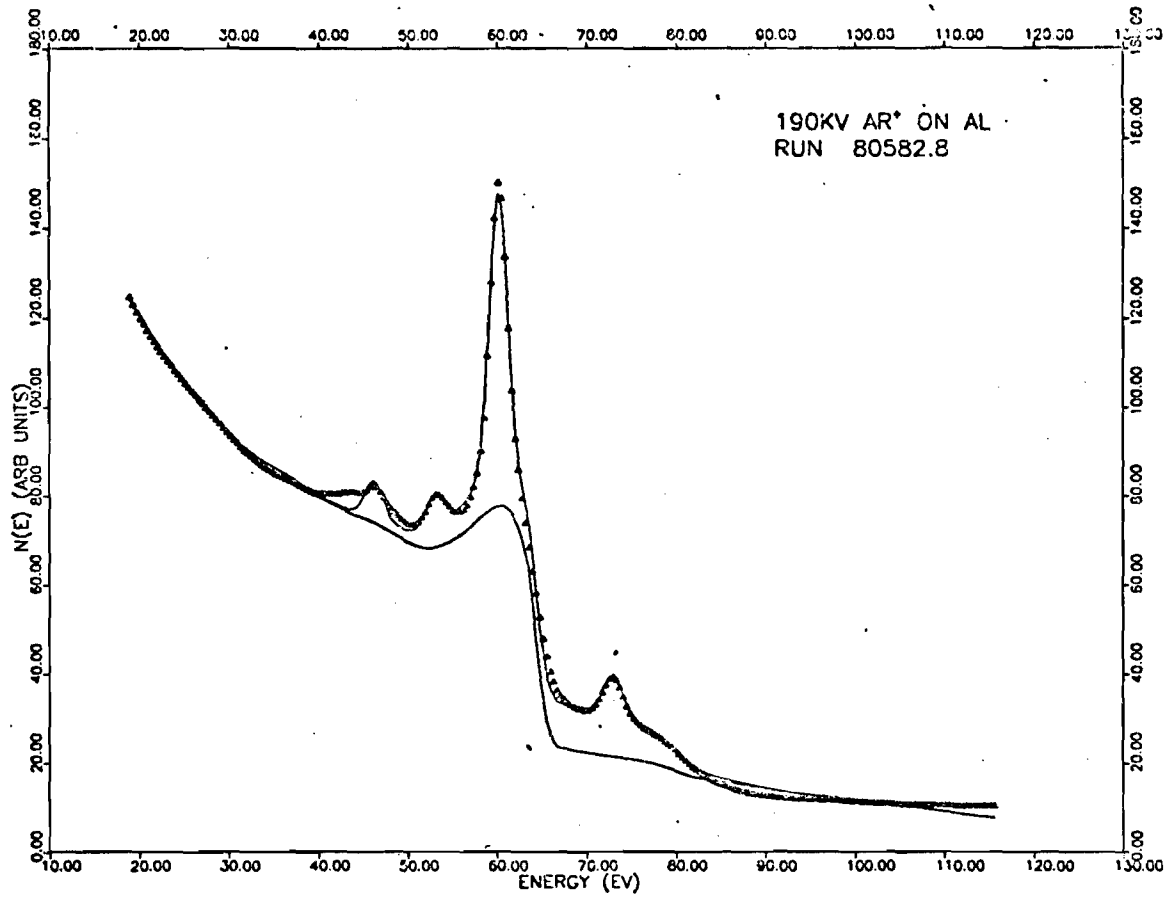

Fig. 3. Integral Auger spectrum induced by 190 keV Ar^+ impact on Al (data points). The lower line is a simulated $L_{23}VV$ spectrum consisting of an electron induced spectrum with an adjusted background. The upper line is a simulated ion induced spectrum composed of the following four components.

(a) The $L_{23}VV$ spectrum--the transitions in the matrix.

(b) Three Gaussian lines at positions predicted for decay of $2p^5\ 3s^2\ 3p^2$ excited states of Al--the transitions of free atoms.

(c) A small subsidiary broad peak, 10 eV in width, centered at 55 eV--the transitions of atoms in the field of the solid.

(d) Features above 65 eV are explained as due to doubly ionized states.

state would be $2s^2 2p^5\ 3s^2 3p^2$. From this we can calculate the energies of Auger electrons emitted in various decay paths and obtain line positions. The lines are broadened by an instrumental function including a small Doppler shift which we can assess separately and to which we arbitrarily assign a Gaussian shape. The relative intensities of the lines may now be adjusted to fit the observations. Fig. 3 shows the result of fitting the continuum and the lines. In general, the overall fit is fairly good, particularly for Mg and less so for Si (see Figs. 4 and 5).

These fitting procedures show quite clearly that the spectrum has both a bulk component and an atomic line component. Thus a certain fraction of the target atoms excited in the collision cascade do not exit from the solid and undergo a conventional $L_{23}VV$ transition. The resulting spectrum shows the expected loss tails, plasmon losses etc. The remaining atoms emerge from the solid picking up an electron in an outer shell to remain neutral. Decay occurs outside the matrix giving rise to discrete atomic lines which are predictable in position and shape. In much of the previous work there has been concern that the existence of three distinct lines, with equal separations for each of the elements Mg, Al and Si indicated some new process with features common to each case. Due to the increasing complexity of states available one would have expected an increase in the number of lines as one progressed from Mg, Al to Si. We have shown this to be an artifact of the problem. An increased number of lines do in fact occur and can be seen in Si as fine structure on the major features. However, the lines do tend to bunch in position and with a low resolution spectrum they fortuitously appear as three peaks in each case.

Two problems remain and are receiving our attention. Firstly the line intensities are quite different from theoretical computations.[11] While no computation has been performed for Al ($2p^5\ 3s^2\ 3p^2$) one would expect relative line strenghts to be similar to Si^+ ($2p^5\ 3s^2\ 3p^2$). Such calculations are available[11] and do not fit the data. Secondly there is for some cases (notably Al and Si) a spectral component underlying the main peaks that is not accomodated by a superposition of $L_{23}VV$ matrix spectrum and the atomic lines. This component is not present in the spectrum of Mg. We believe that these two discrepancies are related to decay of the atoms close to the surface where they are perturbed by the potential field of the solid. For Mg the lifetimes of 2p vacancies are such that most decays from sputtered particles occur in free space; here there is no unexplained spectral component and line intensities bear some resemblance to theory. For Al and more so for Si the lifetimes are lower, more decays occur close to the surface and both problems are present. We are developing a model to predict how these free atomic and perturbed atomic components should vary with lifetime and sputtered particle speed. Preliminary results are encouraging though not yet quantitatively correct.

A substantial effort has been devoted to clarifying erroneous statements in the literature. Hikari et al.,[12] claim that the ion induced line spectra of Si change when it is studied in a compound. This claim was based on derivative spectra and if true would cast in serious doubt the identification

---

[11] D. L. Walters and C. P. Bhalla, Phys. Rev. A 4, 2164 (1971).

[12] A. Hikari, S. C. Kim, T. Imura and M. Iwani, Jap. J. Appl. Phys. 18, 1767 (1979).

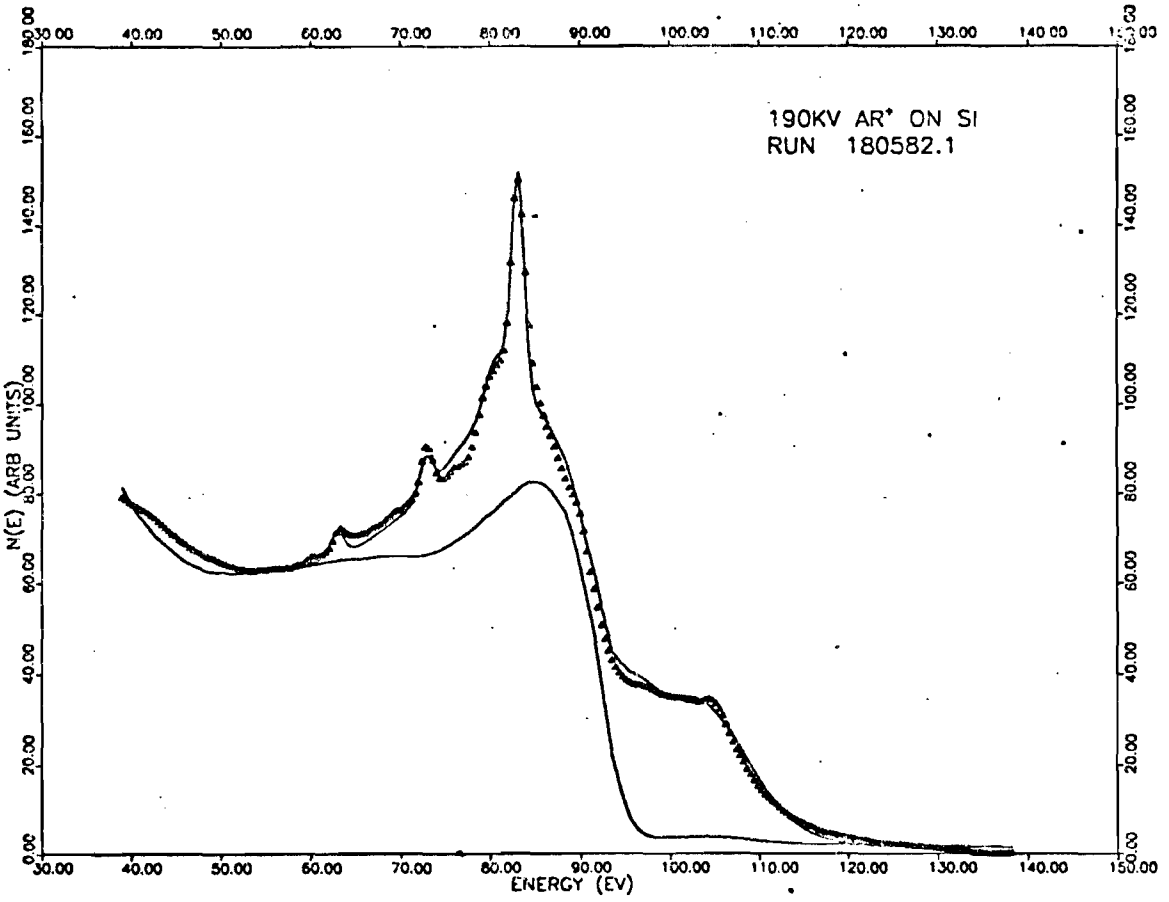

Fig. 4. Integral Auger spectrum induced by 190 keV Ar^+ impact on Si (data points). The lower line is a simulated $L_{23}VV$ spectrum consisting of an electron induced spectrum with an adjusted background. The upper line is a simulated ion induced spectrum composed of the following four components.

(a) The $L_{23}VV$ spectrum--the transitions in the matrix.

(b) Four Gaussian lines at positions predicted for decay of $2p^5\ 3s^2\ 3p^3$ excited states of Si--the transitions of free atoms.

(c) A subsidiary broad peak, 15 eV in width, centered at 75 eV--the transitions of atoms in the field of the solid.

(d) All features above 95 eV are explained as due to doubly ionized states.

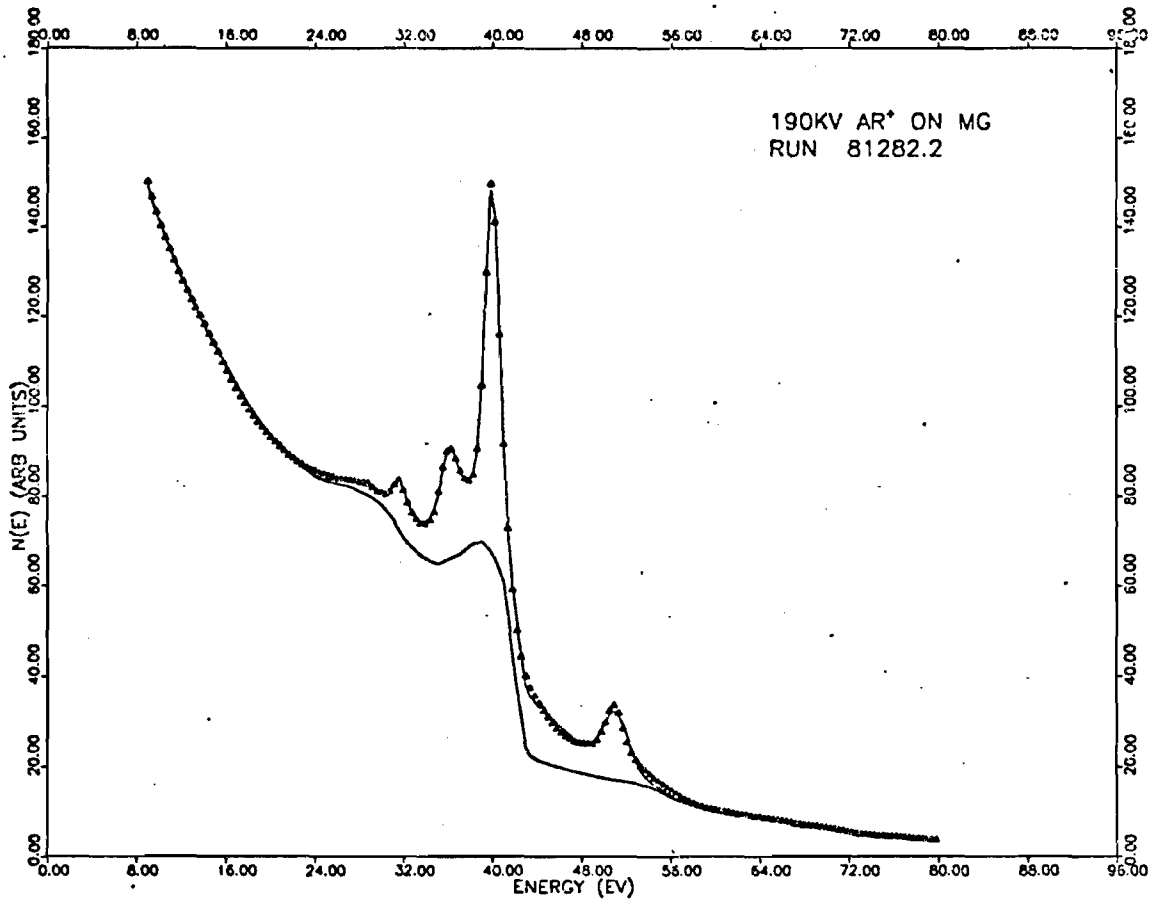

Fig. 5. Integral Auger spectrum induced by 190 keV Ar^+ impact on Mg (data points). The lower line is a simulated $L_{23}VV$ spectrum consisting of an electron induced spectrum with an adjusted background. The upper line is a simulated ion induced spectrum composed of the following three components.

(a) The $L_{23}VV$ spectrum--the transitions in the matrix.

(b) Three Gaussian lines at positions predicted for decay of $2p^5\ 3s^2\ 3p^1$ excited states of Mg--the transitions of free atoms.

(c) All features above 45 eV are explained as due to doubly ionized states.

Note that the subsidiary broad peak mentioned in the captions to Figs. 3 and 4 is not required here. Apparently the long lived Mg excited atoms decay predominantly in free space.

of these lines as due to atoms. We have shown from the integral spectrum that the change with compound occurs only in the underlying $L_{23}VV$ spectrum which does, of course, involve the valence band and should vary with chemical compound. The line spectra are not altered in shape. We have also studied in detail Wittmaack's[13] identification of the line spectra in Si and concluded that many of the identifications are faulty. This again arises from the use of derivative spectra. The problem is compounded by the use of incorrect energies for some of the states.

Experimental work on this subject has now been brought to a conclusion. We have considerable quantitative data for Na, Mg, Al and Si targets bombarded by Ne^+ and Ar^+ at a variety of energies and angles. Fitting routines have been developed to strip out the various contributing spectral features. Some further analysis is necessary as the material is written up as a Ph.D. thesis.

Further detailed pursuit of this problem would require a theoretical analysis of Auger decay occurring close to a surface; this is a subject where we have no local theoretical capability. We therefore do not propose further work on the problem of ion induced spectra at this time.

A brief publication on this subject is included as Appendix VI.

(v) Summary

The project has proceeded generally as expected. Our work on formation of radicals by ion implantation is complete and published. Studies of rotational state populations have suggested the applicability of the hindered rotor model to description of a molecule on a surface. The work on rotational states is of high interest and we plan to continue it. Our studies of Auger spectra have cleared up many inconsistencies in the literature and is being evaluated prior to final publication; no further work on Auger spectra is proposed.

[13] K. Wittmaack, Surf. Sci. 85, 69 (1979).

V. PUBLICATIONS

The following are publications that appeared in print or were published during the period covered by this report (12/31/82 to 1/1/83).

		Support	
		NSF	Other
1.	"Formation of CN^- Radicals by Sequential Implantation of Carbon and Nitrogen Ions into KCl", W. A. Metz and E. W. Thomas, J. Appl. Phys. 53, 3529 (1982).	100%	None
2.	"Formation of CN^- Radicals by Ion Implantation", W. A. Metz and E. W. Thomas, Nucl. Instrum. Meth. 194, 505 (1982).	100%	None
3.	"Excited States of Sputtered Molecules", L. Efstathiou and E. W. Thomas, Nucl. Instrum. Meth. 194, 589 (1982).	100%	None
4.	"Rotational Excitation of Sputtered N_2", L. Efstathiou and E. W. Thomas, Abstracts, 42nd Annual Conference on Physical Electronics, Atlanta, 14-16 June, 1982.	100%	None
5.	"Ion Induced Auger Spectra of Aluminum and Silicon", R. Whaley and E. W. Thomas, Abstracts, 42nd Annual Conference on Physical Electronics, Atlanta, 14-16 June, 1982.	100%	None
6.	"Rotational Excitation of Sputtered N_2", L. Efstathiou and E. W. Thomas (in preparation for Surface Science).	100%	None
7.	"Ion Induced Auger Spectra of Na, Mg, Al and Si", R. A. Whaley and E. W. Thomas (in preparation for J. Appl. Phys.).	100%	None

VI. ABSTRACTS OF THESES

None in this reporting period.

VII. STUDENTS SUPPORTED BY GRANT

(1) R. A. Whaley, Graduate Student, 100% support. Due to finish Ph.D. in April, 1983.

(2) L. Efstathiou, Graduate Student, 100% support. Due to finish Ph.D. in April, 1983.

(3) H. Turner, Graduate Student, 100% support. Started September 1982.

VIII. REPORTS OUTSTANDING

None.

IX. FUNDS EXPECTED TO REMAIN

The following is a summary of the financial situation of this grant as of 11/30/82. The figures given are for the cumulative three year period.

	Expended as of 11/30/82	Encumbered as of 11/30/82	Anticipated Additional Expenditures 11/30/82 to 6/31/83	Total Budget (3 yr.)	Anticipated Residual
Personal Services	$47,054	$11,917	0	$58,971	0
Fringe Benefits	1,571	0	232	1,803	0
Materials and Supplies	7,961	153	6,522	14,636	0
Travel	1,482	0	318	1,800	0
Overhead	31,639	0	10,550	42,190	0
Totals	$89,707	$12,070	$17,622	$119,400	0

Estimated residual funds on 6/31/83 ZERO.

X. EQUIPMENT COSTING OVER $10,000

None.

Formation of CN^- radicals by sequential implantation of carbon and nitrogen ions into KCl

W. A. Metz and E. W. Thomas
School of Physics, Georgia Institute of Technology, Atlanta, Georgia 30332

(Received 14 December 1981; accepted for publication 4 February 1982)

It is shown that the sequential implantation of 20–200 keV C^+ and N^+ ions into a KCl crystal gives rise to formation of the CN^- molecular configuration. Detection of the CN^- is by the characteristic luminescence spectrum induced when He^+ ions are incident on the implanted target, a technique which represents a direct *in situ* determination of their presence. It is shown how the ion-induced optical emission may be used to provide a routine relative measurement of the quantity of CN^- present. We describe a phenomenological model of the formation process which leads to the conclusion that each incoming ion searches a volume of the target approximately 3.4×10^{-21} cm^3 in extent and has a unit probability of combining with an atom of the other species lying in this region. This model explains why saturation of the CN^- density occurs at a N^+ dose independent of the quantity of C^+ implanted previously.

PACS numbers: 61.70.Tm

I. INTRODUCTION

The purpose of this work was to study formation of CN^- radicals by the sequential ion implantation of the constituent C and N into alkali halide crystals. The CN^- so formed was detected by the optical emission of characteristic CN^- bands when the implanted target is subject to bombardment by a beam of energetic light ions, specifically 100 keV He^+. Thus the molecular configuration formed by implantation is detected while located in the bulk of the crystal lattice. There are numerous previous studies of molecules ejected out of solids by the impact of energetic beams, including observations of complexes formed by implanted and substrate particles as well as molecules of the substrate itself. In such cases, however, the molecular complex is detected after it has left the surface and it is not clear whether the complex existed before it was sputtered or was formed during ejection as a consequence of the sputtering process itself. The present work is unique in that the molecule formed, the CN^- radical, is detected while it is still located in the bulk of the target matrix.

Numerous fundamental studies have been made of the CN^- radical introduced chemically into an alkali halide matrix. At temperatures below 78 °K the CN^- occupies an equilibrium orientation along the ⟨100⟩ direction of the crystal lattice[1,2]; above 78 °K it is free to rotate about its lattice site. Broadening of the emission bands is ascribed to the influence of phonons. As temperature is reduced, linewidth decreases becoming comparable, at liquid nitrogen temperatures, to that of the free radical. Phonon frequencies are small compared with the relevant molecular frequencies so there is little coupling and phonon potentials may be well approximated by parabolic curves. As a result line broadening is uniform.[1,2]

This study was largely motivated by the previous work of Bazhin *et al.*[3] where various gases containing N and C atoms were adsorbed onto the surface of alkali halide crystals and then bombarded with He^+ or H^+ ions giving rise to emission of a vibrational band system that was identified as the $D^2\Pi_1\rightarrow X^2\Sigma^2$ band system of CN^- with transitions from the $v=0$ upper vibrational state to $v=6$ to 11 vibrational levels in the lower electronic state. The emission spectrum was identical to that observed under electron and ion-induced fluorescence of alkali halide crystals doped with CN and identical to that observed previously by Von der Heyden *et al.*[4] in the *U-V* induced fluorescence of alkali halide crystals doped with CN. Moreover some of the observed lines correspond to fragments of a CN^- spectrum identified by Douglas and Routly[5] in the gas discharge spectrum of CN. The present work differs conceptually from that of Bazhin *et al.*[3] in that here we implant the molecular constituents and Bazhin *et al.* adsorb the constituents on the surface. The spectra are, however, identical in the two cases and we may confidently rely on the conclusion of Bazhin *et al.*[3] that the spectrum is indeed that of CN^-. Bazhin *et al.* also concluded that excitation of the CN^- radical occurs by recombination of an exciton at the CN^- site and that these excitons are created by the incoming projectile beam used to induce emission of the bands. This conclusion was based on the observed behavior of emission intensity with target temperature which mirrored the expected behavior of exciton mobility and density. Important confirming evidence[3] was the observation that the characteristic CN^- emission was not produced in NaBr for which the band gap (and hence exciton energy) is 6.71 eV and inadequate to excite the observed CN^- state for which the excitation energy is 7.0 eV. In the present work the emission exhibits the same characteristics so we again rely on the conclusions of Bazhin *et al.*[3] that the observed emission is due to excitons created by an incoming ion beam. In summary, then, we shall utilize the work of Bazhin *et al.*[3] and Von der Heyden *et al.*[4] to identify the emission bands as due to CN^- and rely on the work of Bazhin *et al.*[3] to establish that excitation under ion beam impact is due to the excitons created by the ion beam itself.

The present studies involve two distinct parts. In general, we commence by implanting into a KCl crystal both C^+ and N^+ ions, the order of implantation is immaterial. We

 0021-8979/82/053529-07$02.40

believe the evidence indicates that the CN^- radicals are formed directly as a result of this implantation. Subsequently, we bombard the target with a light ion beam, generally He^+, and observe emission of an optical band spectrum characteristic of CN^-. In order to quantitatively relate the observed emission intensity to the density of CN^- and to explore thereby the formation of the CN^- radical, we must first have some clear understanding of the excitation mechanism induced by the He^+ ions. Thus the present report includes both a detailed discussion of the excitation process as well as a discussion of the formation of the CN^- radical.

II. EXPERIMENTAL APPROACH

The source of the ions for both implantation and excitation was a type 200 MPR ion implanter by Accelerators, Inc. It has a useful energy range of 20–200 keV, uses a hot cathode source capable of producing ions of any species, and is provided with conventional mass analysis and collimation facilities to ensure a well-defined ion beam incident on the surface. Ion beam current can be monitored on a Faraday cup placed behind the last defining aperture before the beam is incident on the target. The experimental system is shown schematically in Fig. 1, and is based on a small chamber placed at the end of the beam line. The chamber has a standard manipulator for holding targets and is ion pumped to a base pressure of 10^{-10} Torr before the ion beam is introduced. Differentially pumped beam line sections isolate the experimental system from the relatively poor vacuum of the accelerator.

The target was viewed through a sapphire window at an angle of 90° to the incoming beam. A Jarrel Ash 0.5 meter scanning monochromator with photomultiplier detection was used for detection and analysis of the optical emission from the target. The optical spectrum was recorded by scanning the monochromator and either displaying the photomultiplier output on a pen recorder or else on a multichannel scaler. The latter recording system is generally employed since it permits digital information that can be readily analyzed by a computer. The monochromator has a resolution of 16 Å/mm and was generally employed with a resolution of 48 Å to maximize signal levels. Improved resolution to 2 Å causes no change to the relative intensity of spectral features that we are recording here.

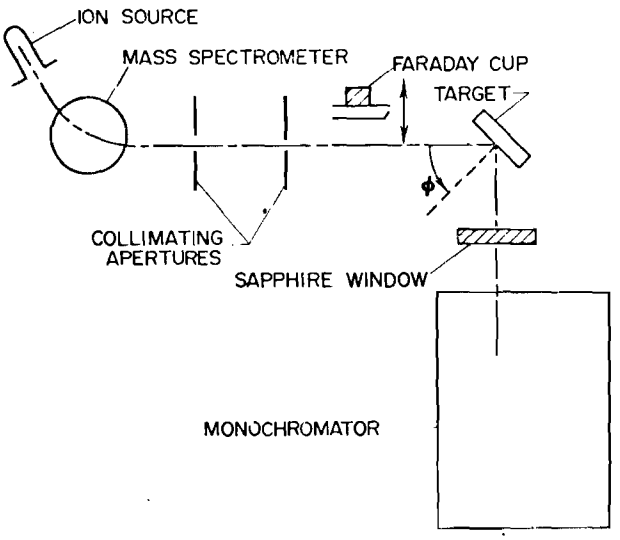

FIG. 1. Experimental arrangement.

The work reported here was confined to KCl crystals, although brief studies were made with NaCl and exhibited similar results. The crystals were optical quality materials freshly cleaved to expose the (100) face before insertion in the vacuum system. Before use they were heated to 250 °C and then bombarded with He^+ ions to confirm that there was no measurable signal from CN^- radicals before commencement of measurements. Sputter cleaning with Ar^+ was shown not to influence the observations and was not normally employed.

Implantation of the C^+ and N^+ ions was with beam densities of the order 1–50 $\mu A/cm^2$ and the beam was rastered over the 5-mm entrance aperture of the chamber to ensure a uniform implant. The analyzing He^+ beam used to induce emission was collimated to a 1.5-mm diameter to ensure that the observed emission was from the center of the implant and not influenced by irregularities at the edge of the implanted region. The targets were always placed with their normal at 60° to the incoming beam and the optical observations made at an angle of 90° to the incoming beam. When probing with a He^+ beam a projectile energy of 100 keV was employed. Minor changes to incidence angle disclosed no substantial changes of emission intensity, confirming that the projectiles were not incident in a channeling direction. Reference to standard tables[6,7] confirms that the range of the probing He^+ beams substantially exceeds the depth distribution of the implanted C^+ and N^+. All implantation and analysis with He^+ beams was performed at room temperature (20 °C).

Figure 2 shows a typical observed spectrum induced by impact of He^+ on a crystal that has been previously implanted with C^+ and N^+. In all significant respects the relative line intensities and line positions of the structures between 2300 and 3400 Å are the same as those recorded by Bazhin *et al.*[3] and by von der Heyden *et al.*[4] and ascribed by both groups of authors to the emission from excited CN^- radicals. The relative magnitudes of line intensities were independent of the conditions used for formation and for excitation; moreover, they show no change as spectral resolution is

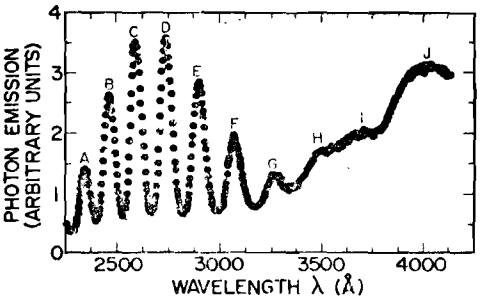

FIG. 2. Typical CN⁻ emission band spectrum induced by a 1-μA 100 keV He^+ ion beam incident of a KCl crystal that has a preliminary dose of 6.3×10^{14} ions cm^{-2} of 80 keV C^+ and 6.3×10^{14} ions cm^{-2} of 80 keV N^+.

altered from 48 to 2 Å. Thus in order to monitor emission intensity from CN^- on a relative basis as a function of excitation or of formation conditions, it is sufficient to record only the magnitude of one peak rather than integrating the whole spectrum. In practice we used a record of the 2730 Å peak for this purpose.

The intensity of the emission bands was a function of the nitrogen and carbon implant doses and of their energy. This is an observation that will be discussed later. The intensity was not a function of the time delay between implanting C and N, not a function of the time delay before analyzing with the He^+ beam, and was not influenced by cycling the target temperature between room temperature and 250 °C. Thus, there is no evidence that the C and N migrate from their implanted position over long time periods. The intensity of the CN^- bands was a function of the analyzing He^+ beam current, a feature that must be understood if the emission intensity is to be related to the density of CN. The signal was not, however, related to the time for which the crystal was exposed to the analyzing beam (i.e., not related to He^+ dose). Radiation damage caused by bombardment with the probing beam does not, therefore, appear to influence the density of CN^-.

Observation of the CN^- bands is not peculiar to a He^+ probing beam. Similar spectra are seen under bombardment by H^+, by Ar^+ and other heavy ions, as well as under bombardment by electrons. For the present studies we wish to employ a probing beam that has a range greater than the implant depth and that will exhibit no chemical reaction with any of the other species present. For these reasons we chose to utilize He^+.

For completeness we also note that the crystals used here exhibited negligible absorption in the spectral region studied, even after the implantation and analysis procedures. Therefore the spectral structures shown in Fig. 2 and the changes of intensity to be discussed later are in no way related to alterations of the absorption coefficients of the crystal.

III. IDENTIFICATION OF THE SPECTRUM

In all essential respects the typical spectrum presented in Fig. 2 is identical to that presented by Bazhin *et al.*,[3] and by Von der Heyden *et al.*,[4] with the lines being about 0.12 eV in width and 0.26 eV in separation. The relative intensities of the lines are independent of formation and excitation conditions and identical to those presented by the earlier workers. Implantation of other species (oxygen and rare gas ions) did not create this spectrum, nor did the implantation of C^+ or N^+ alone. We conclude, therefore, that the emission is indeed from CN^- and that the radical has been created as a result of the implantation of both C^+ and N^+ into the crystal.

There is a certain element of confusion regarding the precise identification of the levels involved in these transitions. All evidence points to the lower state being the $X\,^1\Sigma^+$ ground state and that the various lines represent transitions to various vibrational levels of this state. The line separation (0.26 eV) is in good agreement with the vibrational level spacing in the ground state given by Herzberg[8] (0.256 eV). There is, however, confusion as to whether the excited state is the $v = 0$ level of the $D\,^2\Pi_i$ state or the $v = 0$ level of the $a\,^3\Pi$ state. Bazhin *et al.*[3] point out that the intense lines have the same wavelength as those observed in gas phase discharges by Douglas and Routly[5] and ascribed by them to the transitions from the $D\,^2\Pi_i$ level. By contrast Von der Heyden *et al.*[4] perform some primitive calculations of potential curves and conclude that the excited state is the $a\,^3\Pi$ state. Recently Ha and Zumofen[9] have performed detailed calculations of energy levels and predict similar energies for the $a\,^3\Pi$ state. However, the calculations of Ha and Zumofen also include predictions of Franck Condon factors which show that the $v = 0$ to $v = 0$ transition should be the most intense with the intensity decreasing as one goes to higher vibrational energies of the ground state; this is clearly not in accord with the observations. We prefer to continue to ascribe the emission to the $D\,^2\Pi_i$ excited state. In fact, identification of the level has little impact on the work that follows. There is no doubt that the source of emission is the CN^- radical and that it has been created as a result of the sequential implantation of C^+ and N^+.

IV. MECHANISM FOR EXCITATION OF CN^-

In order to interpret the emission intensities in terms of CN^- densities one must first understand the mechanism by which the radical is excited. Figure 3 shows the CN^- emission intensity as a function of He^+ ion beam current density and clearly there is a saturation effect characteristic of two competing processes coming into equilibrium. We propose that there are three states involved in the process of excitation and decay. There are radicals in the initial ground state with a density $\mathcal{N}^g_{CN}$, radicals in the excited state with a density $\mathcal{N}^i_{CN}$ and radicals in the daughter level to which radiative decay takes place (in fact the vibrationally excited level of the ground state) with a density $\mathcal{N}^f_{CN}$. It is observed that the optical signal is independent of He^+ dose implying that the CN^- is formed by the implantation and not by the detection technique so that the total CN^- density is constant at a value $\mathcal{N}^t_{CN}$ allowing us to write

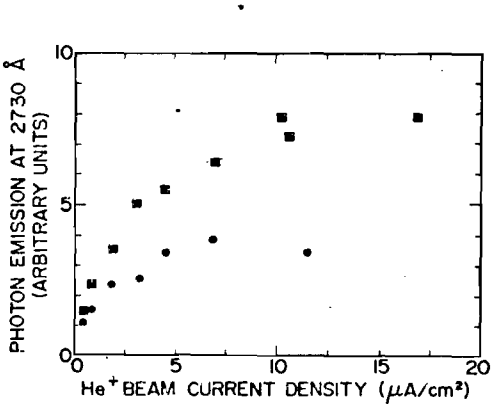

FIG. 3. Intensity at 2730 Å as a function of probing 100 keV He^+ beam current density. The two samples are implanted with a preliminary dose of 100 keV C^+ at 5.5×10^{14} ions cm^{-2}. Both samples have a preliminary N^+ dose of 7×10^{14} ions cm^{-2}; the square data points at 100 keV and the circular data points at 50 keV.

$$\mathcal{N}^{\gamma}_{CN} = \mathcal{N}^{g}_{CN} + \mathcal{N}^{e}_{CN} + \mathcal{N}^{f}_{CN}. \quad (1)$$

Let us first consider the density of excitons that are responsible for excitation of the CN^- from the ground state. Since the observed emission intensity is invariant with time the exciton density must be constant with the rate of exciton formation equal to the rate of loss. We can write the following phenomenological equation:

$$I_B\, \sigma \mathcal{N}_e = N_{ex}\, \mathcal{N}_l\, S_l. \quad (2)$$

The left hand side represents formation at a rate proportional to the incident beam current density, I_B (ions cm^{-2} sec^{-1}), the number density of sites at which excitons may be created $\mathcal{N}_e$ (cm^{-3}), and a constant of proportionality σ (cm^2) being the cross section for exciton production. The term on the right represents exciton loss being proportional to the local number density of excitons N_{ex} (cm^{-3}), to the density of loss sites $\mathcal{N}_l$ (cm^{-3}), and with a constant or proportionality S_l having the form of the product of loss cross section and velocity with which the excitons drift through the crystal. From this expression one can derive the density of excitons.

$$N_{ex} = I_B\, \sigma \mathcal{N}_e / \mathcal{N}_s\, S_l. \quad (3)$$

As a first approximation we would argue that this expression may be taken as independent of penetration depth in the region of the CN^- formed by implantation. The rate of formation will depend on the projectile energy and this will, of course, vary with depth of penetration. However, the range of the implanted C and N is of the order 2000 Å for the energies used here[7] and is some ten times shorter than the range of the 100 keV probing He^+ beam.[6] The energy loss by the projectiles in traversing the implanted region is[6] only some 12.5 keV, leading us to believe that the rate of exciton production is approximately independent of depth in the region of interest. The loss terms will be influenced by damage caused by the implantation of C and N but since their densities are less than 1% of the substrate, we would argue that the loss processes are largely intrinsic functions of the target and therefore also not functions of depth. With these two approximations we will assume as a first approximation that the density of excitons given by Eq.(3)is invariant with depth over the range implanted with C and with N.

Now returning to the excitation process the ground state population in equilibrium is related to the expression

$$N_{ex}\, \mathcal{N}^{g}_{CN}\, S_{CN} = \mathcal{N}^{f}_{CN}\, A_{fg}. \quad (4)$$

The term on the left is the rate of excitation out of the ground state by exciton recombination and is proportional to the density of electrons, and to the density of ground state radicals, $\mathcal{N}^{g}_{CN}$; the factor S_{CN} is a constant of proportionality that has the function of the product of cross section and velocity of exciton drift through the crystal. The term on the right is the rate of repopulation by decay from the daughter state, f, back to the ground state. The nature of this process is unknown but will obviously be proportional to the density of atoms in the excited daughter state f. The quantity A_{if} sec^{-1} is the transition probability for the decay.

The population of the excited state is obtained from the following equation which equates the rate of formation by the term obtained from the left hand side of Eq.(4)to the rate of loss from the state by normal radiative decay with a rate A_{if} sec^{-1}.

$$N_{ex}\, \mathcal{N}^{g}_{CN}\, S_{CN} = \mathcal{N}^{e}_{CN}\, A_{if}. \quad (5)$$

The population of the daughter state is governed by the radiative decay from the excited state, shown on the right hand side of Eq.(5)which is equal, at equilibrium conditions, to the rate of loss of that level by the decay process from the state f to the ground state g which has already appeared as the right hand side of Eq.(4).

$$\mathcal{N}^{e}_{CN}\, A_{if} = \mathcal{N}^{f}_{CN}\, A_{fg}. \quad (6)$$

Combining the above equations one can arrive at the density of the ground, excited, and daughter levels.

The rate of photon emission, $\mathcal{N}_\nu$ photons cm^{-3} sec^{-1}, the physically observed quantity, is equal to the product of the excited state density, $\mathcal{N}^{e}_{CN}$ and the probability for a radiative transition from i to f, A_{if}.

$$\mathcal{N}_\nu = \mathcal{N}^{e}_{CN}\, A_{if} = \frac{\mathcal{N}^{g}_{CN}}{1/N_{ex}\, S_{CN} + 1/A_{if} + 1/A_{fg}}. \quad (7)$$

Combining Eq.(3)with Eq.(7)the functional dependence of the emission intensity on beam current and density of CN^- is given by

$$\mathcal{N}_\nu = \frac{A \mathcal{N}^{g}_{CN}\, I_B}{B I_B + C}, \quad (8)$$

where A, B, and C are parameters associated with exciton formation and loss as well as transitions probabilities, all of which should presumably be constant. In principle, one should now integrate this equation over the full region occupied by CN to get a total emission intensity, and allow for detection sensitivity, to arrive at a prediction of the measured photon signal. Clearly with the assumptions already made concerning the constancy of N_{ex} with depth the result of such an integral is of the same functional form as Eq.(8).

Equation(8)has a number of important consequences. First we now have a representation of the signal strength in terms of beam current density that may be compared with data such as that in Fig. 3. In Fig. 4 we replot those data in the form of $I_B / \mathcal{N}_\nu$ against I_B. Equation(8)predicts that this should be a straight line and indeed this is the form taken by the data. Equation(8)also predicts that the signal observed for

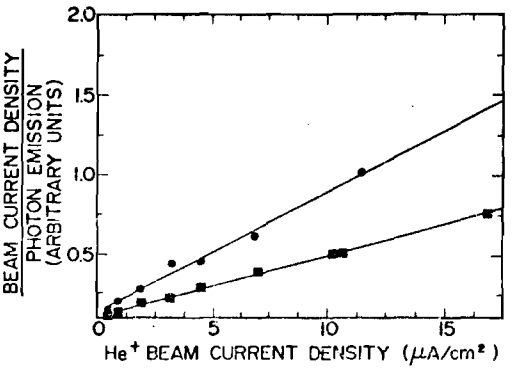

FIG. 4. Data of Fig. 3 replotted in the form of beam current ÷ intensity against beam current density to illustrate agreement with Eq.(8).

a given beam current density should be linearly proportional to the total quantity of CN present. We prepared a number of samples with C and N implanted at the same energy and in the same ratio but to different absolute doses. The observed signals were indeed proportional to the absolute dose. Equation(8)also suggests that the most suitable circumstances for probing the total CN^- density, N_{CN}, is to use a large beam current density where the signal is independent of I_B; that is essentially the saturation region shown in Fig. 3. Such saturation conditions were adopted for all the subsequent measurements.

It is possible to utilize the saturation behavior shown in Fig. 3 and predicted in Eq.(8)to make some useful statements concerning the transition probabilities A_{if} and A_{fg}. Examination of Eq.(7)shows that at high beam current densities, where N_{ex} becomes sufficiently large the observed signal saturates to the following value

$$\mathcal{N}_v(\text{sat}) = \mathcal{N}_{CN}(A_{if}^{-1} + A_{fg}^{-1})^{-1}. \tag{9}$$

If we integrate Eq.(9)over the complete depth occupied by the implanted C and implanted N we have the result that the total amount of CN, divided by the total emission of photons, is equal to $A_{if}^{-1} + A_{fg}^{-1}$. We can make a very rough estimate of the quantities involved here. For a carbon implant density of 2×10^{15} C atoms cm^{-2} the number of C atoms in the 1.5-mm-diam region accessed by the He^+ beam is 3.5×10^{13}; this must represent an upper limit on the amount of CN subject to excitation. The signal, integrated over all of the spectrum, corrected for the limited detection sensitivity and for the spectrometer solid angle, represents a total photonemission of about 10^{14} sec^{-1}. Thus the ratio of total CN present to total photonemission is 0.35 and according to Eq.(9)this is equal to $A_{if}^{-1} + A_{fg}^{-1}$. Now the transition i to f is a normal radiative decay and must therefore exhibit a lifetime of about 10^{-7} sec; this is an insignificant contribution to the denominator of Eq.(9) Clearly then A_{fg}^{-1} must be of the order 0.35 sec impiying a lifetime for decay from f to g of this magnitude. We note that transitions between vibrational levels in isolated molecules are expected to exhibit lifetimes[10] of the order 10^{-2} sec so this present very rough estimate is not unreasonable. In view of the qualitative nature of the model it would be quite misleading to propose the result we have obtained here as a measurement of the lifetime against decay from f to g. It is, however, apparent that the long lifetime for depopulation of the daughter f state is the reason for the saturation behavior in Fig. 3.

At this stage one might be tempted to perform detailed analyses of the data showing how intensity varies with ion beam current in an attempt to determine information concerning the details of the excitation and loss processes. We would regard this as quite hazardous since the equations describing the emission are at best phenomenological and may be incomplete in details. The sole purpose of our discussion here is to establish that the photonemission induced by ion impact can indeed be utilized as a measure of the total CN^- density so that we may proceed further with the analysis of how the radical is formed.

V. THE MECHANISM OF CN^- FORMATION

The above discussion has shown how the ion-induced emission of CN bands may be used as a monitor of CN^- density formed by implantation of C and of N. We now address the problem of modelling the process whereby the CN is formed by studying the relationship of the CN^- density to the implanted dose of C and of N, and to the energies of implantation.

A direct experiment to measure CN^- formation as a function of dose would commence with an implantation of C^+ followed by a series of N^+ implantations alternated with monitoring of the CN^- density by helium ion-induced emisison. This alternation of implanting N^+ beam and probing He^+ beam is inconvenient and time consuming. An alternative giving essentially the same information is to utilize CN^- emission induced while the N^+ ions are implanting into the target. These bands are identical to those excited by He^+ and presumably arise from generally similar mechanisms. We take the target with the preliminary C^+ implantation, then bombard continuously with N^+ and follow the buildup of CN^- by the emission of the CN^- bands induced by the N^+ as it is implanted. Such a data set is shown in Fig. 5 for two different preliminary doses of C^+. It is apparent that there is no signal from CN^- when the N^+ bombardment is commenced and that the signal increases in a generally exponential fashion towards a saturation value that occurs at a N^+ dose of about 5×10^{15} N^+ ions cm^{-2}. Comparing the two sets of observations on Fig. 5 and numerous similar observations that are not displayed here, one is led to the conclusion that the dose of N^+ required to saturate the CN^- signal is independent of the preliminary C^+ dose implanted. When using N^+ both as the probe and implant simultaneously the range of the particle is the same as the depth one is attempting to probe and there is no reason at all for assuming that the number density of excitons, and hence the efficiency for excitation of the CN^-, is the same for the whole depth being probed. Thus the data shown in this figure cannot be related to CN^- density in the same detailed manner as we have claimed for He^+-induced emissions. Never-

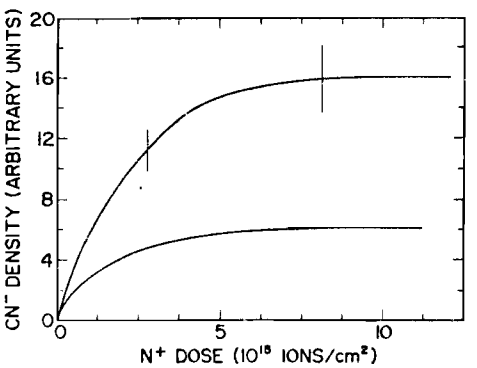

FIG. 5. Intensity at 2730 Å as a function of N^+ implant dose induced by the implanting 115 keV N^+ beam. The upper curve is for a KCl sample with a preliminary 20×10^{16} ions cm^{-2} dose of 100 keV C^+. The lower curve is for a sample with a 1.0×10^{16} ions cm^{-2} dose of 100 keV C^+.

theless, the data of Fig. 5 are a valuable qualitative indication of how the emission intensity, and hence CN^- density, builds up with dose.

As a second test we implanted a series of crystals with C^+ to a fixed dose of 2×10^{15} ions cm^{-2} at an energy of 80 keV, followed by implantation of N^+ to the same dose but with different energies for each sample. The amounts of CN^- formed were monitored by probing with the He^+ beam. The results are shown in Fig. 6 which gives emission intensity, and hence CN^- density, as a function of the N^+ implant energy. We note that the maximum CN^- density occurs for a N^+ implant energy of about 80–120 keV. This is essentially the energy region at which a N^+ implant has the same range as the preliminary 80 keV C^+ implant.

Let us consider the formation of CN^- in a some volume element ΔV. Before N^+ bombardment is commenced this volume has a local number density of carbon, $\mathcal{N}_C(0)$. After bombardment with N^+ with a fixed beam current density I_B for a time t an amount of the carbon has combined with the nitrogen to form CN^- so that the density of free carbon (i.e., carbon not combined with nitrogen) has a number density $\mathcal{N}_C(t) = \mathcal{N}_C(0) - \mathcal{N}_{CN}(t)$ where $\mathcal{N}_{CN}(t)$ is the number density of CN at the time t. The incident beam of current density I_B (ions cm^{-2} sec^{-1}) deposits into the volume ΔV a number of ions $I_B f_N(x)\,\Delta V$ per unit time. Here $f_N(x)$ represents the depth distribution for the implanted species and can be written[7] in the following Gaussian form

$$f_N(x) = \frac{1}{\Delta R_N (2\pi)^{1/2}} \exp -\tfrac{1}{2}\left(\frac{x - R_N}{\Delta R_N}\right)^2. \tag{10}$$

Here R_N is the range of the N^+ ion and ΔR_N is the half width at half-maximum of the range distribution; both these factors can be obtained from the standard calculations of Dearnaley *et al.*[7] If we now simply assume that the number of CN^- radicals formed per unit time in volume ΔV is proportional to the number of N^+ ions entering the volume and to the number of density of free C atoms already present in the volume then the rate of CN^- formation can be written as $k\,[I_B f_N(x)\Delta V]\,\mathcal{N}_C(t)$, where k is a constant of proportionality. Normalizing to unit volume and substituting the value of $\mathcal{N}_C(t)$ we may write

$$\frac{d\,\mathcal{N}_{CN}(t)}{dt} = kI_B f_N(x)[\,\mathcal{N}_C(0) - \mathcal{N}_{CN}(t)]\,. \tag{11}$$

This expression gives the rate of change of CN^- number density with time and can be integrated with the boundary condition that no CN^- is present when bombardment commences (i.e., at $t = 0$) to arrive at

$$\mathcal{N}_{CN}(t) = \mathcal{N}_C(0)[1 - \exp - kI_B f_N(x)t\,]. \tag{12}$$

The local concentration of C before N^+ bombardment commences, $\mathcal{N}_C(0)$ ions cm^{-3}, is a function of depth and can be written $D_C f_C(x)$, where D_C is the preliminary dose of carbon (ions cm^{-2}) and $f_C(x)$ is the depth distribution function of carbon which will have the same form as Eq.(10)but with the ranges for carbon[7] substituted. To find the total amount of CN^- present in the sample we should, in principle, now integrate over the complete volume occupied by C and N as follows:

$$\text{Total CN} = \int_{\text{volume}} \mathcal{N}_{CN}(t)\,\Delta V = D_C\,A \int_{\text{depth}} f_C(c)[1 - \exp - kI_B f_N(x)t\,]\,dx, \tag{13}$$

where in the last equation we have performed the trivial integration over beam area A.

For low doses of N^+ (i.e., for low $I_B t$) we may replace the exponential by a series and retaining only the first significant term arrive at

$$\text{Total CN} = D_C\,AkI_B\,t \int_{\text{depth}} f_C(x) f_N(x)\,dx. \tag{14}$$

Thus the total amount of CN rises linearly with time and is proportional to the integral of the overlap between C and N depth distributions.

Let us now examine the data in the light of the above formulations. Figure 6 shows the relative variation of CN^- signals for different energy N^+ implanted into targets which have a preliminary fixed dose of C^+ at an energy of 80 keV; doses of C and of N are equal. According to Eq.(14)the CN^- signal should vary only as the overlap integral. This integral has been evaluated according to the prescription of Dearnaley *et al.*[7] and is shown in Fig. 6 normalized to the data at an energy of 80 keV. There is good agreement between theory and experiment. We believe that this agreement confirms the basic suggestion that C and N do not significantly migrate after implantation and that the formation of CN^- is simply proportional to the local density of a C and of N in the implant distributions.

The general form of Eq.(12)is also quite consistent with the exponential buildup of CN^- signal illustrated in Fig. 5. We recall, however, that this particular set of data represents CN^- excited by the N^+ beam during implantation and we make no claim concerning the detailed relationship of this signal to CN^- density. One interesting and unambiguous observation from Fig. 5 is that saturation of CN^- density occurs at a dose of about 2×10^{15} ions cm^{-2} independent of the density of CN^- in the target. This low dose for saturation

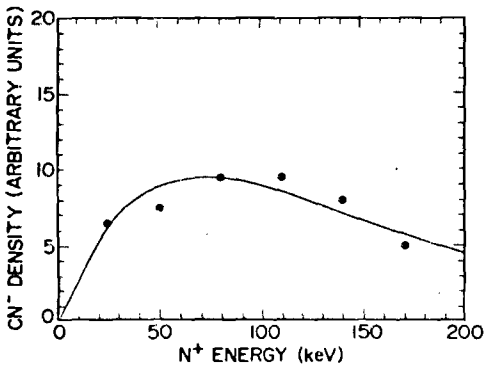

FIG. 6. Intensity of the CN^- bands as a function of N^+ implant energy. The emission is induced by 100 keV He^+. The targets have a preliminary implantation of 80 keV C^+ to a dose of 6.3×10^{14} cm^{-2}. The N^+ was implanted to a dose of 6.3×10^{14} ions cm^{-2} at the indicated energies. The data points are experimental values and the line is a computed value from Eq. (14), normalized to experiment at 80 keV.

is a surprising result. The preliminary carbon implantation presumably is distributed on various lattice sites throughout the carbon range in the crystal. One might have expected that to reach saturation of CN^- density one would need to implant one N^+ ion onto every lattice site in the nitrogen range to ensure that every carbon atom has received an opportunity to combine and form CN^-. The data of Fig. 5 show clearly that saturation occurs at a dose two orders of magnitude lower. Thus apparently CN^- is not formed only when one N^+ ion arrives on a site already occupied by carbon, but the nitrogen ion combines with carbon lying in some region more extensive than a single lattice site. One may understand this by re-evaluation of the meaning of the constant of proportionality k introduced in Eq. (11). Let us suppose that when a N^+ ion comes to rest it has unit probability of combining to make CN^- if a carbon atom lies within a volume $\Delta V'$ about the point where it comes to rest. Our evaluation of the rate of CN^- formation was developed by considering $I_B f_N(x)\Delta V$ ions entering a volume ΔV containing a C atom density $\mathcal{N}_C(t)$. Now each of the $I_B f_N(x)\Delta V$ incoming ions will combine with any C atom lying in a volume $\Delta V'$ about the point where it comes to rest. Thus the rate at which CN^- is formed in the volume ΔV will be $I_B f_N(x)\Delta V \Delta V' \mathcal{N}_c(t)$ and the rate of increase of CN^- density obtained by normalizing to unit volume as before giving

$$\frac{d\mathcal{N}_{CN}(t)}{dt} = \Delta V' I_B f_N(x) \mathcal{N}_C(t). \tag{15}$$

Comparing this with Eq. (11) we see that k has the phenomenological interpretation of being the volume searched by each incoming N^+ ion in its quest to find a free C atom for recombination. Thus the number of N^+ ions required to be incident in order for all available implanted C to be combined is a function only of the volume occupied by C atoms and is in no way related to the number of C atoms present. This is exactly what Fig. 5 demonstrates with the dose of N^+ required to saturate the production of CN^- being independent of how much C was present in the target. We can proceed one step further and evaluate an estimate of $\Delta V'$. Let us assume for the sake of simplicity that the implanted N is distributed over a distance $2\Delta R_p$, where ΔR_p is the half width at half-maximum of the true range depth distribution and can be obtained from the tables of Dearnaley.[7] Thus $f(x) = (2\Delta R_p)^{-1}$. Evaluation of Eq. (13) is now trivial and it indicates that the CN^- density will reach 2/3 of its saturation value when $kI_B t(2\Delta R_p)^{-1} = 1$. Figure 5 shows saturation to occur at a dose $(I_B t)$ of 2×10^{15} ions cm^{-2} and Dearnaley's tables suggest that ΔR_p is approximately 1.7×10^{-5} cm. Thus we would estimate k, which is the same as the volume $\Delta V'$ probed by each incoming N^+ ion, to be 3.4×10^{-21} cm^3 or a spherical volume of radius 15 Å. This represents a distance of some four lattice spacings in KCl.

We note in passing unpublished molecular dynamics calculations by Landman[11] of behavior in a crystal when a single atom is replaced by one with a different potential. The result of the change is a temporarily disordered region having the characteristics of localized melting and being of some four to five lattice spacings in extent. After a period of 10^{-12}–10^{-13} s, recrystallization occurs. We could apply this picture to our present situation arguing that when a N^+ ion comes to rest, it creates a disordered region having a volume of about 3.4×10^{-21} cm^3, or four lattice spacings in radius, where the constituent particles are highly mobile. If a carbon atom lies within this region there is a unit probability of recombination to form CN^-. After some 10^{-12}–10^{-13} s the region recrystallizes and the CN radical falls into a cation lattice position. The present data are consistent with such a picture but in no way confirms any details of the process involved.

VI. SUMMARY

We have demonstrated that separate implantation of C^+ and N^+ ions into a KCl target results in the formation of CN^- radicals. The density of CN^- is simply proportional to the overlap of the C^+ and N^+ implant depth distributions. This represents the first direct demonstration that molecules may be formed by implantation of their constituent parts. It is significant that when implanting N^+ into a crystal containing a preliminary dose of C^+ the amount of CN^- formed saturates at a N^+ dose independent of the amount of C^+ in the crystal. This can be broadly interpreted as indicating that each incoming N^+ ion searches a specific volume of the crystal and combines with any carbon atoms located therein; saturation occurs when the complete implant region has been searched. This requires a N^+ dose independent of the total amount of C^+ present and two orders of magnitude less than the dose which would implant one N^+ ion on each lattice site. The effective volume searched by each N^+ ion is about 3.4×10^{-21} cm^3 and therefore is about four lattice sites in radius.

ACKNOWLEDGMENTS

This work was in part supported by the Solid State Chemistry Program of the National Science Foundation under Grant DMR 8000671. One of us (E. W. T.) wishes to acknowledge the hospitality of the Forskningsinstitutet for Atomfysik, Stockholm, Sweden, during the writing of this paper.

[1] A. Diaz-Gongora and F. Luty, Phys. Status Solidi B **86**, 127 (1978).
[2] H. V. Beyler, Phys. Rev. B **11**, 3078 (1975).
[3] A. I. Bazhin, E. O. Rausch, and E. W. Thomas, Phys. Rev. B **14**, 2583 (1976).
[4] E. Von der Heyden and F. Fischer, Phys. Status Solidi B **69**, 63 (1975).
[5] A. E. Douglas and P. M. Routly, Astrophys. J. Suppl. Ser. **1**, 295 (1955).
[6] J. F. Ziegler, *The Stopping Powers and Ranges of Ions in Matter, Vol. 4* (Pergamon, New York, 1977).
[7] G. Dearnaley, J. H. Freeman, R. S. Nelson, and J. Stephen, *Ion Implantation* (North Holland, Amsterdam, 1973).
[8] G. Herzberg, *Spectra of Diatomic Molecules* (Van Nostrand, New York, 1950).
[9] T-K. Ha and G. Zumofen, Mol. Phys. **40**, 445 (1980).
[10] L. I. Schiff, *Quantum Mechanics* (McGraw Hill, New York, 1968).
[11] U. Landman, Georgia Tech (private communication).

Nuclear Instruments and Methods 194 (1982) 505–508
North-Holland Publishing Company

FORMATION OF CN^- RADICALS BY ION IMPLANTATION

W.A. METZ and E.W. THOMAS
Georgia Institute of Technology, Atlanta, Ga. 30332, U.S.A.

Sequential implantation of C^+ and N^+ ions into KCl is shown to result in formation of CN^- radicals. Detection of the CN^- is by the characteristic optical emission of that molecule when the implanted crystal is bombarded by He^+. The quantity of CN^- formed has been studied as a function of energy of the implanted species (20 to 200 keV) and as a function of dose. The results are consistent with a model where an incoming ion A, slowed to rest, causes a localized melting region of volume ΔV and if a previously implanted species B is already present in this volume then the molecule AB is formed by recombination. The molecule adopts a cation lattice site after recrystallization. The localized melting volume corresponds to a region of radius 9.3 Å which is roughly consistent with unpublished molecular dynamics calculations

1. Introduction

We report here the formation of molecules within a solid as the result of the separate implantation of the molecule's constituent parts. The molecule in question is CN^- created by sequential implantation of C and N into KCl.

Some years ago Bazhin et al. [1] reported that when alkali halides exposed to damp air were bombarded with 20 keV H^+ or He^+ they observed a molecular band spectrum that could be identified as due to CN^-. The spectrum was exactly the same as reported earlier by Von der Heyden and Fischer [2] in studies of X-ray induced fluorescence of NaBr doped with NaCN. The bands were identified as vibrational structure in the $D^2\Pi_i \rightarrow X^1\Sigma^+$ transition. Bazhin et al. [1] argued convincingly that excitation of the CN was by recombination of excitons and these excitons were created by the impact of the incident H^+ or He^+ beam. However, they were unable to explain the nature of the reaction whereby CN^- was created by ion impact on a crystal carrying an adsorbed gas layer. The present work is in large measure an extension of that by Bazhin et al.

Following Bazhin et al. [1] we propose that an He^+ beam incident on an alkali halide creates excitons within its range and these migrate to recombination sites. If recombination occurs where CN^- is located then the molecule may be excited and the characteristic spectrum emitted by its subsequent decay. Thus the emission of the CN^- spectrum is a measure of the CN density along the projectile track. We take crystals of KCl, implant C and implant N to a definite does and then monitor the amount of CN^- by the intensity of the spectrum induced by He^+ impact.

2. Experimental

The target materials were optical purity KCl crystals, cleaved to expose the (100) face before use, and mounted on a conventional target manipulator. The targets were placed in a uhv chamber capable of a 10^{-10} Torr base pressure. A Jarrel–Ash 0.5 m scanning monochromator viewed the samples through a sapphire window; detection was by a cooled photomultiplier serviced by conventional pulse counting electronics. The optical system viewed at 30° to the target normal and at 90° from the incident beam direction.

The ion beams were obtained from a 20 to 200 keV ion implanter. For implantation of C and N the beam was collimated to 4.8 mm diameter. For studies of the CN density so created we use the emission of CN^- molecular bands induced by He^+ impact; for this a 1.6 mm diameter beam is employed so that emission was induced from the center of the implanted spot and non-uniformities at the implant edge were avoided.

In a typical experiment the target was first cleaned by heating to 400°C. The target was then bombarded with He^+, the optical spectrum recorded and the absence of CN^- emission taken as indicating that no CN^- is present as a contaminant. The sample is then implanted with C and then with N to some preselected dose using beam current densities of the order $6\,\mu A/cm^2$. We then return to the He^+ beam, record the ion induced CN^- spectrum and utilize the size of a vibrational peak (2730 Å) as a relative measure of CN^- densities.

All data were taken with room temperature targets. Preliminary annealing to 250°C caused no change to the observations. A typical observed spectrum is shown in

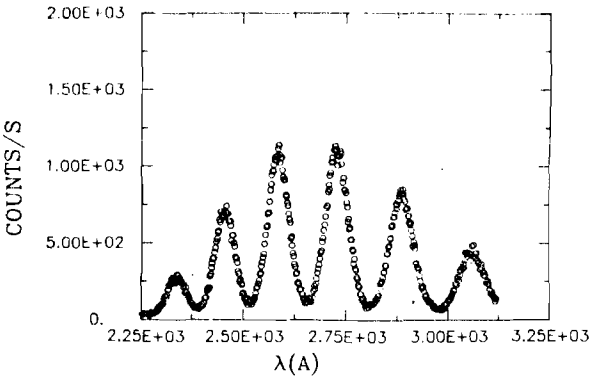

Fig. 1. Typical CN^- emission spectrum induced by 100 keV He^+ on KCl dosed with 3×10^{15}/cm^2 of 100 keV C^+ and 1.2×10^{16}/cm^2 of 150 keV N^+. The most intense peak, at 2731 Å, is identified as the $0\rightarrow10$ vibrational transition in the $D^2\Pi_1\rightarrow X^1\Sigma^+$ decay.

fig. 1. The relative intensities of the different features are independent of the implant doses and energies of C and N as well as independent of the probing He^+ beam intensity and energy. Thus we may monitor a single peak in the spectrum to provide a relative measure of CN^- density.

3. Discussion

Fig. 1 shows a typical CN^- emission spectrum induced by He^+ impact; the implant doses are shown in the figure caption, the spectrum was excited by 100 keV He^+. This spectrum is identical to the spectra reported for CN^- by Bazhin et al. [1], and identical to that reported for CN^- by Von der Heyden and Fischer [2]. It is identified [1,2] as due to a $D^2\Pi_1\rightarrow X^1\Sigma^+$ transition in CN^- with the various peaks representing $0\rightarrow v$ transitions where v is 7 to 12.

In general terms the CN^- signal increases with implant dose, is independent of dose rate, and is independent of the order in which C and N is implanted. Sputter etching of the crystal gives only a slow decrease of CN^- signal with surface erosion showing that the CN^- is in the bulk and not on the surface. There is no doubt that the CN^- is formed by recombination of C and N as the result of their separate implantations into the substrate.

The implantation of C and N as well as the analysis of the CN^- density were all performed at room temperature. We did, however, test the effect of heating the sample to 200°C after implantation to determine whether this might alter the density of CN$^-$. No change was observed suggesting that thermal diffusion of the implanted species was negligible.

There are two major steps in the further understanding of these experiments. In the first place we must understand the mechanism whereby the CN$^-$ is excited so that we know how to interpret the signal in terms of CN$^-$ density. Secondly we must try to understand how the CN$^-$ is formed.

3.1. Excitation by He^+

When the CN$^-$ emission intensity is studied as a function of increasing He^+ beam current we observe first a linear increase, followed eventually by saturation at high current. This can be explained on the following basis employing three distinct molecular states. There is the ground state with a local number density P_g (CN$^-$ ions cm^{-3}), the excited $D^2\Pi_1$ state with local density P_i and the lower vibrationally excited state to which radiative decay occurs having a local density P_k. Under helium bombardment the total density of CN^- remains constant at a value P_T so that

$$P_T = P_g + P_i + P_k. \tag{1}$$

We can now write rate equations describing how the density of each state varies with time. If we assume excitation is by exciton recombination [1] and that the number of excitons is related linearly to beam current density I_B then we can write

$$dP_i/dt = P_g K_e I_B - P_i A_{if}. \tag{2}$$

Here the first term represents rate of excitation from the ground state and is proportional to both the density of ground state molecules and to the beam current density; K_e is simply a constant of proportionality related to the rate of exciton formation. The second term represents spontaneous radiative decay from i to f with the transition probability A_{if}. The rate equation for the vibrational excited state f is related to population by spontaneous radiative decay from the higher state i and depopulation to the ground state by some process having a transition probability A_{fg}.

$$dP_f/dt = P_i A_{if} - P_f A_{fg}. \tag{3}$$

The experimental signals are all invariant with time so that equilibrium has been established for the population densities. Setting the left hand sides of eqs. (2) and (3) to zero, identifying the rate of photon emission N_ν (photons cm^{-3} s^{-1}) as $P_i A_{if}$, and manipulating eqs. (1)–(3) we arrive at

$$N_\nu = \frac{P_T K_E I_B}{1 + K_E I_B\left(1/A_{fg} + 1/A_{fi}\right)}. \tag{4}$$

At this point we should integrate the photon emission rate over the whole range of the He^+ ion allowing for the variation of exciton production rate with depth, and arrive at a total photon emission rate $\mathcal{R}_\nu$(s^{-1}). It is, however, clear that $\mathcal{R}_\nu$ is directly proportional to N_ν and will show the functional relationship to density of CN$^-$.

P_T, and beam current, I_B, given by eq. (4). To confirm the validity of the model we show in fig. 2 a plot of $I_B/\mathfrak{N}_\nu$ as a function of I_B which shows a straight line as predicted by eq. (4). We have performed detailed analysis of the equation, particularly the proportionality constant K_c, placed the data on an absolute basis and shown that the slope and intercept of fig. 1 may be predicted; these considerations will, however, be relegated to a more extensive forthcoming publication. One interesting result is that depopulation of the state f (to which radiative decay occurs) back to the ground state must involve a transition rate A_{fg} of the order 10^4 s^{-1}. This implies that the lifetimes of the vibrationally excited ground state systems are of the order 10^{-4} s. For the moment we need only conclude that the emission intensity is proportional to the density of CN^- provided a constant beam current density and only a single beam energy are used. In practice the data to be presented later were all taken with 100 keV He^+ at a current density of about 50 μA cm^{-2} which is sufficient to cause saturation in eq. (4).

3.2. Formation of CN^-

Whatever may be the details of the recombination mechanism we would certainly expect that the density of CN^- would be directly proportional to the local density of C and to the local density of N. Thus the total amount of CN^- formed in the crystal should be proportional to the convolution of the respective implant depth distributions, integrated over the full depth probed by the incoming beams. In fig. 3 we show the relative CN^- signal for a C implant at a fixed energy of 100 keV and N implants at a variety of energies. Included is the integral of the convolution between the two depth distributions evaluated using the formulations of Dearnaley et al. [3]. Experiment and computation are in good agreement showing the amount of CN^- formed is proportional to the product of densities of C and of N.

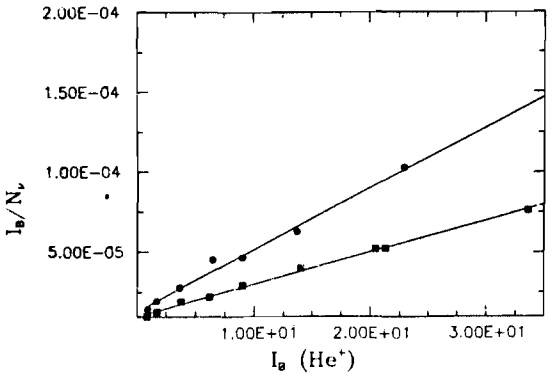

Fig. 2. Plot of $I_B/\mathfrak{N}_\nu$ against I_B for He^+ impact on a crystal with implanted C and N. Here I_B is beam current density, $\mathfrak{N}_\nu$ is emission intensity of the CN^- band in arbitrary units. The straight line confirms validity of eq. (4).

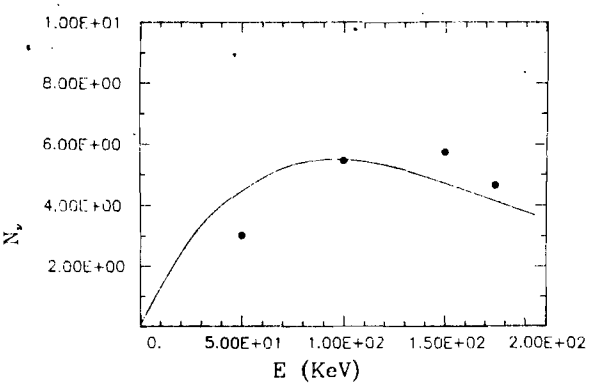

Fig. 3. A curve showing CN^- density as a function of N^+ implant energy for a fixed dose of C^+ implanted at 100 keV. Also shown is a theoretical computation of the overlap between the range distributions of the two implanted species. The experimental data is normalized to computation at 100 keV.

One approach to the mechanism of CN^- formation is simply to argue that the molecule is formed only when an N comes to rest on a lattice site occupied already by C (or vice-versa). If this were the case then to saturate the CN^- signal in a sample previously implanted with C would require an N dose of one atom for every lattice site within the projectile's range. Saturation doses are in fact an order of magnitude lower.

Landman has recently shown by a molecular dynamics simulation technique [4] that when a foreign atom is introduced into a perfect crystal there is created a local region of melting which persists for the order of 10^{-13} s before recrystallization occurs. We adopt this model to explain the present data. The incident N comes to rest, a volume ΔV becomes temporarily disordered, if a C exists within this volume the C and N recombine and after recrystallization adopt a cation lattice site. Thus for an N^+ dose of D_N per unit area a total volume $D_N\,\Delta V$ has been probed and when this volume is equal to the total volume within the projectile range distribution (equal roughly to an area of unity times twice the half width of the range distribution, ΔR_P) we should have achieved saturation. In fig. 4 we show the CN^- emission signal as a function of N^+ dose as excited by the incident N^+ themselves. We see that the CN^- signal saturates at a dose of about 10×10^{15} N^+ ions cm^{-2} independent of the pre-existing C^+ dose. A trivial calculation, using the range data of Dearnaley et al. [3], shows the volume ΔV to be 3.4×10^{-21} cm^3 corresponding to a spherical region of radius 9.3 Å. This figure is in qualitative agreement with the simulation of Landman that implies a melting over a region of the order of four lattice spacings.

We might further inquire whether the C and N

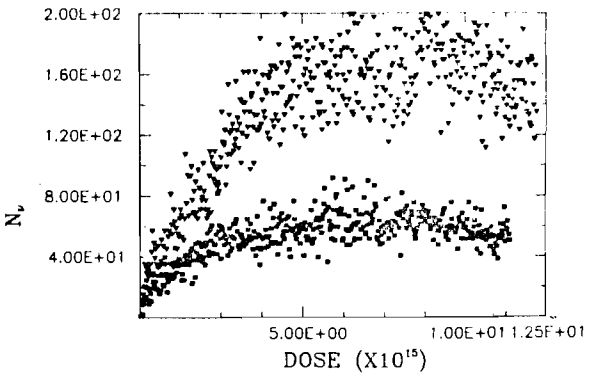

Fig. 4. Intensity of CN^- emission as a function of N dose (at 115 keV) for various preliminary doses of C at 100 keV. The CN^- emission is induced by the N itself. The triangle points are for a preliminary C^+ dose of 8×10^{15} ions/cm^2 and the squares are for a dose of 2×10^{15} ions/cm^2. Saturation occurs at an N dose independent of the preliminary C dose.

atoms might reasonably recombine within the 10^{-13} s that the melt region exists. There is a dearth of information on recombination in high density systems but this problem is now being tackled for the first time by Flannery [6]. He estimates a recombination coefficient of the order 10^{-7} cm^3 s^{-1} for recombination of Kr^+ and F^- in Ar. If we were to assume such a recombination rate was also approximately valid here and apply it to the high density molten region of 9.3 Å radius containing one C and one N we arrive at an average recombination time of 3.4×10^{-14} s. Since the molten region is estimated by Landman to persist for at least 10^{-13} s there is adequate time for the molecule to be formed before recrystallization.

4. Conclusion

We have shown unambiguously that sequential implantation of C and N into KCl gives rise to the formation of the CN^- radical. We have proposed that as an ion comes to rest in the lattice it causes a localized melted region and if the other molecular constituent is present in this region recombination occurs to form CN^-. The density of CN^- created in this manner is related to the convolution of the implant depth distributions.

This work was supported in part by the Solid State Chemistry Program of the National Science Foundation.

References

[1] A.I. Bazhin, E.O. Rausch and E.W. Thomas, J. Chem. Phys. 65 (1976) 3897.
[2] E. Von der Heyden and F. Fischer, Phys. Stat. Sol. (6) 69 (1975) 63.
[3] G.Dearnaley, J.H. Freeman, R.S. Nelson and J. Stephen, Ion implantation (North-Holland, Amsterdam, 1973) Appendix 2.
[4] U. Landman, private communication.
[5] M.R. Flannery, to be published.

Nuclear Instruments and Methods 194 (1982) 589–591
North-Holland Publishing Company

EXCITED STATES OF SPUTTERED MOLECULES

L. EFSTATHIOU and E.W. THOMAS

Georgia Institute of Technology, Atlanta, Georgia 30332, U.S.A.

We present some observations of the N_2 and O_2 molecular spectra induced by ion impact on solids. The N_2 spectra are due to bombardment of a nitrogen implanted silicon sample. The O_2 spectrum is from Ar^+ bombardment of a boron sample with adsorbed oxygen. The nitrogen spectrum shows rotational but not vibrational excitation. A model for its formation is proposed based on surface recombination followed by vibrational deactivation and ejection. The oxygen spectrum appears to contain fragments of the $c^1\Sigma_u^- \rightarrow X^3\Sigma_g^-$ Herzberg II band system and exhibits high vibrational but no rotational excitation.

1. Introduction

We report here some recent observations concerning the excited states of sputtered molecules. In part the work was prompted by an apparent discrepancy between two previous reports on emission of nitrogen molecular lines when a silicon sample is bombarded by a nitrogen ion beam. In the early work of Battacharya et al. [1] the 3371 Å band of neutral N_2 is observed under 10 keV N^+ or N_2^+ bombardment. In the work of Snowdon et al. [2], using 2 keV N_2^+ beams the principal emissions observed were from various states of the molecular nitrogen ion N_2^+. In both the work of Battacharya et al. [1], and that of Snowdon et al. [2], it is suggested that the nitrogen is implanted as individual atoms and either the molecule is formed on the surface and sputtered as one unit or else two individual atoms are sputtered independently and recombine as they emerge from the surface. There is an apparent difference between the two studies in that Battacharya et al. [1], observe the neutral molecule and Snowdon et al. [2], observe an ejected molecular ion. It seems unlikely that these different observations can be due only to differences in cross sections for ejection processes.

The present work was designed to study further the phenomenon of excited molecule ejection by particle impact. We study ejection of nitrogen from silicon by particle impact at energies between 20 and 200 keV as well as providing fragmentary information on ejection of molecular oxygen. The general objective is to study rotational and vibrational excitation in an attempt to understand the mechanism of the molecule's formation.

2. Experimental

The general experimental arrangement is unchanged from that used in our previous studies of collisionally induced light emission from solids [3]. Targets are mounted on a standard manipulator, placed in a vacuum system with a base pressure of 10^{-10} Torr and bombarded with ions from a 20–200 keV ion accelerator. Optical emission from the point of beam impact is analyzed with a 0.5 m Jarrell–Ash scanning monochromator fitted with photomultiplier detection and conventional pulse counting electronics. The monochromator views the target through a sapphire window at an angle of 90° to the beam direction and at a 30° angle from the normal to the target's surface.

The silicon targets were high purity, single crystal targets with the (111) face exposed to the incoming ion beam. For the work with boron we used a polycrystalline sample.

3. Molecular nitrogen spectra

When Si was bombarded with 100 keV N_2^+ we observed weak emissions of the second positive ($C^3\Pi \rightarrow B^3\Pi$) system of N_2 including the $0 \rightarrow 0$, $0 \rightarrow 1$ and $0 \rightarrow 2$ vibrational transitions. The emission intensity was zero when bombardment commenced and built up steadily. Following Bhattacharya et al. [1], we explain this build up as due to erosion of the surface leading to exposure of the ion implanted nitrogen on the surface. If the projectile is changed from N_2^+ to Ar^+ one sees identical features implying that the nitrogen emission arises from sputtering of the implant and is in no way related to scattering of projectiles. In addition to the nitrogen lines there were intense emissions from sputtered Si and Si^+. When molecular oxygen was introduced into the target chamber we observed an increase of the nitrogen intensity along with an increase in intensity of the many Si lines. The intensity ratios of the 0–0, 0–1 and 0–2 transitions are in general agreement with the calculated Franck–Condon factors given by Lofthus and Krupenie

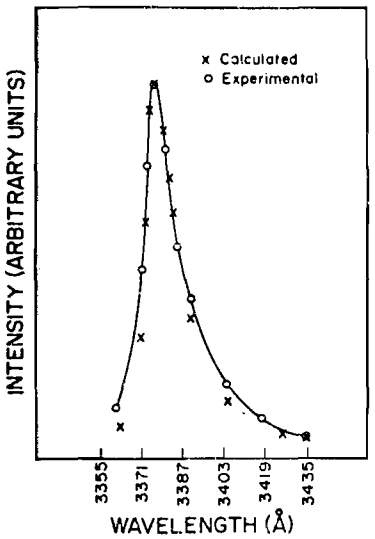

Fig. 1. The $0\rightarrow 0$ spectral line in the $C\,^3\Pi\rightarrow B\,^3\Pi$ second positive system of N_2 induced by 100 keV Ar^+ impact on an Si target implanted with N. Also shown is a calculated line shape assuming a rotational state popultion appropriate to local thermodynamic equilibrium at a temperature of 1100 K.

[4]. We should note that the spectra show no evidence of the N_2^+ emissions that are observed in the studies of Snowdon et al. [2], no evidence of atomic nitrogen system.

A significant feature of these bands is that the lines are broad indicating significant rotational excitation. Due to the low signal strengths we were unable to employ a sufficient spectral resolution to permit a record showing individual rotational lines. We do, however, show in fig. 1 the envelope of the line shape obtained with a resolution of 4 Å. There is obviously significant broadening indicating that many molecules are ejected in excited rotational states. It has often been noted [5] that the state population of electronically excited sputtered atoms is proportional to $\exp(-E_i/kT)$, where E_i is the excitation energy of the state, k is Boltzmann's constant and T has the dimensions of temperature. It has been argued in the past [5] that excitation occcurs in a collision cascade exhibiting local thermodynamic equilibrium; in this case T is the relevant temperature. However, if the LTE model is not appropriate then T is simply an empirical parameter. Without passing any judgement on the models we have computed the line shape for various values of T using the exponential term to predict relative population of rotational states. In fig. 1 we show the calculation for $T = 1100$ K and agreement with experiment is excellent. We note that in the consideration of electronically excited sputtered substrate atoms the value of T is normally found to be much higher [5], typically 3600–5900 K. In summary we observe only the $C\,^3\Pi_u$ state formed in the lowest vibrational state with a rotational state population distribution that decreases exponentially with excitation energy of the state.

To provide some explanation of this phenomenon we may look for guidance to the studies of H_2 desorption from interstellar dust where the ejected molecules are found to be in a ground vibrational state with considerable rotational energy [6,7]. When two N atoms are on adjacent sites of the substrate they will be separated by some 4.5 Å, strongly bonded to the surface and interacting weakly with each other [6]. If one atom migrates to the adjacent site, as a result of a projectile impact, the two atoms will now strongly interact with each other and have an internuclear separation comparable with that in a normal molecule (1.15 Å, see ref. 4). The molecule would, presumably, also have a high degree of rotational and vibrational energy and without some stabilizing event should spontaneously dissociate. If stabilization occurs by some rotational transition, the molecule can remain bound and interact with surface atoms. Internal vibrational energy could be converted into kinetic energy away from the surface in a manner rather like the interaction of a compressed spring with a desk surface. When a molecule with a vibrational frequency of the order $10^{15}\ s^{-1}$ collides with a surface atom that surface atom cannot respond to absorb the vibrational energy if we assume maximum phonon frequencies to be of the order $10^{13}\ s^{-1}$. The molecule will thus rebound, transferring vibrational energy to kinetic energy and the system can be ejected while retaining a high degree of rotational energy.

The $C\,^3\Pi_u$ state of N_2, in the separated atom limit, is composed of a ground state N atom and a metastable $N(^2D^0)$ atom. We would argue that the excited atom is not created by direct particle impact for this would presumably transfer sufficient energy to the nitrogen that it could escape the attractive bonding to the solid altogether. Rather it seems likely that the nitrogen atom could be excited by a secondary electron, a mechanism that would cause no transfer of kinetic energy. It is known that the secondary electron emission coefficient is higher for oxides than for pure materials, which might explain the increase of nitrogen signal when the sample is in an oxygen environment. Due to the excitation, the nitrogen atom will be less strongly bound and lateral surface migration would more readily occur. Barlow and Silk [7] (quoting an unpublished report by Hollenbach) estimate that the time for migration of H between adjacent surface sites of graphite is 3.7×10^{-5} s. If we assume that this figure gives the order of magnitude also for the present case we require that the excited state lifetime be greater than 3.7×10^{-5} s. The $^2D^0$ state of N is in fact metastable with a quoted lifetime in excess of 10^5 s [8] so migration is certainly possible before decay.

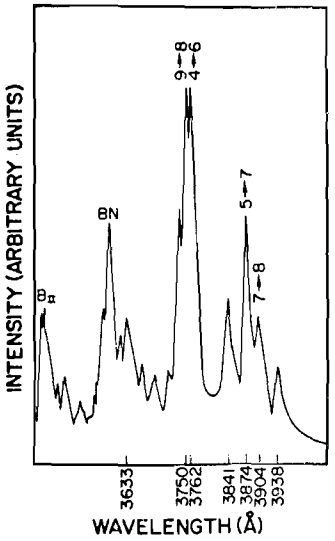

Fig. 2. A fragment of the spectrum induced by Ar^+ impact on a boron target with adsorbed oxygen. The lines are tentatively identified as due to $c^1\Sigma_u^- \rightarrow X^3\Sigma_g^-$ transitions of O_2 between the vibrational states indicated.

5. Molecular oxygen spectrum

We have also studied briefly the spectrum observed from boron with adsorbed oxygen. A boron sample is exposed to oxygen at a pressure of 10^{-5} Torr, the gas removed, and the sample bombarded with 100 keV Ar^+. A part of the observed spectrum is shown in fig. 2. There are a group of peaks that do not correspond to the tabulated wavelengths of BO, nor of O nor of B. Lines of B and B^+ are found at other wavelengths not shown here. We are able to identify these lines only as transitions in the $c^1\Sigma_u^- \rightarrow X^3\Sigma_g^-$ spectrum of O_2 [9]; the identification of vibrational states is shown on the figure. The $c^1\Sigma_u^-$ state of O_2 is in fact metastable, relatively weakly bound and with a large equilibrium internuclear separation. Most of the system has not previously been experimentally observed and the wavelengths quoted by Krupenie [9] are largely from theoretical predictions. These lines show no evidence of rotational broadening. The lifetime for the $c^1\Sigma_u^-$ state is estimated by Slanger [10] to be 25–50 s and if the molecule were to be ejected with any appreciable velocity the bulk of the emission would therefore come from regions outside the detector's field of view. The fact that signal is observed at all implies that the molecules reside on the surface and this is confirmed by observing parallel to the surface whereupon no signal is detected.

6. Discussion

The above observations show two rather different situations. The nitrogen spectra show considerable rotational excitation but no vibration. The oxygen spectrum seems to involve transitions not previously observed in conventional light sources and exhibits substantial vibrational excitation but no rotation. A comon feature of the two spectra is that both involve long lived metastable states, of either the molecule itself, in the case of O_2, or of the constituent atoms, in the case of N_2.

This work was supported in part by the Solid State Chemistry Program of the National Science Foundation.

References

[1] R.S. Bhattacharya, C.B. Kerkdijk, J.F. Van der Veen and F.W. Saris, Rad. Effects 33 (1977) 57.
[2] K.J. Snowdon, W. Heiland and E. Taglauer, Phys Rev. Lett. 46 (1981) 284.
[3] W.E. Baird, M. Zivitz, J. Larsen and E.W. Thomas, Phys. Rev. A 10 (1974) 2063.
[4] A. Lofthus and P.H. Krupenie, J. Phys. Chem. Ref. Data 6 (1977) 113.
[5] C.J. Good-Zamin, M.T. Shehata, D.B. Squires and R. Kelly, Rad. Effects 35 (1978) 139.
[6] R.F. Willis and B. Fitton, At. Space Sci. 34 (1975) 57.
[7] M.J. Barlow and J. Silk, Astrophys. J. 207 (1976) 131.
[8] W.L. Wiese, M.W. Smith and B.M. Glennon, Atomic transition probabilities, volume 1, N.B.S. Report NSRDS-NBS 4 (1966).
[9] P.H. Krupenie, J. Phys. Chem. Ref. Data 1 (1972) 423.
[10] T.G. Slanger, J. Chem. Phys. 67 (1978) 4779.

APPENDIX IV

Abstracts of the 42nd Annual
Conference on Physical Electronics, 1982

Rotational Excitation of Sputtered N_2 †

L. Efstathiou and E. W. Thomas
School of Physics, Georgia Institute of Technology, Atlanta, Georgia 30332

There is a continuing interest in the optical spectra emitted by sputtered atoms and molecules since these provide information on the quantum state distribution of particles ejected in a collision cascade. Excited molecules are particularly interesting since the population of rotational and vibrational states may provide a clue as to the mechanism by which the molecule is formed during the collision.

We have studied the second positive system of N_2 sputtered from an Si surface. Projectiles are 20 to 200 keV N^+ incident on pure Si and the intensity of the N_2 spectrum builds up with dose consistent with the increase of implanted N_2 density at the surface. The use of N^+ ions to both dope the surface and simultaneously eject the molecules is an experimental convenience and not significantly related to the excitation process. Impact of Ar^+ on an Si surface implanted with N^+ gives an identical spectrum.

Analysis of how the N_2 spectral intensity builds up with N concentration shows a linear relationship suggesting that the N_2 is formed by spontaneous recombination of nitrogen atoms on the surface and that formation is not related to the collision process itself.

Detailed study of the N_2 spectral lines discloses a high degree of rotational excitation but negligible population of excited vibrational levles. Rotational state population of lower J levels is approximately Boltzman with an effective temperature of around 1100°K. However, at higher rotational levels the distribution is non-thermal and broad maxima in population occur around J = 30 and 40. Qualitatively there is considerable similarity with the rotational state distributions observed by Kleyn et al. for NO scattered from Ag. These characteristics are independent of the projectile energy, mass and incident angle indicating that the rotational state population is independent of the excitation details.

We conclude that the rotational state populations are related to the transition of an N_2 molecule from a bound surface state to the isolated free molecular state.

---

†Supported in part by Grant DMR-8000671 from the Surface Chemistry Program of the National Science Foundation.

APPENDIX V

Rotational State Populations of NO Scattered from Ag; Comparison with the Hindered Rotor Model

We have taken experimental data of Kleyn et al.[1] on rotational population of NO scattered from Ag and compared them with predictions of the hindered rotor model of Gadzuk, Landman et al.[2] The general objective is to determine whether the hindered rotor model may be applicable.

Kleyn[1] takes rotationally cold NO molecules (5 to 50°K) of energy 0.19 to 0.93 eV and directs them at a clean 111 Ag surface. Rotational populations of the scattered NO are measured by laser induced fluorescence of the $A\ ^2\Sigma \leftarrow X\ ^2\pi_{1/2}$ transition. Signals are divided by laser power and rotational line strengths to yield the relative population N_J of rotational states J. A plot of $\ln [N_J/(2J+1)]$ against J was presented and is reproduced as Fig. 1. For each level J there are, in general, four measurements corresponding to data from the R and P transitions of the $^2\pi_{1/2}$ and $^2\pi_{3/2}$ states. Fig. 1 shows some severe scatter in the derived populations. It is clear that at low J ($J \leq 18$) the plot is a straight line which might be taken as implying a Boltzman population distribution with an appropriate rotational temperature. However, at high J ($J \geq 18$) there is not a straight line and a Boltzman distribution of population is not applicable to the whole distribution.

In Fig. 1 we show the populations as a function of J state derived specifically from the R branch of $^2\pi_{1/2}$ state; calculations were performed for an incident NO energy of 0.3 eV and 0.96 eV. The rotational state populations were predicted for us in the hindered rotor model[2] by C. Cleveland. The theory involves an infinite conical potential well where $V = 0$ for a polar angle (angle between molecular axis and surface normal) of β and $V = \infty$ for larger angles; this angle may be considered as unknown and adjusted to provide a good fit to the data. The theory also includes the parameter B/kT where B is the rotational constant of the molecule about the fixed point (which may be readily computed), k is Boltzman's constant and T is the effective temperature governing rotational population when the molecule is in equilibrium with the surface. The temperature T is taken as the target temperature. The polar angle was varied from 17° to 80° and relative populations compared with the data of Kleyn et al.[1] In Figures 2 and 3 we show the computed values normalized arbitrarily to experiment at $J = 23$. We regard the agreement between the experiment and computation for $\beta = 80°$ as encouraging. The scatter in $\ln [N_J/(2J+1)]$ in the data of Kleyn[1] is as much as 1.2 at large J and is comparable with the difference between experiment and computation. At small J ($J \leq 17$) substantial differences are observed. Kleyn et al.,[1] show that the rotational state population is not a sensitive function of target temperature. This is consistent with the hindered rotor model which shows that rotational population of the molecule in free space is largely governed by the zero point energy of the hindered rotor on the surface.

At the present time we offer no explanation of why the predicted population differs significantly from observations at low J. We must note, however, that the present model is very crude. It utilizes an infinite potential that is certainly unrealistic. Moreover, the large β angle needed to bring the model into agreement with experiment places the molecular axis almost parallel

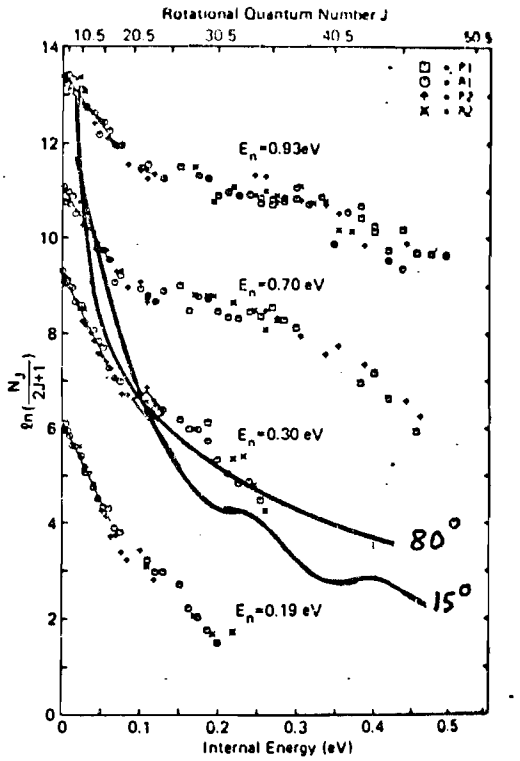

Fig. 1. Rotational state populations of NO scattered from Ag at various incident energies. Data points show the experimental measurements of Kleyn et al.[1] Lines are the result of calculations by Landman's model[2] using cone angles of 15 and 80°. Experiment and computation are normalized together.

to the surface. It is likely that other hindered configurations discussed by Gadzuk and Landman[1] would be more appropriate and these are being explored. At the present stage the agreement is encouraging and refinement of the model to include realistic potentials is under way.

1. A. W. Kleyn, A. C. Luntz and D. J. Auerbach, Phys. Rev. Lett. 47, 1169 (1981).

2. J. W. Gadzuk, U. Landman, E. J. Kuster, C. L. Cleveland and R. N. Barnett, Phys. Rev. Lett. 49, 426 (1982).

APPENDIX VI .

Abstracts of the 42nd Annual Conference on Physical Electronics, 1982

Ion Induced Auger Spectra of Aluminum and Silicon†

R. Whaley and E. W. Thomas
School of Physics, Georgia Tech, Atlanta, GA 30332

Auger spectra induced by heavy ion impact on surfaces differ significantly from electron induced spectra. The details of the excitation process and perhaps even of the decay mechanism are not clear. An understanding of the inner shell excitation and the subsequent decay mechanisms will assist with interpretation of SIMS data and with a general modelling of the quantum state distribution of sputtered particles.

We have concentrated on the study of Al and Si LMM spectra induced by 20 to 200 keV Ar^+ impact on pure Al and Si as well as the compounds of the elements. The spectral lines are sharp and atomic like but do not agree completely with spectra calculated from well established energy level data. Minor structure is observed on the lines when the target is a compound and this structure changes in magnitude, though not energy, as the chemical composition is altered.

Excitation of the inner shell vacancy would appear to be by a curve crossing in the LCAO-MO description of a collision between two atoms. Both direct excitation by projectile-target collisions and indirect excitation by recoil target-target events appear to contribute. Violent collisions that cause such events will transfer sufficient energy to the excited atom that it may be ejected from the lattice and contribute to the sputtered flux. A simple computer model suggests that sputtered particles with inner shell vacancies will generally undergo an Auger decay while still interacting with the surface from which it is receding. Thus, the spectra represents the Auger decay of atoms outside the matrix but still interacting with the field of the surface.

By comparing detailed integral spectra for pure Si with the spectra for its compounds we may synthesize a spectrum representing an Si atom decaying under the influence of the impurity atom. These will be compared for different impurities in an attempt to determine how the decay process is perturbed.

Quantitative comparison of the Auger flux with SIMS data suggests that a substantial fraction of multiply ionized sputtered particles arise from Auger decay of atoms sputtered with inner shell vacancies.

†Supported in part by Grant DMR-8000671 from the Surface Chemistry Program of the National Science Foundation.

Georgia Institute of Technology
Atlanta, Georgia 30332

(404) 894-5200

College of Sciences and Liberal Studies
School of Physics

September 24, 1984

Dr. Fred E. Stafford
Division of Materials Research
National Science Foundation
Washington, D. C. 20550

Subject: Annual Technical Letter Report, DMR-8000671

Dear Dr. Stafford:

This document is to serve as an annual technical letter report of progress on a project supported by NSF Grant No. DMR-8000671. The grant was originally funded in July 1980 with a projected duration of 3 years. A request for renewal was denied but a small grant for one year was awarded to bring the project to a satisfactory conclusion. The project is now into the automatic 6 month extension period with final termination on 31 Dec. 1984. All significant funds have been utilized and remaining resources are committed to the support of a graduate student to the end of the grant period.

Background

The general objective of the research was to study excitation processes occurring during atomic collisions in solids. The experimental techniques are Auger and optical spectroscopy of the point where a projectile beam impacts on a surface. The nature of excitation mechanisms, whether of the matrix, of sputtered atoms, or of scattered projectiles, are not at all well understood and it is often said that there are more theories than there are good experiments. Understanding of such processes should materially assist development of quantitative surface analysis techniques (notably SIMS) and will be a significant factor in the optimization of surface etching by reactive chemistry.

The work of the last twelve months has been largely published in the open literature and reprints are attached. The present letter will be confined to a brief review of three major activity areas.

Auger Spectra

We have brought to a conclusion our study of Auger spectra induced by 20 to 200 keV Ar^+ on targets of Mg, Al and Si. These spectra exhibit a broad underlying continuum roughly similar to that observed under electron impact with, superimposed, a series of atomic like lines. While there is general agreement that the continuum is due to matrix decays of inner shell vacancies the line spectra have been the subject of much controversy.

The line spectra can only be due to 2p vacancies; any other vacancy such as 1s or 2s will certainly give lines at much higher energies than are observed. We have long contended that the lines are from sputtered neutral atoms decaying in free space. We had not, however, been able to unambiguously relate these lines to specific Auger decay transitions.

Auger lines excited (generally by electrons) in gas phase targets are in fact of ions. The projectile impact removes an inner shell electron leaving the particle charged and it is this ion that decays. We suggest that when a target atom is excited in a solid and simultaneously ejected (sputtered) the atom frequently picks up an electron as it emerges across the surface so that

it is neutral. Thus most of the sputtered excited particles have an inner shell vacancy but as extra outer shell electron leading to states like Mg ($1s^2$ $2s^2$ $2p^5$ $3s^2$ $3p$), Al ($1s^2$ $2s^2$ $2p^5$ $3s^2$ $3p^2$) and Si ($1s^2$ $2s^2$ $2p^5$ $3s^2$ $3p^3$). It is the decay of these neutral atoms that we observe - not that of the ions. We have now estimated the energies of such states, calculated energies of the relevant decay channels, estimated line shapes and fitted the predicted to observed spectra. A major step forward was the realization that the so called continuum extended to higher electron energies than would be expected from a conventional matrix decay process. This is due to the presence of atomic lines at the continuum edge that cannot be resolved but are apparent as structural features. With these additional atomic lines our complete identification becomes straightforward. We have, by the fitting procedure, been able to measure the energies of the neutral atom states to about 0.2 eV which is more accurate than the theoretical predictions. Transition probability ratios in the Auger decay processes have been evaluated from relative line strengths.

For the case of sputtered Mg and Al we have successfully modeled the whole spectrum in terms of a continuum from matrix decays and lines from sputtered atom decays. The Si spectrum is also largely explained by these mechanisms but there remains a 10 eV wide band that is not attributable to these mechanisms. We estimate that for Si, which has a shorter lived inner shell vacancy than Mg or Al, a large fraction of the ejected atoms undergo decay within 2-3 A of the surface where energy levels are perturbed by the field of the surface. Here one would broadly expect the spectrum to be intermediate between that for an atom in the matrix and that for the atom in free space. The feature becomes even more obvious for the yet shorter lived sulphur and phosphorous atoms which have been studied by the group at Lyons. Regrettably we can find no tractable theoretical nor experimental techniques to prove that the additional component seen with short lived states does in fact represent decay in a surface field.

We note in passing that the spectra are certainly due to 2p vacancy production and not to 1s nor 2s. Adiabatic molecular orbital curve crossing, for the systems under study, gives rise only to 2p excitation so this presumably is the relevant excitation mechanism.

Two papers on this work have been published and are attached. No further work is planned.

Optical Spectra of Sputtered Molecules

We have been studying for some time the optical spectra of N_2 sputtered from N-implanted Si. Of particular interest is the rotational state population in the $0 \rightarrow 0$ band of the $C\ ^3\Pi \rightarrow B\ ^3\Pi$ transition. We have shown the rotational structure to not be explainable in terms of a thermal equilibrium population of rotational states. By co-operation with Landman's group at Ga. Tech we have devised a possible explanation. Before a molecule is sputtered from a surface it must presumably exist as a configuration bound to the surface. The quantum states of a bound rotator are quite different from a free rotator. As the molecule is ejected it moves from the bound or hindered state to a free state and final population is related to wave function overlap and the bound rotational state population. We have made some simple estimates for the hindered N_2 rotator in terms of an infinite conical well potential. The bound rotator is taken to be in thermal equilibrium with a room temperature surface. With the relevant overlap integrals we can predict the rotational state population after ejection which in turn should represent the rotational structure observed in the optical spectra. There is a broad

correspondence between theory and experiment but with discrepancies in detail that may be due to the oversimplified nature of the model.

There are technical difficulties in working with N_2 spectra sputtered from an N-implanted Si surface. Rotational energies are close and line resolution is almost impossible. We have been searching for a different case where line resolution would be unambiguous and close comparison with prediction more justifiable. BH sputtered from an H_2 exposed B surface has been studied and we are looking also at some other hydrides.

A paper on the N_2 spectra and the hindered rotator model has been published and is attached. The work continues with a search for a case where theory and experiment may be compared with greater sensitivity.

Data Compendium

The writer has long maintained a substantial interest in the assessment and compilation of data. During the last twelve months he has co-operated with three other faculty in the production of a bibliography of major data sources in the area of atomic collisions. The writer was principally responsible for collection of data sources for the area of atomic collisions in solids. The compendium is now complete and has been submitted for publication. Due to its length (some 200 typed pages) I enclose here only the title and abstract page.

Conclusion

The work of this project has largely come to an end and residual activity is confined to one student continuing research on the rotational state population of sputtered molecules. We are attempting to start a new project to study how photo-excitation of surface states can alter excited states of sputtered particles. The idea here is to modify the electron density distribution of the surface in a controlled fashion and then study how this effects the quantum state population of atoms that eject out of the surface. Application is forseen to photo-enhanced etching of microelectronic circuit elements. A proposal for this work is pending with NSF.

Yours sincerely,

Edward W. Thomas
Principal Investigator
Director, School of Physics

EWT:ar

Enc. Preprints as follows.

(1) R. Whaley and E. W. Thomas, J. Applied Physics 56, 1505 (1984).
(2) E. W. Thomas and R. Whaley, Nucl. Instrum. Meth. B2, 571 (1984).
(3) E. W. Thomas and L. Efstathiou, Nucl. Instrum. Meth. B2, 479 (1984).
(4) E. W. McDaniel, M. R. Flannery, E. W. Thomas and S. T. Manson, Atomic and Nuclear Data Tables (submitted). First page of preprint only.

Submitted to Atomic Data and Nuclear Data Tables

BIBLIOGRAPHY ON ATOMIC COLLISIONS

by

E. W. McDaniel, M. R. Flannery, and E. W. Thomas
School of Physics
Georgia Institute of Technology
Atlanta, Ga. 30332

and

S. T. Manson*
Department of Physics and Astronomy
Georgia State University
Atlanta, Ga. 30303

Abstract

This bibliography deals mainly with binary and ternary collisions involving electrons, photons, and heavy particles (i.e., atoms, molecules, and ions). The energy range covered for each kind of collision is such that the interactions might be described as electronic, atomic, or chemical--higher energy collisions involving nuclear forces are not treated. Also covered are particle and photon impact on surfaces, the passage of particles and radiation through bulk matter, and transport phenomena in gases. Practically all of the references cited are data compilations, other bibliographies, review articles, or books. The main objective is to provide easy access to atomic collisions data, although some references are included principally for their tutorial value.

*The authors wish to acknowledge the support of the U. S. Air Force Office of Scientific Research, the U. S. Army Research Office, and the National Science Foundation (Atmospheric Sciences and Solid State Chemistry Divisions).

NATIONAL SCIENCE FOUNDATION
Washington, D.C. 20550

FINAL PROJECT REPORT
NSF FORM 98A

PLEASE READ INSTRUCTIONS ON REVERSE BEFORE COMPLETING

PART I–PROJECT IDENTIFICATION INFORMATION

1. Institution and Address	2. NSF Program	3. NSF Award Number
School of Physics Georgia Institute of Technology Atlanta, Georgia 30332	Div. Materials Research	DMR 8000671
	4. Award Period From 7/1/80 To 2/31/84	5. Cumulative Award Amount $135,900

6. Project Title

Collision Induced Optical and Auger Spectra of Solids

PART II–SUMMARY OF COMPLETED PROJECT *(FOR PUBLIC USE)*

Sputter ejected particles are frequently excited either in the outer or inner atomic shells. This excitation is related to the initial collision event and, more importantly, to the change in local potential and electron density as the ejected particle traverses the surface. Excitation was studied by monitoring the spectra of optical emission or Auger electron emission by conventional spectroscopies.

We discovered that atoms are often ejected in the neutral state with an inner shell vacancy, giving rise to Auger spectra never previously detected. There are also contributions due to decay of such states in the field of the solid. Optical emission studies of sputtered molecules show a non-equilibrium rotational state distribution related to the hindered rotational state of the molecule when bound to the surface.

PART III–TECHNICAL INFORMATION *(FOR PROGRAM MANAGEMENT USE)*

1. ITEM *(Check appropriate blocks)*	NONE	ATTACHED	PREVIOUSLY FURNISHED	TO BE FURNISHED SEPARATELY TO PROGRAM	
				Check (✓)	Approx. Date
a. Abstracts of Theses		2			
b. Publication Citations		12			
c. Data on Scientific Collaborators		X			
d. Information on Inventions	X				
e. Technical Description of Project and Results		X			
f. Other *(specify)*					

2. Principal Investigator/Project Director Name *(Typed)*	3. Principal Investigator/Project Director Signature	4. Date
Edward W. Thomas		7-29-85

INSTRUCTIONS FOR FINAL PROJECT REPORT
(NSF FORM 98A)

This report is due within 90 days after the expiration of the award. It should be submitted in two copies to:

National Science Foundation
Division of Grants and Contracts
Award Accountability Branch
1800 G Street, N.W.
Washington, D.C. 20550

INSTRUCTIONS FOR PART I

These identifying data items should be the same as on the award documents.

INSTRUCTIONS FOR PART II

The summary (about 200 words) must be self-contained and intelligible to a scientifically literate reader. Without restating the project title, it should begin with a topic sentence stating the project's major thesis. The summary should include, if pertinent to the project being described, the following items:

- The primary objectives and scope of the project.
- The techniques or approaches used only to the degree necessary for comprehension.
- The findings and implications stated as concisely and informatively as possible.

NSF may disseminate the project report through the National Technical Information Service (NTIS) of the Department of Commerce. Authors should also be aware that the summary may be used to answer inquiries by nonscientists as to the nature and significance of the research. Scientific jargon and abbreviations should be avoided.

INSTRUCTIONS FOR PART III

Items in Part III may, but need not, be submitted with this Final Project Report. Place a check mark in the appropriate block next to each item to indicate the status of your submission.

a. Self-explanatory.
b. For publications (published and planned) include title, journal or other reference, date, and authors. Provide two copies of any reprints as they become available.
c. Scientific Collaborators: provide a list of co-investigators, research assistants and others associated with the project. Include title or status, e.g. associate professor, graduate student, etc.
d. Briefly describe any inventions which resulted from the project and the status of pending patent applications, if any.
e. Provide a technical summary of the activities and results. The information supplied in proposals for further support, updated as necessary, may be used to fulfill this requirement.
f. Include any additional material, either specifically required in the award instrument (e.g. special technical reports or products such as films, books, studies) or which you consider would be useful to the Foundation.

EXCITATION BY ION IMPACT ON SURFACES

A THESIS

Presented to

The Faculty of the Division

of Graduate Studies

By

Werner Adam Metz, Jr.

In Partial Fulfillment

of the Requirements for the Degree

Doctor of Philosophy

in the School of Physics

Georgia Institute of Technology

December, 1981

SUMMARY

The results of two independent experimental investigations are reported here. The production of Auger electrons due to ion impact on a surface is discussed first. An electron promotion model developed by Barat and Lichten predicts the creation of vacancies in the inner shells of atoms as the result of the interpenetration of atomic orbitals in a violent, binary collision. To test the model Ar^+ ion beams were directed upon targets of Al, Si, and Be. For these systems the electron promotion model predicts the creation of inner shell vacancies in the Al 2p shell, Si 2p shell, and Be 1S shell. Our observed Auger spectra can all be explained on the basis of vacancies in the predicted shells of the target atom. The Auger spectra of Al and Si are consistent with emission from a free particle; Auger spectra of Be is consistent with emission occurring while the Be is interacting with the surface. The difference in the two cases is related to the lifetime of the vacancy. The Al and Si vacancy lifetimes are much longer than that of Be, consequently decay of the vacancy in Al and Si occurs from sputtered particles free of influence from the target matrix. Energy levels of an isolated atom are well known, as we attempt to identify the states responsible for Auger emission from Al and Si as precisely as possible.

The second investigation reported constitutes the first direct evidence that sequential implantation of two distinct species into a target may give rise to the formation of a radical within the solid. Specifically, CN^- is formed by sequential implantations of C^+ and N^+ into KCl. Formation of the radical is explained by a simple model whose main features include the generation of a disordered region as an implanted ion comes to rest in the crystal lattice followed by recombination of the implanted reactants to form the radical. The radical is then identified by photon emission in a molecular transition characteristic of the CN^- radical. The amount of the radical formed is inferred from the emission intensity. We generally excite the CN^- radical by bombarding with a He^+ ion beam. The excitation mechanism is completely independent of the mechanism whereby CN^- is formed. Excitation of the radical is explained in terms of the production of excitons by an impacting ion beam, their subsequent absorption by a CN^- radical inducing formation of an excited state which decays via emission of an UV photon.

Experimental determinations of the formation of CN^- as a function of reactant dose, reactant implantation energy and the emission intensity as a function of beam current density of the He^+ ion beam used as a probe were performed. The model predicts the observed dependencies of the amount of CN^- formed as a function of the experimental parameters.

AUGER SPECTRA INDUCED BY NOBLE GAS ION IMPACT ON MG, AL, AND SI

A THESIS

Presented to

The Faculty of the Division

of Graduate Studies

By

Ray S. Whaley, Jr.

In Partial Fulfillment

of the Requirements for the Degree

Doctor of Philosophy

in the School of Physics

Georgia Institute of Technology

April, 1983

SUMMARY

The Auger spectra resulting from 20-200 keV Ar^+ and Ne^+ impact on Mg, Al, and Si were studied. A mechanism was formulated which explains the sharp features in all three targets as due to atoms with 2p inner shell vacancies sputtered free from the solid surface. The asymmetric continuum underlying these sharp features was found to be due to 2p vacancies decaying within the bulk. A model was formulated consisting of gaussian lineshapes for the predicted atomic transitions from singly ionized and neutral initial states and an experimentally derived electron induced spectrum for the bulk contribution. The model was tested by fitting it to the spectra using a non-linear least squares curve fitting routine. All features of the spectra were completely explained by this fitting routine supporting this interpretation of the ion-induced spectra. Information deduced from the curve fitting included average sputtered atom energies, relative atomic line intensities, dependence of atomic to bulk ratios with Auger lifetimes, and experimental values for the energy of the neutral atoms with 2p vacancies.

Spectra taken using different projectile energies show increased atomic to bulk ratios with projectile energy. This is opposite what would be expected from nuclear stopping power or sputtering data in this energy range.

Auger spectra induced by Ne^+ and Ar^+ impact on Mg, Al, and Si

R. Whaley[a] and E. W. Thomas
School of Physics, Georgia Institute of Technology, Atlanta, Georgia 30332

(Received 4 January 1984; accepted for publication 10 April 1984)

Impact of Ne^+ and Ar^+ at energies of 20–200 keV on targets of Mg, Al, and Si gives rise to an electron spectrum that has sharp atomiclike features superimposed on a continuous background. The continuum is similar to the spectrum observed during electron impact and is generally ascribed to decay of L-shell vacancies in the matrix. We show, however, that this is not completely correct, that the apparent continuum induced by ion impact extends to higher energies than for electron impact and that this is due to the presence of some hitherto unidentified atomiclike lines. We identify the atomiclike transitions as due to particles sputtered with L-shell vacancies. A complete modelling of the spectra is performed which accounts quantitatively for all Auger peaks. We conclude that the major features are due to sputtered neutral atoms with a single inner shell vacancy. The electron configurations and energies are $Mg^0\ 2p^5 3s^2 3p$ (50.6 eV), $Al^0\ 2p^5 3s^2 3p^2$ (73.8 eV), and $Si^0\ 2p^5 3s^2 3p^3$ (101.1 eV). These are states where one electron has been removed from the L shell but an electron added to the $3p$ shell to maintain neutrality. Other weaker lines are identified as due to sputtered Mg^+, Al^+, and Si^+ with single L-shell vacancies. For the case of silicon we identify an additional feature that we tentatively ascribe to sputtered atoms decaying while still within the field of the surface. A detailed modelling of the spectrum with all these components provides a complete explanation of all features of the spectrum lending confidence to the line identifications. Line intensities provide relative transition probabilities for competing decay processes.

I. INTRODUCTION

Impact of heavy ions (Ne^+ and Ar^+) at moderate energies (1–200 keV) on samples of Mg, Al, and Si produce electron spectra with Auger lines at energies in the 40–130 eV region that are certainly due to vacancies in the $2p$ shell of the target species. All reports of these spectra[1–6] agree that there is a continuous spectrum related to the decay of excited atoms in the target matrix and a sharp line spectrum that has the appearance of decays in isolated atoms. Published reports differ, however, on the detailed understanding of the spectra particularly on the question of the origin of the atomiclike lines. The sharp lines in no way resemble the line spectra induced by biparticle collisions of Mg^+, Al^+, and Si^+ impacting on an Ar gas.[7] Vrakking and Kroes[8] argue that the line spectra are due primarily to target atoms displaced from their normal lattice sites and decaying in the disordered region of the collision cascade; the lower intensity lines are said to represent electrons that have lost energy due to plasmon excitation. Negre *et al.*[9] suggest that the atomiclike lines are due to decay of excited atoms localized at the surface. One of the present authors has claimed[5] that the atomiclike lines are largely due to sputtered neutral atoms decaying in free space. The evidence to back up these assertions is generally qualitative in nature leading to imprecision and confusion. An explanation of any spectrum is valid only when the energy, width, and intensity of all spectral features is explained in a quantitative and consistent fashion. The purpose of the present work is to reexamine our suggestion[5] that the lines are principally due to sputtered neutral atoms and that there are also weaker contributions from sputtered ions. To confirm this contention we have completely modelled all the significant features, both continuous and line components, and show that all may be explained in the context of our original proposals. The fitting also permits a measurement of the excitation energy of the neutral states and a measurement of the branching ratio involved in their decay.

II. EXPERIMENT

The present experiments employed the same arrangement as we have described previously.[5] Projectile ions (Ne^+ and Ar^+) are provided by a 20–200 keV accelerator and directed onto the target held in a UHV chamber at 10^{-9} Torr pressure. Ejected electrons are analyzed and detected using a commercial (Varian) cylindrical mirror analyzer (CMA) placed with its axis at 95° to the ion beam and in the plane of the beam and target normal. The CMA has an integral electron gun that permits monitoring also of the electron induced Auger spectrum: Auger spectra are recorded in a derivative mode with repeated scanning of the region of interest and accumulation of signal in a multichannel scalar. Recorded derivative spectra are subsequently integrated to provide spectra showing the number of ejected electrons as a function of electron energy. The derivative recording is performed with a 0.5-eV energy sweep that provides the inherent resolution limit to the spectra we present. Peaks in the derivative electron-induced spectrum were found to agree to within 0.5 eV with a standard compilation.[10] Since we do not seek to draw any conclusions for the magnitude of the data we have not corrected the spectra for detection sensitivity variations with ejected electron energy.

[a] Present address: Modisette Inc., 4223 Richmond Avenue, Houston, TX 77027.

 0021-8979/84/171505-09$02.40

Target samples were high-purity Mg, Al, and Si. The metals were polycrystalline metal stock. The silicon was a (100) single-crystal surface, but undoubtedly the ion bombardment will have largely destroyed the single-crystal structure. Before use all samples were cleaned, chemically etched, and cleaned again. Final cleaning was by Ar^+ ion sputtering at 5 keV after placement in the vacuum system. Electron-induced Auger spectra showed that all contaminants were less than 1%. Targets were held on a conventional manipulator and placed with their normal at 60°–80° from the ion-beam direction. The CMA was aligned at the center of the 5-mm-diam beam spot on the surface so that the spectra should not be effected by edge effects.

III. EXCITATION MECHANISM

In Figs. 1–3 we show, respectively, the spectra recorded for Ar^+ ion impact on Mg, Al, and Si, also shown are the corresponding electron-induced spectra. There is a clear underlying continuous distribution in the ion-induced spectra that bears a close resemblance to the electron-induced Auger spectra of these solids and therefore is due presumably to decay of excited states in the matrix. There are also a series of lines whose limited width suggests that they are not due to decays involving transitions from a valence band of the solid. It has sometimes been suggested that there are three main lines (marked I, II, and III in all spectra) plus a fourth minor line at higher energy in some cases (marked IV on the figures). Some authors[8] have argued that the main three-line structure that appears to be common to all three cases indicates some new mechanism of Auger decay that is similar for all three materials. This argument is quite misleading. Reference to the silicon spectrum shows that there are a variety of subsidiary shoulders and peaks that betray the existence of a multiplicity of transitions. By contrast the magnesium spectrum shows only three distinct lines.

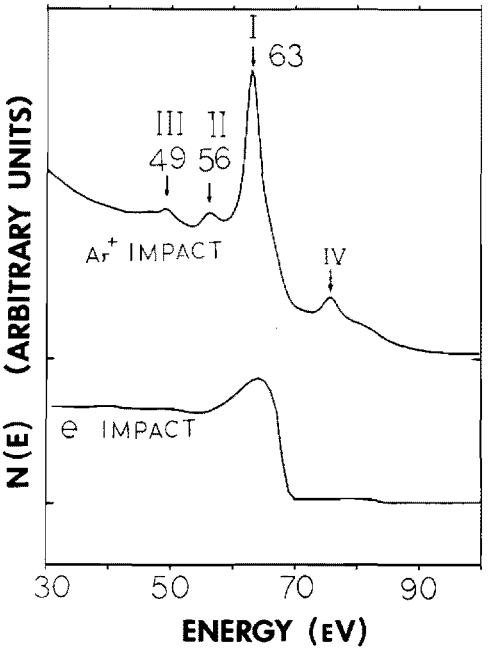

FIG. 2. Auger spectra of aluminum induced by 190-keV Ar^+ and by 1-keV electrons.

There is no serious doubt that the principal features of both lines and continuum are due to decay of single $2p$-shell vacancies of the target material. The energies required to remove one $2p$ electron from Mg, Al, and Si are, respectively,[11] 55.0, 80.7, and 107 eV. A decay of such an excited state, whether in the matrix or in an isolated atom or ion would give spectra at about the observed energy. It is energetically impossible for the spectra to be due to vacancies of the projectile or to $1s$ or $2s$ vacancies of the target.

It is generally argued[1–6] that excitation is by a molecular orbital promotion during small impact parameter collisions in the cascade. The original formulation of such pro-

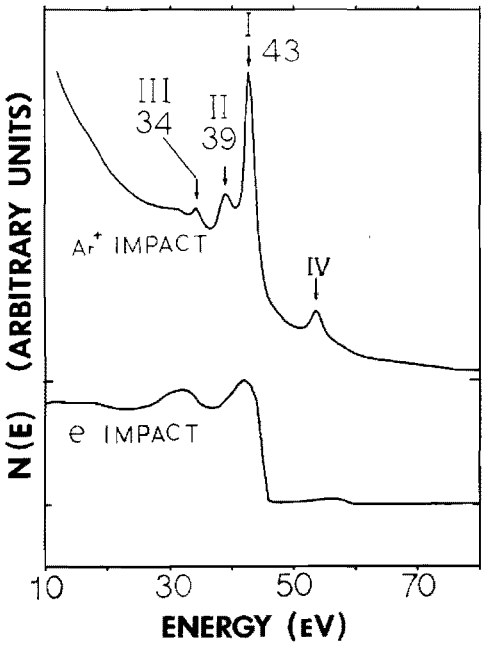

FIG. 1. Auger spectra of magnesium induced by 190-keV Ar^+ and by 1-keV electrons.

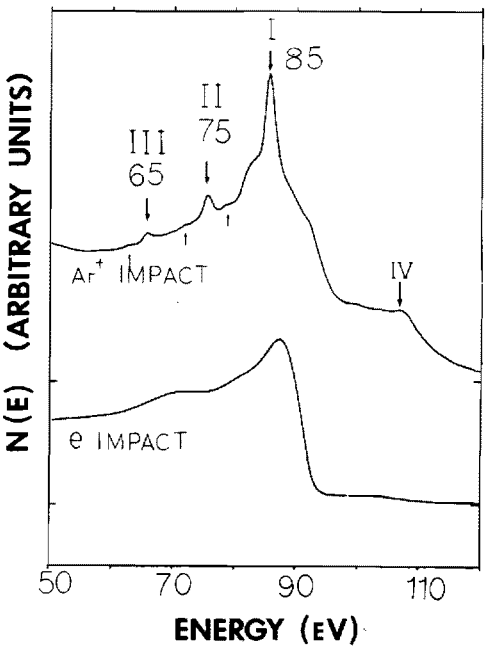

FIG. 3. Auger spectra of silicon induced by 190-keV Ar^+ and by 1-keV electrons.

motions by Barat and Lichten[12] show promotion to occur only to the $2p$ shell of the lightest collision partner. Thus for excitation of silicon during $Ar^+ + Si$ collisions excitation occurs in Si, for $Ne^+ + Si$ collisions excitation occurs in Ne and for Si + Si excitation occurs in either colliding partner. One observes the same ion induced Auger spectrum for Ne^+ impact as for Ar^+ impact on all these targets leading some authors[5,6] to suggest that a major fraction of the excitation events occur in recoil collisions such as Si + Si. However, Schneider *et al.*[13] have recently studied argon silicon collisions in gas phase targets and show that the presence of avoided crossings causes the excitation scheme to be somewhat more complex than envisaged earlier. In fact, $2p$ excitation occurs in both projectile (Ar) and target (Si), although the former has a lower cross section by one to two orders of magnitude. In the present studies impact of Ne^+ produces the same spectra as Ar^+ impact but at lower intensity. The work of Schneider *et al.*[13] tells us that this observation does not allow us to conclude whether excitation is due primarily to projectile target collisions or to target-target recoil collisions. We must therefore accept that both types of event may contribute.

Molecular orbital promotions occur at small impact parameters and therefore require some minimum projectile energy to overcome coulomb repulsion. In turn this means that substantial kinetic energy is transferred to the target nucleus. According to the work of Schneider *et al.*[13] promotion of the $2p$ Si electron in Ar + Si collisions occurs at an internuclear distance of about 0.37 Å. Thus one would anticipate a substantial energy threshold for excitation and this is shown experimentally by Wittmaack[6] to be around 2–3 keV. Close encounters will also involve substantial energy transfer to the target nucleus so that recoils at energies of hundreds of electron volts are anticipated and Auger electrons from decay of such recoils should exhibit detectable Doppler shifts. Wittmaack[6] shows that Doppler widths for $Ar^+ + Si$ collisions increase from 1 to 2.5 eV as projectile energies increase from 2 to 30 keV; at the higher energies the line width appears to saturate. Figure 3 for Ar^+ on Si exhibits line widths of approximately the magnitude reported by Wittmaack. These widths show no detectable change as energy is varied from 20 to 200 keV in the present experiments.

The work of Schneider *et al.*[13] provides us with a cross section for excitation of $2p$ electrons in silicon-argon collision events that is approximately 4×10^{-17} cm^2 in the energy range of the present experiments. Taking the atomic number density of silicon[14] to be 5.0×10^{22} cm^{-3}, one would estimate that approximately 5% of all projectile target collisions would result in excitation of a $2p$ electron of Si. We have not attempted a quantitative measurement of our observed Auger electrons but they are roughly consistent with a yield of this order. One may also consider the absolute yields measured for Ar^+ on solid Al by Hasselkamp and Scharman[15]; cross sections for $2p$ excitation by Ar^+ on Al should be very similar to cross sections for Ar^+ on Si. Hasselkamp and Scharman[15] show a yield in the sharp lines of about 1% (Auger electrons detected per ion incident) and a yield in the broad underlying matrixlike Auger peak of about 2%. The combined yield for Auger electrons ejected from solid aluminum by Ar^+ impact is therefore 3% and comparable to a predicted yield of 5% using cross sections for Ar^+ on silicon and a target thickness appropriate to a single monolayer. A detailed comparison of these figures would require a consideration of how many target monolayers contribute to the measured yield and the fraction of Auger electrons directed into the solid and therefore not detected. Such detailed considerations are beyond the scope of the present work. We wish only to point out that the absolute yield of the Auger electrons is consistent with the cross section for $2p$ shell excitation as measured in a biparticle projectile-target collision experiment.

As we vary projectile energy in the present experiment (from 20 to 200 keV) there is no significant change to strength of the Auger signals which again is consistent with the observations of Schneider *et al.*,[13] that cross sections for target $2p$ shell excitation are almost invariant with energy.

In summary, a yield of a few Auger electrons per hundred ions incident is indicated by the data and is consistent with the separately measured cross section for direct target excitation by projectile impact. A more detailed comparison of the observed signals with measured cross sections would require an assessment of the fraction of electrons emitted back into the solid and therefore not detected; no such assessment was attempted here. There remains also the possibility that part of the observed yield is due to recoil target-target collision events.

IV. DETAILED ANALYSIS OF SPECTRA

It is our objective here to produce a model that reproduces completely all significant observed features of the Auger spectra. We consider first the underlying continuous components that we ascribe to true secondary electron emission and to Auger decay in the matrix. Secondly we propose individual transitions to explain the atomiclike peaks that we believe are due to sputtered atoms and ions decaying in free space. In general terms we are able to predict the locations of spectral lines but have no information on relative intensity. At a final step we fit the predicted lines to the observed spectra and draw some conclusions concerning relative transition probabilities for various decay paths. The unambiguous fitting of these proposed components to the observed spectrum would lead us to conclude that all significant contributions to the spectra have been identified.

A. Underlying continua

Let us consider first the underlying continuous component. Due to ion impact on a surface there is inevitably a secondary electron spectrum that declines in intensity with increasing electron energy. At energies substantially above or below the energy of $2p$ shell decays one would expect the true secondary electron background to be the sole source of electrons. Sickafus[16] describes this spectrum by the empirical formula

$$\text{Yield} = A\,(E + E_0)^{-B}, \tag{1}$$

where E is electron energy and the constants A, E_0, and B are obtained by fitting to the spectrum. We use this equation in the present work establishing the constants by fitting the

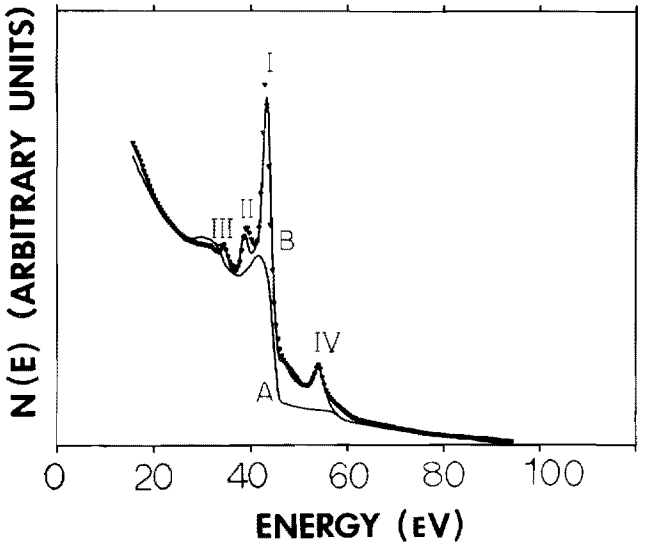

FIG. 4. Auger spectrum of magnesium induced by 190-keV Ar^+ impact. The experimentally determined spectrum is shown as a series of individual data points. Line *A* is the model representation of true secondary electrons plus decay in the matrix. Line *B* represents the model and is essentially coincident with the data of most energies. Roman numerals are used to identify features discussed in the text and listed in Table I.

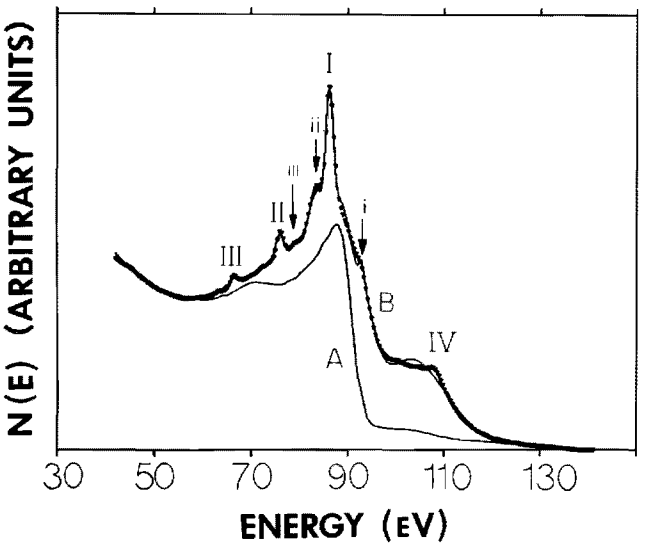

FIG. 6. Auger spectrum of silicon induced by 190-keV impact on silicon. The experimentally determined spectrum is shown as individual data points. Line *A* is the model representation of the true secondary electron and matrix decay components. Line *B* is the final model of the spectrum and is virtually coincident with the data points. The roman numerals designate features discussed in the text and listed on Table III.

formula to the observed spectra at energies above peak IV and below peak III.

L-shell vacancies produced in atoms that remain in the matrix will decay by an *LVV* transition involving two electrons from the valence band. This will produce a broad band of electrons with a width related to the valence band density of states. The observed energy band will in fact be broadened to lower energies by energy loss processes as the electron escapes from the solid. This *LVV* component to the spectrum should be identical to that excited by electron impact on the solid where *LVV* transitions are the only decay channel possible. To model this component we simply record the electron induced Auger spectrum using the built-in electron gun of our Auger system; these spectra are also shown in Figs. 1–3. In our final fitting procedure we adjust the magnitude of the electron induced spectrum to fit the ion induced spectrum.

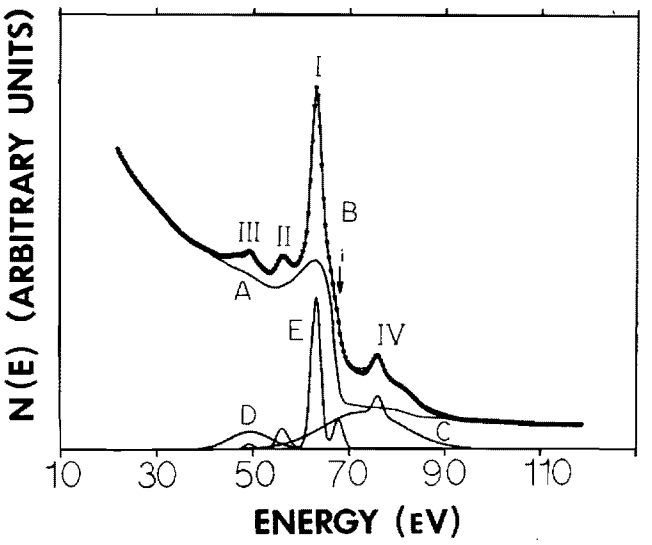

FIG. 5. Auger spectrum of aluminum induced by 190-keV Ar^+ impact. The experimentally determined spectrum is shown as a series of individual data points. Line *A* is the model representation of the true secondary electrons plus decay in the matrix. Line *B* represents the model and is essentially coincident with the data points. Line *C* is the sum of the model components representing decay of two electron vacancies in the matrix and in sputtered ions. Line *D* is the model component representing the enhanced bulk plasmon. Line *E* models the four individual peaks representing decay of single vacancies in neutral atoms and in ions. Roman numerals designate features discussed in the text and listed in Table II.

It is valuable at this stage to anticipate the results of fitting these continuum components. In Figs. 4, 5 and 6 we again reproduce the ion-induced spectra and show for each case, as line A, the sum of the true secondary electron and matrix decay spectra. The component shown is that required in the final fitting where we include also the discrete lines. In the case of Al and Si one could increase the magnitude of matrix (electron-induced) component to force a better correspondence to the observed spectrum but then the individual atomiclike lines would not fit.

The reader's attention is drawn to the location of the "high-energy edge" of the electron-induced spectra located at 45 eV in Mg, 66 eV in Al and 91 eV in Si. For Mg this edge lies at essentially the location of the rapid decrease in the ion-induced spectrum, suggesting that the matrix decay component does indeed explain the underlying continuous part of the spectrum. For Al, however, (Fig. 5) there is a small discrepancy. For Si there is a major difference of some 5 eV between the location of the high-energy edge in the matrix component (at 91 eV) and the rapid decrease of the ion-induced spectrum (at 96 eV). These discrepancies in Al and Si have been noted previously. Baragiola[4] observes the discrepancy in Al and ascribes it to a changed density of states in the collision cascade induced by ion impact. Wittmaack[6] observes the discrepancy in Si and ascribes it to a charging of the sample during ion impact. Hasselkamp and Schar-

mann[15] observe the discrepancy in Al and offer no explanation. We would contend that the apparent discrepancy is explained by the presence of an additional atomiclike line feature lying just above the electron-induced spectrum edge. This is fairly apparent in the case of Si where there is a distinct shoulder at 96 eV betraying the presence of an additional feature. Thus, in explaining the line spectra we must allow for a line at about 66 eV in Al and 93 eV in Si in addition to the main features numbered I–IV and the subsidiary shoulders. No such additional line is necessary for Mg. We shall show later that introduction of these extra lines is a critical step in properly classifying the atomiclike spectra. We conclude that explanations of the discrepancies given by Baragiola[4] and Wittmaack[6] are wrong.

B. Energies of atomic states

We must now address the question of the nature of the states that give rise to the discrete lines. It is our contention that the lines are due to sputtered atoms and ions with one or two $2p$ vacancies decaying in free space outside the solid. If the atom is excited by a projectile-target collision event then close encounters are necessary to permit molecular orbital promotion and this will transfer substantial kinetic energy to the target nucleus. Thus the target atoms may acquire sufficient energy to be ejected and if decaying after ejection we expect a Doppler broadening of Auger peaks related to the atom's velocity.

We propose that the major line feature in each spectrum is from a sputtered neutral atom with a $2p$ shell vacancy; for example, in aluminum this would be a $2p^5 3s^2 3p^2$ configuration. In essence a $2p$ electron has been removed and a $3p$ electron added to maintain neutrality. The notion of a neutral atom with an inner shell vacancy introduces a group of states that are not routinely observed in conventional Auger spectroscopy. Excitation modes such as electron or light ion impact will remove an inner shell electron leaving an ion to engage in the decay process. Neutral atom states have however been identified previously[7] in heavy particle gas-phase collisions where the added outer shell electron can be acquired by a charge transfer process. In the present case we could speculate on two mechanisms for the formation of such neutral states. Firstly, it is quite possible for the $2p$ electron to be promoted to a $3p$ level by the curve crossing mechanism. Secondly, an ion with a single $2p$ vacancy, recoiling from the target, could possibly abstract an electron from the valence band into the $3p$ level by a charge transfer process. The present work provides no clue as to formation process.

Let us consider first the proposed neutral atom states. In the case of aluminum we suggest a $2p^5 3s^2 3p^2$ configuration where one electron has been removed from the L shell but an electron has been added to the $3p$ shell to maintain neutrality. Following Dahl *et al.*,[6] one may estimate the energy of this state by assuming that the energy difference between $2p^5 3s^2 3p^2$ and $2p^5 3s^2 3p$ states of aluminum is equal to the energy difference between the $2p^6 3s^2 3p^2$ and $2p^6 3s^2 3p$ states of the element next highest in Z, namely silicon. In essence one argues that the increased potential of the outer electrons caused by removal of one inner shell electron is equivalent to the increase of nuclear charge by unity. The required energy difference for Si is the first ionization potential of Si which we take from Moore[17]; the energy of the $2p^5 3s^2 3p$ state of Al^+ is taken from the work of Shirley *et al.*[11] In this manner we estimate the energy of the $2p^5 3s^2 3p^2$ state of Al to be 72.35 eV. By a similar argument magnesium in a $2p^5 3s^2 3p$ state would have an energy of 48.82 eV and silicon in a $2p^5 3s^2 3p^3$ state would have an energy of 98.3 eV. These energies are only rough estimates and we should anticipate a possible error of a few eV. We shall shortly discuss the decay paths of these states and predict Auger line energies. By adjusting the line energies to fit the observed spectra we arrive at a more accurate value of the excitation energy lying within two eV of the above estimates.

We anticipate also some contribution from sputtered ions such as Al^+ $2p^5 3s^2 3p$ where one electron is missing from the inner shell but the outer shells are in the configuration of a ground state atom. In these cases the energies of the states are known accurately and can be taken directly from the work of Shirley *et al.*[11] The Auger energies resulting from decay of these states should be accurately predictable since the parent level energy is well known. In comparing these lines with observed spectra we find a direct correspondence of energy.

There is in each spectrum a high energy line designated IV on Figs. 1–3. Most authors agree that this is from an atomic (or atomiclike) state with two L-shell vacancies. For the case of Al we propose a structure $2p^4 3s^2 3p^2$ and calculate an excitation energy of 178 eV by again assuming that for energy differences between different electron configurations the change of screening by removal of each inner shell electron is equivalent to a unity increase of nuclear charge. For magnesium we propose a state of $2p^4 3s^2 3p$ configuration of energy 129 eV and for silicon a state of $2p^4 3s^2 3p^3$ configuration with energy 238 eV. One might question the choice of a state where two electrons have been removed from an inner shell and one added to the outer shells to give a singly ionized state. Why not a doubly ionized configuration with two $2p$ electrons removed and more added to the outer shells? The configuration is chosen because for the single vacancy states a configuration where one electron is added to the outer shells fits the largest feature of the whole spectrum; we surmise that the same should be true here for the doubly ionized states. In practice, the energy estimate for doubly ionized shells is likely to be quite crude and our fitting does not permit us to unambiguously confirm that this proposed state is present. Configurations involving two $2p$ vacancies and no added $3p$ electrons would also fit the data adequately.

C. Auger line energies

We turn now to the prediction of Auger line energies. From the above discussion we have proposed three configurations of sputtered particles for each target case and estimated excitation energies. We consider Auger transitions involving loss of electrons from the $n = 3$ shells. In Tables I, II, and III we show the proposed transitions and the energies of the emitted electrons. Energies are determined using the parent state energies discussed in Sec. IV B above and final

TABLE I. Proposed identification of lines in the magnesium spectrum.

Species	Transition	Predicted Auger energy (eV)	Observed Auger energy (eV)	Peak identification
Mg^0	$2p^5 3s^2 3p$—$2p^6 3s(^2S)$	41.18	43.0	I
	$2p^6 3p(^2P)$	36.75	39.0	II
Mg^+	$2p^5 3s^2$—$2p^6(^1S)$	32.13	34.0	III
Mg^+	$2p^4 3s^2 3p$—$2p^5 3s$	56	54	IV

state energies from Moore.[17] For the double $2p$ vacancy states we list only one transition involving one electron from each of the $3s$ and $3p$ states; other transitions involving two $3s$ or two $3p$ electrons are also possible. We shall find that for the neutral atom transitions the most intense is that involving one $3s$ and one $3p$ electron. We guess that for the double vacancy state, which has the same outer shell configuration, the same type of transition will be most intense. In practice, only a single distinct line from the two vacancy state is observed and this at low intensity; other lines of lower magnitude may be present but would be obscured by instrumental noise.

For certain of the transitions listed in Tables I and II there are previous energy estimates by Dahl *et al.*,[6] using Hartree–Fock calculations. These are generally given for the centroid of the outer-shell multiplet structure and not for individual structures as we list them here. In general the Hartree–Fock calculations give energies a few eV higher than our present estimates and we shall find after the detailed fitting that indeed our estimates are low by this amount.

Let us compare first the lines tabulated in Table II for aluminum with the lines observed on the spectrum of Fig. 5. The two transitions predicted from the Al^+ parent level agree exactly with the positions of peaks II and III in Fig. 5. This is as expected because the energies of the parent and daughter states are well known. The larger group of lines from the Al^0 state do not fit the observed lines. We must recall however that the energy of this parent level is in fact only a rough estimate and an error of a few eV is quite possible. If we increase the $2p^5 3s^2 3p^2$ energy by 1.4 to 73.8 eV then two of these peaks fit exactly onto lines I and II, while a third occurs at 67.8 eV and falls right at the high energy edge of the electron-induced spectrum. The existence of this last line

TABLE II. Proposed identification of lines in the aluminum spectrum.

Species	Transition	Predicted Auger energy (eV)	Observed Auger energy (eV)	Peak identification
Al^0	$2p^5 3s^2 3p^2$—$2p^6 3s^2\ (^1S)$	66.37	67.8	i
	—$2p^6 3s\ 3p\ (^3P)$	61.74	62.2	I
	—$2p^6 3s\ 3p\ (^1P)$	58.95	Absent	
	—$2p^6 3p^2\ (^1D)$	55.78	Absent	
	—$2p^6 3p^2\ (^3P)$	54.71	56.2	II
Al^+	$2p^5 3s^2 3p$—$2p^6 3s\ (^2S)$	55.7	55.7	II
	—$2p^6 3p\ (^2P)$	49.0	49.0	III
Al^+	$2p^4 3s^2 3p^2$—$2p^5 3s 3p\ (^3P)$	75.3	76.0	IV

TABLE III. Proposed identification of lines in the silicon spectrum.

Species	Transition	Predicted Auger energy (eV)	Observed Auger energy (eV)	Peak identification
Si^0	$2p^5 3s^2 3p^3$—$2p^6 3s^2 3p(^2P)$	90.15	93.0	i
	—$2p^6 3s 3p^2\ (^4P)$	84.70	Absent	
	—$2p^6 3s 3p^2\ (^2D)$	83.30	86.0	I
	—$2p^6 3s 3p^2\ (^2S)$	80.65	83.0	ii
	$2p^6 3s 3p^2(^2P)$	79.71		
	$2p^6 3p^3\ (^4S)$	74.75	78.0	iii
Si^+	$2p^5 3s^2 3p^2$—$2p^6 3s^2\ (^1S)$	82.01	82.5	ii
	$2p^6 3s 3p\ (^3P)$	75.47	76.0	II
	$2p^6 3s 3p\ (^1P)$	71.74	Absent	
	$2p^6 3p^2\ (^1D)$	66.90	Absent	
	$2p^6 3p^2\ (^3P)$	65.34	66	III
Si^+	$2p^4 3s^2 3p^3$—$2p^5 3s 3p^2$	103.0	107.0	IV

was predicted earlier to explain the difference between the high-energy edge of the bulk spectrum and the edge of the ion-induced spectrum. Two lines are not observed which may simply mean that the relevant transition probabilities are lower than those of the other components. We note that the decay process involving one electron from each of the $3s$ and $3p$ shells explains peak I, which is the most intense line. It is the same type of transition that we suggest is responsible for decay of the two $2p$ vacancy Al^+ state. The energy for this single transition is shown on Table II as 75.3 eV and agrees well with peak IV on Fig. 5, which lies at 76.0 eV. The agreement may be fortuitous as the estimated energy for the parent level is subject to uncertainty. In conclusion, the major line features of the aluminum spectrum can be explained by the transitions listed in Table II if we allow the energy of the Al^0 $(2p^5 3s^2 3p^2)$ state to be 73.8 eV.

Let us now turn to the magnesium spectrum and compare the predicted lines of Table I with the observed lines in Fig. 4. There are in fact only four lines predicted and four are observed. The line from Mg^+ is located approximately where expected. The two predicted lines of Mg^0 may be brought into agreement with peaks I and II if the $2p^5 3s^2 3p$ state energy is set at 50.6 eV rather than our estimated energy of 48.82 eV. The two-vacancy Mg^+ state also is in satisfactory agreement with the observed line at 54 eV. It is important to note that here the high-energy edge of the electron-induced spectrum agrees with the rapid fall of the ion-induced spectrum so no hidden line is expected at this point and none is required for the group of transitions invoked in Table I.

Turning finally to the silicon case we have a very large number of lines predicted in Table III but a much smaller number of features indicated on the data of Fig. 6. Table III shows that many lines are close together and line width causes overlapping rendering separate identification difficult. A proper identification of line position is possible only by the detailed fit to the data which we shall discuss later. However, some major features are reasonably clear. The Si^0 state of configuration $2p^5 3s^2 3p^3$ was estimated to have an energy of 98.3 eV. This is likely to be inaccurate by some eV and for the similar Al^0 case we found that the estimated

energy was too low by 1.8 eV. If we raise the Si^0 state energy by 2.8 to 101.1 eV then the major peak I and the minor features i, ii, and iii all correspond to lines in the table. We note that the major peak I is a transition involving both a $3s$ and $3p$ electron; such transitions were responsible also for the largest features in the Al^0 and Mg^0 spectra. For the Si^+ spectrum we are dealing with similiar electron configurations to the Al^0 spectrum discussed earlier. For Al^0 two of the proposed transitions do not show lines of any significant intensity; those same transitions are apparently absent here. The predicted Si^+ spectrum appears to explain accurately, with no need for energy shifts, the features labelled II, III, and iii. The two-vacancy state of Si^+ is invoked to explain the very weak feature labelled IV and the estimated energy corresponds satisfactorily with observation. We note particularly that the clear discrepancy between the high-energy edge of the electron-induced spectrum with the rapid signal drop in the ion-induced spectrum corresponding to the feature labelled i is satisfactorily explained by a line of the Si^0 spectrum.

D. Line shape and width

Molecular orbital promotion of electrons requires close encounters and substantial energy transfer to the target species. We therefore anticipate that the sputtered excited particles will have substantial kinetic energy and that the Auger Lines will exhibit a Doppler broadening. Thus in a modelling of the spectrum we must assign a width and shape to each line. We have not attempted to estimate a line shape since the velocity distribution of the recoils is not known independently. Moreover, the annular collection geometry and the inherent resolution limit of the analyzer produce further contributions to line width that are not readily quantified. Rather we represent each line by a Gaussian function and adjust the width and height to match observation. The linewidth will then be used to give a measure of the projectile velocity distribution. Line magnitude will of course give a measure of relative transition probability.

E. Detailed fitting to the observed spectra

In principle, the detailed fitting of components to the observed spectra proceeds as follows. We have already established in Sec. IV A how the underlying secondary electron background is modelled by a Sickafus-type function. To this we add the electron-induced spectrum to represent the decay of vacancies in atoms of the matrix. The intensity of the electron-induced spectrum is allowed to vary as the magnitude of this component is unknown. We add also a Gaussian function for each line listed in Tables I, II, and III. All lines in a given spectrum are held at the same width but this is varied to fit the data. Height of the lines is also allowed to vary since we do not have any information on transition probabilities. Within any one group of lines shown in Tables I, II, or III, having a common parent state, the line separations are accurate and therefore should not be allowed to vary. However the energy of the parent level is in some cases only an estimate with an uncertainty of a few eV. Thus we permit the whole group to vary in energy by a few eV to fit the data and determine, from the best fit, a more accurate value of parent level energy. In practice, for the ion states with single $2p$ vacancies the energy shift required to fit the data is less than three tenths of an eV and therefore less than the resolution of the Auger spectra to which we are fitting. This is expected as the parent level energies are well established for these cases. For the neutral spectra, and the spectral line from an ion with two vacancies, the required shift will be few electron volt.

One further contribution common to all spectra must be included to account for the broad feature under line IV. This is undoubtedly due to decay of two electron vacancies in the solid matrix and will be related to valence band density of states and to energy loss processes experienced by electrons as they exit the solid. This feature is observed also on electron induced spectra such as we show in Figs. 1–3 but at a low relative amplitude. Apparently two electron excitation by ion impact is more efficient than the corresponding process under electron impact. We have not attemped any detailed model of this feature but represent it simply by a broad Gaussian adjusted in width and height to fit the data. While a Gaussian function is of course unrealistic, the location, height, and width of the atomiclike transitions are not significantly affected even if this component is left out entirely; its function is primarily to account for the broad feature under peak IV.

A further small problem arises in the handling of a contribution from the bulk plasmon. The component due to matrix decays should exhibit small plasmon loss structures at well-known energies. Such plasmon loss peaks should also be present in the electron-induced spectrum which we use to model the decay of vacancies in the matrix, thus they should be automatically taken into account. We find, however, that the plasmon loss peak in the ion-induced spectrum is of different magnitude from the corresponding peak in the electron spectrum. This is clearly shown in Fig. 4, where line A, representing the underlying continuum, overestimates the signal at about 30 eV, here the bulk plasmon loss peak is greater under electron impact than under ion impact. We accomodate this by adding yet another broad Gaussian at the location expected for bulk plasmon loss features in the electron-induced spectrum. For magnesium, the required amplitude to fit the data is actually negative showing that the plasmon loss peak must be reduced in magnitude. For aluminum and silicon the amplitude is positive indicating that ion impact produces a higher plasmon loss component than electron impact. The influence of this feature on the identification and location of atomiclike lines is quite negligible and we include it only to demonstrate that every feature of our observed spectra can be accounted for.

One may now perform the fit to the data. A nonlinear curve fitting routine based on the gradient expansion algorithm of Marquardt[18] was used for this purpose. The principal parameters that we seek from the fit are relative height of peaks, the width of the peaks and the location of the peak groups which in turn gives us the energy of the Auger decay parent levels.

The fitted spectrum for magnesium is shown on Fig. 4 as the line through the data points. The fit is excellent except for a minor discrepancy around 40 eV that we cannot ex-

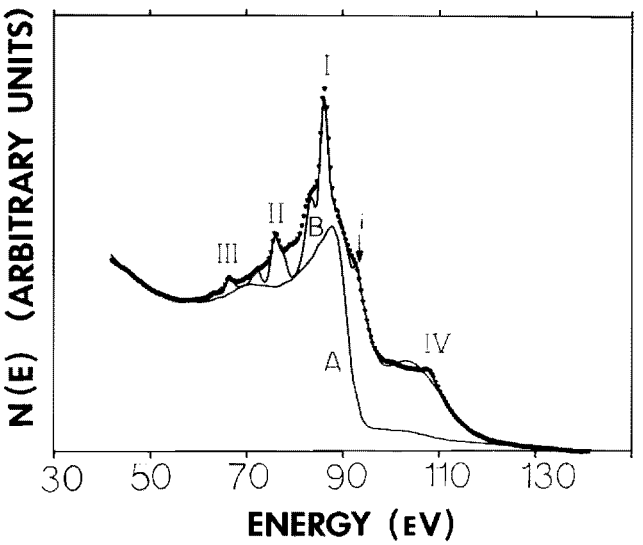

FIG. 7. Auger spectrum induced by 190-keV Ar^+ impact on Si is again indicated by data points. Line *A* is again the model component representing true secondary electrons and matrix decays. Line *B* represents the model prediction when only line *A*, the individual atomic transitions and decay of two electron vacancies are considered. Clearly, Line *B* does not reproduce the data points.

plain. Similarly for aluminum we show the fitted line in Fig. 5 and for the aluminum case we show separately the individual model components. For these two cases we would conclude that all relevant contributing processes have been properly accounted for and that the sharp lines are indeed from the proposed transitions.

For the case of silicon the fitted spectrum designated as line *B* in Fig. 7 fails to match the observed spectrum in a significant manner. Line positions and widths can be reproduced leading us to believe that the suggested Auger transitions do account for the observed atomiclike lines. There is some discrepancy at around 100 eV that is probably due to our inadequate model of the two-vacancy decays in the matrix; this is of little consequence. The great concern is that in the region 60–90 eV, there is a general underestimate of the observed signal. The discrepancy can be accommodated by adding yet a further term. We add a very broad Gaussian centered at about 80 eV, repeat the fitting and achieve the agreement shown by line *B* on Fig. 6. For silicon we must conclude that the peaks are due to the suggested Auger transitions and that the underlying continuum is broadly explained by the decays in the matrix and by true secondary electrons. There is however an unexplained component which must represent an additional decay mechanism.

V. DISCUSSION

Let us first address the explanation of the component for the Si spectrum that was arbitrarily introduced to force a fit between experiment and model. Our explanation of the spectra has proceeded on the basis that the major contributions are from atoms decaying in the matrix and giving a broad $L_{23}VV$ spectrum and sputtered atoms (or ions) decaying in free space giving atomic lines in an $L_{23}MM$ spectrum. The lifetimes of $2p$ vacancies in Mg, Al, and Si are, respectively,[19] 930, 134, and 37 f sec. If we consider the sputtered atoms (or ions) to have an energy of about 100 eV as suggested by Wittmaack[6] from his Doppler broadening data, then the decay distance (lifetime times speed) for Mg, Al, and Si are, respectively, 260, 35.6, and 9.7 Å. If we assume that surface potential is significant to a range of, say, 5 Å, then clearly most Mg and Al decays will occur far from the surface, effectively in free space, and atomic lines should be observed characteristic of free atoms. For the case of silicon, however, a large fraction of the decays from moving atoms will occur within the field of the surface. We tentatively suggest that the additional component added to curve *B* of Fig. 7 to get curve *B* of Fig. 6 represents decays of $2p$ vacancies in Si atoms emerging from the surface and decaying within the field of the surface. The component may be thought of as centered at approximately the location of both $L_{23}VV$ (matrix) and $L_{23}MM$ (atomic) transitions but broadened due to a mixing of the various outer-shell electron configurations. It is valuable to consider also ion-induced spectra of phosphorus and sulphur which have been recorded by Viel *et al.*[3] using these targets in compound form. For phosphorus and sulphur the lifetimes become yet shorter implying further increases in the fraction of sputtered atoms decaying close to the solid. One finds that for sulphur there are no distinct atomic lines at all and the spectrum has merged into a broad peak with distinct shoulders. For this case the decay length of 100-eV particles is only 2.33 Å and 90% of all decays would occur within our assumed 5 Å surface potential range. For phosphorus the conditions are intermediate with a broad underlying peak carrying weak individual atomic lines. We conclude then that the silicon spectrum has evidence for a substantial component due to free atoms undergoing Auger decay while within the field of the surface. We suggest that our introduction of a broad Gaussian is a satisfactory expedient for representing this component and allowing us to separately consider the size and width of the atomic lines superimposed upon it.

Let us turn now to the question of relative line intensities obtained from our fitting procedure. Comparing Table II with Table III, we see that for both aluminum and silicon we propose five decays from a $2p^5 3s^2 3p^2$ configuration; for aluminum the configuration is a neutral atom, for silicon it is a singly ionized particle. Since the electron configurations are the same it is reasonable to expect the relative line strengths, and hence transition probabilities to be in the same ratios for both cases. Transitions from the $2p^5 3s^2 3p^2$ configuration to, respectively, $2p^6 3s^2(^1S)$, $2p^6 3s 3p(^3P)$, and $2p^6 3p^2(^3P)$ levels are in the intensity ratios 0.23:1:0.07 for Al^0 and 0.45:1:0.09 for Si^+. Transitions to the $2p^6 3s 3p\,(^1P)$ and $2p^6 3p^2(^1D)$ states appear in both cases to be absent or of very low intensity. Similarly comparing magnesium and aluminum transitions from the $2p^5 3s^2 3p$ state to, respectively, the $2p^6 3s(^2S)$ and $2p^6 3p(^2P)$ states are in the ratio 1:0.2 for Mg^0 and 1:0.4 for Al^+. Dahl *et al.*[7] have considered this ratio theoretically and show it to be 1:0.25. There is substantial uncertainty on a number of these lines since they occur at essentially the same energy as features from other configurations; also we have made no correction for varying detection sensitivity. Nevertheless, the agreement of ratios for different atomic species and also with the one theoretical estimate

is quite satisfactory. This observation gives us some confidence that the assigned configurations are correct.

The widths of atomic lines in these spectra are respectively, for magnesium, aluminum, and silicon, 1.9, 2.8, and 2.2 eV. Approximately one half this width is due to instrumental broadening. Assuming that the remaining width is due to Doppler broadening and taking into account the particular geometry of our analyzer we would conclude that the decaying atoms (and ions) have speeds of about 120 eV.

The location of the line groups allows us to determine the energy of the parent level. For Mg^+, Al^+, and Si^+ spectra the line location after fitting differs from the predicted positions in Tables I, II, and III by less than 0.3 eV, which is less than the inherent resolution of the analyzer. We would conclude therefore that the predicted lines are correct and that the energy of the parent levels is completely consistent with the values tabulated by Shirley *et al.*[11] For the neutral atom states our measured Auger energies are no more than 2.5 eV from our estimated energies. From the fitting procedure we derive the observed line energies and determine the parent level energies as follows: for Mg^0 $(2p^5 3s^2 3p)$ 50.6 eV, for Al^0 $(2p^5 3s^2 3p^2)$ 73.8 eV, and for $Si^0(2p^5 3s^2 3p^3)$ 101.1 eV. We can also use the fitting of the $2p$-vacancy ion states to conclude that the energies are for Mg^+ $(2p^4 3s^2 3p)$ 127 eV for Al^+ $(2p^4 3s^2 3p^2)$ 179 eV, and for Si^+ $(2p^4 3s^2 3p^3)$ 242 eV. These are within, respectively, 2, 1, and 4 eV of our estimates. We could, however, suggest that this latter group of energies should be treated with caution as the features on which they are based are weak and energies poorly defined. These various defined state energies are quite consistent with the Hartree–Fock predictions of Dahl *et al.*[7]

VI. CONCLUSION

The objective here was to reexamine the ion-induced Auger spectra of Mg, Al, and Si to provide a quantitative explanation of all observed features in terms of well-understood mechanisms. For magnesium and aluminum this has been achieved and for silicon also there is a large measure of success. In general terms our original explanation[5] is shown to be correct. The underlying continuum is due to decay of atoms located in the matrix, superimposed on a true secondary electron background. The sharp features are largely from sputtered neutral atoms in a configuration where one electron has been removed from a $2p$ shell but an electron also added to the $3p$ shell to maintain neutrality. The energies of these states have now been determined experimentally by fitting to the observations. In all cases there are also lines from sputtered ions with single $2p$ vacancies that have energies that agree well with predictions based on well-established energies. We also show quantitatively how sputtered ions with two $2p$ vacancies can account for a high-energy feature in all spectra. Relative transition probabilities for similar electron configurations are shown to be independent of the target and consistent with available theoretical predictions. A critical factor in the identification of the lines has been the realization that for aluminum and silicon there is a discrepancy between the high-energy edge of the electron induced Auger spectrum and the rapid drop in the ion-induced spectrum. This betrays the existence of additional lines that must be identified. Explanations that the discrepancy is due to band structure perturbations[4] or to instrumental effects[6] are shown to be unnecessary.

Linewidths all exceed instrumental resolution and are interpreted as a Doppler broadening related to the speed of the sputtered particles; an average energy of some 100 eV is consistent with the observations.

In the case of silicon we identify a 10-eV-wide feature that is due neither to matrix decays nor to decay of free atoms. We propose that this is due to atomic decays close to the surface where the fields cause energy levels to be broadened into a continuous distribution. It is suggested that the work of Viel *et al.*[3] on sulfur, where decay times are yet shorter, provides a further example of decay within the potential field of the surface.

The present data do not provide a quantitative measure of total Auger signal and cannot be used to compare with cross sections. We do, however, point out that a comparison of the recent absolute measurement of Auger flux by Hasselkamp and Scharmann[15] with the recent cross-section measurements of Schneider *et al.*[13] show that direct excitation in projectile-target collisions is capable of explaining the observed Auger signal.

ACKNOWLEDGMENTS

This work has at all stages benefited from the advice and assistance of Dr. K. O. Legg. It was in part supported by the Solid State Chemistry program of NSF under Grant no. DMR-80007.

[1] J. T. Grant, M. P. Hooker, R. W. Springer, and T. W. Haas, J. Vac. Sci. Technol. **12**, 481 (1975).
[2] F. Louchet, L. Viel, C. Benazeth, B. Fagot, and N. Coloumbie, Radiat. Eff. **14**, 123 (1972).
[3] L. Viel, C. Benazeth, and N. Benazeth, Surf. Sci. **54**, 635 (1976).
[4] R. A. Baragiola, Springer Ser. Chem. Phys. **17**, 39 (1981).
[5] W. A. Metz, K. O. Legg, and E. W. Thomas, J. Appl. Phys. **51**, 2888 (1980).
[6] K. Wittmaack, Surf. Sci. **85**, 69 (1979).
[7] P. Dahl, M. Rodbro, G. Hermann, B. Fastrup, and M. E. Rudd, J. Phys. B **9**, 1581 (1976).
[8] J. J. Vrakking and A. Kroes, Surf. Sci. **84**, 153 (1979).
[9] M. Negre, J. Mischler, and N. Benazeth, Surf. Sci. **107**, 562 (1981).
[10] Paul W. Palmberg, Gerald E. Riach, Roland E. Weber, and Noel C. MacDonald, *Handbook of Auger Electron Spectroscopy* (Physical Electronics Industries, Inc. Eden Prairie, Minnesota, 1972).
[11] D. A. Shirley, R. L. Martin, S. P. Kowalczyk, F. R. McFeely, and L. Ley, Phys. Rev. B **15**, 544 (1977).
[12] M. Barat and W. Lichten, Phys. Rev. A **6**, 211 (1972).
[13] D. Schneider, G. Nolte, U. Wille, and N. Stolterfoht, Phys. Rev. A **28**, 161 (1983).
[14] H. H. Andersen and J. F. Ziegler, *Hydrogen Stopping Powers and Ranges in All the Elements* (Pergamon, New York, 1977).
[15] D. Hasselkamp and A. Scharmann, Vak. Tech. **32**, 9 (1983).
[16] E. N. Sickafus, Phys. Rev. B **16**, 1436 (1977).
[17] C. E. Moore, National Bureau of Standards Circ. (U.S.) **467** (1949).
[18] D. W. Marquardt, J. Soc. Ind. Appl. Math. **11**, 431 (1963).
[19] E. J. McGuire, Phys. Rev. A **3**, 587 (1971).

Nuclear Instruments and Methods 170 (1980) 561–564

AUGER SPECTRA INDUCED BY ION IMPACT ON METALS

K.O. LEGG, W.A. METZ and E.W. THOMAS
School of Physics, Georgia Tech, Atlanta, Ga. 30332, U.S.A.

The Auger electron spectra induced by 20–200 keV Ar^+ ion impact on Al and Fe are examined and the spectral lines identified. For Al the spectrum is due to sputtered Al and Al^+ with one or two vacancies in the 2p shell. For Fe there are Doppler broadened lines from Ar plus subsidiary structure from interatomic transitions.

1. Introduction

Heavy ion impact on metal targets induces an intense emission of Auger electrons. The excitation mechanism is understood in terms of the electron promotion model of Barat and Lichten [1], involving the formation of a quasi-molecule AB from the interaction of a projectile A with an atom of the target B. The electron energy levels of the two particles are perturbed as they approach one another, allowing levels from one atom to become degenerate with levels of the second atom. This permits electron promotion from a filled inner shell on one atom to an unfilled shell on either atom, creating an inner shell hole which can subsequently decay by an Auger process. We have studied the Auger spectra induced by heavy ion impact on metals. Taking as examples the cases of Ar^+ on Al and Ar^+ on Fe which are studied most closely in this paper, the simple promotion model would suggest that Ar^+ on Al will result in 2p vacancies of Al while Ar^+ on Fe will result in 2p vacancies of the projectile Ar. It is also possible that the collision cascade resulting from the projectile impact will cause symmetric collisions Al + Al and Fe + Fe with sufficient energy to permit electron promotions; in this case there will be vacancy production in the 2p level of the target species.

We have performed a study of the Auger spectra induced by 20–200 keV Ar^+ and Kr^+ impact on Be, Al, Si, Cr, Mn, Fe, and Co. Due to space limitations this report will be restricted to discussion of Ar^+ + Al and Ar^+ + Fe which respectively represent cases where the vacancy production should occur in the 2p shell of the target (Ar^+ + Al) and the 2p shell of the projectile (Ar^+ + Fe). Details of the other cases will be presented elsewhere [2].

The experimental arrangement consisted of an ultra high vacuum chamber capable of base pressures below 10^{-10} Torr linked via a differentially pumped beam line to a 20–200 keV ion implantation accelerator. A standard commercial cylindrical mirror analyzer (CMA) with an axial electron gun was used to monitor ion-induced electron emission and surface cleanliness. The ion beam was 95° from the CMA axis with the sample normal lying between and coplanar with the two axes at an angle of 60° from the ion beam. Electrons were detected in a 42° annulus about the CMA axis. Typical ion beam currents were 1–20 μA in a 3 mm^2 spot. The targets were polycrystalline Al and Fe mechanically and chemically polished followed by further sputter cleaning with a 100 keV Ar^+ or Kr^+ beam from the accelerator. The Auger spectra shown here were all taken in the differential mode commonly used in Auger measurements and built up over a period of several minutes using a multichannel analyzer to increase signal-to-noise ratio.

2. Ar^+ impact on aluminum

The ion induced spectrum is shown in fig. 1 along with a conventional elctron induced spectrum for comparison; the spectrum is similar to that published earlier by Benazeth and others [4]. Clearly the major feature of the ion induced spectrum is at about the same energy as that in the electron induced spectrum; the feature is certainly due to filling of a 2p shell vacancy which is anticipated on the basis of the pro-

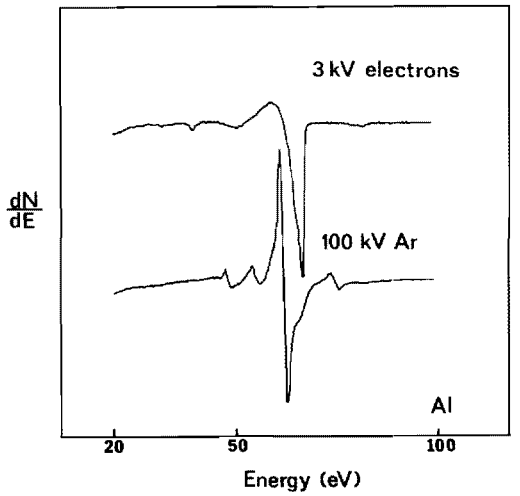

Fig. 1. Auger spectra induced by impact of 3 keV electrons and 100 keV Ar^+ incident on an aluminium target. The spectra are taken in the derivative mode.

motion model. The electron induced line shows a long tail to lower energies which causes the asymmetry in the 67 eV peak; the tail is due to energy loss by electrons emitted below the surface of the target. No such tail is seen on the ion induced spectrum No such tail is seen on the ion induced spectrum. The electron induced spectrum shows a peak at 51 eV, 16 eV below the main peak, representing excitation of bulk plasmons; no such plasmon loss is seen 16 eV below the major peak of the ion induced spectrum. Oxidation of the aluminum surface causes a major change to the electron induced spectrum [3] due to alteration of the valence band structure; the ion induced spectrum remains unchanged on oxidation. Thus the ion induced Auger spectrum shows none of the characteristics expected for emission by an atom in the solid; there is no loss tail, no plasmon loss and no change on oxidation. Vrakking and Kroes [5] have recently argued that the Auger spectrum comes from atom-like structures formed deep in the solid within the disturbed region of the collision cascade. Cross sections for ionization of atoms are of the order 10^{-16} cm^2 or greater so that an electron emerging from deep in the solid will almost certainly cause one or more ionization events with a loss of energy equal to the relevant ionization potential. Thus on oxidizing the surface there should be a large increase of a peak at 13.6 eV below the main Auger structure. While such a peak is indeed present (see fig. 1) it is observed for a clean aluminum surface and shows no change on oxidation. We therefore conclude that the Auger electrons come from aluminum atoms or ions sputtered out of the surface and not from deep in the solid as claimed by Vrakking and Kroes [5].

We propose that the major feature of the ion induced spectrum is due to sputtered neutral Al with a 2p vacancy having a $2p^5 3s^2 3p^2$ configuration. The energy of this state can be estimated as follows. $E(2p^5 3s^2 3p^2)$–$E(2p^5 3s^2 3p)$ for Al should be approximately equal to the difference between $E(2p^6 3s^2 3p^2)$ and $E(2p^6 3s^2 3p)$ for Si; the latter difference is the ionization potential of Si which from standard tables [6] is 8.149 eV. Taking $E(2p^5 3s^2 3p)$ for Al as 80.5 eV from the calculations of Shirley et al.[7], we arrive at an energy of 72.35 eV for the $2p^5 3s^2 3p^2$ configuration of Al. We can now calculate the energies of five transitions leading to filling of the 2p vacancy and ejection of an outer shell electron.

$$2p^5 3s^2 3p^2 \rightarrow 2p^6 3s^2 : \quad E_{\text{Auger}}\ 66.37\ \text{eV}, \quad (1a)$$

$$\rightarrow 2p^6 3s\ (^3P^0) : E_{\text{Auger}}\ 61.74\ \text{eV}, \quad (1b)$$

$$\rightarrow 2p^6 3s3p\ (^1P^0) : E_{\text{Auger}}\ 58.95\ \text{eV}, \quad (1c)$$

$$\rightarrow 2p^6 3p^2\ (^1D) : E_{\text{Auger}}\ 55.78\ \text{eV}, \quad (1d)$$

$$\rightarrow 2p^6 3p^2\ (^3P) : E_{\text{Auger}}\ 54.71\ \text{eV}, \quad (1e)$$

In each case the energy of the final state is readily obtained from standard tables [5]. Transitions (1b) and (1c) explain the principal peak in fig. 1; the cross-over point of the major peak is at about 61 eV. Transitions (1d) and (1e) can explain the secondary peak at 56 eV. Transition la coincides with the shoulder on the main peak at 67 eV. In a similar manner we can identify the small peak at 76 eV as being due to decay of a neutral atom with two 2p vacancies; that is to say a $2p^4 3s^2 3p^3$ configuration. Finally the small peak at 49 eV can be identified as decay of an Al^+ ion with a single 2p vacancy; a $2p^5 3s^2 3p$ configuration. In summary the Auger spectrum induced by Ar^+ on Al has the form expected for target atoms ejected out of the solid and the lines can be completely identified as due to one or two 2p vacancies in Al atoms or Al^+ ions.

3. Ar^+ impact on iron

In fig. 2 we show the Auger spectrum induced by Ar^+ of various energies incident on Fe. Unlike the aluminum case shown in fig. 1 the spectrum is not readily recognizable as being from an Fe target. According to the promotion model [1] vacancies should occur in the 2p shell of the argon projectile; this is the origin of the broad peak at about 216 eV which is simply the $L_{23}M_{23}M_{23}$ transition of Ar. At about 45 eV there is a large peak which coincides exactly with the $M_{23}M_{45}M_{45}$ peak seen in the electron induced Auger spectrum of Fe. According to the promotion model an M_{23} vacancy (i.e. 3p vacancy) in Fe can occur in the direct Ar^+ + Fe primary collision as well as in Fe + Fe collisions occurring in the collision cascade. A second small peak at about 75 eV occurs in both the ion and electron induced spectra of Fe; it is probably the $M_1M_{45}M_{45}$ transition of Fe. There remains a considerable additional structure in the region 90–200 eV that is not readily identified as arising from either Fe or Ar.

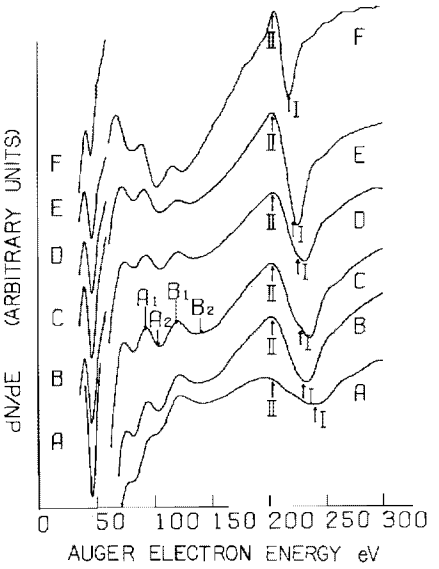

Fig. 2. Auger spectra induced by 20–200 keV Ar^+ incident on an irong target. The spectra are taken in a derivative mode. The peak designated I–II is identified as a Doppler-broadened LMM transition in backscattered argon. Peaks A and B are identified as interatomic transitions involving Ar vacancies filled by electrons from Fe (see text). Curves A to F are for 200, 100, 80, 60, 40 and 20 keV Ar^+ ions respectively.

Let us examine first the Ar $L_{23}M_{23}M_{23}$ peak lying at about 216 eV. We can demonstrate that the changing line width is consistent with a Doppler shift of electron energy due to the source of electrons being backscattered Ar^+ ions. According to Werme et al. [8], the major feature of the $L_{23}M_{23}M_{23}$ transition from an isolated Ar^+ ion is a group of lines lying between 203 and 206 eV. We can predict that if such a group were to be recorded using the derivative mode of our CMA and detector then there would be a conventional single peak with the positive excursion at about 203 eV and the negative excursion at 206 eV. We perform the calculation for the case of ions scattered through 43° from their original direction and emitting their Auger electron in the direction of their motion. This seemingly arbitrary choice represents scattering and electron emission in the plane of the incident ion beam, target surface normal and CMA axis, with the direction of motion directly towards one side of the CMA annular entrance aperture. This choice will serve for an illustration of qualitative behaviour. The scattered Ar^+ ion energy is calculated from conservation of energy and momentum; the Doppler effect is computed from the formula given by Dahl et al. [9]. This Doppler shift is then added to the negative excursion of the expected peak from an isolated Ar ion and gives the points labeled I in fig. 2. For the geometry of the present experiment there will be very few particles scattered out of the surface and away from the detector giving a shift to lower electron energies. Thus the positive excursion of the Ar $L_{23}M_{23}M_{23}$ peak should remain essentially unchanged with projectile energy; the expected position of the positive excursion is indicated by the symbol II in fig. 2. The positions of points I and II evaluated in this manner do in fact agree quite well with the observed positions of the positive and negative excursions, confirming that the changes in peak shape and position are consistent with the Doppler effect. It is also clear that in the limit as projectile energy tends to zero the argon line extrapolates to the position expected for a free Ar^+ ion. We offer no definite explanation of the weak double peak seen on the argon line for 60 and 80 keV impact. We do note, however, that the backscattered energy spectrum of Ar^+ ions from polycrystalline materials is a broad continuum with superimposed a sharp peak due to surface scattering [10]; such an energy distribution

would produce a double peak structure on the negative excursion.

In the region 90–200 eV there are other peaks which cannot be identified as due to Fe or to Ar. The peaks are not seen in an electron induced Auger spectrum of the target and are not seen when a different heavy projectile is used (e.g. Kr^+). We will argue that these features are interatomic Auger transitions involving a core hole in the projectile being filled by electrons for a neighboring Fe atom. The transitions are of the type $L_{Ar}M_{Fe}M_{Fe}$ or $L_{Ar}M_{Fe}M_{Ar}$ where L_{Ar}, L_{Fe}, etc., are energy levels of Ar and Fe atoms. Transitions of this type have been seen in a number of systems [11]. The interatomic transition rate depends on the spatial overlap of the initial hole state (L_{Ar}) and the annihilating electron state (M_{Ar} or M_{Fe}) as well as the initial state of the ejected electron and its continuum wave function. There appear to be two lines designated A and B in fig. 2; line A extends from the positive excursion A_1 to the negative excursion at A_2 and similarly the line B extends from B_1 to B_2. Clearly the width of line A (measured as the energy $E_{A_2} - E_{A_1}$) is small and decreases slightly from 13 to 6 eV as the projectile energy increases from 20 to 200 keV. By contrast the width of line B ($E_{B_2} - E_{B_1}$) increases with increasing projectile energy with the negative excursion moving to higher energy and the positive excursion remaining unchanged; this behaviour is exactly similar to that of the argon Auger line therefore representing a Doppler effect and indicating that the source of the electrons is a moving projectile. We ascribe peak A to an Ar (L_{23}) Fe (M_1, M_{23}) transition whose energy can be estimated (from the binding energies of Shirley et al.) [7], to be 95.5 eV. The small decrease in peak width with increasing projectile energy is consistent with the "Berry effect" whereby the emitted electron is affected by the Coulomb fields of both the source ion (Fe) and the Ar projectile [13]. There is no Doppler effect because the source of the monitored electron is an Fe atom in the matrix. We ascribe peak B to a transition of the type Ar (L_{23}) Fe (M_1) Ar (M_{23}) whose energy from a stationary system should be [7] about 138 eV. The broadening with projectile energy occurs because the source of the detected electron is an argon projectile which is in motion. There are in fact at least eight interatomic transitions which occur in the region 90–200 eV and we do not claim positive identification of these two major peaks. We do, however, conclude that the structures *A* and *B* are interatomic transitions with the ejected electron coming from an Fe atom for peak A and from the Ar atom for peak B.

4. Conclusion

The ion induced Auger spectra of metals occur due to electron promotion mechanisms and exhibit different lines from those seen in electron induced spectra. For Ar^+ on Al the vacancies occur in the L_{23} shell of Al and the spectrum is identified as being due to sputtered Al and Al^+. For Ar^+ on Fe the promotion model predicts vacancy formation in the 2p level of Ar. We observe a Doppler-broadened LMM line of Ar from backscattered atoms and also certain interatomic transitions involving decays in the Ar Fe quasi-molecular system.

This work was supported in part by the Solid State Chemistry Program of the NSF and by the Magnetic Fusion Energy program of the D.O.E.

References

[1] M. Barat and W. Lichten, Phys. Rev. A 6 (1972) 211.
[2] W.A. Metz, K.O. Legg and E.W. Thomas, to be published.
[3] H. Guennou, G. Dufour and C. Bonnelle, Surface Sci. 41 (1976) 547.
[4] C. Benazeth, N. Benazeth and L. Viel, Surface Sci. 78 (1978) 625; see also references cited therein.
[5] J.J. Vrakking and A. Kroes, Surface Sci. 84 (1979) 153.
[6] C.E. Moore, Atomic energy levels, NBS Circular 467, 15 June 1949.
[7] D.A. Shirley, R.L. Martin, S.P. Kowalczyk, F.R. McFeely and L. Ley, Phys. Rev. B 15 (1977) 544.
[8] L.O. Werme, T. Bergmark and K. Siegbahn, Phys. Scripta 8 (1973) 169.
[9] P. Dahl, M. Rodbro, G. Hermann, B. Fastrup and M.E. Rudd, J. Phys. B 9 (1976) 1581.
[10] T.M. Buck, Y.S. Chen, G.H. Wheatley and W.F. Van der Weg, Surface Sci. 47 (1975) 244.
[11] For a brief review see P.H. Citrin, J. Elec. Spectr. 5 (1974) 273.
[12] R.B. Barker and H.W. Berry, Phys. Rev. 151 (1966) 14.
[13] P. Dahl, M. Rodbro, B. Fastrup and M.E. Rudd, J. Phys. B 9 (1976) 1567.

Identification of Auger spectra induced by Ar^+ and Kr^+ ion impact on transition metals

K. O. Legg, W. A. Metz, and E. W. Thomas
School of Physics, Georgia Tech, Atlanta, Georgia 30332

(Received 29 October 1979; accepted for publication 8 February 1980)

The production of Auger electrons from Cr, Mn, Fe, and Co by 20–200-keV Ar^+, 100-keV Kr^+, and 3-keV electrons has been studied. The metal $M_{23}M_{45}M_{45}$ and the Argon LMM peaks are clearly identifiable, the latter broadened consistent with electron emission from backscattered Argon ions. Various other features are produced which cannot be due to target or projectile Auger emission. These are believed to result from interatomic transitions between the ions of the beam and those of the target.

PACS numbers: 79.20.Nc, 79.20.Fv, 32.80.Hd

I. INTRODUCTION

Although Auger electron emission from gaseous targets under ion bombardment has been studied for many years,[1] relatively little data exist for ion bombarded solids. Because electron emission is particularly strong from some light elements, most of the work to date has concentrated on Be, Mg, Al and Si Refs. 2–12, although Li and Na, (Ref. 5) K, Ca, Sc, and V (Ref. 13), Ge (Ref. 14), Ag (Ref. 5), Ti (Refs. 8, 12, and 13), Cr (Refs. 8, 13), Fe (Ref. 8), and Cu (Refs. 5, 8, 14), the alloys Al-15% Mg and Fe_3Al (Ref. 10) and the compound GaP (Ref. 12) have also been examined. The bombarding species has usually been Ar^+ in the energy range from a few keV to several hundred keV, although some workers have used He^+ (Ref. 6), Ne^+, and Xe^+ (Ref. 9), Kr^+ (Refs. 8 and 9), and protons.[15] The energy spectra of the emitted electrons usually comprise a low-energy secon-

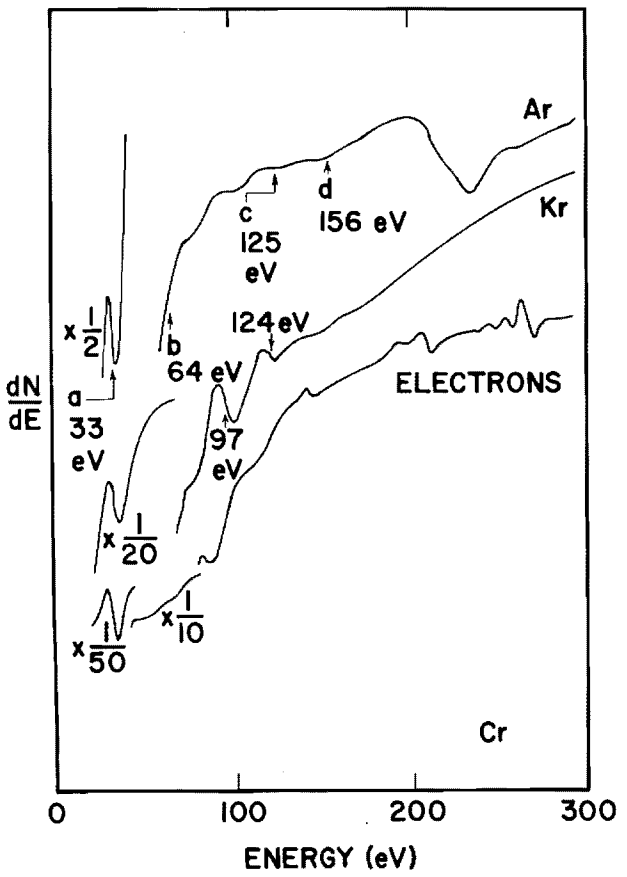

FIG. 1. Auger spectra induced by impact of 3-keV electrons and 100-keV Ar^+ and Kr^+ on a chromium target. The various indicated features are identified in the text.

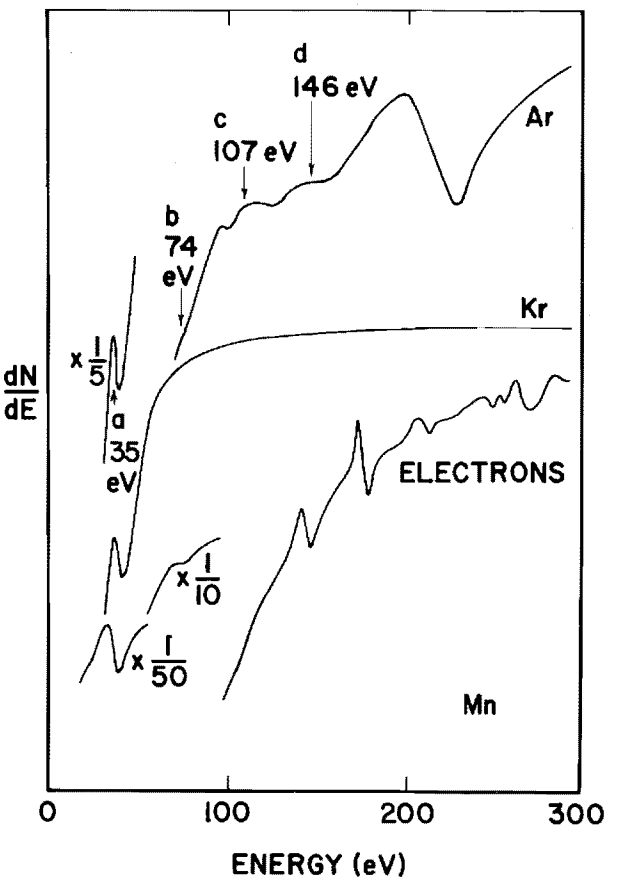

FIG. 2. Auger spectra induced by impact of 3-keV electrons and 100-keV Ar^+ and Kr^+ ions on a manganese target. The various indicated features are identified in the text.

 0021-8979/80/084437-07$01.10

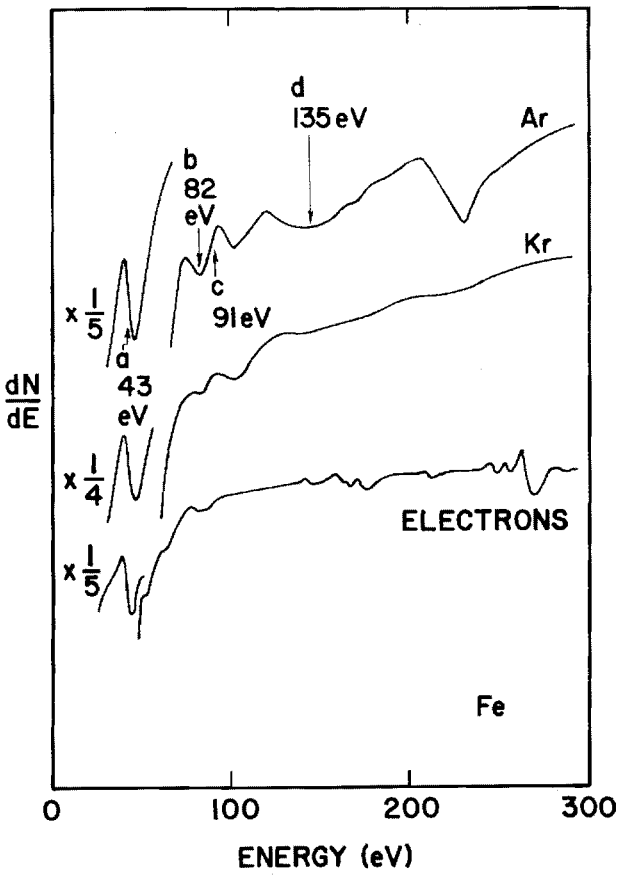

FIG. 3. Auger spectra induced by impact of 3-keV electrons and 100-keV Ar^+ and Kr^+ ions on an iron target. The various indicated features are identified in the text.

dary electron peak, on which some workers have found a great deal of structure,[16-18] with higher-energy Auger peaks from the target and the bombarding species up to about 300 eV.

The mechanism for formation of the inner-shell hole required to create an Auger electron is understood in terms of the electron promotion model of Barat and Lichten.[19] In this model, the electron energy levels of the two ions are perturbed as they approach each other, allowing levels on different ions to become degenerate. This permits electron promotion from a filled inner shell on one atom to an unfilled shell on either atom, creating an inner-shell hole which can subsequently decay by an Auger process.

The ion-induced Auger spectrum is not identical to that observed with electron bombardment,[7,11] the metal peaks tending to be sharper, more symmetric and largely independent of surface contamination.[20] We have proposed that in the case of Be, Al, and Si targets bombarded by Ar^+ the Auger electrons are primarily from sputtered neutral atoms.[21]

In the work reported here we have examined in some detail the ion-induced Auger spectrum of transition metals (Cr, Mn, Fe, and Co) in order to understand the mechanisms giving rise to the Auger emission.

II. EXPERIMENTAL METHODS

Our experimental arrangement consisted of an UHV chamber capable of base pressures below 10^{-10} Torr linked via a differentially pumped beam line to a 20–200-keV ion-implantation accelerator. A standard commercial cylindrical-mirror electron energy analyzer (CMA) with an axial electron gun was used to monitor ion-induced electron emission and surface cleanliness.

The ion-beam axis was 95° from the CMA axis with the sample normal lying between, and coplanar with, the two axes at an angle of 60° or 65° from the ion beam. Thus electrons were detected in an annulus 53°–137° from the ion beam. Ion-beam currents were between 1 and 20 μA, while the pressure varied from 7×10^{-10} to 6×10^{-9} Torr with the beam on. Ion-beam energies of 20–200 keV were used for all the data reported here. Comparison electron-induced Auger spectra were taken with a 3-keV 10-μA beam. Modulation of the CMA was 5 V peak to peak. Polycrystalline samples of Cr, Mn, Fe, and Co were mechanically and chemically polished and cleaned *in situ* by 100 keV Ar^+ or Kr^+ bombardment to remove most of the carbon and oxygen contamination. Specta were taken in the differential mode commonly used in Auger measurements and built up over a period of several minutes using a multichannel ana-

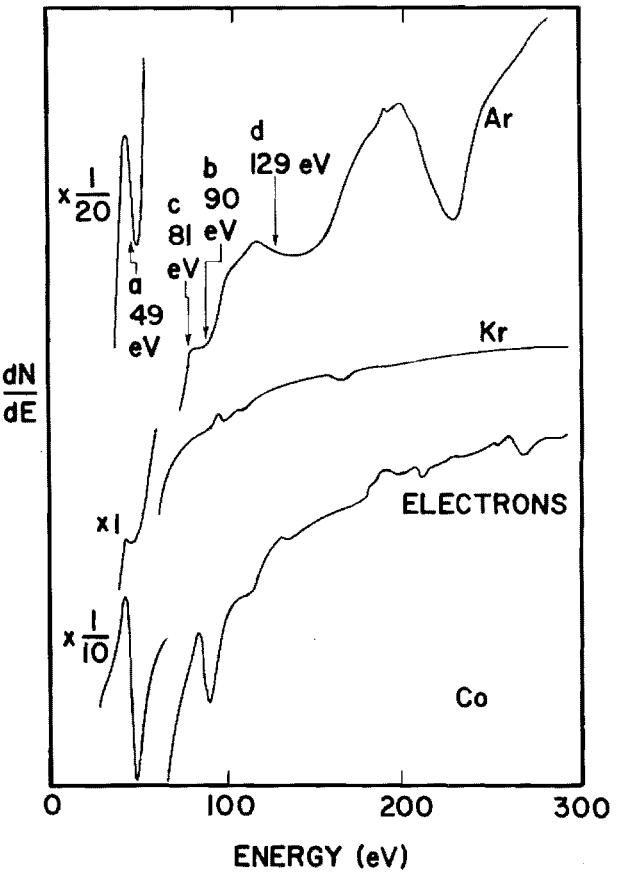

FIG. 4. Auger spectra induced by impact of 3-keV electrons and 100-keV Ar^+ and Kr^+ ions on a cobalt target. The various indicated features are identified in the text.

TABLE I. Relative intensities under 100-keV Ar $^+$ bombardment.

	Metal $M_{23}M_{45}M_{45}$ peak	Ar LMM peak
Cr	1	1
Mn	1.2	0.9
Fe	0.6	0.2
Co	0.2	0.02
	$L_{2,3}$ MM peak	
Si	7.3	0

lyzer to increase the signal/noise ratio. The surface chemical composition was routinely monitored by Auger spectroscopy. After cleaning the surfaces contained no more than 0.02 monolayers of carbon and 0.2 monolayers of oxygen. The targets were periodically heated to 150 °C, but no attempt was made to anneal ion-induced defects.

III. RESULTS

The Auger spectra of Cr, Mn, Fe, and Co are shown in Figs. 1–4 for 100-keV Ar $^+$ and Kr $^+$ bombardment; for each case we show for comparison a spectrum induced by 3-keV electron impact. The spectra are as directly measured by the CMA and therefore the energies are referenced to vacuum. Certain features are readily identifiable. The lowest-energy peak on each ion-induced spectrum (indicated by the letter a on Figs. 1–4) occurs also under electron bombardment and is well-known to be a $M_{23}M_{45}M_{45}$ transition in the target metal. At around 216 eV there is a broad peak which is observed under Ar $^+$ bombardment, but not for Kr $^+$ or electron impact. This peak is at the position expected for LMM transitions in Argon; the breadth will be explained later in terms of a Doppler effect due to the motion of the Argon projectiles. Between these two peaks there is a variety of additional structure particularly for Kr $^+$ on Cr and Ar $^+$ on Fe. These ion-induced spectra were independent of whether the surface was cleaned and analyzed with the same inert-gas ions or cleaned with one ion species and analyzed with the other. No time-dependent effects were observed once the surface was clean although on a dirty surface the metal $M_{23}M_{45}M_{45}$ peak was less pronounced than on a clean surface. The relative sizes of the various Auger peaks was independent of beam intensity, beam focusing, and angle of incidence on the target. We are, therefore, confident that the various peaks are not artifacts of the apparatus nor of of the CMA.

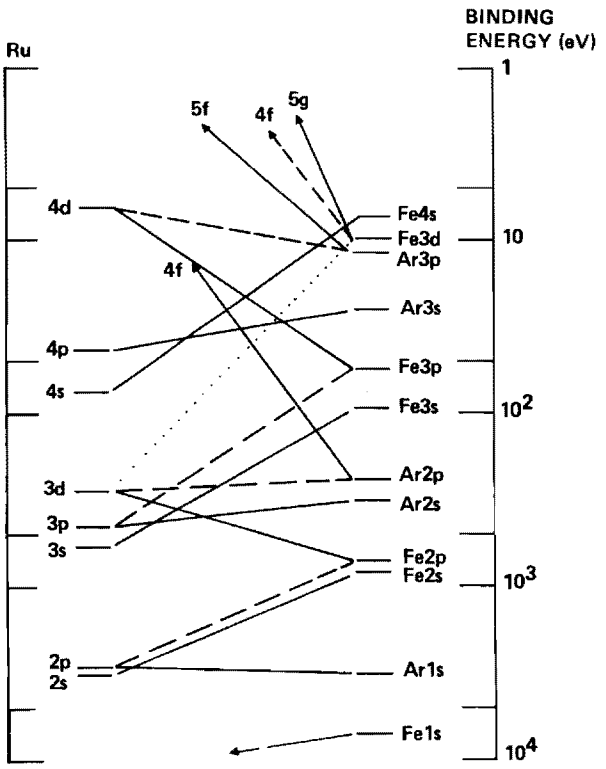

FIG. 5. Correlation diagram for Ar $^+$ + Fe collisions.

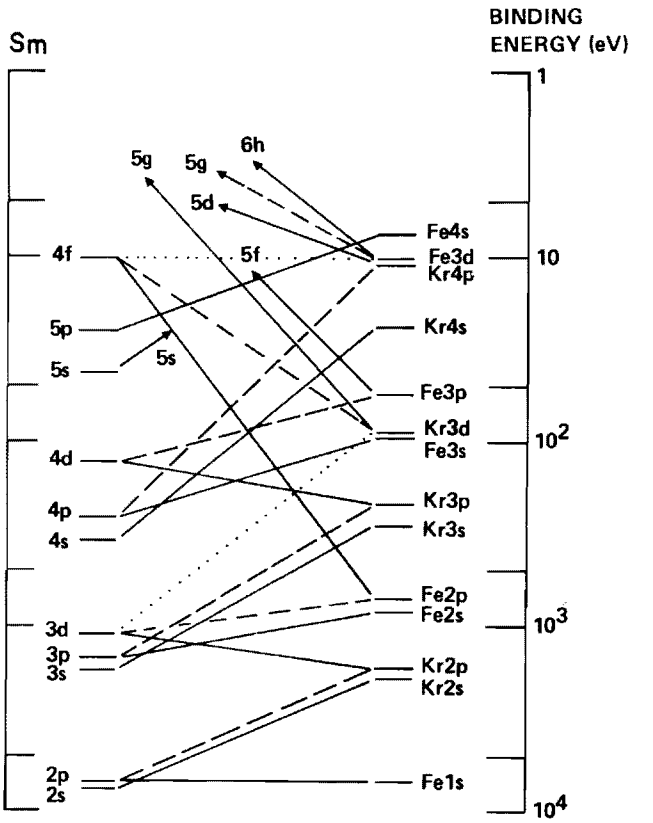

FIG. 6. Correlation diagram for Kr $^+$ + Fe collisions.

With some uncertainty in the beam current density distribution and detection sensitivity over the beam spot, it is not possible to measure absolutely the intensity of the various features. It is however, of interest to measure the relative intensity of the features utilizing fixed ion beam and detection conditions. For this purpose we define intensity as the peak-to-peak height of an Auger feature. In Table I we show the relative intensities of the metal $M_{23}M_{45}M_{45}$ peak and Ar $L_{23}MM$ peak for Ar $^+$ on Cr, Mn, Fe, and Co and the $L_{23}MM$ peak of Si for Ar $^+$ on Si; the values for Cr are set to unity.

IV. DISCUSSION

In Figs. 5 and 6 we show the Fe-Kr and Fe-Ar correlation diagrams drawn according to the prescriptions of Barat

and Lichten[19]; the diagrams for the other target cases are approximately the same and have not been drawn here. Figure 5 shows immediately that strong promotions should occur from the $2p$ shell of Ar leading to LMM lines of Argon. This is in fact seen in Figs. 1–4 as the broad peak at about 216 eV. From Fig. 6 we would expect no promotions from the $2p$ shell of Kr so explaining the absence of a Krypton LMM or LNN transition in the observed spectra. From both Figs. 5 and 6 one would expect promotions from the $3p$ shell of the metal leading to $M_{23}M_{45}M_{45}$ Auger electrons. These are observed as the lowest-energy peak in the ion-induced spectra of Figs. 1–4 and are also seen in the electron-induced spectra. Promotion of the metal $3p$ electron can occur also in symmetric collisions (e.g., Fe + Fe) in the collision cascade.

A. Metal $M_{23}M_{45}M_{45}$ transitions

These are the lowest-energy peaks, visible in all the spectra. The are indicated by the letter a on Figs. 1–4. The ion-induced Auger peaks show an increase in energy of about 1.7 eV over the corresponding peaks due to electron impact, although the width (measured as the energy difference between positive and negative excursions) is similar. The excitation event is caused by a collision between heavy particles resulting in substantial energy transfer to the excited atom. This motion of the species which emits the Auger electron may give rise to shifts of the Auger line. If the excited species is ejected out of the solid, the emitted line will be that of an isolated atom. Using the solid-state correction of Larkin[22] and allowing for the work function, this should lower the Auger line energy for the $3d$ transition metals by about 4.5 ± 2 eV. This is not consistent with our observations which show an increase in Auger line energy. Auger electrons emitted by atoms ejected out of the target will also exhibit a Doppler shift and for the configuration of the present experiment, the majority of sputtered atoms will move towards the observer causing an increase in the observed Auger line energy. This would produce a shift in the observed direction, but we would require the ejected particle energies to be of the order of 2 keV or more to explain the magnitude of the shift, calculated by the formula given by Dahl *et al.*,[23] which seems to be unreasonably high. We are, therefore, unable to offer any convincing explanation of the small energy shift of the metal $M_{23}M_{45}M_{45}$ lines.

Table I shows that the $M_{23}M_{45}M_{45}$ line intensity varies rapidly through the transition-metal series and is considerably smaller than the LMM intensity for a light element such as Si.

B. Metal $M_1M_{45}M_{45}$ transitions

Peaks seen weakly at 64, 74, 82, and 90 eV in Cr, Mn, Fe, and Co, respectively, are[24] the metal $M_1M_{45}M_{45}$ Auger transitions; in Figs. 1–4 they are indicated by the letter b. According to the promotion diagram of Fig. 5 the metal $3s$ level should not be ionized by the direct projectile-target collision. Some more complicated event or sequence of events is taking place. Possibly a target atom recoiling from a projectile-target collision with a $3p$ vacancy collides subsequently with a further target atom causing the vacancy to be transferred to a $3s$ level.

C. Ar LMM transitions

The argon $L_{23}M_{23}M_{23}$ peak lying at about 216 eV in Figs. 1–4 is much broader than one would expect from an isolated stationary atom. We propose that the principal source of such electrons is Ar^+ ions scattered out of the surface and that the line width and shift is due to the Doppler effect related to the recoil speeds and directions of the Ar^+ ions. Figure 7 shows the Auger spectrum induced by Ar^+ impact on Fe for a variety of projectile energies from 20 to 200 keV; the angle of incidence in this case is 65° from the target surface normal. The negative excursion of the line shifts progressively to higher energies as projectile energy is increased; this is to be expected if the Auger electrons come primarily from Ar^+ ions scattered towards the observer and the average recoil energy increases with projectile energy. The most satisfactory method of confirming this contention would be to compute the line shape and compare to the experiment. This is not readily possible due to the complicated annular geometry of the CMA and the lack of detailed information on energy distributions of scattered Ar^+ ions. As an alternative we shall perform a simple calculation of the Doppler shift expected for recoils into a somewhat arbitrar-

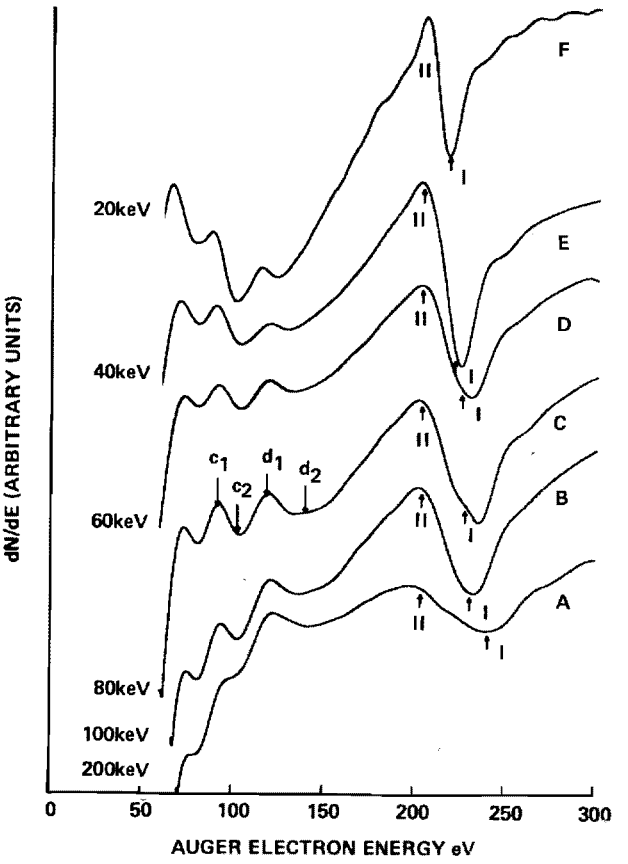

FIG. 7. Auger spectra induced by Ar^+ impact on Fe at energies from 20 to 200 keV. The various indicated features are identified in the text.

ily chosen direction and demonstrate that this is consistent with the progressive change in line shape.

To perform the calculation we consider the case of Ar^+ ions scattered specularly from the surface; this should represent a direction where a large flux of projectiles will occur. We further consider only those Auger electrons emitted in the plane of the projectile and recoil beams. The scattered Ar^+ ion energy is calculated from conservation of energy and momentum in a biparticle $Ar^+ + Fe$ collision on the surface. The Doppler shift is calculated from the formula by Dahl *et al.*[23] An Auger $L_{23}M_{23}M_{23}$ line from a stationary atom will have[25] a group of lines between 203 and 206 eV which in the derivative mode of recording spectra with our CMA will produce a single peak with a positive excursion at 203 eV and a negative excursion at 206 eV. We take the calculated shift obtained by the prescription given above and simply add it to 206 eV to provide a prediction of how the negative excursion should vary with projectile energy; this calculated energy is designated by the symbol I on Fig. 7. On this simple model there should be no downward shift of Auger electron energy since we include no projectiles scattered away from the observer; the positive excursion should therefore remain invariant with projectile energy at the stationary atom value of 203 eV, and this is shown by the symbol II on Fig. 7. The positions of points I and II evaluated in this manner do in fact agree very well with the position of the negative and positive excursions, confirming that the changes in peak position and width are consistent with the Doppler effect. It is also clear that in the limit as projectile energy tends to zero the argon line position extrapolates to the value expected for a free Ar^+ ion. We offer no definite explanation of the weak structure seen on the negative excursion of the argon line for 60- and 80-keV impacts. We do note that the backscattered energy spectrum for Ar^+ ions on polycrystalline materials does show a broad continuum with a sharp peak superimposed due to surface scattering.[26] If recoils with L-shell vacancies have such an energy distribution, the Doppler-broadened line shape of the emitted Auger electrons will have a double-peak structure on the negative excursion.

The lifetime of the argon L_{23} vacancy is estimated by McGuire[27] to be 3.5×10^{-15} sec. Thus for an argon ion with a speed of 2.2×10^{7} cm sec^{-1} (10-keV energy) the decay length is 7.7 Å. Recoils with low energy will therefore frequently undergo the Auger decay event while still interacting with the metal surface. Inevitably this will cause some shift or broadening of the emitted Auger line, further adding to the complexity of the line shape.

The data in Table I shows that the cross section for excitation of the argon Auger line decreases rapidly with increasing atomic number. This in accord with the results found at lower energies.[13,28]

D. Kr Auger lines

According to the promotion diagram of Fig. 6 one would have expected formation of $3d$ vacancies in Kr followed by emission of $M_{45}NN$ Auger electrons at 63 eV.[24] No such line is observed.

The 97-eV line in the $Kr^+ + Cr$ spectrum (Fig. 1) has an energy corresponding to that expected for a $M_3M_{45}N_{23}$ transition in Kr.[24] According to Coghlan and Clausing[24] this should be the most intense line resulting from a $3p$ vacancy. The line width (about 10 eV) is consistent with the Doppler broadening to be expected if the krypton atom is recoiling from the target. It is, however, puzzling that this line does not occur in the case of the other targets. Moreover, according to Fig. 6 the $3p$ vacancy in Kr should not occur due to a single promotion in a Kr^+ collision with a target atom. We consequently regard the identification of this line as only tentative and offer no explanation as to why it occurs only for Cr targets.

Discussion of the krypton spectrum in terms of the correlation diagram of Fig. 6 is probably inadequate. Many of the curve crossings shown in Fig. 6 will be avoided; this occurs specifically when the two intersecting levels have the same angular momentum and parity.[29] Thus the $5g\,\sigma$ level (connecting Kr $3d$ to the $5g$ state of the united atom) will not cross the $4s\,\sigma$ level (connecting Kr $4s$ to the $4s$ state of the united atom). Consequently, the apparently strong $5g$ promotion shown in Fig. 6 will not occur and vacancies will not appear in the $3d$ level of Kr. This may explain the absence of the $M_{45}NN$ transitions. We also note that the whole concept of "crossing" is questionable when the subshell splitting is comparable with the promotion energy,[29] a situation which certainly holds for the M and N shells of the projectile and target.

E. Other features

In the Ar^+ ion induced spectra there are a number of weak features in the 90–200-eV region that cannot be identified as either metal or rare-gas Auger lines. Care was taken to ensure that they were not spurious or impurity related. Movement of these peaks with sample bias showed that they were not an artifact of the beam or of its interaction with, for example, the CMA aperture. They did not result from contaminants since they were independent of the surface condition after initial cleaning. Moreover, the only element with an Auger line close to our observed peaks is phosphorus, which was not detected in the electron-induced Auger spectrum. Deliberately implanting enough phosphorus to be detectable in the electron-induced Auger spectrum did not effect the ion-induced spectrum.

It is impossible that the extra features are interatomic Auger peaks resulting from transitions between the bombarding and target ions. In this type of transition a core hole on one atom is filled by an electron either from that atom or from a neighboring atom, with the ejection of an Auger electron from the neighboring atom. Thus one obtains transitions of the type $K_AM_BM_B$ or $K_AM_AM_B$, where K_A, K_B, etc., are energy levels on the atoms A and B. Transitions of this type have been seen in a number of systems.[30,31] The interatomic transition rate depends on the spatial overlap of the initial hole state (K_A) and the annihilating electron state (M_A or M_B), as well as the initial state of the ejected electron and its continuum wave function.

When two atoms collide, the spatial overlap of different energy levels is greatly enhanced over the overlap in an alloy or compound. To create an Ar $2p$ hole in an Ar-Fe collision, for example, the nuclear separation must be less than about[28] 0.2 Å. This would make possible a large number of interatomic transitions which cannot usually occur in alloys or compounds.

From Figs. 5 and 6 it can be seen that the most readily ionized core levels of the projectile are the Ar $2p$, Kr $3d$, and possibly Kr $3p$. Thus, to account for the peaks we observe, any interatomic transition must involve a core hole in one of these levels. Further, the ejected electron will probably come from a delocalized orbital such as Fe $3d$ or $4s$ or an orbital which tends to become delocalized during the collision such as Fe $3p$, Ar $3p$, Kr $3p$, or Kr $4p$. There are a large number of transitions of the type Ar (L_{23}) Metal (MM) and Kr (M_3) Metal (MM) which would produce Auger electrons in the energy range under consideration. Allowing for the resolution of the analyzer and possible small Doppler broadening effects, most of these transitions would not be resolved. It is also not possible to determine *a priori* which of the many possible transitions are the most likely to occur. To illustrate that the interatomic transitions can provide an explanation of the observed features we shall concentrate on the case of Ar^+ colliding with Fe. Figure 7 shows the collisionally induced Auger spectrum for this case as a function of projectile energy. There are two distinct lines indicated as a c and d, which lie well below the Ar LMM Auger group and do not appear in the electron-induced spectrum of the target material (see Fig. 3).

Peak c extends from a positive excursion at c_1 to a negative excursion at c_2. The width (measured as energy $E_{c_1} - E_{c_2}$) decreases slightly from 13 to 6 eV as the projectile energy increases from 20 to 200 keV. We ascribe this peak to an Ar (L_{23}) Fe (M_1, M_{23}) transition; from the solid-state binding energies of Coghlan and Clausing[24] we would estimate the energy of this transition to be 91 eV which is in good agreement with the observed peak position. An interatomic transition will involve perturbed energy levels of the colliding partners. Furthermore, the energy of the emitted electron will be depressed due to its interaction with the potential of the other atom; this causes a depression and broadening of the emitted line known as the "Berry" effect.[23] This line broadening ΔE_B for a projectile of mass M (amu) with an energy T_i (keV) interacting with a second atom of charge ne and having a core-hole lifetime of τ sec is given by[23]

$$\Delta E_B = 1.07\, b = 1.07\, \frac{n 3.30\times 10^{-15}}{\tau} \left(\frac{M}{T_i}\right)^{1/2} \text{eV}. \quad (1)$$

Clearly the line width decreases with increasing projectile energy, in accordance with the observed behavior of line c. If we plot the line width as a function of $T_i^{1/2}$ and n is taken as unity, then we derive an effective value of τ of about 3.3×10^{-16} sec. In this time a 20-keV Ar^+ ion will move only about 1 Å, and a 200-keV Ar^+ ion only about 3 Å. It is therefore reasonable to argue that the decay of the Ar L_{23} vacancy occurs while the projectile interacts with the target atom and therefore an interatomic transition is possible. This lifetime is, of course, and order of magnitude shorter than that of an isolated argon atom.[27] However, it is known that the interatomic transitions can greatly reduce hole lifetimes[30] and that the lifetime of L_{23}, shell vacancies are reduced by an order of magnitude when in a matrix.[32] Thus our lifetime estimate is not unreasonable. There is no appreciable Doppler effect because the source of the monitored electron is an Fe atom which is either at rest in the matrix or recoils with a relatively low velocity. It is to be noted that as projectile energy increases to 200 keV the magnitude of this peak becomes small compared with the other features. This is to be expected since with the increased projectile speed the time of interaction between projectile and target will decrease, so reducing the probability of an interatomic transition.

Peak d has a width ($E_{d_1} - E_{d_2}$) which increases significantly with increasing projectile energy. We ascribe this peak to a transition of the type Ar (L_{23}) Fe (M_1) Ar (M_{23}) whose energy from a stationary system is about 135 eV.[24] The increase of width with projectile energy is similar to that of the argon line designated I and II on Fig. 7. This shows that the width change is again a Doppler effect due to the fact that the observed electron comes from the projectile Ar which is in motion.

There are in fact at least eight interatomic transitions for Ar^+ projectiles in the energy region 90–200 eV and we would not claim that the above discussion provides positive identification of peaks c and d. We do, however, conclude that these peaks are due to interatomic transitions and that the electron in peak c comes from an Fe atom in the matrix, and for peak d the electron comes from a moving projectile. We have also indicated the position of the corresponding transitions for Cr, Mn, Fe, and Co targets on Figs. 1–4 and there is a correspondence between observed features and the predicted line position particularly for Mn, Fe, and Co.

In the case of krypton impact there are few distinct features other than the metal $M_{23}M_{45}M_{45}$ peak. In the case of Kr^+ on Cr, there is a distinct line at 97 eV which we have ascribed to the $M_{23}M_{45}M_{45}$ transition in krypton, meaning that in this case there are inner-shell vacancies produced in the projectile. The second subsidiary (peak e on Fig. 1) could be an Kr (M_3) Cr ($M_{23}M_{23}$) peak for which we would calculate[24] an energy of 124 eV in essential agreement with the observed peak position. In the remaining Kr^+ impact spectra there is no definite identification of krypton peaks and no definite subsidiary structures. We would conclude that vacancy formation in the krypton has a small cross section and therefore interatomic lines (which involve the projectile vacancy) are not observed.

CONCLUSIONS

The Auger spectra induced by impact of Ar^+ and Kr^+ ions on Cr, Mn, Fe, and Co differ markedly from the spectra induced by electron impact on these same metals. The only common feature is excitation of the metal $M_1M_{45}M_{45}$ and $M_{23}M_{45}M_{45}$ lines which lie at quite low energies. Ar^+ impact also produces the Doppler-broadened

$L_{23}M_{45}M_{45}$ line of argon whose width and shape is consistent with the primary source of electrons being projectiles scattered out of the surface. Formation of the L_{23} vacancy is consistent with electron promotion during the interaction of the projectile with a target atom. With the possible exception of a $M_{23}M_{45}M_{45}$ line in $Kr^+ + Cr$ collisions we identify no sizeable spectral features from krypton induced by Kr^+ impact on the various targets. For Ar^+ impact there are a variety of additional features in the energy region 90–200 eV which cannot be identified as due either to the target system or to the projectile system. We propose that these lines are interatomic transitions where the vacancy created in the inner shell of a projectile by the promotion mechanism is filled by a transition involving electrons of the target atom.

ACKNOWLEDGMENT

This work was supported in part by the solid-state chemistry program of the NSF.

[1]See, for example, the references cited by M. Barat and W. Lichten, Phys. Rev. A **6**, 211 (1972).
[2]J. -F. Hennequin and P. Viaris de Lesegno, Surf. Sci. **42**, 50 (1974).
[3]P. Viaris de Lesegno, G. Rivais, and J. -F. Hennequin, Phys. Lett. **49A**, 265 (1974).
[4]P. Viaris de Lesegno and J. -F. Hennequin, Rev. Phys. Appl. **12**, 927 (1977).
[5]N. Benazeth, J. Agusti, C. Benazeth, J. Mischler, and L. Viel, Nucl. Instrum. Methods **132**, 477 (1976).
[6]C. Benazeth, N. Benazeth, and L. Viel, Surf. Sci. **65**, 165 (1977).
[7]J. T. Grant, M. P. Hooker, R. W. Springer, and T. W. Haas, J. Vac. Sci. Technol. **12**, 481 (1975).
[8]F. Louchet, L. Viel, C. Benazeth, B. Fagot, and N. Colombie, Radiat. Eff. **14**, 123 (1972).
[9]J. Ferrante and S. V. Pepper, Surf. Sci. **57**, 420 (1976); **58**, 613 (1976).
[10]L. Viel, C. Benazeth and N. Benazeth, Surf. Sci. **54**, 635 (1976).
[11]R. A. Powell, J. Vac. Sci. Technol. **15**, 125 (1978).
[12]P. Viaris de Lesegno and J. -F. Hennequin, Surf. Sci. **80**, 656 (1979).
[13]P. Viaris de Lesegno and J. -F. Hennequin, J. Phys. (Paris) **35**, 759 (1974).
[14]A. A. Dorozhkin, A. A. Petrov, and N. N. Petrov, Sov. Phys. Solid State **20**, 1660 (1978).
[15]P. B. Needham, Jr., T. J. Driscoll, C. J. Powell, and R. J. Stein, Appl. Phys. Lett. **30**, 357 (1977).
[16]S. Ya. Lebedev, N. M. Omel'yanovskaya, and V. I. Krotov, Sov. Phys. Solid State **11**, 1294 (1969).
[17]W. Kruger, A. Scharmann, and N. Stiller, Nucl. Instrum. Methods **132**, 483 (1976).
[18]W. Soszka, Surf. Sci. **74**, 636 (1978).
[19]M. Barat and W. Lichten, Phys. Rev. A **6**, 211 (1972).
[20]E. W. Thomas, K. O. Legg, and W. A. Metz, Nucl. Instrum. Methods. **168**, 379 (1980).
[21]W. A. Metz, K. O. Legg, and E. W. Thomas, J. Appl. Phys. (unpublished).
[22]F. P. Larkins, At. Data and Nucl. Data Tables **20**, 311 (1977).
[23]P. Dahl, M. Rodbro, B. Fastrup, and M. E. Rudd, J. Phys. B **9**, 1567 (1976).
[24]W. A. Coghlan and R. E. Clausing, At. Data **5**, 318 (1973).
[25]L. O. Werme, T. Bergmark, and K. Siegbahn, Phys. Scr. **8**, 169 (1973).
[26]T. M. Buck, Y. S. Chen, G. H. Wheatley, and W. F. Van der Weg, Surf. Sci. **47**, 244 (1975).
[27]E. J. McGuire, Phys. Rev. A **3**, 587 (1971).
[28]F. W. Saris, Physica (Urecht) **52**, 290 (1971).
[29]W. Lichten, Phys. Rev. **164**, 131 (1967).
[30]For a brief review see P. H. Citrin, J. Electron. Spectrosc. Relat. Phenom. **5**, 273 (1974).
[31]P. H. Citrin and D. R. Hamman, Phys. Rev. B **10**, 4948 (1974).
[32]P. Joyes and J. -F. Hennequin, J. Phys. (Paris) **29**, 483 (1968).

516 Nuclear Instruments and Methods in Physics Research B2 (1984) 516–519
North-Holland, Amsterdam

INNER SHELL VACANCIES IN SPUTTERED ATOMS

E.W. THOMAS and R. WHALEY

School of Physics, Georgia Institute of Technology, Atlanta, GA 30332, USA

Impact of heavy ions (Ne^+, Ar^+) on surfaces of Mg, Al and Si are known to produce Auger spectra characteristic of 2p vacancies in the target species. Excitation is largely by recoil collisons in the target matrix leading to curve crossing events. A detailed modelling of the observed spectrum is performed which accounts for all significant features. An underlying continuum is shown to be due to secondary electrons and to decay of atoms in the matrix. An apparent discrepancy between the high energy edge of electron and ion induced spectra is due to a hitherto unidentified line in the ion induced spectrum. Dominant line features of the ion-induced spectra are due to sputtered neutral atoms with a single L-shell vacancy. Electron configurations and measured excitation energies are for Mg ($2p^5 3s^2 3p$) 50.6 eV, for Al ($2p^5 3s^2 3p^2$) 73.8 eV and for Si ($2p^5 3s^2 3p^3$) 101.1 eV.

1. Introduction

Auger spectra induced by impact of heavy ions (e.g. Ne^+ and Ar^+) on Mg, Al,, and Si show a group of sharp lines superimposed on an underlying continuous background [1]. Grant et al. [2] first pointed out that the underlying continuum is similar to the spectrum induced by electron impact and suggested that the origin is decay by LVV transitions of atoms in the solid matrix. The line spectra bear no resemblance to LVV transitions of the matrix and have been variously ascribed to sputtered particles decaying in free space [1] to plasmon losses within the collision cascade [3] or to decays of "quasi-atomic" atoms displaced from normal lattice sites by the collision cascade [4]. It is generally agreed that excitation is by formation of a 2p vacancy due to an adiabatic curve crossing event [1]; since the spectra are similar for both Ne^+ and Ar^+ impact [5] the predominant excitation events are collisions between recoiling atoms rather than projectile–target events.

We have previously suggested [1] that the sharp lines are due to sputtered atoms and ions with one L-shell vacancy. We were, however, unable to provide an accurate match between predicted and observed line energies. The present work was undertaken to revise the identification of lines by providing a detailed model of the whole spectrum. We shall show that a key factor of this procedure is the identification of a hitherto unrevealed line.

2. Experimental

Auger spectra induced by 20–200 keV Ne^+ and Ar^+ impact on polycrystalline Mg, Al and Si were recorded using the experimental facilities described earlier [1]. The ion beam was produced by a conventional ion implanter and impacts on the surface at 70° to the surface normal. Auger spectra are analyzed with a conventional Varian CMA placed with its axis at 95° to the ion beam direction. Spectra were generally similar to those we have presented earlier [1] but with an improved energy resolution of 0.5 eV. We prefer to show the integral forms of the spectra believing that these provide a better indication of relative importance of features than do derivative spectra. In fig. 1 we show as

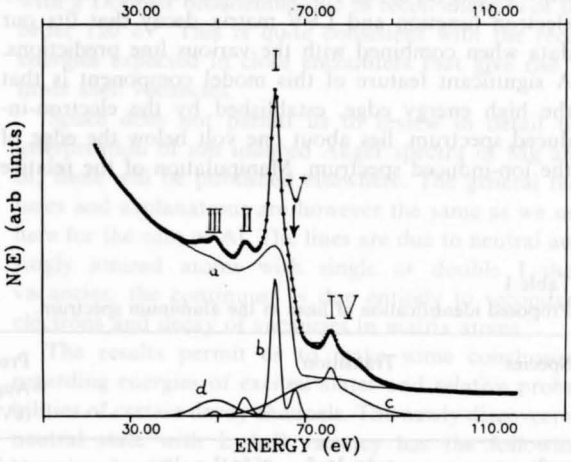

Fig. 1. Auger spectrum induced by impact of 100 keV Ar^+ on Al. The data points are the experimental record, while the line through them is the result of our modelling procedure. Certain components of the model are also shown separately. Line (a) is the secondary electron and matrix decay component alone; line (b) represents the individual lines from one-electron vacancies in sputtered atoms and ions; line (c) is the matrix and line component due to two-electron vacancies; line (d) represents the enhanced surface plasmon.

an example of the spectrum induced by Ar^+ impact on Al. This is similar to integral spectra published previously by Viel et al. [4] and is consistent also with derivative spectrum by Grant et al. [1].

The spectra for Mg, Al and Si are qualitatively similar. There are three sharp peaks (labelled I, II and III) which are generally ascribed to an L shell vacancy in an atomic like state plus a fourth peak (IV) that is often ascribed to a double L shell vacancy. Underlying the peaks is a continuous distribution. We shall see later that there is in fact a fifth distinct line.

3. Discussion

To define our detailed modelling procedure we concentrate on the case of the Al spectrum shown in fig. 1. As a first step to understanding this spectrum we shall attempt to model the underlying continuum distribution. We anticipate a contribution due to true secondary electrons peaking at low energies. This we describe by the function given by Sickafus [6] and we normalize this to the observed spectrum at low energies (< 20 eV) and high energies (> 100 eV) where no atomic like features are anticipated. We expect also an LVV peak with a loss tail to lower energies that is due to decay of excited atoms in the matrix. This should be identical to an electron induced Auger spectrum and we record this within our own apparatus. The LVV component must also be adjusted in magnitude to fit the observed spectrum. Anticipating our final result we show as line (a) in fig. 1 a sum of the Sickafus secondary electron function and LVV matrix decay that fits our data when combined with the various line predictions. A significant feature of this model component is that the high energy edge, established by the electron-induced spectrum, lies about one volt below the edge of the ion-induced spectrum. Manipulation of the relative magnitudes of the contributing components does not eliminate the discrepancy. The effect has been noted previously in Al by Baragiola [7] and is also seen in Si both in our own spectra and in the work of Wittmaack [5]. We have examined the apparent shift carefully and conclude that it is real. Thus the apparent edge of the ion-induced spectrum is not at the same location as the LVV matrix transition edge. We shall see later that there is in fact an additional peak at this location due to an atomic transition. Identification of this peak is a major step in fixing the location of other atomic transitions and the feature occurs also for Si as a very distinct shoulder. We shall for convenience refer to this as peak V.

We turn now to the detailed identification of the peak. Following our previous work [1] we will identify peaks I, II, III and V as due to sputtered Al^+ and Al^0 particles with single L-shell vacancies and peak IV as due to sputtered particles with two L-shell vacancies. We have proposed [1] that the neutral Al is in the state $2p^5 3s^2 3p^2$; thus an electron has been removed from the 2p-shell but an electron added to the 3p-shell to maintain neutrality. We estimate the energy of this state to be 72.35 eV by an argument [1] that the difference between energies of a state $2p^5 3s^2 3p^2$ and $2p^5 3s^2 3p$ in an element of atomic number Z is the same as the energy difference between states of configuration $2p^6 3s^2 3p^2$ and $2p^6 3s^2 3p$ in an element $Z+1$. All required energies can be obtained from the work of Shirley et al. [8] and of Moore [9]. In table 1 we propose various transitions leading to decay of this state and estimate Auger electron energies. As indicated previously [1] these predicted transitions are in only approximate agreement with the observed features I and II in fig. 1. However the energy of the parent level is only a crude estimate and we may permit some variations in the energies of this group provided always that energy separation of lines is held fixed. If we raise the energy of

Table 1
Proposed identification of lines in the aluminum spectrum.

Species	Transition		Predicted Auger energy (eV)	Observed Auger energy (eV)	Peak identification
Al^0	$2p^5 3s^2 3p^2$	$-2p^6 3s^2$ (^1S)	66.37	67.8	V
		$-2p^6 3s3p$ (^3P)	61.74	62.2	I
		$-2p^6 3s3p$ (^1P)	58.95	absent	
		$-2p^6 3p^2$ (^1D)	55.78	absent	
		$-2p^6 3p^2$ (^3P)	54.71	56.2	II
Al^+	$2p^5 3s^2 3p$	$-2p^6 3s$ (^2S)	55.7	55.7	II
		$-2p^6 3p$ (^2P)	49.0	49.0	III
Al^+	$2p^4 3s^2 3p^2$	$-2p^5 3s3p$ (^3P)	75.3	76.0	IV

the $2p^5 3s^2 3p^2$ state to 73.8 eV then all lines are shifted up by 1.45 eV and three of the proposed transitions agree exactly with the location of peak I, peak II and with the newly identified peak V. We suggested also [1] that lines due to decay of the $2p^5 3s^2 3p$ state of Al^+ are present. The proposed transitions and their energies predicted from the work of Shirley et al. [8] and of Moore [9] are given also in table 1. In the case of these Al^+ lines the energy levels are well known and no significant error is anticipated; the two predicted Auger energies coincide exactly with peaks II and III of fig. 1. At this point we should also examine line IV which is generally ascribed [1,4,7] to a two electron vacancy. We propose that the line is a sputtered Al^+ ion with two L-shell vacancies ($2p^4 3s^2 3p^2$) and that decay is to a $2p^5 3s3p$ (^3P) configuration. We chose this particular decay path since the analogous transition in the one vacancy state appears to be responsible for the most intense line of the Al^0 spectrum; line I in fig. 1. Other transitions giving different final state configurations are of course also possible but if branching ratios are the same as for Al^0 the lines should be of negligible intensity. The energy level of the parent level is estimated by assuming the energy difference between $2p^4 3s^2 3p^2$ and $2p^5 3s^2 3p^2$ configurations in Al is the same as that for the $2p^5 3s^2 3p^2$ and $2p^6 3s^2 3p^2$ states of Si. The energy difference for the Si states comes from the work of Shirley et al. [8] and the energy of the $2p^5 3s^2 3p^2$ state of Al has been estimated above. The estimated energy of the parent level is 178.4 eV and the predicted energy of Auger electrons in the assumed transition is 75.3 eV agreeing almost exactly with the location peak IV in fig. 1. The agreement is undoubtedly fortuitous as the energies of both parent and daughter level are crude estimates. We do not regard the present work as a unique identification of this feature.

In principle we may now attempt a fit to the observed spectrum. The underlying background has already been represented by a superposition of Sickafus function and the electron induced spectrum. Each individual line given in table 1 is represented by a Gaussian line shape, line width and height is adjusted to fit the observations. We also permit a variation in line position (though not separation) for all lines from Al^0 to allow for a possible error in estimate of parent level energy. Such a fitting allows a modelling of most major features but two areas of discrepancies occur. The first, and most obvious, is a broad feature underlying line IV. This corresponds exactly to the expected location of matrix transitions from double L-shell vacancies. Such a feature is seen weakly on electron induced spectra. Apparently under ion impact this feature is more strongly excited. The second discrepancy is a weak feature to the low energy side of line III. This is precisely the location of the bulk plasmon in Al and while present in the electron induced spectrum is more intense under ion impact. To take these two features into account we add to the model broad Gaussian features centered at 74 and 49 eV. With these additions the observed spectrum can be reproduced exactly as is shown in fig. 1; the figure shows also certain of the individual components in the fit.

4. Conclusion

We would conclude that the general explanation of the ion-induced spectrum published earlier [1] is indeed correct. The general underlying background is due to true secondary electrons and to decay of vacancies created in atoms that are located in the matrix. The bulk plasmon peak and matrix component due to double L-shell ionization are more prominent under ion impact than under electron impact. The line structure consists of five major peaks rather than the four peaks identified in all previous publications. All peak locations can be explained in terms of decaying isolated atoms or ions. Line IV is appropriate to a double L-shell vacancy and the decay given in table I is a plausible though not unique explanation. Decay of the newly identified Al^0 state with $2p^5 3s^2 3p^2$ configuration would account for lines I, II and V; this requires the energy of the parent level to be 73.8 eV which agrees satisfactorily with our rough estimate of 72.35 eV. Al^+ with a $2p^5 3s^2 3p$ configuration can account for line III and would also contribute at the location of line II. The width of the lines is about 1.5 eV which is consistent with a Doppler broadening due to recoil energies of the order 120 eV. This is quite consistent with the recoil energies expected in close encounters that give rise to inner shell vacancies.

Space does not permit us to review in detail the interpreation of ion induced Auger spectra of Mg and Si; these will be published elsewhere. The general features and explanations are however the same as we use here for the case of Al. The lines are due to neutral and singly ionized atoms with single or double L-shell vacancies; the continuum is due entirely to secondary electrons and decay of vacancies in matrix atoms.'

The results permit us to make some conclusions regarding energies of excited states and relative probabilities of certain decay channels. The newly discoveered neutral state with L-shell vacancy has the following energies; for Mg ($2p^5 3s^2 3p$) 50.6 eV, for Al ($2p^5 3s^2 3p^2$) 73.8 eV and for Si ($2p^5 3s^2 3p^3$) 101.1 eV. The various decay channels shown in table 1 for Al^0 ($2p^5 3s^2 3p^2$) should occur also for $Si^+(2p^5 3s^2 3p^2)$ in an ion induced spectrum of an Si target. One might also expect that since electron configurations are identical the ratios of intensities in each case should be the same. This is in fact observed when we compare the fit to the aluminum spectrum with that for Si (not reproduced here). Refer-

ring to table 1 we observe only transitions to the $2p3s^2$ (^1S), $2p^63s3p$ (^3P) and $2p^63p^2$ (^3P) levels and they are in the ratio 0.23 : 1 : 0.07 for aluminum and 0.45 : 1 : 0.09 for silicon. The other two transitions postulated in table 1 for Al^0 are not observed and neither do we detect the corresponding transitions in the Si^+ spectrum of silicon. This may simply be due to low probabilities for these decay paths. For the three observed transitions the intensity ratios, and therefore transition probabilities, are essentially the same in Al^0 and Si^+; differences are well within error estimates as some peaks may suffer distortion due to overlap with other structures particularly in Si.

The present conclusions permit us to reject many previous explanations of these spectra. Both Wittmaack [5] and Baragiola [7] have pointed out that there is an apparent discrepancy between the high energy edges of the electron and ion induced spectra. Baragiola [7] suggests that this is due to a collisonally induced change in electron energy distribution of the solid; Wittmaack [5] claims it is due to charging of the solid. We find that the discrepancy is due to the presence of an additional atomic peak from the ejected neutral particles. This identification shows that there are in fact five significant peaks (labelled I–V) in the spectra of Mg, Al and Si not four as has been claimed previously by all workers in the area [1,4,7]. The complete explanation of all peaks in terms of predictable atomic energy levels would appear to be in contradiction to the suggestion [3] that the smaller peaks are due to energy losses due to plasmon excitation in an excited lattice. It has often been suggested [4] that the spectral features are related to decay of the atoms in a disturbed region created by the collision cascade. The present work shows that the underlying continuum is completely explainable by secondary electrons and decay in the unperturbed matrix; the lines are entirely explicable as due to sputtered atoms and ions decaying in free space. These conclusions are completely consistent with the work of Saiki and Tanaka [10] presented at this conference.

This work was supported in part by the Solid State Chemistry program of the NSF under grant number DMR 80007.

References

[1] W.A. Metz, K.O. Legg and E.W. Thomas, J. Appl. Phys. 51 (1980) 4437.
[2] J.T. Grant, M.P. Hooker, R.W. Springer and T.W. Haas, J. Vac. Sci. Tech. 12 (1975) 481.
[3] J.J. Vrakking and A. Kroes, Surf. Sci. 84 (1979) 153.
[4] L. Viel, C. Benazeth and N. Benazeth, Surf. Sci. 54 (1976) 635.
[5] K. Wittmaack Surf. Sci. 85 (1979) 69.
[6] E.N. Sickafus, Phys. Rev. B. 16 (1977) 1436.
[7] R.A. Baragiola, Springer series in chemical physics, vol. 17 (1981) p. 39.
[8] D.A. Shirley, R.L. Martin, S.P. Kowalczyk, F.R. McFeely and L. Ley, Phys. Rev. B 15 (1977) 544.
[9] C.E. Moore, National Bureau of Standards Circ. (US) 467 (1949).
[10] K. Saiki and S. Tanaka, these Proceedings (ICACS-10) p. 512.

Surface Science 109 (1981) 11–19
North-Holland Publishing Company

AN INELASTIC MECHANISM FOR ION INDUCED DESORPTION OF OXYGEN FROM TITANIUM AND IRON

K.O. LEGG, R. WHALEY and E.W. THOMAS
School of Physics, Georgia Institute of Technology, Atlanta, Georgia 30332, USA

Received 11 February 1981; accepted for publication 21 April 1981

Measurements are reported of the cross sections for desorption or sputtering of oxygen from polycrystalline Ti, and Fe by H^+, H_2^+ and H_3^+ in the energy range 20 to 200 keV. At low energies the desorption cross sections are a few times 10^{-18} cm^2 and are believed due to a conventional sputtering mechanism involving kinematic transfer of energy. At energies above 40 keV/proton for Fe and 80 keV/proton for Ti the cross sections for desorption by molecular ions show a sharp rise indicating onset of some new inelastic desorption mechanism. We propose that this mechanism is electron stimulated desorption initiated by electrons stripped from the projectiles and having the same speed as the projectile.

1. Introduction

Sputtering from solids has usually been modelled in terms of dynamical interactions between the incoming particle and the lattice or in terms of the creation of thermal spikes. Removal of atoms adsorbed on a surface should occur also by these same mechanisms. However removal of adsorbed species by electron impact (electron stimulated desorption or ESD) or by photon impact (photon stimulated desorption or PSD) cannot, at low energies, be due to a kinematic process and must instead be due to some sort of inelastic excitation mechanism. Typically ESD shows a sharp threshold energy indicating that a specific excitation process is involved in the desorption. The earliest picture of ESD formulated by Menzel and Gomer [1] and by Redhead [2] supposes that an incident electron excites a bonding (valence) electron into a nonbonding or antibonding state. The surface species is then assumed to be in a repulsive potential which causes it to be ejected. On this model ESD would exhibit a definite threshold related to the energy required to excite the bonding electron. While this picture may be adequate for a covalently bonded situation it does not explain desorption of ionically bonded species where several electrons must be removed before the adsorbate finds itself in a repulsive situation. Knotek and Feibelman [3–5] discuss ESD of ionically bonded species and it is useful to consider as an example their consideration of O^+ desorption from TiO_2. One would expect the oxygen to be bonded as O^{2-} so that three electrons must be

0039-6028/81/0000–0000/$02.50

removed to liberate O^+; this cannot occur by the Menzel, Gomer, Redhead [1,2] model. Knotek and Feibelman provide convincing evidence that ESD from TiO_2 occurs by the electrons creating a 3p hole in the Ti which cannot be filled by intra-atomic Auger transition because the titanium is in a Ti^{4+} configuration with no outer shell electrons; instead there is an interatomic Auger transition involving removal of electrons from the O^{2-} leaving it as O or O^+ and permitting desorption. Knotek and Feibelman also suggest that desorption can be initiated by inner shell excitation of the bonded species (e.g. the 2s shell of O) followed by intra-atomic Auger decay reducing the number of electrons associated with the oxygen and again placing it in a repulsive situation in the form O^0 or O^+. They point out that for desorption from TiO_2 the energy involved in inner shell excitation of the oxygen is insufficient to give rise to desorption as O^+ but might cause desorption as neutral O. Clearly the position of the ESD threshold should show whether the inner shell excitation is of the substrate or of the adsorbate, and is a major factor in confirming the applicability of the mechanism.

The purpose of the present experiment is to explore whether ion induced desorption might also occur by an inelastic excitation mechanism. We study the total oxygen sputtering (or desorption) cross section as a function of ion energy between 20 and 200 keV for removing oxygen from titanium and iron by impact of H^+, H_2^+, and H_3^+. To enhance the possibility of detecting inelastic processes we use light ions (the three molecular ions of hydrogen) rather than heavy ions (e.g. Ar^+) where conventional sputtering by kinematic energy transfer might dominate.

2. Experiment

The experiment arrangement has been described previously in the context of other experiments [6] and will not be discussed in detail. The targets are placed in a uhv chamber where they can be bombarded by an ion beam from an accelerator, incident at an angle of 60° from the surface normal. A conventional cylindrical mirror Auger spectrometer views the target at 95° to the beam direction and is used to monitor the composition of the surface. The targets were electropolished polycrystalline high purity Ti and Fe cleaned prior to use by low energy argon ion bombardment. Typically the Auger spectrum of the nominally clean target showed a C and O contamination level of less than 10% of a monolayer. About one monolayer of oxygen was adsorbed at room temperature and at a pressure of 10^{-6} Torr. The approximate coverage was determined by continuous Auger monitoring and comparing the O-KLL peak height with the data of Palmberg [7]. The oxygen was then pumped out and the target bombarded by a broad H^+, H_2^+, or H_3^+ beam centered about the Auger electron gun beam. The ion current density at the electron impact point was measured with a small aperture faraday cup. During sputtering, the O-KLL Auger signal was continuously monitored using 3 keV electron excitation. In order to check readsorption rates and to ensure that there was negligible electron

beam desorption, the same experiment was run with no ion beam. It should be noted that, because only the oxygen remaining on the surface was measured, only the total desorption cross section was determined.

For sputtering with readsorption from the ambient the surface coverage at time t is given by the differential equation

$$dN/dt = -(J/e)\sigma N + \alpha P s(N^0 - N), \tag{1}$$

where N is the number density of adsorbed atoms (cm^{-2}) at time t and N^0 is the number density for a monolayer coverage. J is current density and e electronic charge so J/e is the number of incident ions cm^{-2} s^{-1}. The first term therefore represents collisional removal of adsorbed oxygen with a sputtering or desorption cross section σ. The second term represents replacement of oxygen from the ambient gas with s being average sticking coefficient, P the partial pressure of oxygen in the background gas and α being a constant of proportionality ($\alpha = (2\pi mkT)^{-1/2}$ in ideal gas theory). The formulation assumes that there are $N^0 - N$ adsorption sites vacant at any one time and the sticking coefficient for these sites is s; for the N sites already occupied the sticking coefficient is zero and thus only one monolayer of oxide can be formed. Integrating, one arrives at the density as a function of time

$$N(t) = \left(N(0) - \frac{N^0 \alpha P s}{(J/e)\sigma + \alpha P s}\right) \exp\{-[(J/e)\sigma + \alpha P s]\}t + \frac{N^0 \alpha P s}{(J/e)\sigma + \alpha P s}, \tag{2}$$

where $N(0)$ is the coverage at time $t = 0$ when the oxygen atmosphere has been

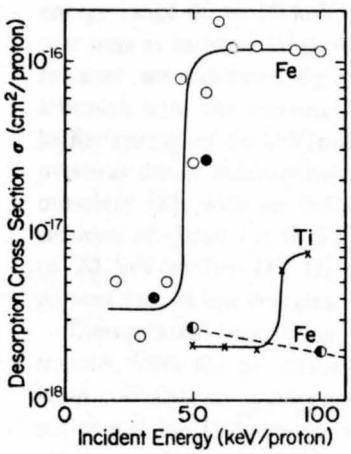

Fig. 1. Cross sections for desorption of oxygen adsorbed on Ti and Fe. Circles are for the Fe substrate; open circles for H_2^+ impact; closed circles for H_3^+ impact; half filled circles for H^+ impact. The crosses are for H_2^+ impact on Ti. Data are shown as the cross section per proton as a function of energy per proton. The lines are meant only to guide the eye and do not represent measurements.

removed and bombardment by the ion beam is commenced. As $t \to \infty$

$$N(t) \to N(\infty) = N^0 \alpha Ps/[(J/e)\sigma + \alpha Ps]. \quad (3)$$

We find that the O-KLL line shape does not change significantly during sputtering so we take the peak to peak height in the derivative spectrum as being proportional to adsorbate surface density $N(t)$. Plotting $\ln[N(t) - N(\infty)]$ versus t yields a straight line of slope $-[(J/e)\sigma + \alpha Ps]$. We determine αPs from the rate of rise of $N(t)$ with time when the ion beam is removed, and with our measured value of J (typically about 30 μA cm^{-2}) we can evaluate the desorption cross section σ. With the relatively low sputtering rates involved in this work the equilibrium coverage $N(\infty)$ is attained at about half a monolayer so that the measured cross section is relevant only to the removal of the first one half monolayer. The inaccuracies in measuring $N(\infty)$ and in the experimental determination of current density J are the major factors contributing to the large scatter of the data points.

In fig. 1 we show the cross sections for desorbing oxygen from Ti and Fe. For a projectile H_n^+ the measured desorption cross sections have been divided by n to give cross section per incident proton; the data are presented as a function of incident energy $\div n$, or energy per proton.

3. Discussion

The cross sections for removal of adsorbed oxygen by impact of H_2^+ and H_3^+ on iron (fig. 1) show a remarkable increase of more than an order of magnitude in the energy range 40 to 50 keV/nucleon. This effect is peculiar to the impact of molecular ions as incident H^+ shows a very low and energy invariant cross section. Similar features are exhibited by the cross section for removing oxygen from titanium although here the increase is only a factor of four and occurs at the somewhat higher energy of 80 keV/nucleon. To the best of our knowledge there is only one previous direct measurement of oxygen removal by hydrogen ions, performed by ourselves [8], with an indirect optical technique. This previous work gives cross sections of about 1.6 to 3.5 $\times 10^{-18}$ cm^2/proton for removing O from Mo by 6.7 to 20 keV/proton H^+, H_2^+ and H_3^+; these figures are quite comparable with the present data at low energies.

Conventional sputtering theories involve consideration of kinematic energy transfer from the projectile to the target atoms either by direct projectile–target atom collisions or as the result of the collision cascade. Such calculations have been performed by Taglauer et al. [9], for removal of S from Ni by H^+ and give cross sections of 2 to 6 $\times 10^{-16}$ cm^2 (depending on the model used) at 2.0 keV decreasing towards higher impact energies. Sputtering of bulk metals by H^+ at energies below 10 keV has been studied extensively and fits a kinematic energy transfer model [10]. A typical sputtering coefficient (e.g., for Fe [10]) for 10 keV H^+ impact is 10^{-3} which implies a sputtering cross section of the order of 10^{-18} cm^2 and

is roughly comparable with the low energy data in fig. 1. None of the sputtering models involving kinematic energy transfer are capable of predicting rapid cross section rises such as those shown in fig. 1.

We would argue that the low cross sections exhibited for sputtering by H^+ indicate that for this species one is observing only the effect of kinematic energy transfer. The cross section values are very similar to what one would expect from extrapolation of low energy sputtering data for homogeneous solids where kinematic energy transfer is certainly a satisfactory explanation of the ejection mechanism; the cross section exhibits the expected (slow) decrease with increasing energy. If this is accepted then the present data for H_2^+ and H_3^+ impact at lower energies ($E < 40$ keV/proton for Fe and $E < 80$ keV/proton for Ti) could be explained also as due to kinematic energy transfer.

The rapid cross section rises exhibited on fig. 1 must indicate the onset of some other ejection mechanism. The rapidity of the onset would strongly imply an inelastic process with a definite threshold. For guidance in the explanation of the high cross sections we must turn to the allied fields of electron and photon stimulated desorption where removal of oxygen is related to inelastic excitation mechanisms.

Let us first examine the possibility that ionization of an inner shell electron by direct ion impact is the precursor to desorption. The threshold for ion-induced excitation of an inner shell will be at an ion energy equal to the required excitation energy. For excitation of L or M shell electrons from the adsorbate or substrate species in the present experiments the threshold should be below 1 keV and cannot explain the sharp rise seen here at 40 or 80 keV. Moreover, an H_2^+ molecular ion should act simply as two hydrogen atoms or ions and there would not be the extreme difference between H^+ and H_2^+ that we observe here. We must conclude that excitation of inner shells by the projectile is not the origin of the large desorption cross sections seen for H_2^+ although it might possibly represent a small underlying contribution at all energies.

Let us focus now on the difference between H^+ and H_2^+. When a projectile traverses a solid one finds at the exit point not only the heavy ion but also a considerable flux of electrons with a velocity distribution centered on the speed of the ion. In part these electrons arise from charge exchange to the continuum states of the projectile. For H_2^+ there is a second component [11] comprising electrons stripped from the projectile. A general discussion of mechanisms leading to the production of electrons with speeds close to that of the ion is provided by Meckback and Baragiola [11]. A very significant observation is that the flux of electrons for H_2^+ impact can be 17 times greater than for H^+ impact at the same speed [12] due to the efficient stripping mechanism. It is therefore clear that when H^+ and H_2^+ are incident on a solid there is in addition to the ion core also a flux of energetic electrons having a speed distribution peaked at the speed of the ion. If stripped projectile electrons are responsible for initiating desorption then one should expect desorption by H_2^+ impact to be far more efficient than by H^+ since there are more

electrons associated with the molecule; this is, of course, in accord with the present data.

Let us now examine the desorption mechanism under the assumption that electrons are stripped from the projectile as it traverses the first monolayer and that these electrons moving with the same speed as the projectile cause electron stimulated desorption. One would hope to find that the rising cross sections, exhibited on fig. 1, occurs at the same projectile velocity as one would expect electron stimulated desorption to exhibit a threshold. We shall consider the situation on the assumption that the oxygen is ionically bonded so that desorption should be in accordance with the Knotek and Feibelman model [3–5] which invokes inner shell ionization followed by Auger decay. The binding energy of the oxygen 2s electron in a solid is given as about 24 eV in the catalogue of Coghlan and Clausing [13] and observed by Knotek and Feibelman [4] to lie at about 20 eV in a variety of ionic solids. Thus the threshold for ESD by excitation of the 2s oxygen shell would be 20 to 24 eV. Hydrogen projectiles of energy 44 to 63.5 keV/nucleon would carry with them electrons of energy 20 to 24 eV. In fig. 1 the onset of the large cross section for removal of oxygen from Fe occurs at an H_2^+ ion energy of about 44 keV/nucleon. Thus, the onset of the large desorption cross section occurs at a projectile energy where the projectile electrons are energetically able to excite the 2s shell of oxygen on the surface. We should also examine the magnitude of the desorption cross section. If electrons stripped from the H_2^+ projectile are the principal contributors to desorption then we expect one electron to every two protons. If indeed the electrons are causing desorption, via inner shell ionization, then the data of fig. 1 imply an electron ionization cross section for 2s electrons in bound O of about 2×10^{-16} cm^2. While large this is not necessarily unreasonable as the total cross section for ionization of isolated atomic oxygen is estimated to be 5×10^{-17} cm^2 at 20 eV [14]. It is not clear at this point why a threshold at 44 keV is not also observed for desorption of oxygen from Ti. One would also anticipate, at a somewhat higher energy, the onset of a second desorption mechanism when the convoy electrons are able to ionize the 3p electrons of the substrate nuclei leading to interatomic Auger events leaving the adsorbate in a repulsive state. For Fe the binding energy of the 3p electrons is 56 eV [13] which could be excited by stripped projectile electrons associated with 102 keV/nucleon H_2^+; this is outside our present energy range. For ESD of O^+ from bulk TiO_2 by excitation of 3p electrons in Ti, the threshold is found experimentally to be 34 eV [3,4] which in our model would require electrons associated with 62 keV/proton projectiles; this energy is somewhat below the point where the onset is observed. We would note, however, that the ESD data of Knotek and Feibelman for bulk TiO_2 actually exhibits not only a 34 eV threshold but also an equally large structure at about 44 eV that has the appearance of a threshold for a second mechanism. That apparent threshold at 44 eV would require electrons associated with 80 keV/nucleon projectiles which is about where we observe the increase in cross section.

In summary, if the stripped projectile electrons are responsible for inner shell

excitation which, in turn, leads to desorption then the rise in desorption from Fe is completely consistent with excitation of the 2s electron in the oxygen and the rise in desorption from Ti is approximately where one expects excitation of the 3p level of titanium. There are, however, two problems with this explanation. On the one hand one would have expected O to desorb from Ti by excitation of the 2s level in oxygen leading to a threshold at about 44 keV, the same as for desorption from Fe. Secondly the threshold for desorption via excitation of the 3p level in Ti is expected to be at 62 keV/proton while we observe it slightly higher at 70 to 80 keV/proton. These two apparent discrepancies do not necessarily cast doubt on our proposal that electrons are responsible, they may simply indicate inadequacies in our understanding of the ESD process. We must point out that the ESD work that we have used for comparison is in fact for ejection of O^+ ions from the surface of bulk oxides (such as TiO_2) not the total removal of adsorbed oxygen from the surface of the bulk metal that we are studying here.

We have some direct evidence of differences between bonding in the bulk oxide and adsorbed oxygen situations. One may study the energy loss spectrum for electrons scattered from a surface with adsorbed oxygen; peaks in the loss spectrum should represent energies at which interband transitions and plasmon creation occur. For bulk TiO_2 Knotek and Feibelman [3,4] find a loss peak at 32 eV which they identify as due to excitation of the Ti 3p electron leading to the conclusion that ESD should have a threshold at 32 eV; this is in fact the impact energy at which O^+ ESD commences. In our own work with adsorbed oxygen on a Ti substrate the loss curve shows a strong peak at 44 eV which disappears when oxygen is removed. This peak has in fact been seen by others and explained as due either to excitation of a chemically shifted 3p electron of Ti [15] or excitation of a momentum conservation interband transition in the manner suggested by Viatskin [16]. Whatever the explanation, if indeed the peak represents excitation of a 3p electron in Ti one would expect an electron stimulated desorption threshold at 44 eV and a threshold for desorption by stripped projectile electrons at a hydrogen projectile energy of 80 keV/proton. In fact the ESD data for TiO_2 by Knotek and Feibelman show a significant structure at 44 eV electron energy and the present ion induced desorption of adsorbed oxygen from Ti shows its rise at about 80 keV/proton. A similar situation exists in photon stimulated desorption of O^+ from V_2O_5 [17] where the threshold is at the energy for exciting 3p electrons but there is a second very large structure at 50 eV; this second structure occurs at the same energy as a peak in the electron energy loss spectra of V_2O_3 [18] which is ascribed to a momentum conservation interband transition. Irrespective of whether the explanation of these energy loss peaks is correct it is clear that they are related to structure in ESD and PSD studies and that their relative importance may depend on whether the oxygen is present as an adsorbate or in the bulk oxide phase.

4. Conclusions

The cross sections for removal of adsorbed oxygen from Ti and Fe by impact of H^+, H_2^+, and H_3^+ are of the order 10^{-18} cm^2/proton for low energy (20–40 keV/proton) impact and the removal mechanism presumably involves kinematic energy transfer from the projectile to the target. As energy is increased the cross section exhibits a sharp rise (at 40 to 50 keV/proton for Fe and circa 80 keV/proton for Ti) for removal by molecular ions (H_2^+ and H_3^+) but no significant change for the monatomic species (H^+). The sharp rise cannot be explained on the basis of kinematic energy transfer mechanisms and must represent onset of desorption by an inelastic event. We postulate that the new process is electron stimulated desorption initiated by electrons stripped from the projectile and having a speed distribution peaked sharply at the speed of the projectile. The flux of such electrons will be quite large for molecular ion impact where they arise primarily from stripping with a small contribution from charge transfer to the continuum; for the H^+ projectile they arise only from charge transfer and will be of a much lower flux. On this basis we identify the sharp increase of cross section for removal of adsorbed oxygen from iron as due to ionization of the 2s shell of O by stripped projectile electrons followed by Auger processes leaving it in a repulsive state. The enhanced removal of O from Ti is identified as due to ionization, by stripped projectile electrons, of the 3p shell in Ti followed by interatomic Auger transitions involving electrons from the oxygen leaving it in a repulsive configuration.

Acknowledgements

This work was supported in part by subcontract from the Oak Ridge National Laboratory, operated by Union Carbide for the Department of Energy under Contract No. W-7405-eng-26.

References

[1] D. Menzel and R. Gomer, J. Chem. Phys. 41 (1964) 3311.
[2] P.A. Redhead, Can. J. Phys. 42 (1964) 886.
[3] P.J. Feibelman and M.L. Knotek, Phys. Rev. B18 (1978) 6531.
[4] M.L. Knotek and P.J. Feibelman, Phys. Rev. Letters 40 (1978) 964.
[5] M.L. Knotek and P.J. Feibelman, Surface Sci. 90 (1979) 78.
[6] W.A. Metz, K.O. Legg and E.W. Thomas, J. Appl. Phys. 51 (1980) 2888.
[7] L.E. Davis et al., Handbook of Auger Electron Spectroscopy, 2nd ed. (Physical Electronics Industries Inc., Eden Prarie, Minnesota, 1976).
[8] E.O. Rausch, M.W. Murray, H. Inouye and E.W. Thomas, J. Appl. Phys. 48 (1977) 4347.
[9] E. Taglauer, U. Beitat, G. Marin and W. Heiland, J. Nucl. Mater. 63 (1976) 193.
[10] Experimental data for Fe and a useful bibliography of sputtering data is to be found in the paper of R. Behrisch, G. Maderlechner, B.M.U. Scherzer and M.T. Robinson, Appl. Phys. 18 (1979) 391.

[11] W. Meckback and R.A. Baragiola, Processes of Charge Exchange Into the Continuum of Ionic Projectiles Interacting with Gases and Solids, in: Inelastic Ion–Surface Collisions, Eds. N.H. Tolk, J.C. Tully, W. Heiland and C.W. White (Academic Press, New York, 1976).
[12] M.M. Duncan and M.G. Menendez, Phys. Letters 56A (1976) 177.
[13] W.A. Coghlan and R.E. Clausing, Atomic Data 5 (1973) 317.
[14] E.J. McGuire, Phys. Rev. A16 (1977) 73.
[15] J. Frandon, B. Brousseau and F. Pradel, J. Physique 39 (1978) 839.
[16] A.Ia. Viatskin, Zh. Tekh. Fiz. 28 (1958) 2217 [Soviet Phys.-Tech. Phys. 3 (1958) 2038].
[17] J.F. Van der Veen, F.J. Himpsel, D.E. Eastman and P. Heimann, Solid State Commun. 36 (1980) 99.
[18] F.J. Szalkowski, P.A. Bertrand and G.A. Somorjai, Phys. Rev. B9 (1974) 3369.

Nuclear Instruments and Methods in Physics Research B2 (1984) 479–483
North-Holland, Amsterdam

THE ROTATIONAL POPULATION OF SPUTTERED N_2 – EVIDENCE FOR HINDERED ROTATIONAL STATES

E.W. THOMAS and L. EFSTATHIOU

School of Physics, Georgia Tech., Atlanta, Ga 30332, USA

We report on the study of excited N_2 molecules sputtered from a N^+ implanted Si surface by an N^+ ion beam. Analysis of how N_2 emission intensity varies with implant dose suggests that N_2 molecules are formed by recombination of N atoms before being collisionally ejected by the sputtering mechanism. Such N_2 molecules, localized on the surface, must inevitably exhibit a quantum mechanical rotational configuration that differs from an isolated molecule in free space. We observed that the rotational state distribution implied by the rotational structure of the N_2 emission is a non-Boltzmann distribution and we relate this to a hindered rotor configuration of the N_2 molecule when localized on the surface.

1. Introduction

Battacharya et al. [1] reported that during N^+ bombardment of Si an optical emission of N_2 molecular lines was observed that increased with cumulative N^+ dose. Apparently N^+ was implanted first and then further bombardment sputtered the surface to reveal the implant and both eject and excite molecular species. The line studied by Battacharya et al. [1] was the 3371 Å band which is the $0 \rightarrow 0$ transition in the $C\ ^3\Pi \rightarrow B\ ^3\Pi$ band. We previously examined the detailed shape of the 3371 Å N_2 transition [2] and showed that there was substantial rotational excitation which could be roughly characterized by an apparent rotational temperature of 1100 K. In the present work we re-examine this phenomenon to study the details of how intensity builds up with cumulative dose and to perform more detailed studies of the rotational line shape.

The study of N_2 emissions due to sputtering of nitrogen implanted silicon is the subject of some controversy in the literature. Snowdon et al. [3] using low energy (0.5–6 keV) N_2^+ beams observe a broad band emission spectrum which they identify as due to sputtered N_2^+ in very high rotational states; an associative ionization mechanism is used to explain the formation process. Loxton et al. [4,5] criticize this work, claiming that some of the observed features identified by Snowdon et al. [3] are in fact sputtered Si N. The work we report here sheds no light on this controversy. The observed lines have been carefully measured and are due to the neutral N_2 molecule as observed earlier by Battacharya et al. [1]; the line studied is neither from N_2^+ as observed by Snowdon et al. [3] nor from Si N as observed by Loxton et al. [4]. The present work is performed with ion energies of 100 keV compared with the 6 keV used by Snowdon, Loxton and co-workers. It is quite possible that the energy variation of excitation cross sections places our work in a somewhat different regime from that of Snowdon, Loxton and co-workers [3–5].

2. Experimental

The general experimental arrangement is unchanged from that used in our previous studies of collisionally induced light emission from solids [6]. Targets are mounted on a standard manipulator, placed in a vacuum system with a base pressure of 10^{-10} Torr and bombarded with ions from a 20–200 keV ion accelerator at a dose rate of about 3×10^{14} N^+ ions $\cdot$ cm$^{-2} \cdot$ s^{-1}. Optical emission from the point of beam impact is analyzed with a 0.5 m scanning monochromator fitted with photomultiplier detection. The monochromator views the target through a sapphire window at an angle of 90° to the beam direction; the beam impact on the surface at an angle of 60° to the normal.

The silicon target was a single crystal with the (111) face exposed to the incoming ion beam. Preliminary heating of the crystal to 250°C or sputter cleaning with Ar^+ ions did not alter the observations reported here.

The general procedure was to bombard the virgin crystal with a 100 keV N_2^+ beam and monitor the dependence of the 3371 Å line intensity on dose. The signal was observed to rise and become constant. After saturation had been achieved the complete spectrum was scanned (from 3000 to 5000 Å) at a 2 Å resolution to record the detailed shape of the 3371 Å line, to establish background levels and to ensure no interference from other spectral systems. Very intense emissions of Si and Si^+ lines were also observed that were generally similar to the spectra published by others [7].

0168-583X/84/$03.00

There must be some concern when using an N_2^+ beam to simultaneously implant and sputter the target that observed N_2 emission might be from the projectile beam passing through residual gas in the target chamber. To check this we first bombarded the target with N_2^+ to reach a saturation intensity of N_2 emission and then changed the ion beam to Ar^+ (also at 100 keV). Under Ar^+ bombardment the same N_2 emission was observed and the intensity decreased with cumulative dose in a manner consistent with the sputter erosion of the N_2^+ implanted region. We also substituted N^+ for the N_2^+ beam and observed a similar dependence of N_2 emission on dose and an identical N_2 rotational line shape. We conclude therefore that the observed N_2 emission is due to sputtering of implanted N and is not related to the beam used for sputtering.

The data reported here was all obtained using 100 keV N_2^+ ion beams. We shall assume that each incident molecular ion dissociates on impact and that further motion of the fragments is uncorrelated. Thus a 100 keV N_2^+ ion is treated as two N^+ ions at 50 keV. Direct test using an N^+ beam showed this assumption to be valid. The N_2^+ beam was used rather than N^+ because a higher current was obtainable in our apparatus permitting use of higher optical resolution.

We searched also for other lines related to nitrogen. A very weak emission of Si N was observed consistent with the reports of Loxton et al. [4]. We observed also other weak emissions of N_2 from the same spectral system as the 3371 Å line; these included the 3577 Å ($0 \rightarrow 1$) and 3805 Å ($0 \rightarrow 2$) bands. The relative intensity of all three bands was in approximately the ratios observed in discharge spectra [8].

We studied briefly the impact of N_2^+ on a single crystal Ge surface to determine whether N_2 emissions could also be seen in this case – no emission was observed. Performing Auger analysis of the ion implanted Si and Ge we found nitrogen only in the Si targets with no significant trace in the Ge. We conclude therefore that no significant density of nitrogen builds up in Ge under these circumstances and for this reason there is no nitrogen available to be sputtered.

3. Mechanism for N_2 formation

The first step in an analysis of the observations is to determine whether the N_2 molecules are formed before they are ejected or whether two N atoms are independently sputtered and associate in space to form the molecule. This question has a major bearing on understanding rotational state distributions observed by optical emission. We show how one may distinquish between the two formation mechanisms by studying the intensity of emission as a function of implant dose.

The relevant experimental observation is given in fig. 1 where we show how emission intensity of 3371 Å band increases with dose. The measurements are taken with a 16 Å optical resolution to automatically integrate over all rotational structures of significant intensity. The data are very similar to that of Battacharya et al. [1] with signal rising from zero to attain a constant level. Following Battacharya et al. [1] we would explain this behaviour as due to sputter erosion of the surface down to the depth of the initial implant with simultaneous replenishment of nitrogen at greater depths by implantation. To model this behaviour in detail we must first estimate how surface density of N varies with dose since one would anticipate sputtering to occur principally from the surface monolayer.

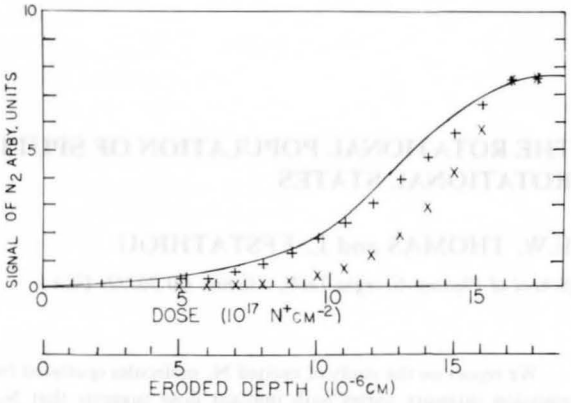

Fig. 1. Intensity of the 3371 Å line as a function of dose for impact of 50 keV (or 100 keV N_2^+) on a Si target is shown as the solid line. Shown parallel to the dose scale is an estimate of erosion depth derived as indicated in text. Also indicated is a prediction of how intensity varies with dose if sputtering is related linearly (+) or quadratically (×) to surface concentration of N. Prediction and experiment are all relative and normalized together at saturation.

We consider the implantation occurring during small time intervals δt centered on a series of time steps t_0, t_1, $t_2 \cdots t_n$. We suppose the interval to be substantially less than the time step (i.e. $\delta t \ll t_n - t_{n-1}$). At the first step the ions are implanted for an interval δt and are taken to be at a Gaussian depth distribution of range R_p and straggling ΔR_p given by the tables of Dearnaley et al. [9]. During the time between steps the incoming ion beam sputters a thickness Δx off the surface. Thus the depth distribution of implants during the second interval δt at the time t_2 is centered at a distance of $R_p + \Delta x$ from the original surface location. At the nth step (time t_n) implantation is a Gaussian centered at a distance $R_p - n\Delta x$ from the original surface. In this manner one may model the distribution of implants with respect to the original location of the surface. The density of implants on the surface at any time t_n is obtained from the sum of the Gaussian distributions

occurring in the previous time steps evaluated at the location of the surface at the time t_n; this location will be at a distance nd from the original surface governed by sputtering coefficient.

This simple modelling procedure shows that the maximum surface density of N, and therefore presumably maximum N_2 emission, occurs when the depth eroded by the ion beam is equal to the range of the projectiles. That is to say the surface has been eroded to the original depth of the implant maximum at the first time step. From this we may calculate a value for sputtering coefficient S in terms of dose to maximum signal strength N_D (ions cm^{-2}), projected range R_p (cm) and density of silicon atoms of the target N_{Si}.

$$S = R_p N_{Si}/N_D. \quad (1)$$

We use R_p from Dearnaley et al. [9] and N_{Si} from Andersen and Ziegler [10] leading to a value of S of 0.53. This value of sputtering coefficient is in excellent agreement with a value for sputtering of pure Si given by Hofer and Liebl [11].

From the variation of signal with dose one may come to some understanding of how the molecules of N_2 are formed. Two mechanisms may be envisaged. It is in principle possible for two N atoms to be simultaneously sputtered from adjacent locations so that the total energy in the center of mass frame of the two atoms is less than the binding energy of N_2. In this case the probability of ejecting any atom is proportional to the surface density of N and the probability of ejecting two atoms is proportional to the square of surface density. On the basis of our general spectra which show no lines from N atoms we would surmise that ejection of excited N under any circumstances is unlikely and ejection simultaneously with a second atom is not expected at all. Nevertheless this mechanism was invoked by Snowdon et al. [3] at lower projectilve energies and must be considered. Alternatively N_2 molecules could be formed by recombination on (or in) the solid so that all the nitrogen present is in the molecular form; in this case the probability of ejection is linearly dependent on surface density. Thus a study of how N_2 signal varies with surface density of N should in principle permit us to determine whether the formation of N_2 occurs before or after ejection.

From the model described above one may estimate surface density of N after different erosion depths. Using the derived sputtering coefficient one may relate depth to projectile dose. In fig. 1 we show a plot of surface N density against dose and also the square of surface N density against dose; in both cases the plot is normalized to experiment at high dose. It is observed that the linear relationship of N density to dose fits the data exactly. We conclude therefore that the N_2 molecule forms before the sputtering event and the molecule is ejected and excited as a single unit. Recombination to form molecules may occur at the surface after the N has been revealed by erosion; this mechanism is invoked for formation of D_2 on steel [12]. Alternatively the N_2 may be formed by some recombination mechanism in the bulk as has been discovered for CN formation in alkali halides [13]. The present observations do not permit differentation between these two mechanisms.

4. Rotational state populations

The N_2 molecule localized on the surface must inevitably have a different rotational state configuration than a molecule in full space. In principle the rotational state population derived from the observed emission spectrum should be related to the rotational configuration of the molecule on the surface before sputter ejection.

We recorded the 3371 Å band using a 2 Å resolution. This is substantially greater than rotational line separation so that only the envelope of line intensities can be recorded. The 3371 Å transition has both P and R branches with the R branch being concentrated near the band head. For the moment let us analyze the line shape on the assumption that only the P branch is present.

From the standard references on molecular spectroscopy the frequency of a transition $J \rightarrow J-1$ is given by.

$$\nu = \nu_0 + B_u(J-1)J - B_e J(J+1). \quad (2)$$

The values of the constants are taken from Herzberg [14] and for each upper rotational state J one may determine frequency or wavelength of the transition. The measured line shape as a function of wavelength may then be re-drawn as intensity as a function of rotational state J.

The intensity of a transition is given by

$$I = AS_J P_J. \quad (3)$$

Here A is a constant of proportionality, P_J is the state population and S_J is the Hönl–London factor which is $(J+2)J/(J+1)$ for the P branch of this line [14]. Thus dividing I by the Hönl–London factor gives a quantity proportional to population density P_J. In fig. 2 we plot $\ln P_J/2J+1$ against $J(J+1)$. If the population density were appropriate to a local thermodynamic equilibrium (LTE) situation of temperature T then a Boltzmann state population should hold given by

$$P_J = (2J+1)\exp - \frac{BJ(J+1)\,hc}{kT}, \quad (4)$$

where B is a constant associated with the molecule and h, c, k have their usual meaning. If LTE holds then eq. (4) shows that the plot of fig. 2 should be a straight line from which T may be determined. Clearly this is not the case.

Non-Boltzmann distributions of rotational states in

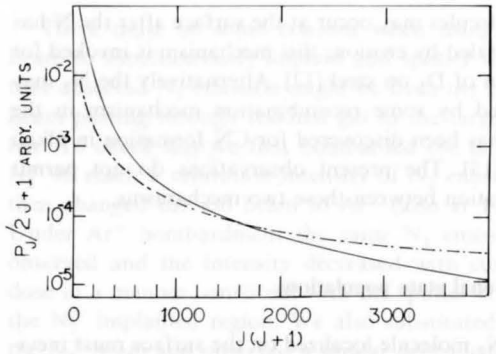

Fig. 2. Plot of rotational state population P_J as a functional of rotational quantum number J plotted in the form ln P_J/J $(J+1)$. Shown as a solid line is the experimental data for the 3371 Å band of N_2 excited by 50 keV N^+ (or 100 keV N_2^+) impact on Si. Population is derived by dividing intensity by the Hönl–London factors. Also shown as a dashed–dotted line are the predictions for a hindered rotor model with an infinite conical well of half-angle 90°.

molecules emerging from surfaces have been noted in a number of recent experiments; a good example is the work of Kleyn et al. [15] on rotational state populations of NO scattered from Ag. This observation has been explained by Gadzuk et al. [16] in terms of a hindered rotor model to describe the molecule when it is attached to the surface. Certainly a molecule attached to a surface does not have the same rotational state description as a molecule in free space. Gadzuk et al. [16] have formulated the quantum mechanics of this state. They assume the molecule to be represented as a dumb-bell with one end located on the surface and the axis rotating in an infinite conical well of angle β; for an inclination of molecular axis to the surface normal at an angle θ the potential is zero for $0 \leq \beta$ and infinity for $\beta < \theta < 90°$. Angles θ greater than 90° are of course impossible due to the presence of the surface. With this formulation the hindered rotational states may be described and populated according to a Boltzmann distribution appropriate to the room temperature surface. Removal of the molecule is simulated by simply removing the hindering potential so that the molecule rotates freely. The rotational state population of the free rotor is simply given by the overlap integral between rotational states of the hindered and free rotational configurations. The result given by Gadzuk et al. [16] is a very dramatic non-Boltzmann distribution in the free rotor with oscillations of population under some circumstances.

We have applied this model directly to the prediction of rotational state populations of ejected N_2. We have shown above that the N_2 molecule exists as a molecular entity before the sputtering event so that the hindered rotational states may be predicted by the theory of Gadzuk et al. [16]. We assume these states are thermally populated appropriate to a room temperature target. As a result of the sputtering event the hindering potential is removed, a free molecule results, and the rotational state distribution can be evaluated by the overlap between hindered and free rotational configurations. We assume that the ejection event transfers no rotational energy to the molecules. Using the formulation of Gadzuk et al. [16] we may predict the rotational state distribution of the excited molecule and compare it with experiment; the sole unknown is the angle of the conical well. In fig. 2 we show a rotational state population prediction for a conical well angle $\theta = 90°$. The simulation shows a general agreement with experiment and clearly predicts a non-Boltzmann state distribution. Use of smaller well angles provides a less satisfactory fit.

It must be admitted that there are numerous inadequacies in the use of this experiment and this model. The experiment includes an R-branch contribution that will increase signal at low J in fig. 2; the experiment also has a limited resolution so obscuring detail. A simulation of these effects suggests that their inclusion would improve agreement between experiment and theory. The computation is based on an infinite well that is clearly unrealistic. In view of large conical angle indicated by our data one should repeat the computation for a molecule in a hindered rotor configuration where the hindering potential increases as the angle between molecular axis and surface normal decreases; such a potential was envisaged by Gadzuk et al. [16] but no explicit calculations formulated.

5. Conclusion

During N_2^+ bombardment of Si we observe the 3371 Å band of N_2 increasing with dose to reach a plateau. We conclude that the implanted nitrogen is revealed by surface sputter erosion and is ejected and excited by particle impact. The dose dependence is consistent with the N_2 molecule being formed on the surface by recombination before the collisional ejection event. A coefficient of 0.53 is deduced for sputtering of Si by 50 keV N^+ incident at 60° to the surface normal. Analysis of the rotational line shape of the 3371 Å band shows a non-Boltzmann distribution. This is consistent with the use of the hindered rotor model of Gadzuk et al. [16] to describe a molecule's rotation when bound to a surface. A simple formalism of the hindered rotor in terms of an infinite conical well is consistent with our data provided the angle of the well is taken as 90°. Such an angle is quite feasible for a molecule where one atom is bound to the surface and the other is free to rotate.

This work was supported in part by the Solid State Chemistry Program of the NSF under grant DMR 8000671.

References

[1] R.S. Battacharya, J.F. Van Der Veen, C.B.W. Kerkdijk and F.W. Saris, Rad. Eff. 32 (1977) 25.

[2] L. Efstathiou and E.W. Thomas, Nucl. Instr. and Meth. 194 (1982) 589.

[3] K.J. Snowdon, E. Taglauer and W. Heiland, Phys. Rev. Lett. 46 (1981) 284.

[4] C.M. Loxton, I.S.T. Tsong and S.H. Lin, Phys. Rev. Lett. 50 (1983) 1331.

[5] K. Snowdon and W. Heiland, Phys. Rev. Lett. 50 (1983) 1332.

[6] W.E. Baird, M. Zivitz, J. Larsen and E.W. Thomas, Phys. Rev. A10 (1974) 2063.

[7] P.J. Martin and R.J. MacDonald, Phys. Lett. 55A (1976) 483.

[8] A. Lofthus and P.H. Krupenie, J. Phys. Chem. Ref. Data 6 (1977) 113.

[9] G. Dearnaley, J.H. Freeman, R.S. Nelson and J. Stephen, Ion implantation (North-Holland, Amsterdam, 1973).

[10] H.H. Andersen and J.F. Ziegler, Hydrogen stopping power and ranges in all elements (Pergamon, New York, 1977).

[11] W.O. Hofer and H. Liebl, Appl. Phys. 8 (1975) 359.

[12] I. Ali-Khan, K.J. Dietz, F. Waelbroeck and P. Wienhold, J. Nucl. Mat. 76/77 (1978) 337.

[13] W.A. Metz and E.W. Thomas, J. Appl. Phys. 53 (1982) 3529.

[14] G. Herzberg. Spectra of diatomic molecules (Van Nostrand, Princeton, 1950).

[15] A.W. Kleyn, A.C. Luntz and D.J. Auerbach, Phys. Rev. Lett. 47 (1981) 1169.

[16] J.W. Gadzuk, U. Landman, E.J. Kuster, C.L. Cleveland and R.N. Barnett, Phys. Rev. Lett. 49 (1982) 426.

Nuclear Instruments and Methods 194 (1982) 589–591
North-Holland Publishing Company

EXCITED STATES OF SPUTTERED MOLECULES

L. EFSTATHIOU and E.W. THOMAS

Georgia Institute of Technology, Atlanta, Georgia 30332, U.S.A.

We present some observations of the N_2 and O_2 molecular spectra induced by ion impact on solids. The N_2 spectra are due to bombardment of a nitrogen implanted silicon sample. The O_2 spectrum is from Ar^+ bombardment of a boron sample with adsorbed oxygen. The nitrogen spectrum shows rotational but not vibrational excitation. A model for its formation is proposed based on surface recombination followed by vibrational deactivation and ejection. The oxygen spectrum appears to contain fragments of the $c\,^1\Sigma_u^- \rightarrow X\,^3\Sigma_g^-$ Herzberg II band system and exhibits high vibrational but no rotational excitation.

1. Introduction

We report here some recent observations concerning the excited states of sputtered molecules. In part the work was prompted by an apparent discrepancy between two previous reports on emission of nitrogen molecular lines when a silicon sample is bombarded by a nitrogen ion beam. In the early work of Battacharya et al. [1] the 3371 Å band of neutral N_2 is observed under 10 keV N^+ or N_2^+ bombardment. In the work of Snowdon et al. [2], using 2 keV N_2^+ beams the principal emissions observed were from various states of the molecular nitrogen ion N_2^+. In both the work of Battacharya et al. [1], and that of Snowdon et al. [2], it is suggested that the nitrogen is implanted as individual atoms and either the molecule is formed on the surface and sputtered as one unit or else two individual atoms are sputtered independently and recombine as they emerge from the surface. There is an apparent difference between the two studies in that Battacharya et al. [1], observe the neutral molecule and Snowdon et al. [2], observe an ejected molecular ion. It seems unlikely that these different observations can be due only to differences in cross sections for ejection processes.

The present work was designed to study further the phenomenon of excited molecule ejection by particle impact. We study ejection of nitrogen from silicon by particle impact at energies between 20 and 200 keV as well as providing fragmentary information on ejection of molecular oxygen. The general objective is to study rotational and vibrational excitation in an attempt to understand the mechanism of the molecule's formation.

2. Experimental

The general experimental arrangement is unchanged from that used in our previous studies of collisionally induced light emission from solids [3]. Targets are mounted on a standard manipulator, placed in a vacuum system with a base pressure of 10^{-10} Torr and bombarded with ions from a 20–200 keV ion accelerator. Optical emission from the point of beam impact is analyzed with a 0.5 m Jarrell–Ash scanning monochromator fitted with photomultiplier detection and conventional pulse counting electronics. The monochromator views the target through a sapphire window at an angle of 90° to the beam direction and at a 30° angle from the normal to the target's surface.

The silicon targets were high purity, single crystal targets with the (111) face exposed to the incoming ion beam. For the work with boron we used a polycrystalline sample.

3. Molecular nitrogen spectra

When Si was bombarded with 100 keV N_2^+ we observed weak emissions of the second positive ($C\,^3\Pi \rightarrow B\,^3\Pi$) system of N_2 including the $0 \rightarrow 0$, $0 \rightarrow 1$ and $0 \rightarrow 2$ vibrational transitions. The emission intensity was zero when bombardment commenced and built up steadily. Following Bhattacharya et al. [1], we explain this build up as due to erosion of the surface leading to exposure of the ion implanted nitrogen on the surface. If the projectile is changed from N_2^+ to Ar^+ one sees identical features implying that the nitrogen emission arises from sputtering of the implant and is in no way related to scattering of projectiles. In addition to the nitrogen lines there were intense emissions from sputtered Si and Si^+. When molecular oxygen was introduced into the target chamber we observed an increase of the nitrogen intensity along with an increase in intensity of the many Si lines. The intensity ratios of the 0–0, 0–1 and 0–2 transitions are in general agreement with the calculated Franck–Condon factors given by Lofthus and Krupenie

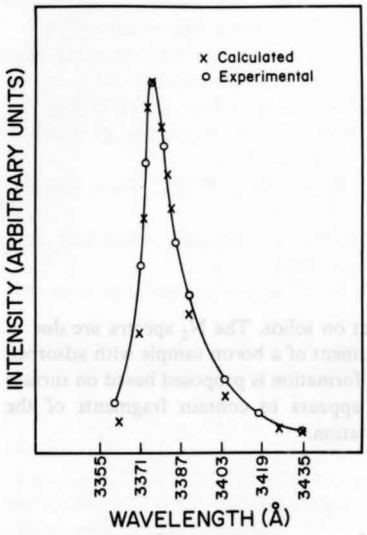

Fig. 1. The $0 \rightarrow 0$ spectral line in the $C\,^3\Pi \rightarrow B\,^3\Pi$ second positive system of N_2 induced by 100 keV Ar^+ impact on an Si target implanted with N. Also shown is a calculated line shape assuming a rotational state popultion appropriate to local thermodynamic equilibrium at a temperature of 1100 K.

[4]. We should note that the spectra show no evidence of the N_2^+ emissions that are observed in the studies of Snowdon et al. [2], no evidence of atomic nitrogen system.

A significant feature of these bands is that the lines are broad indicating significant rotational excitation. Due to the low signal strengths we were unable to employ a sufficient spectral resolution to permit a record showing individual rotational lines. We do, however, show in fig. 1 the envelope of the line shape obtained with a resolution of 4 Å. There is obviously significant broadening indicating that many molecules are ejected in excited rotational states. It has often been noted [5] that the state population of electronically excited sputtered atoms is proportional to $\exp(-E_i/kT)$, where E_i is the excitation energy of the state, k is Boltzmann's constant and T has the dimensions of temperature. It has been argued in the past [5] that excitation occcurs in a collision cascade exhibiting local thermodynamic equilibrium; in this case T is the relevant temperature. However, if the LTE model is not appropriate then T is simply an empirical parameter. Without passing any judgement on the models we have computed the line shape for various values of T using the exponential term to predict relative population of rotational states. In fig. 1 we show the calculation for $T = 1100$ K and agreement with experiment is excellent. We note that in the consideration of electronically excited sputtered substrate atoms the value of T is normally found to be much higher [5], typically 3600–5900 K. In summary we observe only the $C\,^3\Pi_u$ state formed in the lowest vibrational state with a rotational state population distribution that decreases exponentially with excitation energy of the state.

To provide some explanation of this phenomenon we may look for guidance to the studies of H_2 desorption from interstellar dust where the ejected molecules are found to be in a ground vibrational state with considerable rotational energy [6,7]. When two N atoms are on adjacent sites of the substrate they will be separated by some 4.5 Å, strongly bonded to the surface and interacting weakly with each other [6]. If one atom migrates to the adjacent site, as a result of a projectile impact, the two atoms will now strongly interact with each other and have an internuclear separation comparable with that in a normal molecule (1.15 Å, see ref. 4). The molecule would, presumably, also have a high degree of rotational and vibrational energy and without some stabilizing event should spontaneously dissociate. If stabilization occurs by some rotational transition, the molecule can remain bound and interact with surface atoms. Internal vibrational energy could be converted into kinetic energy away from the surface in a manner rather like the interaction of a compressed spring with a desk surface. When a molecule with a vibrational frequency of the order 10^{15} s^{-1} collides with a surface atom that surface atom cannot respond to absorb the vibrational energy if we assume maximum phonon frequencies to be of the order 10^{13} s^{-1}. The molecule will thus rebound, transferring vibrational energy to kinetic energy and the system can be ejected while retaining a high degree of rotational energy.

The $C\,^3\Pi_u$ state of N_2, in the separated atom limit, is composed of a ground state N atom and a metastable $N(^2D^0)$ atom. We would argue that the excited atom is not created by direct particle impact for this would presumably transfer sufficient energy to the nitrogen that it could escape the attractive bonding to the solid altogether. Rather it seems likely that the nitrogen atom could be excited by a secondary electron, a mechanism that would cause no transfer of kinetic energy. It is known that the secondary electron emission coefficient is higher for oxides than for pure materials, which might explain the increase of nitrogen signal when the sample is in an oxygen environment. Due to the excitation, the nitrogen atom will be less strongly bound and lateral surface migration would more readily occur. Barlow and Silk [7] (quoting an unpublished report by Hollenbach) estimate that the time for migration of H between adjacent surface sites of graphite is 3.7×10^{-5} s. If we assume that this figure gives the order of magnitude also for the present case we require that the excited state lifetime be greater than 3.7×10^{-5} s. The $^2D^0$ state of N is in fact metastable with a quoted lifetime in excess of 10^5 s [8] so migration is certainly possible before decay.

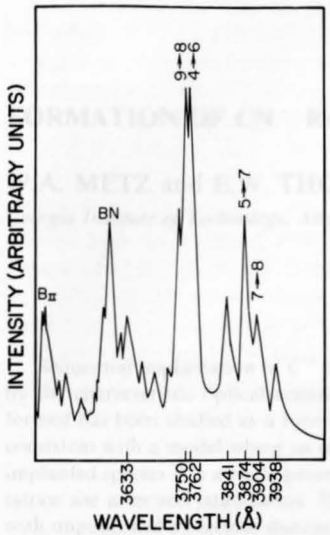

Fig. 2. A fragment of the spectrum induced by Ar^+ impact on a boron target with adsorbed oxygen. The lines are tentatively identified as due to $c^1\Sigma^- \rightarrow X^3\Sigma_g^-$ transitions of O_2 between the vibrational states indicated.

5. Molecular oxygen spectrum

We have also studied briefly the spectrum observed from boron with adsorbed oxygen. A boron sample is exposed to oxygen at a pressure of 10^{-5} Torr, the gas removed, and the sample bombarded with 100 keV Ar^+. A part of the observed spectrum is shown in fig. 2. There are a group of peaks that do not correspond to the tabulated wavelengths of BO, nor of O nor of B. Lines of B and B^+ are found at other wavelengths not shown here. We are able to identify these lines only as transitions in the $c^1\Sigma_u^- \rightarrow X^3\Sigma_g^-$ spectrum of O_2 [9]; the identification of vibrational states is shown on the figure. The $c^1\Sigma_u^-$ state of O_2 is in fact metastable, relatively weakly bound and with a large equilibrium internuclear separation. Most of the system has not previously been experimentally observed and the wavelengths quoted by Krupenie [9] are largely from theoretical predictions. These lines show no evidence of rotational broadening. The lifetime for the $c^1\Sigma_u^-$ state is estimated by Slanger [10] to be 25–50 s and if the molecule were to be ejected with any appreciable velocity the bulk of the emission would therefore come from regions outside the detector's field of view. The fact that signal is observed at all implies that the molecules reside on the surface and this is confirmed by observing parallel to the surface whereupon no signal is detected.

6. Discussion

The above observations show two rather different situations. The nitrogen spectra show considerable rotational excitation but no vibration. The oxygen spectrum seems to involve transitions not previously observed in conventional light sources and exhibits substantial vibrational excitation but no rotation. A comon feature of the two spectra is that both involve long lived metastable states, of either the molecule itself, in the case of O_2, or of the constituent atoms, in the case of N_2.

This work was supported in part by the Solid State Chemistry Program of the National Science Foundation.

References

[1] R.S. Bhattacharya, C.B. Kerkdijk, J.F. Van der Veen and F.W. Saris, Rad. Effects 33 (1977) 57.
[2] K.J. Snowdon, W. Heiland and E. Taglauer, Phys Rev. Lett. 46 (1981) 284.
[3] W.E. Baird, M. Zivitz, J. Larsen and E.W. Thomas, Phys. Rev. A 10 (1974) 2063.
[4] A. Lofthus and P.H. Krupenie, J. Phys. Chem. Ref. Data 6 (1977) 113.
[5] C.J. Good-Zamin, M.T. Shehata, D.B. Squires and R. Kelly, Rad. Effects 35 (1978) 139.
[6] R.F. Willis and B. Fitton, At. Space Sci. 34 (1975) 57.
[7] M.J. Barlow and J. Silk, Astrophys. J. 207 (1976) 131.
[8] W.L. Wiese, M.W. Smith and B.M. Glennon, Atomic transition probabilities, volume 1, N.B.S. Report NSRDS-NBS 4 (1966).
[9] P.H. Krupenie, J. Phys. Chem. Ref. Data 1 (1972) 423.
[10] T.G. Slanger, J. Chem. Phys. 67 (1978) 4779.

Nuclear Instruments and Methods 194 (1982) 505–508
North-Holland Publishing Company

FORMATION OF CN^- RADICALS BY ION IMPLANTATION

W.A. METZ and E.W. THOMAS

Georgia Institute of Technology, Atlanta, Ga. 30332, U.S.A.

Sequential implantation of C^+ and N^+ ions into KCl is shown to result in formation of CN^- radicals. Detection of the CN^- is by the characteristic optical emission of that molecule when the implanted crystal is bombarded by He^+. The quantity of CN^- formed has been studied as a function of energy of the implanted species (20 to 200 keV) and as a function of dose. The results are consistent with a model where an incoming ion A, slowed to rest, causes a localized melting region of volume ΔV and if a previously implanted species B is already present in this volume then the molecule AB is formed by recombination. The molecule adopts a cation lattice site after recrystallization. The localized melting volume corresponds to a region of radius 9.3 Å which is roughly consistent with unpublished molecular dynamics calculations

1. Introduction

We report here the formation of molecules within a solid as the result of the separate implantation of the molecule's constituent parts. The molecule in question is CN^- created by sequential implantation of C and N into KCl.

Some years ago Bazhin et al. [1] reported that when alkali halides exposed to damp air were bombarded with 20 keV H^+ or He^+ they observed a molecular band spectrum that could be identified as due to CN^-. The spectrum was exactly the same as reported earlier by Von der Heyden and Fischer [2] in studies of X-ray induced fluorescence of NaBr doped with NaCN. The bands were identified as vibrational structure in the $D\,^2\Pi_i \rightarrow X\,^1\Sigma^+$ transition. Bazhin et al. [1] argued convincingly that excitation of the CN was by recombination of excitons and these excitons were created by the impact of the incident H^+ or He^+ beam. However, they were unable to explain the nature of the reaction whereby CN^- was created by ion impact on a crystal carrying an adsorbed gas layer. The present work is in large measure an extension of that by Bazhin et al.

Following Bazhin et al. [1] we propose that an He^+ beam incident on an alkali halide creates excitons within its range and these migrate to recombination sites. If recombination occurs where CN^- is located then the molecule may be excited and the characteristic spectrum emitted by its subsequent decay. Thus the emission of the CN^- spectrum is a measure of the CN density along the projectile track. We take crystals of KCl, implant C and implant N to a definite does and then monitor the amount of CN^- by the intensity of the spectrum induced by He^+ impact.

2. Experimental

The target materials were optical purity KCl crystals, cleaved to expose the (100) face before use, and mounted on a conventional target manipulator. The targets were placed in a uhv chamber capable of a 10^{-10} Torr base pressure. A Jarrel–Ash 0.5 m scanning monochromator viewed the samples through a sapphire window; detection was by a cooled photomultiplier serviced by conventional pulse counting electronics. The optical system viewed at 30° to the target normal and at 90° from the incident beam direction.

The ion beams were obtained from a 20 to 200 keV ion implanter. For implantation of C and N the beam was collimated to 4.8 mm diameter. For studies of the CN density so created we use the emission of CN^- molecular bands induced by He^+ impact; for this a 1.6 mm diameter beam is employed so that emission was induced from the center of the implanted spot and non-uniformities at the implant edge were avoided.

In a typical experiment the target was first cleaned by heating to 400°C. The target was then bombarded with He^+, the optical spectrum recorded and the absence of CN^- emission taken as indicating that no CN^- is present as a contaminant. The sample is then implanted with C and then with N to some preselected dose using beam current densities of the order $6\,\mu A/cm^2$. We then return to the He^+ beam, record the ion induced CN^- spectrum and utilize the size of a vibrational peak (2730 Å) as a relative measure of CN^- densities.

All data were taken with room temperature targets. Preliminary annealing to 250°C caused no change to the observations. A typical observed spectrum is shown in

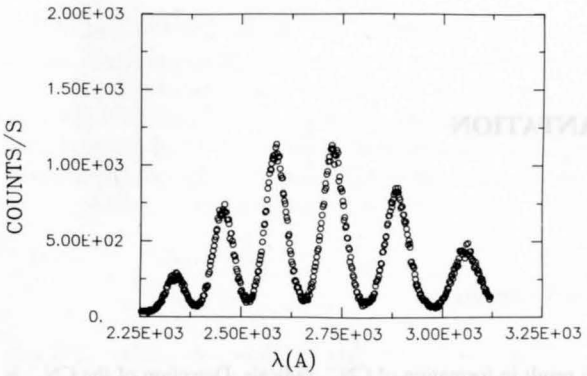

Fig. 1. Typical CN^- emission spectrum induced by 100 keV He^+ on KCl dosed with $3\times10^{15}/cm^2$ of 100 keV C^+ and $1.2\times10^{16}/cm^2$ of 150 keV N^+. The most intense peak, at 2731 Å, is identified as the $0\rightarrow10$ vibrational transition in the $D\,^2\Pi_1\rightarrow X\,^1\Sigma^+$ decay.

fig. 1. The relative intensities of the different features are independent of the implant doses and energies of C and N as well as independent of the probing He^+ beam intensity and energy. Thus we may monitor a single peak in the spectrum to provide a relative measure of CN^- density.

3. Discussion

Fig. 1 shows a typical CN^- emission spectrum induced by He^+ impact; the implant doses are shown in the figure caption, the spectrum was excited by 100 keV He^+. This spectrum is identical to the spectra reported for CN^- by Bazhin et al. [1], and identical to that reported for CN^- by Von der Heyden and Fischer [2]. It is identified [1,2] as due to a $D\,^2\Pi_1\rightarrow X\,^1\Sigma^+$ transition in CN^- with the various peaks representing $0\rightarrow v$ transitions where v is 7 to 12.

In general terms the CN^- signal increases with implant dose, is independent of dose rate, and is independent of the order in which C and N is implanted. Sputter etching of the crystal gives only a slow decrease of CN^- signal with surface erosion showing that the CN^- is in the bulk and not on the surface. There is no doubt that the CN^- is formed by recombination of C and N as the result of their separate implantations into the substrate.

The implantation of C and N as well as the analysis of the CN^- density were all performed at room temperature. We did, however, test the effect of heating the sample to 200°C after implantation to determine whether this might alter the density of CN^-. No change was observed suggesting that thermal diffusion of the implanted species was negligible.

There are two major steps in the further understanding of these experiments. In the first place we must understand the mechanism whereby the CN^- is excited so that we know how to interpret the signal in terms of CN^- density. Secondly we must try to understand how the CN^- is formed.

3.1. Excitation by He^+

When the CN^- emission intensity is studied as a function of increasing He^+ beam current we observe first a linear increase, followed eventually by saturation at high current. This can be explained on the following basis employing three distinct molecular states. There is the ground state with a local number density P_g (CN^- ions cm^{-3}), the excited $D\,^2\Pi_1$ state with local density P_i and the lower vibrationally excited state to which radiative decay occurs having a local density P_k. Under helium bombardment the total density of CN^- remains constant at a value P_T so that

$$P_T = P_g + P_i + P_k. \tag{1}$$

We can now write rate equations describing how the density of each state varies with time. If we assume excitation is by exciton recombination [1] and that the number of excitons is related linearly to beam current density I_B then we can write

$$dP_i/dt = P_g K_e I_B - P_i A_{if}. \tag{2}$$

Here the first term represents rate of excitation from the ground state and is proportional to both the density of ground state molecules and to the beam current density; K_e is simply a constant of proportionality related to the rate of exciton formation. The second term represents spontaneous radiative decay from i to f with the transition probability A_{if}. The rate equation for the vibrational excited state f is related to population by spontaneous radiative decay from the higher state i and depopulation to the ground state by some process having a transition probability A_{fg}.

$$dP_f/dt = P_i A_{if} - P_f A_{fg}. \tag{3}$$

The experimental signals are all invariant with time so that equilibrium has been established for the population densities. Setting the left hand sides of eqs. (2) and (3) to zero, identifying the rate of photon emission N_ν (photons $cm^{-3}\ s^{-1}$) as $P_i A_{if}$, and manipulating eqs. (1)–(3) we arrive at

$$N_\nu = \frac{P_T K_E I_B}{1 + K_E I_B (1/A_{fg} + 1/A_{fi})}. \tag{4}$$

At this point we should integrate the photon emission rate over the whole range of the He^+ ion allowing for the variation of exciton production rate with depth, and arrive at a total photon emission rate $\mathfrak{N}_\nu(s^{-1})$. It is, however, clear that $\mathfrak{N}_\nu$ is directly proportional to N_ν and will show the functional relationship to density of CN^-,

P_T, and beam current, I_B, given by eq. (4). To confirm the validity of the model we show in fig. 2 a plot of $I_B/\mathcal{N}_\nu$ as a function of I_B which shows a straight line as predicted by eq. (4). We have performed detailed analysis of the equation, particularly the proportionality constant K_e, placed the data on an absolute basis and shown that the slope and intercept of fig. 1 may be predicted; these considerations will, however, be relegated to a more extensive forthcoming publication. One interesting result is that depopulation of the state f (to which radiative decay occurs) back to the ground state must involve a transition rate A_{fg} of the order $10^4\ s^{-1}$. This implies that the lifetimes of the vibrationally excited ground state systems are of the order 10^{-4} s. For the moment we need only conclude that the emission intensity is proportional to the density of CN^- provided a constant beam current densty and only a single beam energy are used. In practice the data to be presented later were all taken with 100 keV He^+ at a current density of about 50 $\mu A\ cm^{-2}$ which is sufficient to cause saturation in eq. (4).

3.2. Formation of CN^-

Whatever may be the details of the recombination mechanism we would certainly expect that the density of CN^- would be directly proportional to the local density of C and to the local density of N. Thus the total amount of CN^- formed in the crystal should be proportional to the convolution of the respective implant depth distributions, integrated over the full depth probed by the incoming beams. In fig. 3 we show the relative CN^- signal for a C implant at a fixed energy of 100 keV and N implants at a variety of energies. Included is the integral of the convolution between the two depth distributions evaluated using the formulations of Dearnaley et al. [3]. Experiment and computation are in good agreement showing the amount of CN^- formed is proportional to the product of densities of C and of N.

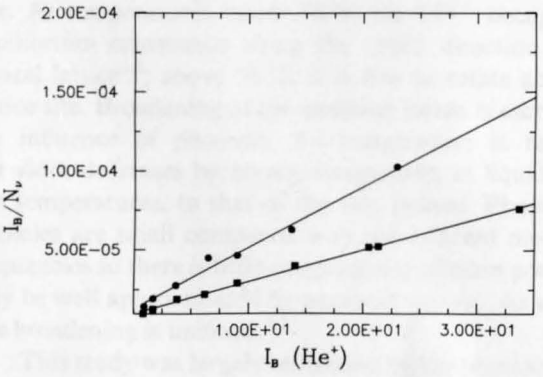

Fig. 2. Plot of $I_B/\mathcal{N}_\nu$ against I_B for He^+ impact on a crystal with implanted C and N. Here I_B is beam current density, $\mathcal{N}_\nu$ is emission intensity of the CN^- band in arbitrary units. The straight line confirms validity of eq. (4).

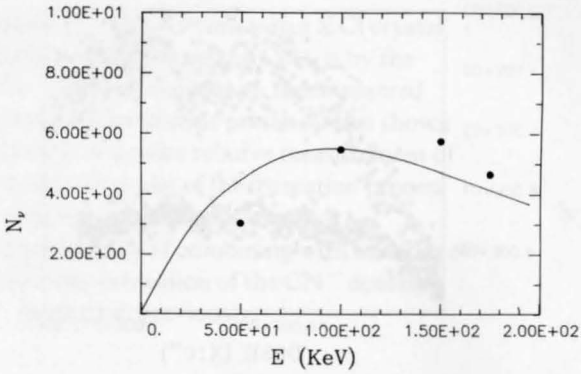

Fig. 3. A curve showing CN^- density as a function of N^+ implant energy for a fixed dose of C^+ implanted at 100 keV. Also shown is a theoretical computation of the overlap between the range distributions of the two implanted species. The experimental data is normalized to computation at 100 keV.

One approach to the mechanism of CN^- formation is simply to argue that the molecule is formed only when an N comes to rest on a lattice site occupied already by C (or vice-versa). If this were the case then to saturate the CN^- signal in a sample previously implanted with C would require an N dose of one atom for every lattice site within the projectile's range. Saturation doses are in fact an order of magnitude lower.

Landman has recently shown by a molecular dynamics simulation technique [4] that when a foreign atom is introduced into a perfect crystal there is created a local region of melting which persists for the order of 10^{-13} s before recrystallization occurs. We adopt this model to explain the present data. The incident N comes to rest, a volume ΔV becomes temporarily disordered, if a C exists within this volume the C and N recombine and after recrystallization adopt a cation lattice site. Thus for an N^+ dose of D_N per unit area a total volume $D_N\ \Delta V$ has been probed and when this volume is equal to the total volume within the projectile range distribution (equal roughly to an area of unity times twice the half width of the range distribution, ΔR_p) we should have achieved saturation. In fig. 4 we show the CN^- emission signal as a function of N^+ dose as excited by the incident N^+ themselves. We see that the CN^- signal saturates at a dose of about $10 \times 10^{15}\ N^+$ ions cm^{-2} independent of the pre-existing C^+ dose. A trivial calculation, using the range data of Dearnaley et al. [3], shows the volume ΔV to be $3.4 \times 10^{-21}\ cm^3$ corresponding to a spherical region of radius 9.3 Å. This figure is in qualitative agreement with the simulation of Landman that implies a melting over a region of the order of four lattice spacings.

We might further inquire whether the C and N

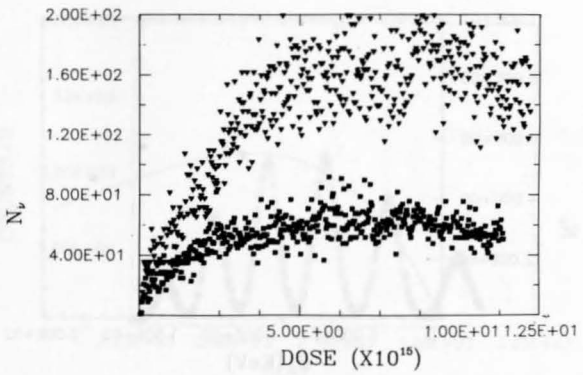

Fig. 4. Intensity of CN^- emission as a function of N dose (at 115 keV) for various preliminary doses of C at 100 keV. The CN^- emission is induced by the N itself. The triangle points are for a preliminary C^+ dose of 8×10^{15} ions/cm^2 and the squares are for a dose of 2×10^{15} ions/cm^2. Saturation occurs at an N dose independent of the preliminary C dose.

atoms might reasonably recombine within the 10^{-13} s that the melt region exists. There is a dearth of information on recombination in high density systems but this problem is now being tackled for the first time by Flannery [6]. He estimates a recombination coefficient of the order 10^{-7} cm^3 s^{-1} for recombination of Kr^+ and F^- in Ar. If we were to assume such a recombination rate was also approximately valid here and apply it to the high density molten region of 9.3 Å radius containing one C and one N we arrive at an average recombination time of 3.4×10^{-14} s. Since the molten region is estimated by Landman to persist for at least 10^{-13} s there is adequate time for the molecule to be formed before recrystallization.

4. Conclusion

We have shown unambiguously that sequential implantation of C and N into KCl gives rise to the formation of the CN^- radical. We have proposed that as an ion comes to rest in the lattice it causes a localized melted region and if the other molecular constituent is present in this region recombination occurs to form CN^-. The density of CN^- created in this manner is related to the convolution of the implant depth distributions.

This work was supported in part by the Solid State Chemistry Program of the National Science Foundation.

References

[1] A.I. Bazhin, E.O. Rausch and E.W. Thomas, J. Chem. Phys. 65 (1976) 3897.
[2] E. Von der Heyden and F. Fischer, Phys. Stat. Sol. (6) 69 (1975) 63.
[3] G.Dearnaley, J.H. Freeman, R.S. Nelson and J. Stephen, Ion implantation (North-Holland, Amsterdam, 1973) Appendix 2.
[4] U. Landman, private communication.
[5] M.R. Flannery, to be published.

Formation of CN^- radicals by sequential implantation of carbon and nitrogen ions into KCl

W. A. Metz and E. W. Thomas
School of Physics, Georgia Institute of Technology, Atlanta, Georgia 30332

(Received 14 December 1981; accepted for publication 4 February 1982)

It is shown that the sequential implantation of 20–200 keV C^+ and N^+ ions into a KCl crystal gives rise to formation of the CN^- molecular configuration. Detection of the CN^- is by the characteristic luminescence spectrum induced when He^+ ions are incident on the implanted target, a technique which represents a direct *in situ* determination of their presence. It is shown how the ion-induced optical emission may be used to provide a routine relative measurement of the quantity of CN^- present. We describe a phenomenological model of the formation process which leads to the conclusion that each incoming ion searches a volume of the target approximately 3.4×10^{-21} cm^3 in extent and has a unit probability of combining with an atom of the other species lying in this region. This model explains why saturation of the CN^- density occurs at a N^+ dose independent of the quantity of C^+ implanted previously.

PACS numbers: 61.70.Tm

I. INTRODUCTION

The purpose of this work was to study formation of CN^- radicals by the sequential ion implantation of the constituent C and N into alkali halide crystals. The CN^- so formed was detected by the optical emission of characteristic CN^- bands when the implanted target is subject to bombardment by a beam of energetic light ions, specifically 100 keV He^+. Thus the molecular configuration formed by implantation is detected while located in the bulk of the crystal lattice. There are numerous previous studies of molecules ejected out of solids by the impact of energetic beams, including observations of complexes formed by implanted and substrate particles as well as molecules of the substrate itself. In such cases, however, the molecular complex is detected after it has left the surface and it is not clear whether the complex existed before it was sputtered or was formed during ejection as a consequence of the sputtering process itself. The present work is unique in that the molecule formed, the CN^- radical, is detected while it is still located in the bulk of the target matrix.

Numerous fundamental studies have been made of the CN^- radical introduced chemically into an alkali halide matrix. At temperatures below 78 °K the CN^- occupies an equilibrium orientation along the ⟨100⟩ direction of the crystal lattice[1,2]; above 78 °K it is free to rotate about its lattice site. Broadening of the emission bands is ascribed to the influence of phonons. As temperature is reduced, linewidth decreases becoming comparable, at liquid nitrogen temperatures, to that of the free radical. Phonon frequencies are small compared with the relevant molecular frequencies so there is little coupling and phonon potentials may be well approximated by parabolic curves. As a result line broadening is uniform.[1,2]

This study was largely motivated by the previous work of Bazhin *et al.*[3] where various gases containing N and C atoms were adsorbed onto the surface of alkali halide crystals and then bombarded with He^+ or H^+ ions giving rise to emission of a vibrational band system that was identified as the $D\,^2\Pi_i \rightarrow X\,^2\Sigma^2$ band system of CN^- with transitions from the $v=0$ upper vibrational state to $v=6$ to 11 vibrational levels in the lower electronic state. The emission spectrum was identical to that observed under electron and ion-induced fluorescence of alkali halide crystals doped with CN and identical to that observed previously by Von der Heyden *et al.*[4] in the *U-V* induced fluorescence of alkali halide crystals doped with CN. Moreover some of the observed lines correspond to fragments of a CN^- spectrum identified by Douglas and Routly[5] in the gas discharge spectrum of CN. The present work differs conceptually from that of Bazhin *et al.*[3] in that here we implant the molecular constituents and Bazhin *et al.* adsorb the constituents on the surface. The spectra are, however, identical in the two cases and we may confidently rely on the conclusion of Bazhin *et al.*[3] that the spectrum is indeed that of CN^-. Bazhin *et al.* also concluded that excitation of the CN^- radical occurs by recombination of an exciton at the CN^- site and that these excitons are created by the incoming projectile beam used to induce emission of the bands. This conclusion was based on the observed behavior of emission intensity with target temperature which mirrored the expected behavior of exciton mobility and density. Important confirming evidence[3] was the observation that the characteristic CN^- emission was not produced in NaBr for which the band gap (and hence exciton energy) is 6.71 eV and inadequate to excite the observed CN^- state for which the excitation energy is 7.0 eV. In the present work the emission exhibits the same characteristics so we again rely on the conclusions of Bazhin *et al.*[3] that the observed emission is due to excitons created by an incoming ion beam. In summary, then, we shall utilize the work of Bazhin *et al.*[3] and Von der Heyden *et al.*[4] to identify the emission bands as due to CN^- and rely on the work of Bazhin *et al.*[3] to establish that excitation under ion beam impact is due to the excitons created by the ion beam itself.

The present studies involve two distinct parts. In general, we commence by implanting into a KCl crystal both C^+ and N^+ ions, the order of implantation is immaterial. We

 0021-8979/82/053529-07$02.40

believe the evidence indicates that the CN^- radicals are formed directly as a result of this implantation. Subsequently, we bombard the target with a light ion beam, generally He^+, and observe emission of an optical band spectrum characteristic of CN^-. In order to quantitatively relate the observed emission intensity to the density of CN^- and to explore thereby the formation of the CN^- radical, we must first have some clear understanding of the excitation mechanism induced by the He^+ ions. Thus the present report includes both a detailed discussion of the excitation process as well as a discussion of the formation of the CN^- radical.

II. EXPERIMENTAL APPROACH

The source of the ions for both implantation and excitation was a type 200 MPR ion implanter by Accelerators, Inc. It has a useful energy range of 20–200 keV, uses a hot cathode source capable of producing ions of any species, and is provided with conventional mass analysis and collimation facilities to ensure a well-defined ion beam incident on the surface. Ion beam current can be monitored on a Faraday cup placed behind the last defining aperture before the beam is incident on the target. The experimental system is shown schematically in Fig. 1, and is based on a small chamber placed at the end of the beam line. The chamber has a standard manipulator for holding targets and is ion pumped to a base pressure of 10^{-10} Torr before the ion beam is introduced. Differentially pumped beam line sections isolate the experimental system from the relatively poor vacuum of the accelerator.

The target was viewed through a sapphire window at an angle of 90° to the incoming beam. A Jarrel Ash 0.5 meter scanning monochromator with photomultiplier detection was used for detection and analysis of the optical emission from the target. The optical spectrum was recorded by scanning the monochromator and either displaying the photomultiplier output on a pen recorder or else on a multichannel scaler. The latter recording system is generally employed since it permits digital information that can be readily analyzed by a computer. The monochromator has a resolution of 16 Å/mm and was generally employed with a resolution of 48 Å to maximize signal levels. Improved resolution to 2 Å causes no change to the relative intensity of spectral features that we are recording here.

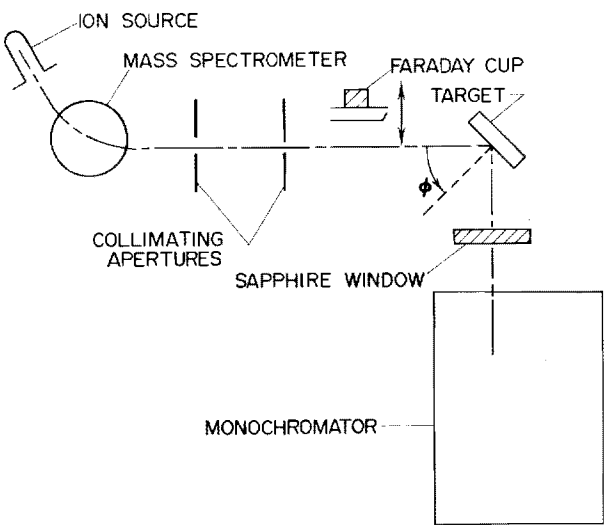

FIG. 1. Experimental arrangement.

The work reported here was confined to KCl crystals, although brief studies were made with NaCl and exhibited similar results. The crystals were optical quality materials freshly cleaved to expose the (100) face before insertion in the vacuum system. Before use they were heated to 250 °C and then bombarded with He^+ ions to confirm that there was no measurable signal from CN^- radicals before commencement of measurements. Sputter cleaning with Ar^+ was shown not to influence the observations and was not normally employed.

Implantation of the C^+ and N^+ ions was with beam densities of the order 1–50 $\mu A/cm^2$ and the beam was rastered over the 5-mm entrance aperture of the chamber to ensure a uniform implant. The analyzing He^+ beam used to induce emission was collimated to a 1.5-mm diameter to ensure that the observed emission was from the center of the implant and not influenced by irregularities at the edge of the implanted region. The targets were always placed with their normal at 60° to the incoming beam and the optical observations made at an angle of 90° to the incoming beam. When probing with a He^+ beam a projectile energy of 100 keV was employed. Minor changes to incidence angle disclosed no substantial changes of emission intensity, confirming that the projectiles were not incident in a channeling direction. Reference to standard tables[6,7] confirms that the range of the probing He^+ beams substantially exceeds the depth distribution of the implanted C^+ and N^+. All implantation and analysis with He^+ beams was performed at room temperature (20 °C).

Figure 2 shows a typical observed spectrum induced by impact of He^+ on a crystal that has been previously implanted with C^+ and N^+. In all significant respects the relative line intensities and line positions of the structures between 2300 and 3400 Å are the same as those recorded by Bazhin *et al.*[3] and by von der Heyden *et al.*[4] and ascribed by both groups of authors to the emission from excited CN^- radicals. The relative magnitudes of line intensities were independent of the conditions used for formation and for excitation; moreover, they show no change as spectral resolution is

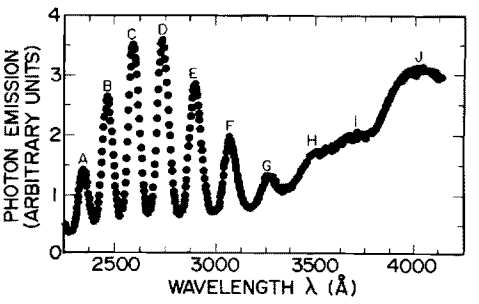

FIG. 2. Typical CN emission band spectrum induced by a 1-μA 100 keV He^+ ion beam incident of a KCl crystal that has a preliminary dose of 6.3×10^{14} ions cm^{-2} of 80 keV C^+ and 6.3×10^{14} ions cm^{-2} of 80 keV N^+.

altered from 48 to 2 Å. Thus in order to monitor emission intensity from CN^- on a relative basis as a function of excitation or of formation conditions, it is sufficient to record only the magnitude of one peak rather than integrating the whole spectrum. In practice we used a record of the 2730 Å peak for this purpose.

The intensity of the emission bands was a function of the nitrogen and carbon implant doses and of their energy. This is an observation that will be discussed later. The intensity was not a function of the time delay between implanting C and N, not a function of the time delay before analyzing with the He^+ beam, and was not influenced by cycling the target temperature between room temperature and 250 °C. Thus, there is no evidence that the C and N migrate from their implanted position over long time periods. The intensity of the CN^- bands was a function of the analyzing He^+ beam current, a feature that must be understood if the emission intensity is to be related to the density of CN. The signal was not, however, related to the time for which the crystal was exposed to the analyzing beam (i.e., not related to He^+ dose). Radiation damage caused by bombardment with the probing beam does not, therefore, appear to influence the density of CN^-.

Observation of the CN^- bands is not peculiar to a He^+ probing beam. Similar spectra are seen under bombardment by H^+, by Ar^+ and other heavy ions, as well as under bombardment by electrons. For the present studies we wish to employ a probing beam that has a range greater than the implant depth and that will exhibit no chemical reaction with any of the other species present. For these reasons we chose to utilize He^+.

For completeness we also note that the crystals used here exhibited negligible absorption in the spectral region studied, even after the implantation and analysis procedures. Therefore the spectral structures shown in Fig. 2 and the changes of intensity to be discussed later are in no way related to alterations of the absorption coefficients of the crystal.

III. IDENTIFICATION OF THE SPECTRUM

In all essential respects the typical spectrum presented in Fig. 2 is identical to that presented by Bazhin *et al.*,[3] and by Von der Heyden *et al.*,[4] with the lines being about 0.12 eV in width and 0.26 eV in separation. The relative intensities of the lines are independent of formation and excitation conditions and identical to those presented by the earlier workers. Implantation of other species (oxygen and rare gas ions) did not create this spectrum, nor did the implantation of C^+ or N^+ alone. We conclude, therefore, that the emission is indeed from CN^- and that the radical has been created as a result of the implantation of both C^+ and N^+ into the crystal.

There is a certain element of confusion regarding the precise identification of the levels involved in these transitions. All evidence points to the lower state being the $X\,^1\Sigma^+$ ground state and that the various lines represent transitions to various vibrational levels of this state. The line separation (0.26 eV) is in good agreement with the vibrational level spacing in the ground state given by Herzberg[8] (0.256 eV). There is, however, confusion as to whether the excited state is the $v = 0$ level of the $D\,^2\Pi_i$ state or the $v = 0$ level of the $a^3\Pi$ state. Bazhin *et al.*[3] point out that the intense lines have the same wavelength as those observed in gas phase discharges by Douglas and Routly[5] and ascribed by them to the transitions from the $D\,^2\Pi_i$ level. By contrast Von der Heyden *et al.*[4] perform some primitive calculations of potential curves and conclude that the excited state is the $a^3\Pi$ state. Recently Ha and Zumofen[9] have performed detailed calculations of energy levels and predict similar energies for the $a^3\Pi$ state. However, the calculations of Ha and Zumofen also include predictions of Franck Condon factors which show that the $v = 0$ to $v = 0$ transition should be the most intense with the intensity decreasing as one goes to higher vibrational energies of the ground state; this is clearly not in accord with the observations. We prefer to continue to ascribe the emission to the $D\,^2\Pi_i$ excited state. In fact, identification of the level has little impact on the work that follows. There is no doubt that the source of emission is the CN^- radical and that it has been created as a result of the sequential implantation of C^+ and N^+.

IV. MECHANISM FOR EXCITATION OF CN^-

In order to interpret the emission intensities in terms of CN^- densities one must first understand the mechanism by which the radical is excited. Figure 3 shows the CN^- emission intensity as a function of He^+ ion beam current density and clearly there is a saturation effect characteristic of two competing processes coming into equilibrium. We propose that there are three states involved in the process of excitation and decay. There are radicals in the initial ground state with a density $\mathcal{N}^g_{CN}$, radicals in the excited state with a density $\mathcal{N}^i_{CN}$ and radicals in the daughter level to which radiative decay takes place (in fact the vibrationally excited level of the ground state) with a density $\mathcal{N}^f_{CN}$. It is observed that the optical signal is independent of He^+ dose implying that the CN^- is formed by the implantation and not by the detection technique so that the total CN^- density is constant at a value $\mathcal{N}^t_{CN}$ allowing us to write

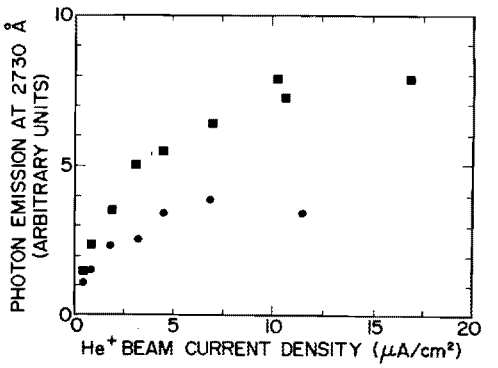

FIG. 3. Intensity at 2730 Å as a function of probing 100 keV He^+ beam current density. The two samples are implanted with a preliminary dose of 100 keV C^+ at 5.5×10^{14} ions cm^{-2}. Both samples have a preliminary N^+ dose of 7×10^{15} ions cm^{-2}; the square data points at 100 keV and the circular data points at 50 keV.

$$\mathcal{N}^t_{CN} = \mathcal{N}^g_{CN} + \mathcal{N}^i_{CN} + \mathcal{N}^f_{CN}. \quad (1)$$

Let us first consider the density of excitons that are responsible for excitation of the CN^- from the ground state. Since the observed emission intensity is invariant with time the exciton density must be constant with the rate of exciton formation equal to the rate of loss. We can write the following phenomenological equation:

$$I_B\, \sigma \mathcal{N}_e = N_{ex}\, \mathcal{N}_l\, S_l. \quad (2)$$

The left hand side represents formation at a rate proportional to the incident beam current density, I_B (ions $cm^{-2}\,sec^{-1}$), the number density of sites at which excitons may be created $\mathcal{N}_e$ (cm^{-3}), and a constant of proportionality σ (cm^2) being the cross section for exciton production. The term on the right represents exciton loss being proportional to the local number density of excitons N_{ex} (cm^{-3}), to the density of loss sites $\mathcal{N}_l$ (cm^{-3}), and with a constant or proportionality S_l having the form of the product of loss cross section and velocity with which the excitons drift through the crystal. From this expression one can derive the density of excitons.

$$N_{ex} = I_B\, \sigma \mathcal{N}_e / \mathcal{N}_s\, S_l. \quad (3)$$

As a first approximation we would argue that this expression may be taken as independent of penetration depth in the region of the CN^- formed by implantation. The rate of formation will depend on the projectile energy and this will, of course, vary with depth of penetration. However, the range of the implanted C and N is of the order 2000 Å for the energies used here[7] and is some ten times shorter than the range of the 100 keV probing He^+ beam.[6] The energy loss by the projectiles in traversing the implanted region is[6] only some 12.5 keV, leading us to believe that the rate of exciton production is approximately independent of depth in the region of interest. The loss terms will be influenced by damage caused by the implantation of C and N but since their densities are less than 1% of the substrate, we would argue that the loss processes are largely intrinsic functions of the target and therefore also not functions of depth. With these two approximations we will assume as a first approximation that the density of excitons given by Eq.(3)is invariant with depth over the range implanted with C and with N.

Now returning to the excitation process the ground state population in equilibrium is related to the expression

$$N_{ex}\, \mathcal{N}^g_{CN}\, S_{CN} = \mathcal{N}^f_{CN}\, A_{fg}. \quad (4)$$

The term on the left is the rate of excitation out of the ground state by exciton recombination and is proportional to the density of electrons, and to the density of ground state radicals, $\mathcal{N}^g_{CN}$; the factor S_{CN} is a constant of proportionality that has the function of the product of cross section and velocity of exciton drift through the crystal. The term on the right is the rate of repopulation by decay from the daughter state, f, back to the ground state. The nature of this process is unknown but will obviously be proportional to the density of atoms in the excited daughter state f. The quantity $A_{if}\,sec^{-1}$ is the transition probability for the decay.

The population of the excited state is obtained from the following equation which equates the rate of formation by the term obtained from the left hand side of Eq.(4)to the rate of loss from the state by normal radiative decay with a rate $A_{if}\ sec^{-1}$.

$$N_{ex}\, \mathcal{N}^g_{CN}\, S_{CN} = \mathcal{N}^i_{CN}\, A_{if}. \quad (5)$$

The population of the daughter state is governed by the radiative decay from the excited state, shown on the right hand side of Eq.(5)which is equal, at equilibrium conditions, to the rate of loss of that level by the decay process from the state f to the ground state g which has already appeared as the right hand side of Eq.(4).

$$\mathcal{N}^i_{CN}\, A_{if} = \mathcal{N}^f_{CN}\, A_{fg}. \quad (6)$$

Combining the above equations one can arrive at the density of the ground, excited, and daughter levels.

The rate of photon emission $\mathcal{N}_v$ photons $cm^{-3}\,sec^{-1}$, the physically observed quantity, is equal to the product of the excited state density $\mathcal{N}^i_{CN}$ and the probability for a radiative transition from i to f, A_{if}.

$$\mathcal{N}_v = \mathcal{N}^i_{CN}\, A_{if} = \frac{\mathcal{N}^i_{CN}}{1/N_{ex}\, S_{CN} + 1/A_{if} + 1/A_{fg}}. \quad (7)$$

Combining Eq.(3)with Eq.(7)the functional dependence of the emission intensity on beam current and density of CN^- is given by

$$\mathcal{N}_v = \frac{A \mathcal{N}^i_{CN}\, I_B}{BI_B + C}, \quad (8)$$

where A, B, and C are parameters associated with exciton formation and loss as well as transitions probabilities, all of which should presumably be constant. In principle, one should now integrate this equation over the full region occupied by CN to get a total emission intensity, and allow for detection sensitivity, to arrive at a prediction of the measured photon signal. Clearly with the assumptions already made concerning the constancy of N_{ex} with depth the result of such an integral is of the same functional form as Eq.(8).

Equation(8)has a number of important consequences. First we now have a representation of the signal strength in terms of beam current density that may be compared with data such as that in Fig. 3. In Fig. 4 we replot those data in the form of $I_B / \mathcal{N}_v$ against I_B. Equation(8)predicts that this should be a straight line and indeed this is the form taken by the data. Equation(8)also predicts that the signal observed for

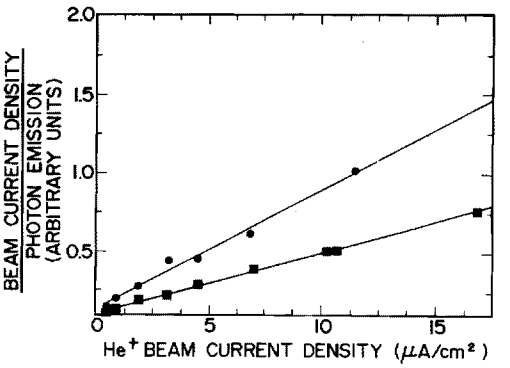

FIG. 4. Data of Fig. 3 replotted in the form of beam current ÷ intensity against beam current density to illustrate agreement with Eq.(8).

a given beam current density should be linearly proportional to the total quantity of CN present. We prepared a number of samples with C and N implanted at the same energy and in the same ratio but to different absolute doses. The observed signals were indeed proportional to the absolute dose. Equation(8)also suggests that the most suitable circumstances for probing the total CN^- density, $\mathcal{N}^t_{CN}$, is to use a large beam current density where the signal is independent of I_B; that is essentially the saturation region shown in Fig. 3. Such saturation conditions were adopted for all the subsequent measurements.

It is possible to utilize the saturation behavior shown in Fig. 3 and predicted in Eq.(8)to make some useful statements concerning the transition probabilities A_{if} and A_{fg}. Examination of Eq.(7)shows that at high beam current densities, where N_{ex} becomes sufficiently large the observed signal saturates to the following value

$$\mathcal{N}_v(\text{sat}) = \mathcal{N}^t_{CN}(A_{if}^{-1} + A_{fg}^{-1})^{-1}. \tag{9}$$

If we integrate Eq.(9)over the complete depth occupied by the implanted C and implanted N we have the result that the total amount of CN, divided by the total emission of photons, is equal to $A_{if}^{-1} + A_{fg}^{-1}$. We can make a very rough estimate of the quantities involved here. For a carbon implant density of 2×10^{15} C atoms cm^{-2} the number of C atoms in the 1.5-mm-diam region accessed by the He^+ beam is 3.5×10^{13}; this must represent an upper limit on the amount of CN subject to excitation. The signal, integrated over all of the spectrum, corrected for the limited detection sensitivity and for the spectrometer solid angle, represents a total photonemission of about 10^{14} sec^{-1}. Thus the ratio of total CN present to total photonemission is 0.35 and according to Eq.(9)this is equal to $A_{if}^{-1} + A_{fg}^{-1}$. Now the transition i to f is a normal radiative decay and must therefore exhibit a lifetime of about 10^{-7} sec; this is an insignificant contribution to the denominator of Eq.(9). Clearly then A_{fg}^{-1} must be of the order 0.35 sec implying a lifetime for decay from f to g of this magnitude. We note that transitions between vibrational levels in isolated molecules are expected to exhibit lifetimes[10] of the order 10^{-2} sec so this present very rough estimate is not unreasonable. In view of the qualitative nature of the model it would be quite misleading to propose the result we have obtained here as a measurement of the lifetime against decay from f to g. It is, however, apparent that the long lifetime for depopulation of the daughter f state is the reason for the saturation behavior in Fig. 3.

At this stage one might be tempted to perform detailed analyses of the data showing how intensity varies with ion beam current in an attempt to determine information concerning the details of the excitation and loss processes. We would regard this as quite hazardous since the equations describing the emission are at best phenomenological and may be incomplete in details. The sole purpose of our discussion here is to establish that the photonemission induced by ion impact can indeed be utilized as a measure of the total CN^- density so that we may proceed further with the analysis of how the radical is formed.

V. THE MECHANISM OF CN^- FORMATION

The above discussion has shown how the ion-induced emission of CN^- bands may be used as a monitor of CN^- density formed by implantation of C and of N. We now address the problem of modelling the process whereby the CN is formed by studying the relationship of the CN^- density to the implanted dose of C and of N, and to the energies of implantation.

A direct experiment to measure CN^- formation as a function of dose would commence with an implantation of C^+ followed by a series of N^+ implantations alternated with monitoring of the CN^- density by helium ion-induced emisison. This alternation of implanting N^+ beam and probing He^+ beam is inconvenient and time consuming. An alternative giving essentially the same information is to utilize CN^- emission induced while the N^+ ions are implanting into the target. These bands are identical to those excited by He^+ and presumably arise from generally similar mechanisms. We take the target with the preliminary C^+ implantation, then bombard continuously with N^+ and follow the buildup of CN^- by the emission of the CN^- bands induced by the N^+ as it is implanted. Such a data set is shown in Fig. 5 for two different preliminary doses of C^+. It is apparent that there is no signal from CN^- when the N^+ bombardment is commenced and that the signal increases in a generally exponential fashion towards a saturation value that occurs at a N^+ dose of about 5×10^{15} N^+ ions cm^{-2}. Comparing the two sets of observations on Fig. 5 and numerous similar observations that are not displayed here, one is led to the conclusion that the dose of N^+ required to saturate the CN^- signal is independent of the preliminary C^+ dose implanted. When using N^+ both as the probe and implant simultaneously the range of the particle is the same as the depth one is attempting to probe and there is no reason at all for assuming that the number density of excitons, and hence the efficiency for excitation of the CN^-, is the same for the whole depth being probed. Thus the data shown in this figure cannot be related to CN^- density in the same detailed manner as we have claimed for He^+-induced emissions. Never-

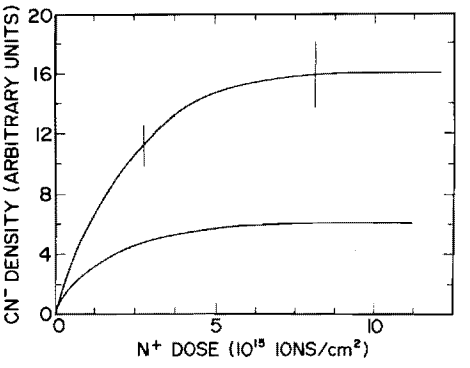

FIG. 5. Intensity at 2730 Å as a function of N^+ implant dose induced by the implanting 115 keV N^+ beam. The upper curve is for a KCl sample with a preliminary 20×10^{16} ions cm^{-2} dose of 100 keV C^+. The lower curve is for a sample with a 1.0×10^{16} ions cm^{-2} dose of 100 keV C^+.

theless, the data of Fig. 5 are a valuable qualitative indication of how the emission intensity, and hence CN^- density, builds up with dose.

As a second test we implanted a series of crystals with C^+ to a fixed dose of 2×10^{15} ions cm^{-2} at an energy of 80 keV, followed by implantation of N^+ to the same dose but with different energies for each sample. The amounts of CN^- formed were monitored by probing with the He^+ beam. The results are shown in Fig. 6 which gives emission intensity, and hence CN^- density, as a function of the N^+ implant energy. We note that the maximum CN^- density occurs for a N^+ implant energy of about 80–120 keV. This is essentially the energy region at which a N^+ implant has the same range as the preliminary 80 keV C^+ implant.

Let us consider the formation of CN^- in a some volume element ΔV. Before N^+ bombardment is commenced this volume has a local number density of carbon $\mathcal{N}_C(0)$. After bombardment with N^+ with a fixed beam current density I_B for a time t an amount of the carbon has combined with the nitrogen to form CN^- so that the density of free carbon (i.e., carbon not combined with nitrogen) has a number density $\mathcal{N}_C(t) = \mathcal{N}_C(0) - \mathcal{N}_{CN}(t)$ where $\mathcal{N}_{CN}(t)$ is the number density of CN at the time t. The incident beam of current density I_B (ions cm^{-2} sec^{-1}) deposits into the volume ΔV a number of ions $I_B f_N(x)\,\Delta V$ per unit time. Here $f_N(x)$ represents the depth distribution for the implanted species and can be written[7] in the following Gaussian form

$$f_N(x) = \frac{1}{\Delta R_N (2\pi)^{1/2}} \exp -\tfrac{1}{2}\left(\frac{x - R_N}{\Delta R_N}\right)^2. \tag{10}$$

Here R_N is the range of the N^+ ion and ΔR_N is the half width at half-maximum of the range distribution; both these factors can be obtained from the standard calculations of Dearnaley *et al.*[7] If we now simply assume that the number of CN^- radicals formed per unit time in volume ΔV is proportional to the number of N^+ ions entering the volume and to the number of density of free C atoms already present in the volume then the rate of CN^- formation can be written as $k\,[I_B f_N(x)\Delta V]\mathcal{N}_C(t)$, where k is a constant of proportionality. Normalizing to unit volume and substituting the value of $\mathcal{N}_C(t)$ we may write

$$\frac{d\mathcal{N}_{CN}(t)}{dt} = kI_B f_N(x)[\mathcal{N}_C(0) - \mathcal{N}_{CN}(t)]. \tag{11}$$

This expression gives the rate of change of CN^- number density with time and can be integrated with the boundary condition that no CN^- is present when bombardment commences (i.e., at $t = 0$) to arrive at

$$\mathcal{N}_{CN}(t) = \mathcal{N}_C(0)[1 - \exp - kI_B f_N(x)t\,]. \tag{12}$$

The local concentration of C before N^+ bombardment commences, $\mathcal{N}_C(0)$ ions cm^{-3}, is a function of depth and can be written $D_C f_C(x)$, where D_C is the preliminary dose of carbon (ions cm^{-2}) and $f_C(x)$ is the depth distribution function of carbon which will have the same form as Eq.(10)but with the ranges for carbon[7] substituted. To find the total amount of CN^- present in the sample we should, in principle, now integrate over the complete volume occupied by C and N as follows:

$$\text{Total CN} = \int_{\text{volume}} \mathcal{N}_{CN}(t)\Delta V = D_C A \int_{\text{depth}} f_C(c)[1 - \exp - kI_B f_N(x)t\,]\,dx, \tag{13}$$

where in the last equation we have performed the trivial integration over beam area A.

For low doses of N^+ (i.e., for low $I_B t$) we may replace the exponential by a series and retaining only the first significant term arrive at

$$\text{Total CN} = D_C\, AkI_B\, t \int_{\text{depth}} f_C(x) f_N(x)\,dx. \tag{14}$$

Thus the total amount of CN rises linearly with time and is proportional to the integral of the overlap between C and N depth distributions.

Let us now examine the data in the light of the above formulations. Figure 6 shows the relative variation of CN^- signals for different energy N^+ implanted into targets which have a preliminary fixed dose of C^+ at an energy of 80 keV; doses of C and of N are equal. According to Eq.(14)the CN^- signal should vary only as the overlap integral. This integral has been evaluated according to the prescription of Dearnaley *et al.*[7] and is shown in Fig. 6 normalized to the data at an energy of 80 keV. There is good agreement between theory and experiment. We believe that this agreement confirms the basic suggestion that C and N do not significantly migrate after implantation and that the formation of CN^- is simply proportional to the local density of a C and of N in the implant distributions.

The general form of Eq.(12)is also quite consistent with the exponential buildup of CN^- signal illustrated in Fig. 5. We recall, however, that this particular set of data represents CN^- excited by the N^+ beam during implantation and we make no claim concerning the detailed relationship of this signal to CN^- density. One interesting and unambiguous observation from Fig. 5 is that saturation of CN^- density occurs at a dose of about 2×10^{15} ions cm^{-2} independent of the density of CN^- in the target. This low dose for saturation

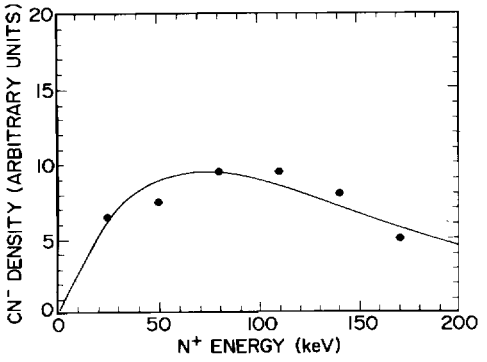

FIG. 6. Intensity of the CN bands as a function of N^+ implant energy. The emission is induced by 100 keV He^+. The targets have a preliminary implantation of 80 keV C^+ to a dose of 6.3×10^{14} cm^{-2}. The N^+ was implanted to a dose of 6.3×10^{14} ions cm^{-2} at the indicated energies. The data points are experimental values and the line is a computed value from Eq. (14), normalized to experiment at 80 keV.

is a surprising result. The preliminary carbon implantation presumably is distributed on various lattice sites throughout the carbon range in the crystal. One might have expected that to reach saturation of CN^- density one would need to implant one N^+ ion onto every lattice site in the nitrogen range to ensure that every carbon atom has received an opportunity to combine and form CN^-. The data of Fig. 5 show clearly that saturation occurs at a dose two orders of magnitude lower. Thus apparently CN^- is not formed only when one N^+ ion arrives on a site already occupied by carbon, but the nitrogen ion combines with carbon lying in some region more extensive than a single lattice site. One may understand this by re-evaluation of the meaning of the constant of proportionality k introduced in Eq. (11). Let us suppose that when a N^+ ion comes to rest it has unit probability of combining to make CN^- if a carbon atom lies within a volume $\Delta V'$ about the point where it comes to rest. Our evaluation of the rate of CN^- formation was developed by considering $I_B f_N(x)\Delta V$ ions entering a volume ΔV containing a C atom density $\mathcal{N}_C(t)$. Now each of the $I_B f_N(x)\Delta V$ incoming ions will combine with any C atom lying in a volume $\Delta V'$ about the point where it comes to rest. Thus the rate at which CN^- is formed in the volume ΔV will be $I_B f_N(x)\Delta V\Delta V'\mathcal{N}_c(t)$ and the rate of increase of CN^- density obtained by normalizing to unit volume as before giving

$$\frac{d\mathcal{N}_{CN}(t)}{dt} = \Delta V' I_B f_N(x)\mathcal{N}_C(t). \tag{15}$$

Comparing this with Eq. (11) we see that k has the phenomenological interpretation of being the volume searched by each incoming N^+ ion in its quest to find a free C atom for recombination. Thus the number of N^+ ions required to be incident in order for all available implanted C to be combined is a function only of the volume occupied by C atoms and is in no way related to the number of C atoms present. This is exactly what Fig. 5 demonstrates with the dose of N^+ required to saturate the production of CN^- being independent of how much C was present in the target. We can proceed one step further and evaluate an estimate of $\Delta V'$. Let us assume for the sake of simplicity that the implanted N is distributed over a distance $2\Delta R_p$, where ΔR_p is the half width at half-maximum of the true range depth distribution and can be obtained from the tables of Dearnaley.[7] Thus $f(x) = (2\Delta R_p)^{-1}$. Evaluation of Eq. (13) is now trivial and it indicates that the CN^- density will reach 2/3 of its saturation value when $kI_B t(2\Delta R_p)^{-1} = 1$. Figure 5 shows saturation to occur at a dose $(I_B t)$ of 2×10^{15} ions cm^{-2} and Dearnaley's tables suggest that ΔR_p is approximately 1.7×10^{-5} cm. Thus we would estimate k, which is the same as the volume $\Delta V'$ probed by each incoming N^+ ion, to be 3.4×10^{-21} cm^3 or a spherical volume of radius 15 Å. This represents a distance of some four lattice spacings in KCl.

We note in passing unpublished molecular dynamics calculations by Landman[11] of behavior in a crystal when a single atom is replaced by one with a different potential. The result of the change is a temporarily disordered region having the characteristics of localized melting and being of some four to five lattice spacings in extent. After a period of 10^{-12}–10^{-13} s, recrystallization occurs. We could apply this picture to our present situation arguing that when a N^+ ion comes to rest, it creates a disordered region having a volume of about 3.4×10^{-21} cm^3, or four lattice spacings in radius, where the constituent particles are highly mobile. If a carbon atom lies within this region there is a unit probability of recombination to form CN^-. After some 10^{-12}–10^{-13} s the region recrystallizes and the CN radical falls into a cation lattice position. The present data are consistent with such a picture but in no way confirms any details of the process involved.

VI. SUMMARY

We have demonstrated that separate implantation of C^+ and N^+ ions into a KCl target results in the formation of CN^- radicals. The density of CN^- is simply proportional to the overlap of the C^+ and N^+ implant depth distributions. This represents the first direct demonstration that molecules may be formed by implantation of their constituent parts. It is significant that when implanting N^+ into a crystal containing a preliminary dose of C^+ the amount of CN^- formed saturates at a N^+ dose independent of the amount of C^+ in the crystal. This can be broadly interpreted as indicating that each incoming N^+ ion searches a specific volume of the crystal and combines with any carbon atoms located therein; saturation occurs when the complete implant region has been searched. This requires a N^+ dose independent of the total amount of C^+ present and two orders of magnitude less than the dose which would implant one N^+ ion on each lattice site. The effective volume searched by each N^+ ion is about 3.4×10^{-21} cm^3 and therefore is about four lattice sites in radius.

ACKNOWLEDGMENTS

This work was in part supported by the Solid State Chemistry Program of the National Science Foundation under Grant DMR 8000671. One of us (E. W. T.) wishes to acknowledge the hospitality of the Forskningsinstitutet for Atomfysik, Stockholm, Sweden, during the writing of this paper.

[1] A. Diaz-Gongora and F. Luty, Phys. Status Solidi B **86**, 127 (1978).
[2] H. V. Beyler, Phys. Rev. B **11**, 3078 (1975).
[3] A. I. Bazhin, E. O. Rausch, and E. W. Thomas, Phys. Rev. B **14**, 2583 (1976).
[4] E. Von der Heyden and F. Fischer, Phys. Status Solidi B **69**, 63 (1975).
[5] A. E. Douglas and P. M. Routly, Astrophys. J. Suppl. Ser. **1**, 295 (1955).
[6] J. F. Ziegler, *The Stopping Powers and Ranges of Ions in Matter, Vol. 4* (Pergamon, New York, 1977).
[7] G. Dearnaley, J. H. Freeman, R. S. Nelson, and J. Stephen, *Ion Implantation* (North Holland, Amsterdam, 1973).
[8] G. Herzberg, *Spectra of Diatomic Molecules* (Van Nostrand, New York, 1950).
[9] T-K. Ha and G. Zumofen, Mol. Phys. **40**, 445 (1980).
[10] L. I. Schiff, *Quantum Mechanics* (McGraw Hill, New York, 1968).
[11] U. Landman, Georgia Tech (private communication).

Volume 10 Number 4 1980

Progress in Surface Science

An International Review Journal

EDITOR: Professor Sydney G. Davison

ISBN 0 08 029116 3
ISSN 0079 6816
PSSFBP 10(4) 383-490 (1980)

PERGAMON PRESS
New York / Oxford / Toronto
Paris / Frankfurt / Sydney

Progress in Surface Science, Vol. 10, pp. 383-490, 1980
Printed in the USA.

0079-6816/80/04083-108$05.00/0

FORMATION OF EXCITED STATES BY ION IMPACT ON SURFACES

E.W. THOMAS

School of Physics, Georgia Institute of Technology
Atlanta, Ga., 30332, USA

Abstract

Impact of energetic ions on surfaces gives rise to a variety of excited states in the sputtered particles, in the reflected projectiles and sometimes of molecular species bound to the surface. Where the outer shell of the system is excited the state will normally decay with emission of optical photons that may be detected with conventional spectroscopy. Where there are vacancies in the inner shells the species may be detected by subsequent emission of Auger electrons or x-rays. The review provides a comprehensive catalogue of the available data and attempts to correlate the various observations. Optical emissions from sputtered and recoil particles are strongly influenced by radiationless de-excitation processes and this is incorporated into models that describe both line shape and line intensity. There is, however, no well developed description of how the excited states are formed. Thermal excitation models that describe excitation in terms of a Local Thermodynamic Equilibrium plasma are shown to be poorly founded. Alternative models ascribing excitation to bi-particle collision events have not yet been quantitatively tested. Inner shell excitation certainly appears to be governed by electron promotion events in the transient quasi-molecule formed by a projectile and target atom. We review briefly the possible applications of ion induced optical emission to the analysis of surface composition.

Contents

The writing of this review was in part supported by the Solid State Chemistry Program of the National Science Foundation.

Vacuum/volume 34/number 12/pages 1031 to 1044/1984
Printed in Great Britain

0042-207X 84$3.00 + 00
Pergamon Press Ltd

Ion bombardment induced photon and Auger emission for surface analysis

Edward W Thomas, *School of Physics, Georgia Institute of Technology, Atlanta, GA 30332 USA*

Impact of heavy ions on surfaces induces Auger electron and photon spectra characteristic of the surfaces. In general such spectra are dominated by decay of excited sputtered particles. Auger decays are very fast so decay may sometimes occur while the particle is under the influence of the surface field, leading to complex spectral features. By contrast, radiative decay is slow so that ejected atoms are in free space before photon emission occurs and the spectra are readily recognized by reference to standard tables. We review the present understanding of both types of spectra and consider the circumstances under which they may be useful for determination of surface properties or surface composition.

1. Introduction

Impact of heavy ions on surfaces gives rise to a variety of inelastic collision events leading to ejection of ions, electrons, and photons. Photons occur as a result of a single electron decay process and are therefore related to excitation of outer shell electrons. Ejected electrons of specific energy are due to two electron decay processes and are related to excitation of inner shell electrons. When ejected ions are detected as a current we have no knowledge of whether they are excited or not. In principle each of these ejected species, photons, electrons and ions represent a characteristic signature of the surface and could lead to a method of surface analysis. In practice the only mechanism to find wide acceptance is the detection of secondary ions which leads to the technique known as secondary ion mass spectroscopy or SIMS. In this review we shall concentrate on the other two processes-ejection of photons and ejection of Auger electrons—to determine whether these can be valuable for surface analysis.

There are many important differences between radiative and Auger processes. A radiative decay involves one outer shell electron. The lifetime is of the order 10^{-8} s so that an atom ejected with any appreciable kinetic energy will move thousands of Å from the surface before the transition occurs. The decay therefore involves unperturbed energy levels which are well known from standard spectroscopic tables. The participating electrons have, however, undergone an evolution from the band structure in the solid to discrete levels of the atom. One might, therefore, anticipate that excited state populations of sputtered atoms are intimately related to surface band structure. Photon emission may occur also from transition in the solid or from atoms resident on the surface. Since the relevant energy levels are here related to the band structure of the solid we anticipate broad, ill-defined, spectral features; due to the long lifetime, decay will occur after the transient disruptions of the collision cascade have long since disappeared. Auger transitions are two electron processes leading to decay of inner shell vacancies. The lifetime is short (typically 10^{-14} s) so that if the excited atom is in the matrix it may undergo decay while the local environment is still disturbed by the effects of the collision cascade. If the relevant atom is ejected from the solid then the product of lifetime and speed may be only a few Å so that decay occurs while the atom still interacts with the surface. It is therefore not at all clear what detailed form to expect from the Auger line shape. Thus the interpretation of the spectrum remains the focus of present research and little attention has been directed to using the spectra to understand the collision process or the nature of the surface.

We shall discuss in general terms the present level of understanding of ion-induced Auger and optical spectra. Our work can be regarded as an update of previous reviews of optical emissions by White *et al*[1], on Auger emission by Baragiola[2,3] and on both subjects by Thomas[4]. The latter review in particular contains a complete bibliography of all publications before 1980. In the present discussions we shall pay particular attention to the application of these phenomena to surface analysis. We will, therefore, concentrate particularly on spectra of ejected (sputtered) particles. Spectra are also seen from the solid matrix itself but often they are not understood and are therefore not useful for analysis. This is particularly true of optical emissions.

2. Ion-induced Auger spectra

Ion-induced Auger spectra were first detected by Snoek *et al*[5] during studies of Ar^+ impact on Cu. The energy spectrum of ejected electrons showed a number of peaks that were ascribed to Auger decays of the solid copper target. The peaks were however broad and ill-defined, in part due to the poor resolution of the electron energy analyser and in part, as we shall see later, to a smearing of energies inherent in this case. The work of Snoek *et al*[5], was not pursued. The next observations were by Haas *et al*[6], during sputter etching of Al by Ar^+ ions. They found that the Ar^+ ions induced Auger signals just as strong as the electron beam and that the spectra for ion impact and for electron impact were in fact

different. From these observations has sprung a steadily increasing study of ion induced Auger spectra.

The technique for investigating the ion induced Auger spectra is quite straightforward and can be illustrated by one of the author's own arrangements[7] shown as Figure 1. The ion beam is directed onto the target and the ejected electrons analysed by a commercial cylindrical mirror analyser (CMA). This CMA has on its axis an electron gun and together they represent a conventional electron-induced Auger analyser arrangement. A great advantage for fundamental studies is that the electron-induced and ion-induced Auger spectra may be recorded with the same experimental arrangement. Retarding potential analysis has been used by Hasselkamp and Scharmann[8] and a simple curved plate system by Nègre *et al*[9].

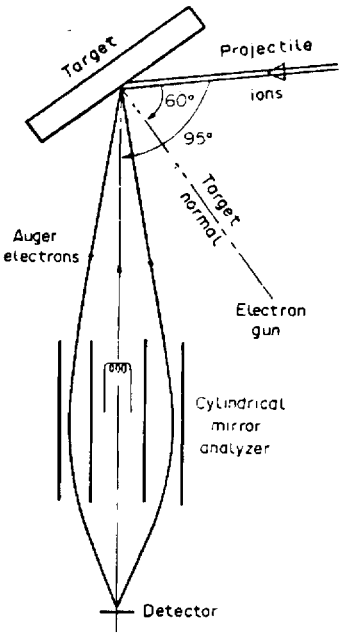

Figure 1. Schematic diagram of the arrangement used for study of ion induced Auger Spectra by Metz *et al*[7].

Reported experiments use ion beams of energies from 1 - 400keV and generally H^+, He^+ or rare gas ions as the projectile. For fundamental studies one must of course use well defined targets, good quality vacuum systems and flat target surfaces. One must take some care that the axes of electron detector and ion beam interesect at the same point on the target. For analysers that have definite focusing properties it is essential that the analyser be located at the correct distance from the irradiated spot on the target otherwise considerable spectral distortion will occur. With the arrangement shown in Figure 1 one can check focusing very conveniently by using the electron gun to induce a spectrum and comparing this with standard spectral atlases. The arrangement shown in Figure 1 detects only the electrons emitted into specific directions. The retarding field analyser used by Hasselkamp and Scharmann[8] analyses and detects all electrons ejected from the surfaces. Nègre *et al*[9], used a moveable detector and studied Auger signals as a function of detector orientation relative to crystallographic directions. In this last case it must be recognized that a heavy ion beam creates substantial damage and the order in a single crystal is rapidly destroyed by bombardment. Thus study of ion-induced spectra from single crystals may prove quite difficult.

Auger spectra taken with electron impact and used for analytical purposes are generally recorded in a derivative mode since this enhances line features and de-emphasizes the continuous background. This is also convenient for the ion induced spectra. However we prefer to record the integral spectra believing that they are more satisfactory when attempting to perform basic studies.

The conventional technique of Auger surface analysis is to excite inner-shell electrons by an electron beam of some 2 10 keV energy. The mechanism of excitation is a direct Coulomb interaction and no significant momentum is transferred to the target atom so that it remains in place in the lattice. The subsequent Auger decay will generally involve valence band electrons so that the ejected electron energy spectrum is related to the valence band density of states. A transition resulting from an L-shell vacancy with decay and ejection of valence band electrons is designated LVV. These electron-induced mechanisms are quite well understood and the major research activity relates to extraction of the valence band density of states from the Auger electron line shape. Clearly line shape and position will be a function of the chemical composition of the target under study.

Proton impact on a solid target can excite electrons only by Coulomb excitation and, in general, little momentum is transferred to the matrix so that again the excited atom is not displaced. A subsequent Auger decay process will involve the same features as decay of an electron-excited Auger decay process so the line shape and position is again related to the valence band density of states. Protons and electrons will, according to the Born approximation, exhibit identical excitation cross-sections at sufficiently high energies. Thus, we expect no significant differences between electron and proton excited Auger lines. This expectation is confirmed in the very limited work published on the subject[10]. In principle Auger spectra excited by high energy protons should be just as useful for analytical purposes as electron-induced spectra. In practice the complexity and cost of a proton accelerator precludes routine use of the technique.

Excitation by a heavy particle beam is somewhat different. Very large excitation cross-sections can occur at low projectile energies by promotion of inner shell electrons through crossing of molecular orbitals. Such excitation processes were described first, for bi-particle gas phase collisions, by Barat and Lichten[11]. Moreover substantial momentum may be transferred from projectile to target because masses are similar. Thus the target atom, with an inner shell vacancy, may be displaced from its normal lattice location leading to the possibility of decay while in motion in the solid or when in free space after ejection (sputtering). Clearly the spectra induced by heavy particle impact may be quite different from those induced by electrons. We show in Figures 2 and 3 typical spectra[12] induced by 190 keV Ar^+ on Mg and Si surfaces compared with electron induced spectra of the same samples. The ion-induced spectra have three major components. There is an underlying continuous distribution decreasing with increasing electron energy that is true secondary electron emission; subtracting this from the spectrum would leave us with the Auger decay contribution. Within the Auger component is a further underlying broad structure that strongly resembles the electron-induced spectrum and is therefore probably related to decays of excited atoms located in the matrix. Thirdly we have a number of sharp peaks (labelled I, II, III, IV on Figures 2 and 3) whose limited width suggests that they emanate from atomic-like structures. It is these atomic-like features that provide the most significant distinction between electron- and ion-induced spectra.

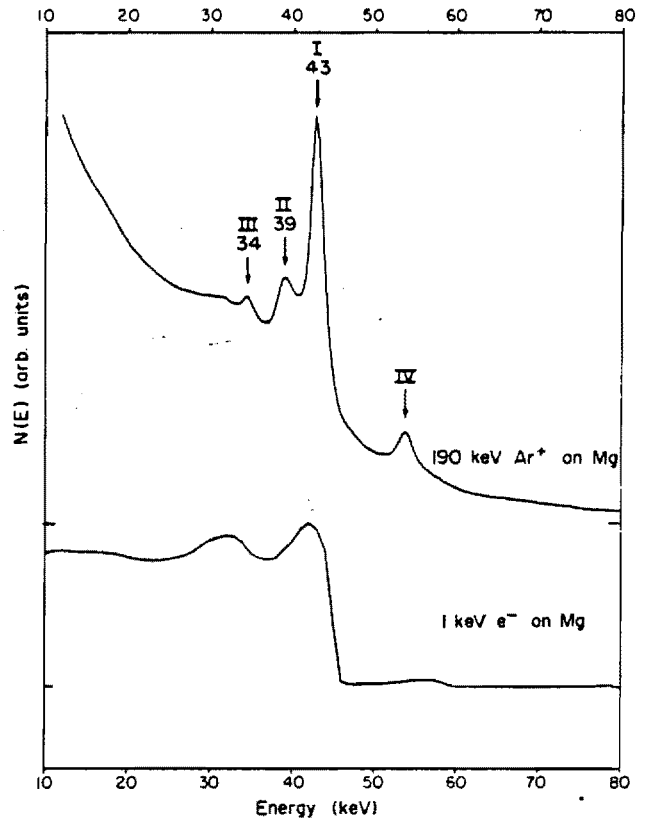

Figure 2. Auger Spectra of magnesium induced by 190 keV Ar^+ and 1 keV electrons[12].

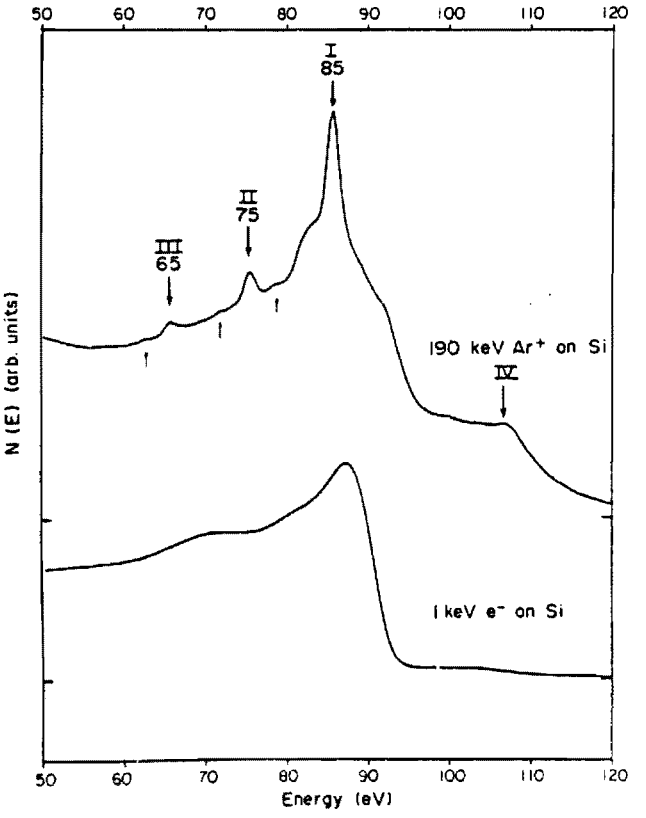

Figure 3. Auger spectra of silicon induced by 190 keV Ar^+ and 1 keV electrons[12].

In both Mg and Si the lines are at about the energy expected from decay of a 2p vacancy (of the target) but bear no close resemblance to lines from isolated atoms excited in gas phase collisions.

Explanation of the ion-induced Auger spectra requires separate consideration of the excitation and decay processes. To an extent the characteristics of these spectra and their excitation mechanisms have been discussed in earlier reviews[2-4]. We shall concentrate entirely on heavy particle (Ne^+, Ar^+, etc) excitation since light particle (H^+) induced processes are similar to electron impact processes and are therefore well understood.

2.1. Excitation mechanisms. All authors agree that the excitation mechanism involves electron promotion by curve crossing of molecular orbitals in the scheme originally formulated by Barat and Lichten[11]. Consider an Ar + Si collision event. The energy levels for the Ar Si 'molecule' at zero internuclear separation will be those of a Ge atom and are well known; similarly at infinite separation the energies of electrons are those appropriate to the isolated atoms. Energy levels at intermediate separations must connect the two extremes and may be sketched out using the prescriptions of Barat and Lichten. A general result is that as internuclear separation decreases the $4f\sigma$ orbital rises in energy and crosses many other orbitals some of which will be empty; at such crossing one or more of the electrons in the $4f\sigma$ orbital may in principle transfer to a state with a vacancy. As the atoms recede from the collison event the orbitals return to their separated atom limits and the $4f\sigma$ vacancy may be retained. The $4f\sigma$ orbital terminates on the 2p level of the colliding partner of lowest Z leaving it with a vacancy. Thus the promotion model, in its simplest form, predicts that for an Ar + Si collision vacancies will be formed only in the 2p level of the lighter species (i.e. Si), for a Ne^+ + Si collision the promotion would be of a 2p electron in the neon projectile and one should observe no decay of 2p vacancies in Si. Experiment does not conform to this simple rule as Si Auger spectra from 2p vacancies are observed for both Ar^+ and Ne^+ impact on Si with the latter differing only by exhibiting a lower signal[13] than for Ar^+. This paradox was ascribed by some authors[14a] to a large contribution from Si + Si recoil collisions which also will promote 2p electrons of Si. There may however be another explanation. The molecular orbital picture provided by Barat and Lichten[11] is apparently overly simplistic and has been modified by Schneider *et al.*[15], to include avoided crossings and other detailed features; this revised picture is based on a detailed study of promotion in bi-particle gas-phase Ar + Si collisions. While excitation of the 2p electron in the lightest species (Si) is indeed the predominant mechanism there is observed also excitation of the 2p electron of the heavier species (Ar) but at a substantially lower cross-section. Assuming that the same picture holds for Ne + Si collisions one cannot use the similarity between signals from Ne + Si and Ar + Si to determine whether projectile target or recoil target target collisions are the principal mechanisms. Some further guidance may be obtained by considering absolute magnitudes of signals and of cross-sections. The work of Schneider *et al*[15], gives a cross-section of 4×10^{-17} cm^2 for excitation of Si 2p electrons in Ar + Si collisions (at energies of 50–500 keV) which with a Si number density of 5×10^{22} cm^{-3} would suggest that 5% of all projectile target collision events in the first monolayer will result in excitation of 2p electrons of Si. The excitation rate in Ar^+ solid Si collisions has not been measured but for Ar^+ + Al, which should be similar, the data of Hasselkamp and Scharman[8] show a total Auger yield from Al-2p decays that suggests 2% of all incoming projectiles cause ejection

from the surface of an electron from the decay of an Al-2p vacancy. If we consider that one half of all Auger decays in a particle-solid experiment give rise to an Auger electron directed into the solid—and therefore not detected—we would estimate roughly that the total experimental yield is 4%. Thus the yield of electrons is approximately equal to what we would estimate from projectile-target collisions in the first monolayer alone. Two other factors suggest also that the observed signal is due only to collisions in the first one or two monolayers. Firstly, the escape depth of the Auger electrons is only[16] about 4 Å so that no signal of any type from a greater depth should be observed. Secondly, direct calculation of recoil and primary collision event probabilities predicts that recoil collisions contribute no more than 15% of all excitation events[17]. Thus we would suggest that the 2p-shell excitation events probably occur by direct projectile target collisions in the first one or two monolayers of the surface and that recoil collisions do not contribute significantly to the observed Auger signals: this contention does, however, require more detailed analysis.

Molecular orbital promotion occurs only at small internuclear separations where there is a strong repulsive interaction of nuclei. For example, in the Ar + Si system $4f\sigma$ promotion occurs at[15] 0.37 Å. Consequently there should be an energy threshold for the excitation event corresponding to repulsive energy at the internuclear separation where curve crossings occurs. Such thresholds have been demonstrated by Wittmaack[13] in rare gas-Si collisions, the signals rising by three orders of magnitude from a 2-3 keV threshold to 30 keV. According to the gas phase collision studies of Schneider *et al*[15], the cross-sections and therefore signals, should become constant for higher energies. A second consequence of the large repulsive energy at molecular orbital crossings is that substantial momentum will be transferred to the target nucleus. Consequently the nucleus will be displaced from its original lattice site and either recoil into the solid or be ejected out of the solid. In the latter case decay may take place in free space so that the Auger transition is appropriate to a free particle. As we shall see later this is indeed the explanation of the sharp atomic-like features in spectra like Figures 2 and 3. We would expect also that the lines should show a Doppler broadening and that this will vary with momentum transferred and hence with projectile energy. Wittmaack[13] showed that the line width of atomic-like features is in fact energy dependent consistent with a Doppler broadening.

The above discussion has been based on studies of rare-gas ion impact on third row elements but the same general features hold also for other collision events. We would note particularly our own work on Auger spectra induced by Ar^+ on transition metals[18] where the principal feature is due to 2p vacancies in the Ar projectile, as expected from the molecular orbital model. The line shows substantial energy dependent broadening consistent with the emitting species being backscattered particles.

In summary then, the general observation in cases studied to date is an excitation of 2p vacancies by projectile target events in the first one or two monolayers. This is generally in accord with the molecular orbital promotion model provided one takes into account the full details of avoided crossings and rotational coupling. An energy threshold is anticipated and observed in practice. Momentum transfer to target species may be significant leading to ejection so that decay occurs in free space. In this case one anticipates sharp atomic like features which may be those of Figures 2 and 3, and Doppler shifts of energy which have been measured by Wittmaack[13]. For cases where the target is heavier than the projectile we expect substantial backscattering so that large Doppler shifts from backscattered projectiles will be observed: this phenomenon also has been detected[18].

2.2. Decay mechanisms and spectral details. The above discussion of mechanisms would lead us to believe that ion-induced Auger spectra should consist of two distinct components related to whether the excited atom is in the matrix when it decays or whether it has been ejected into free space. A matrix decay should presumably involve valence electrons and be describable as an $L_{23}VV$ transition. This should be just the same as an $L_{23}VV$ transition induced by electron impact and indeed both Figures 2 and 3 appear to show such a component underlying the sharp peaks of the ion-induced Auger spectra. There is, however, a discrepancy in the case of Si where the high energy edge at the electron induced spectrum (at 91 eV) does not coincide with the sharp drop of the ion induced spectrum which occurs at 95 eV. An atom ejected into free space, by contrast, should decay as a free atom with distinct sharp lines designated $L_{23}MM$, perhaps broadened by Doppler-effects. This, in principal, explains the atomic-like features but the observed lines do not coincide properly with spectra induced in gas phase collisions. Thus, although qualitatively the spectra are as expected, there is some question about the fine details.

The literature contains many abortive attempts to explain the atomic-like features. The basic problem is that for an ejected particle with a single 2p vacancy the calculated Auger line energies do not agree with observation. For example $L_{23}MM$ decay of the $2p^5\,3s^2$ structure of magnesium gives only a single energy peak[19] of about 35 eV explaining perhaps line III of Figure 2 but not the more significant features I and II. Consequently there has been a search for other mechanisms. It is often noted that the excited state lifetime (10^{-14} s) may be comparable with the time for which the collision cascade persists so that decays in the solid are in a disordered environment. Thus, entirely new spectra characteristic of neither solid nor atom might be observed and study of the decays might provide a unique method of probing directly the physical conditions in the cascade. Vrakking and Kroes[14a] suggest that the matrix particles in the disordered collision cascade have 'atomic like' structures that give rise to peak I; peak II is electrons from the same source that have lost energy by exciting a plasmon. Decay in the disordered matrix is invoked also by Benazeth *et al*[14b]. Such suggestions are never quantified to the point of a detailed prediction of line positions. One mistake in these analyses is that the authors ignore the possibility that *neutral* atoms with inner shell vacancies may also occur. For magnesium the relevant parent level would be $2p^5\,3s^2 3p$ where one electron is removed from the 2p shell to form the vacancy, but another is added to the outer shell to maintain neutrality. Such configuration were suggested by Dahl *et al*[19], to explain certain details of Auger spectra induced by $Mg^+ + Ar$ gas phase collisions. From Hartree Fock calculations they estimate Auger energies of 44 eV for a $2p^5 3s^2 3p \rightarrow 2p^6 3s$ transition and 40 eV for $2p^5 3s^2 p \rightarrow 2p^6 3p$; these fit, within accuracy limitations, both peaks I and II. Moreover Dahl *et al*[19], provide a theoretical calculation which suggests that the relative probabilities of decay by these two paths should be 4:1 which is roughly the ratio between features I and II. We must not neglect the possibility also of ions and an Mg^+ $2p^5 3s^2$ configuration decaying to Mg^{2+} $2p^6$ is estimated by Dahl *et al*[19], to have an energy of between 34 and 35 eV (depending on the calculation procedure) which would explain peak III. One should also note that the weak high energy feature designated peak IV could be explained as a $2p^4 3s^2 3p \rightarrow 2p^5 3s$ transition for

which the estimated energy[19] is 54 eV. Thus in a purely qualitative fashion one can completely explain all significant features of Figure 2 relaying on anticipated transitions with decays of the unusual *neutral* atom as the cause of the most prominent peaks. There is apparently no need to invoke a new class of atomic-like states[14], peculiar to collision cascades, for explanation of these observations.

Our discussion has been largely qualitative and these explanations can only be considered reliable if we may use them to explain in quantitative detail the observed spectrum. Basically one wishes to take each of the suggested contributing components and use them to simulate in complete detail the observed spectrum. This we have recently done[12,20] for spectra of Mg, Al and Si induced by Ar^+ impact and the reader is referred to these publications for full details. We shall here confine ourselves to a brief description of the procedure for a magnesium target. The spectrum of Figure 2 shows a background decreasing to higher energies that is due to true secondary electrons. We simulate this by the mathematical function introduced by Sickafus normalized to the data at low (<20 eV) and high (>60 eV) energies where no features are observed. We add to this the electron induced Auger spectrum of Mg (see Figure 2) to account for matrix decays and thereby simulate the main feature underlying peaks I, II and III. Then the Auger energies listed in the previous paragraph are taken to give individual lines which we represent by Gaussian functions. These various components are then added together and fitted to the data by a non-linear curve fitting routine based on the gradient expansion algorithm of Marquand[21]. We allow the intensities of all components to vary and also the width of the line Gaussian functions. Since the energy of the $2p^53s^23p$ state is only roughly estimated we allow this to vary also though the separation of lines from decay to $2p^63s$ and $2p^63p$ configuration is kept fixed since this is well known. We show in Figure 4 the results of this fit and clearly all significant features are properly represented. The width of the atomic features is consistent with Doppler broadening due to the particles having energies of around 100 eV.

The same modelling and fitting procedure has been used also for the ion-induced Auger spectrum of aluminium with similar excellent results[20]. Again the key to the procedure is recognizing that the major atomic like features are due to Al^0 atoms in a $2p^53s^23p^2$ configuration.

As we proceed on up the periodic table we find a deterioration of agreement between model and experiment. For silicon, which obviously has an outer electron structure far more complex than magnesium, our model gives line B of Figure 5. The predicted peak positions are properly reproduced. We show that there is a line (designated i) that lies at an energy above the electron induced LVV spectrum edge. This extra line explains the apparent discrepancy between the high energy edge of the matrix components in electron and ion-induced spectra. Baragiola[2] and Wittmaack[13] explained this discrepancy as due to a change in local density of states in the collisions cascade. These explanations are not necessary and should be considered without foundation. Despite this general agreement on location of features there remains a substantial discrepancy between line B and the data which betrays the existence of yet another Auger feature. Atoms with excited core holes have short lifetimes[22] which for the 2p levels of Mg, Al and Si are respectively 930, 134 and 37 fs. If we assume, following Wittmaack's Doppler shift measurements, that the excited atom emerges from the solid with an energy of 100 eV then decay occurs within a distance of 260, 35.6 and 9.7 Å for Mg, Al and Si respectively. If we assume that the potential of the surface extends some 5 Å from the first monolayer then for Mg essentially all decays of emerging atoms occur in free space while for Si many decays will occur within the field of the surface. We have tentatively suggested[12] that the additional component of the spectrum is due to emerging atoms undergoing Auger decay while still within the field of the surface. One would anticipate the outer shell electrons having a configuration intermediate between that of the solid and that of the isolated atom and a broad line should result. Cursory analysis of the spectra for sulphur and phosphorus[23] suggests that this new component is even more significant, consistent with the shorter lifetimes of S and P.

Regrettably, very few studies have been reported for ion-induced Auger spectra of elements outside the third row of the

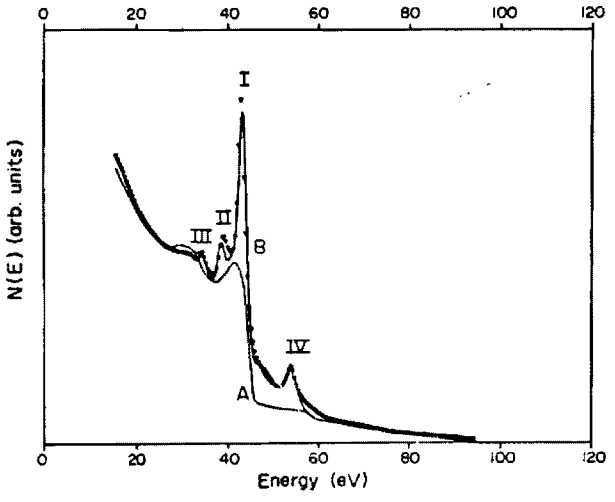

Figure 4. The Auger spectrum of magnesium induced by 190 keV Ar^+ impact. The experimentally determined spectrum is shown as a series of individual data points. Line A is the representation of true secondary electrons plus decay in the matrix. Line B represents the complete model including atomic lines and is essentially coincident with the data at most energies. Roman numerals are used to identify features discussed in the text. From Whaley and Thomas[12].

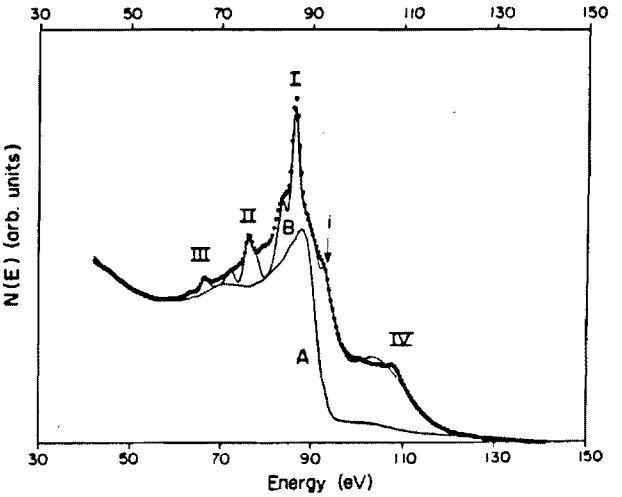

Figure 5. The Auger spectrum induced by 190 keV Ar^+ impact on Si is indicated by data points. Line A is the component representing true secondary electrons and matrix decays. Line B represents the model prediction when only Line A, the individual atomic transitions and decay of two electron vacancies is considered. Clearly Line B does not reproduce the data points. From Whaley and Thomas[12].

periodic table. Boron has been studied a number of times[7,23] and shows a broad line from excitation of 1s electrons. Copper was studied by Dorozhkin *et al*[24,25] and shows a broad structure at about the energy expected for 3s excitations. In both these cases the structures cannot be described as 'atomic-like' and the authors suggest that decay is occurring within the field of the surface. Dorozhkin *et al*[26] study also Ar^+ ion induced Auger spectra of BeO and LiF showing that the Auger peaks of Be and Li are the same as that of the pure metal. This is as expected since for both metal and compound the particle of interest is sputtered from the lattice and decays as a free atom (or ion).

The broad conclusion is that the ion-induced Auger spectra of the solid are due to decays of excited atoms in one of three locations. In all cases some atoms will decay while in the solid either while in motion or while at a lattice site. It would appear that the line shape is the same as that of an electron excited Auger decay. In some cases a significant fraction of the excited atoms are sputtered from the surface and decay in free space giving a predictable line spectrum. It is particularly important in this case to consider neutral particles with inner shell vacancies since these provide the predominant features for elements in row three of the periodic table. Finally one also observes in some cases an Auger component that appears to arise from atoms emerging out of the surface but decaying while still within the field of the surface; the result is a broad feature that is intermediate in form between the matrix decay and atom decay spectra. The relative importance of these three components is directly related to the lifetime of the excited state and to the speed (and direction) of the excited particle. These broad conclusions are supported by recent measurements of how the matrix and atomic decay components vary with projectile impact angle where good agreement with a theoretical model is demonstrated[27].

It is appropriate to speculate briefly on the mechanism which leads to the majority of ejected atoms with inner shell vacancies being neutral rather than ionized. This is certainly not the case for the corresponding bi-particle collisions in gas-phase targets where multiply ionized species predominate[19]. The electron promoted by a curve crossing of molecular orbitals will of course transfer to a vacant state. It is possible that an electron from a 2p level may promote to the 3p level of the same atom so that neutrality is maintained. However, such a mechanism should occur equally well in gas-phase bi-particle collisions but in practice[19] is not a major feature in the spectra. Alternatively as the inner-shell excited particle ejects from the surface it may pick up electrons by charge transfer from the valence band to maintain neutrality. It is well known[28] from gross charge state analysis that the majority of sputtered particles are neutral. There are many theories that argue the particle starts as an ion but picks up electrons to become neutralized as it traverses the surface edge[29]. We speculate that this occurs also for ejected particles with inner shell vacancies.

2.3. Applications to surface analysis. Ion induced Auger spectroscopy is at present an area of research and not a diagnostic tool. We must however examine whether it has any potential for routine analytical purposes. Spectra induced by protons will be essentially the same as by equi-velocity electrons and could in principle be utilized routinely. To produce protons of the same velocity as 3 keV electrons would require a 6 MeV accelerator. The difference in cost and complexity between a 3 keV electron gun and a 6 MeV proton accelerator effectively precludes routine use of protons. Spectra induced by rare-gas ion impact are a mixture of matrix, atomic and perturbed-state decays that render them inherently more complex than electron-induced spectra. In the few cases where detailed analysis has been performed the signal is predominantly from sputtered atoms and so gives no information on the band structure, nor chemical composition of the surface. High energy (>30 keV) impact of heavy ions may sometimes exhibit cross-sections for inner shell excitation that exceed those for electron impact and provide, for limited cases, a potential improvement in sensitivity. Nevertheless this is not of general value for surface analysis.

It is worth noting that ion-induced Auger spectra may be a hindrance in attempts to analyse depth distributions using sputter etching and electron-induced Auger analysis of the surface. If the etching beam (usually Ar^+) and electron gun are employed simultaneously then both may produce detectable spectra and these will be different. To avoid confusion the two beams should be used alternately or the ion beam energy kept below the threshold for electron promotion.

A major reason for pursuing the academic study of ion-induced Auger spectra is the opportunity to probe the electron structure of atoms perturbed by the surface. As we showed earlier short lived states undergo their Auger decay while interacting with the surface so that the energy levels involved are those of an atom perturbed by the field of the surface. In principle the energy levels can be unfolded from the data allowing some assessment of how electron energies evolve from the band structure of the solid to the discrete level structure of the isolated atom. There is an active program on the study of orientational effects in ion-induced Auger spectra. Kitov and Parilis[30] have treated theoretically the anisotropy of Auger yields due to H^+ impact on single crystal Al; shadowing and channelling effects are significant. Nègre *et al*[9], provide experimental measurements of (very weak) orientation effects for Ne^+ and Ar^+ impact on single crystal Al. With the interpretation of spectra that we have suggested[12,20] and discussed above, the orientation effects should occur only for matrix decays and, therefore, be essentially similar to those for electron induced spectra. There are also published studies[31] of how the ion induced Auger spectra change with chemical composition but these have not been quantitatively analysed and the chemically-induced changes may all be due to the matrix decay and therefore essentially the same as for electron impact.

3. Ion induced photon spectra

Optical spectra induced by ion impact on solids were studied as early as the 1920s and 1930s with publications by von Hippel[32] and Sporn[33] on emission from sputtered cathodes in discharges. The first clearly defined experiment was that of Snoek *et al*[34], in 1964 on spectra induced by Ar^+ impact on solid Cu. Since that time there have been many papers on the subject.

The techniques necessary for a properly defined experiment are quite straightforward. An ion beam is directed onto a surface and the optical emission observed by a suitable spectrometer. Photomultiplier detection is essential. An arrangement drawn from the author's own work[35] is shown as Figure 6. For fundamental studies attention must of course be paid to surface cleanliness, vacuum environment and surface structure.

Radiative decay involves a one electron transition, normally in the outer shells only. Lifetimes are typically 10^{-8}–10^{-7} s so that if the excited particle is sputtered from the surface the emission may occur at a macroscopic distance from the point of ejection. In setting up experiments to detect this emission the optics should be arranged to collect with equal efficiency light from all parts of the

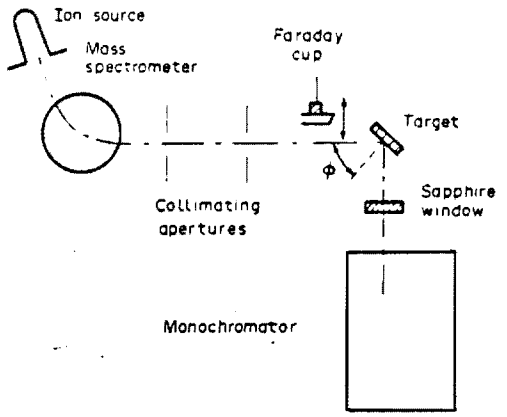

Figure 6. Equipment for the study of optical emissions induced by ion impact on solids[35].

emitting region. Calibrating the optical system to perform absolute measurements requires use of a standard lamp and considerable attention to detail: procedures have been reviewed earlier by the author in the context of gas phase collisions[36]. Calibration of relative sensitivity at different wavelengths is a necessary step to permit proper interpretation of spectral intensities. Absolute calibration, and therefore absolute measurements of emission, are rarely performed.

A very wide variety of projectiles and targets have been used in such studies and they are too numerous to mention here. Much of the recent work is devoted to silicon and its oxides bombarded by Ar^+ ions; this relates to the opportunity for sputter etching of electronic device materials.

Radiative decay of excited outer electron shells of atoms (and ions) is quite well understood and the wavelengths of all significant transitions are tabulated in numerous works of reference. Thus, there is no confusion in analysing spectra of sputtered particles that decay in free space. Radiative decay in the solid involves electron energy bands and gives rise to broad spectral features. These are often not understood and must be studied before they can be used for analytical purposes. Many of the experiments in this area have been devoted to study of excited reflected projectiles. This does not assist with surface analysis and will not be considered here as little work has been done since the review by Thomas[36].

We shall discuss separately the mechanisms for excited state formation, the process of decay and the possible applications to surface analysis. We shall find that excitation is not at all well understood, decay is generally unambiguous and that applications to surface analysis are quite specialized.

3.1. Excitation mechanisms. Photon emission results from excitation of an electron to a bound state. Excitation of an electron to a continuum state results in the formation of an ion and must have an essentially similar theoretical formulation. Thus mechanisms leading to ion-induced photons and to ejected ions must be essentially similar. It is to be admitted that the theoretical understanding of excitation events in solids is very weak. One would prefer to treat the excitation process in a detailed quantum mechanical fashion following evolution of wave function and state populations as an atom is ejected from the solid. This is, of course, very difficult in practice and must be formulated individually for each case of interest. Consequently much attention has been devoted to formulation of general descriptions based on statistical population of states, or local thermodynamic equilibrium in collision cascades.

A general approach developed by Anderson and Hinthorne[37,38] but tested also for optical emissions is to treat the collision cascade region as being at high temperature T. Atoms are excited, ionized and ejected from this region. Yield of a species having an excitation energy E_j will be given by

$$Y_j = C\left(\frac{w_j}{Q}\right)\exp -\frac{E_j}{kT}. \qquad (1)$$

Here w_j is the statistical weight of the state of interest, Q is a constant for a given target, T is the effective temperature of the plasma region and C is the concentration of the species of interest at the surface. Anderson and Hinthorne[37,38] proposed this formulation to interrelate the yield of different ions in SIMS; here w_j is unity and E_j is the ionization energy of the state of interest. Good-Zamin *et al*[39], have demonstrated that this equation also correlates well with the yield of different excited states. Here w_j is the statistical weight of the state, E_j is the excitation energy and Y_j is the total yield obtained by summing all decays out of the excited state. For excitation Good-Zamin *et al* find that a temperature T of 3600-5900 K fits data from a wide variety of materials. Figure 7 is drawn from their work and the straight lines drawn through the data have a slope $1/kT$, allowing T to be determined. Snowdon has effectively demolished this approach, he points out that there is no physical basis for the LTE model, that excited atoms are too large to exist in a solid[40], that experimentally the same relative state populations occur also in excitation of gas phase targets[41] (where no high temperature LTE region can exist) and that the whole formulation is often incorrectly applied to the data[42].

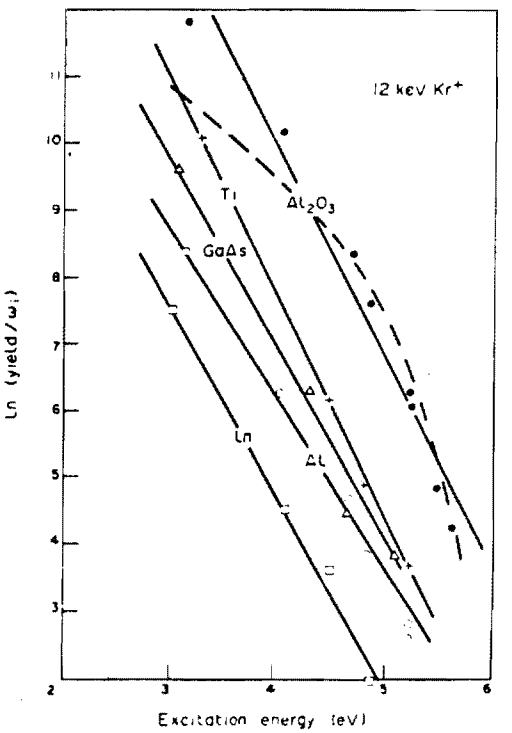

Figure 7. Photon yield in decay of state, as a function of level excitation energy E_j. For Al, Al_2O_3, GaAs, In and Tl bombardment by 12 keV Kr^+. From the work of Good-Zamin *et al*[39]. The straight solid lines are drawn to fit the data on the assumption that the LTE model is valid and that equation (1) is applicable. The dashed line is a calculation for Al (fitted to the data for an Al_2O_3 target) by the statistical model of Kelly[58].

Nevertheless there have been some attempts[43-47] to develop the techniques for analysis of stainless steel in the following manner. The procedure is to establish Q in equation (1) by a standard sample, then for the material of interest to plot the relative line intensities for the constituent materials in the form of equation (1). The plots give the effective value of temperature T and one can determine the ratio of concentrations C for the different constituents. As Tsong[48] points out the LTE model requires that a single temperature should describe all constituents since they evolve from the same collision cascade. He shows that in steel different temperatures are required for Ni and for Fe contrary to expectation. In general terms one must conclude that the LTE model is quite invalid.

A second approach based on the collective properties of the solid is to consider electron transfer between an emerging atom and the surface. In Figure 8 we show the potential well of an atom located at a short distance from the potential well of the solid. We neglect the question of how the excited state was created and concentrate instead on its possible destruction by resonance tunnelling. In Figure 8 the excited electron is at an energy where an allowed but vacant state exists in the solid; the excited electron may tunnel into the solid leaving the excited particle as an ion. The rate $R_i(s)$ (units of s^{-1}) of resonance ionization can be written in the form.

$$R_i(s) = A \exp(-\alpha s) \tag{2}$$

where s is the particle-surface distance (cm), A is a constant (s^{-1}) related to barrier height and a (cm^{-1}) is constant related to barrier width. If a particle is emerging with a velocity component normal to the surface of $v_\perp$ (cm s^{-1}) then it is a simple matter[49] to show that the probability of emerging to $s = \infty$ without electron loss is given by

$$P(\infty, v) = \exp -\frac{A}{av_\perp}. \tag{3}$$

Since radiative decay involves long lifetimes and will occur at macroscopic distances from the surface this equation gives the probability that an excited atom will emerge to decay radiatively. Introducing a further constant B to represent the (unknown) rate of excited state formation then the yield of a given excited state may be written

$$Y = B \exp -\frac{A}{av_\perp}. \tag{4}$$

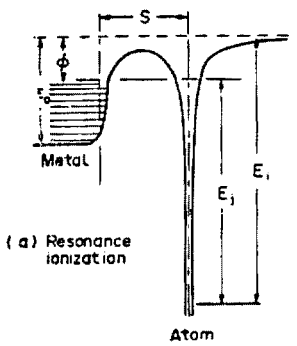

Figure 8. Potential configuration for an atom at a distance S from a surface with an electron in the excited state of energy E_j to demonstrate resonance ionization. E_i is the ionization function of the ground state atoms, ϕ is the target work function and E_0 is the depth of the target valence band.

This formulation has been tested in a number of ways. It should apply to projectiles backscattered from a surface. Backscattered projectiles will have a velocity distribution which may be modelled and from this distribution a Doppler broadened line shape can be evaluated. If the radiationless decay process is not included then the predicted line shape does not agree with experiment. Applying equation (4) to modify the velocity distribution of excited recoil atoms one can fit[50] the observed line shape by altering the ratio A/a. By the same token if backscattered flux is modelled theoretically and equation (4) is used to represent excited state yield then one can also model the projectile energy dependence of optical emission intensity[51]. Thomas and co-workers have performed a number of such analyses for hydrogen backscattering from metals[50,51] and conclude that A/a is of the order 10^8 cm s^{-1}. The formulation may also be used to consider dependence on projectile energy of sputtered excited particle yield. The velocity distribution of sputtered particles may be estimated theoretically and as projectile energy increases then momentum transfer, and hence recoil velocity ($v_\perp$ of equation (4)) increases also. Thus, one may model projectile energy dependence of sputtered particle emission intensity and choose a value of A/a that fits the data. An example from the work of White *et al*[52] is shown in Figure 9. At low projectile velocities there will be low recoil velocities and a high probability of radiationless decay leading to low signals. As projectile energies increase, so do recoil velocities and the time for which the recoil interacts with the surface decreases; this results in a reduced rate of loss and an increased intensity. The data of Figure 9 generally follow the expected behaviour; the discrepancy between experiment and theory is ascribed to the energy dependence of the initial excitation rate (B in equation 4) which is not included here.

A most significant feature of ion-induced optical emissions is that the signal strength is strongly dependent on the matrix from which an atom is ejected. This is dramatically illustrated by Figure 10 from the work of White *et al*[53], which shows the Si 2882 Å line observed in sputtering of SiO_2 compared with that from Si. For the oxide the signal is far stronger than for the pure material with a broader line shape peaking at the wavelength of unshifted radiation. This can be qualitatively explained by the radiationless de-excitation model. The excited electron in Si is at a level opposite a forbidden band of the SiO_2. Thus resonance ionization cannot occur and all excited atoms emerge and radiate. For Si that same level is opposite an allowed but vacant state so

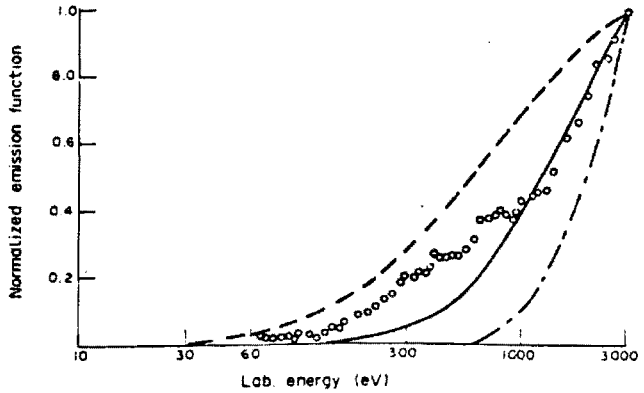

Figure 9. Comparison of three calculated emission functions computed using A/a values of 7.5×10^5 cm s^{-1} (dashed line) 2×10^6 cm s^{-1} (solid line), and 5×10^6 cm s^{-1} (dot-dash line) with measured emission function (open circles) for CuI 3247 Å in the case of Ar^+ on Cu. From White *et al*[52].

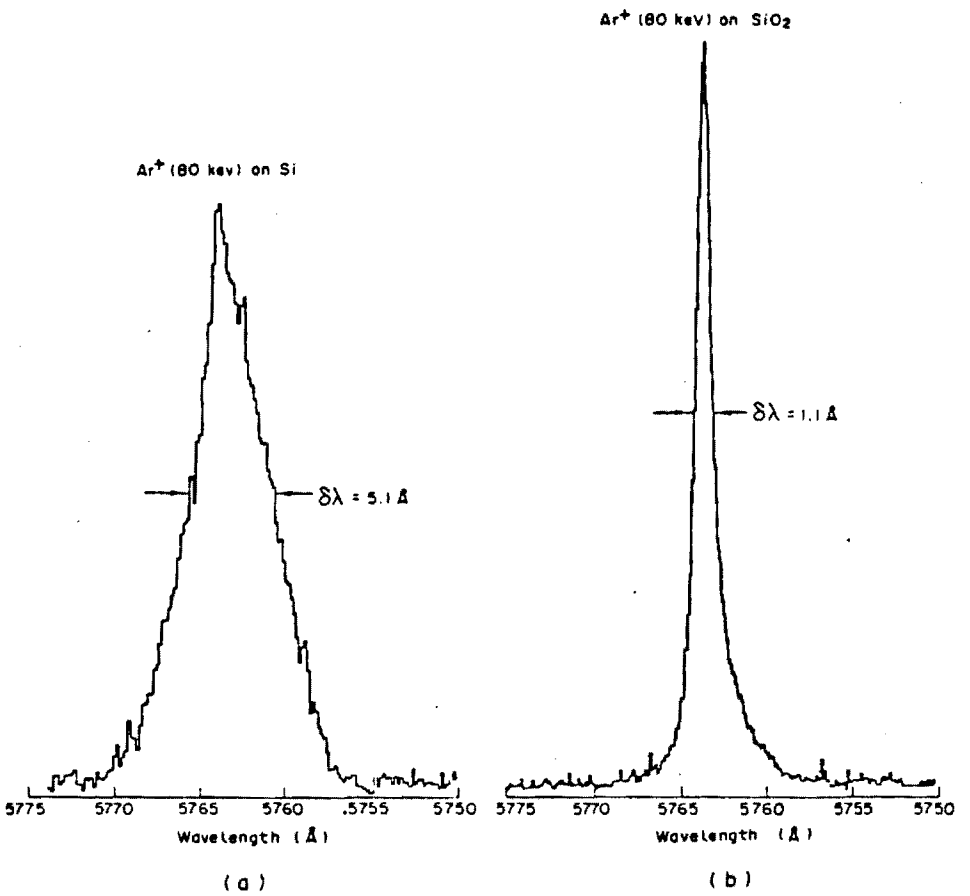

Figure 10. Measured line shapes of the 2882 Å SI line by 80 keV Ar^+ ion sputtering from Si and from SiO_2. The vertical scales are distorted in that the intensity from Si is a factor fifty lower than for SiO_2. The change of total intensity of this line is demonstrated in Figure 12. From White *et al*[53].

that resonance ionization is possible. In the latter case slow recoiling particles are lost causing a reduction in signal particularly at wavelengths close to those of stationary atoms. The high velocity component of the sputtered particles is less severely effected and the intensity at large Doppler shifts does not differ greatly between Si and SiO_2. Hippler *et al*[54] have performed similar experiments on Zn with and without oxygen coverage giving a similar behaviour as illustrated in Figure 11. they have modelled both lines using equation (4) and found A/a for the clean surface to be 5×10^4 cm s^{-1} and for the oxygen covered surface to be 5×10^6 cm s^{-1}.

The general picture of radiationless de-excitation provides an understanding of many qualitative features. It explains energy dependence, line shape and matrix effects. The picture is not however of universal validity as for some lines[55] (specifically of magnesium sputtered from Mg and MgO) the effect of oxidation is not as predicted. The formulation, of course, gives no guidance on the probability of forming the excited state in the first place and the constants A and a cannot be accurately predicted. Finally the model is based on unperturbed energy levels and that is clearly unrealistic for particle surface separations of 2 5 Å where the radiationless decay processes are expected to occur. We conclude that radiationless de-excitation is a useful tool for qualitative understanding but does not provide detailed quantitative predictions and is not always qualitatively consistent with observations.

The procedures based on LTE and on radiationless de-excitation are designed to act as simple explanations applicable to

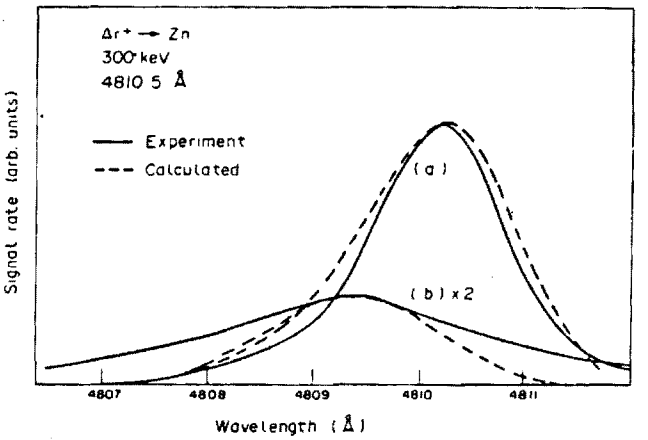

Figure 11. Comparison of experimental and calculated line shape of the indicated Zn line for (a) surface covered with oxygen and (b) a clean metal. Experiment and model calculations are normalized at the peak intensity. From Hippler *et al*[54].

all materials. When examined in detail they fail. This is not at all surprising. In the much simpler case of bi-particle inelastic collision events one must perform detailed quantum mechanical calculations for each case of interest. One would expect the same thing to be true also for excited state formation in solids. Indeed there is evidence that inelastic events in solids are dominated by bi-particle collisions between the particle of interest and only one

atom of the solid. For example oscillations in the neutralization probability[56,57] of He^+ ions incident on lead are due to a near-resonant charge transfer reaction between the helium and a single lead atom. Also excitation of Zn by $Zn^+ + Ar$ bi-particle collisions gives essentially the same spectra[41] as excitation by Ar^+ impact on solid Zn. If bi-particle collisions are to be the predominant excitation mechanism then we must first decide which collisions are involved. Kelly[58] argues that since excited atoms are too 'large' to exist in the solid they must be created as they cross a surface. Moreover since excited particles are ejected at normal projectile incidence one cannot ascribe ejection -excitation events primarily to direct projectile target collisions. Kelly argues therefore that the principle source of ejected particles is recoil collisions in the cascade where a low lying atom collides from behind with a surface atom so ejecting it into free space. This approach is also confirmed by work of Symonski *et al*[59]. Kelly[58] states that ideally excitation would be described in terms of curve crossing processes as the ejected atom departs from its neighbours. We have already encountered the concept of curve crossing in our discussion of inner shell excitation, for which it is a relatively simple concept as energy levels are well defined. For outer shells, however there is little detailed information on the evolution of energy levels with particle separation and the matter is further confused by broadening of energy levels due to the uncertainty principle. Some attempts have been made to formulate the problem as in the work of Sroubek *et al*[60] on the state of sputtered ions and the work of Blaise[61] on sputtering of metal atoms in excited states from oxides. In principle the problem could perhaps be formulated in a stationary state approximation predicting energy levels and occupation probabilities at successively increasing particle surface separations. Such an approach has been formulated completely for the interaction of H with a jellium target[62]. However for any situation involving more complex electron structures the formulation problems become formidable and no generally applicable scheme is available. One would expect to await guidance from theoretical consideration of bi-particle collisions where problems are similar. Kelly[58] admits defeat on the matter and adopts a statistical model. This involves an estimate of the probability that the recoil collision event will lead to an energy transfer required to cause excitation, E_i, followed by a distribution of population into the various degenerate states of energy E_j. Assuming that unperturbed energy levels are appropriate to the interacting particles one can then develop an expression for yield as a function of excitation energy E_i. The general prediction is of excitation probability decreasing with excitation energy E_j and having a distribution very similar to that predicted by the discredited LTE model, (equation (4)). We show in Figure 7 the prediction by Kelly[58] for Al which reproduces the curvature of the data while the LTE model predicts a straight line. the new statistical model still shows substantial discrepancy with experiment.

Our general conclusion is that the models based on collective and purely solid state concepts do not permit any detailed predictions; in the case of the LTE model the initial assumptions cannot be justified. We prefer, following Kelly, to argue that we must consider the detailed interaction of the ejected atom with the recoil particle that caused ejection. A quantum mechanical treatment should in principle permit description of the process. Since that is technically unfeasible at present one can provide some useful predictions of relative intensity from the statistical model of Kelly[58]. That model has not yet been applied to compounds or alloys.

3.2. Decay mechanisms. Radiative decay of sputtered atoms will occur in free space so that lines will be from isolated atoms which are well known. Numerous standard listings of wavelengths are available. There are however practical concerns in relating emission intensity to state population. In general an excited state decays by more than one transition. To determine level population one should, in principle, measure intensities of all decays of the excited state and add them together. This will require that the relative detection sensitivities be accounted for and if some transitions lie in unfavorable wavelength regions this may not be very accurate. An alternative procedure is to use tabulated transition probabilities to estimate branching ratios and thereby estimate level population from measurement at a single wavelength. A further complication is that an excited state may be populated by cascade from higher levels so that the measured population is not that for the original excitation process. All cascading transitions should be measured and subtracted from the signal due to decay of the state of interest. Again relative detection sensitivity must be calibrated. In practice cascade population is often small and can be ignored. Further if only relative measurements are required then branching in decay may also be ignored. While sputter ejected species are generally monatomic one sometimes observes spectra of molecules particularly of N_2[63,64], O_2[63] and CH. These are readily recognized. Sometimes, however, populations of high rotational states can be unexpectedly large[65] leading to broad continua that are not easily identified. Furthermore there are a number of reports of broad continua[66–72] that emanate from sputtered molecules with repulsive ground state configurations. Study of such continua is a continuing project and the relevant states are not yet well understood so that they are of little value for analytical purposes.

3.3. Applications to surface analysis. The use of ion induced optical emissions for surface analysis was suggested first by White *et al*[60] who coined the acronym SCANIIR (surface composition analysis by neutral and ion induced radiation). They demonstrated its potential by producing spectra of dried blood, meteorites, and glasses induced by Ar^+ ion impact[73]. A manufacturer of scientific equipment even produced a device for sale consisting of an ion accelerator and optical multichannel analyser; this was not a commercial success. SCANIIR should have advantages and disadvantages very similar to the well established SIMS technique. The inelastic processes leading to sputtered ions and to sputtered excited particles should be essentially the same. The basic process is not understood in either case and matrix effects confuse interpretation of data. Both involve sputter erosion destroying the surface under study. A major potential advantage of the optical technique is that a high optical resolution is very easy to achieve and spectral identification is unambiguous. In SIMS the mass analysis is quite complex and overlapping of peaks, particularly involving molecular complexes, can confuse interpretation. SCANIIR is a simple technique only for wavelengths between say 2000 and 6000 Å. Lower wavelengths are possible if the complete optical path is evacuated and higher wavelengths suffer from poor detector sensitivity. If a species does not have a strong radiative decay in the 2000–6000 Å region then it is not readily detected.

A true quantitative analysis of a surface is possible only when there is a theoretical understanding of the signal one is detecting. This is certainly not the case for ion induced photon emission although one could still provide an analysis by reference to standard sample if excitation efficiencies were independent of the

matrix. This turns out to be a severe problem for ion induced optical emission—as indeed it is also for SIMS. Frequently as one moves from a pure metal to an oxide or to an oxygen covered surface the signal increases greatly as illustrated in Figure 12. The same phenomenon occurs for nitrides[74], CO covered[75] surfaces, etc. A further, perhaps related, problem is that in most situations little or no signal is observed from H, C, N and O when they are incorporated into the surface. The problem here may be that they sputter principally as negative ions which have no excited states. One might anticipate useful analyses when the species of interest is present in the matrix as only a trace element. Since the ejecting atom interacts only with its immediate neighbours the matrix effects will be constant provided the element of interest is present only in a small fraction of the lattice sites.

Ion-induced optical spectra will of course always be a direct characteristic of the surface and can act as a 'finger-print' to permit its identification. This is, however, not as valuable as a compositional analysis.

We shall discuss first circumstances under which optical emission has already proved useful in quantitative and qualitative analysis. We turn then to an application that has the potential for determining surface structure.

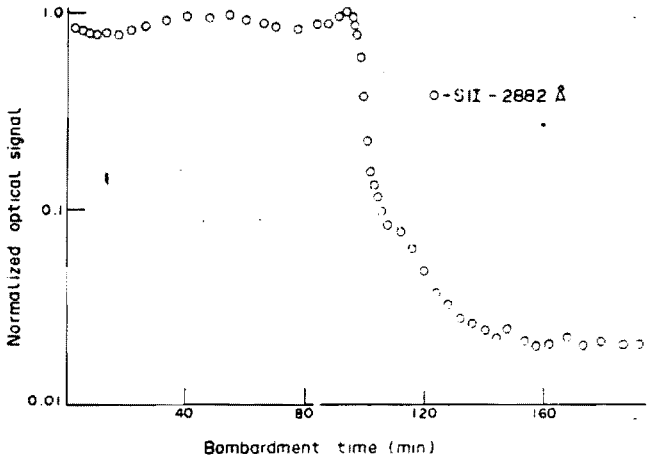

Figure 12. Intensity of the Si I 2882 Å line induced by 80 keV Ar^+ impact shown as a 1200 Å thick SiO_2 surface on an Si substrate is profiled. Note that the intensity scale is logarithmic. Signal is shown as a function of bombardment time (and hence dose). The authors made no attempt to convert to a depth scale. From White *et al*[43].

3.3.1. Quantitative and qualitative analysis. Quantitative analysis will be possible when the element of interest is present in relatively small quantities. Detection sensitivities were assessed by Tsong and Yusuf[76] for a variety of elements using NBS glass samples of known composition. For each element the chosen wavelength was that which gave maximum signal provided always that the excited state lifetime was of the order 10^{-8} s or less so that decay took place in a small spatial region. In Table 1 we show the chosen lines and estimated detection sensitivities. An estimate is given also of the fraction of ejected atoms that radiate at the wavelength of detection. It is noted that the highest sensitivity is achieved using states of low excitation energy and that for alkali metals a sensitivity of 1 ppm (by weight) is attainable. Knudsen *et al*[77] have also provided spectra from various metals and shown what wavelengths in the range 1000–3000 Å are most favorable for analysis of certain metals and semiconductors. The fraction of sputtered Si and Ni atoms in excited states is provided by measurements of Williams *et al*[78]. The various absolute figures of sensitivity or of yield per sputtered particle are applicable only for the matrix used in the original study. The data of Table 1 are applicable to silicate glasses and may be valid also for other insulators. For metals, however, radiationless de-excitation may occur reducing both signal and sensitivity.

Tsong and co-workers[74,81,82,84] have used optical emissions to study composition of a variety of mineralogical specimens. Relative concentrations of Si, Al, Fe, Ca, Na and K have been determined[81] in a variety of Feldspar samples and agree to within a few per cent with electron microprobe analysis. Of particular interest is the determination of hydrogen in natural gem diamond[79], in GdF_3[83] in topaz[80], silicon[80] and titanium[80]. The depth profiles of H in an α-Si film on Ge and GdF_3 films on glass were determined by following the H_α intensity as a function of dose as the film was eroded by the projectile ion beam. The study of H is particularly significant since it cannot be detected by the conventional technique of Auger spectroscopy. Tsong and Liebert estimate[80] that the detection limit of H by this technique is 1500 ppm. A problem in depth profiling is that the dose of the exciting beam must be related to eroded depth by a sputtering coefficient determined in a subsidiary experiment. Depth resolution is defined primarily by homogeneity of the incident beam. A further group of studies on glasses by Bach[84–86] studies interdiffusion of Si from an SiO_2 layer with Pb and B within the substrate glass.

A general attempt to perform analysis of metals has been made by MacDonald and co-workers[43–46] as well as Okatani[47] using steel samples of known composition as standard targets. They invoke the Anderson–Hinthorne LTE model[37,38] to permit estimates of relative concentration. We have discussed this model earlier and shown that it has no physical basis. Moreover Tsong *et al*[48] point out that each constituent of the steel must be represented by a different (and unpredictable) effective temperature. While a rough assessment of composition may be obtained the results are not encouraging.

We should mention also an interesting suggestion of Meriaux *et al*[87] to use the optical emission for mapping purposes. They illuminate a sample with a broad projectile beam and view it through a microscope fitted with a narrow band optical filter (a Fabry Perot etalon) at the wavelength of one of the expected constituents. In practice a vidicon camera and screen is used to enhance detection sensitivity. One achieves a picture of the surface taken at the wavelength of one of its constituents and therefore showing the distribution of that constituent over the surface. By changing the transmission wavelength of the filter one may map the distribution of different elements. The technique was demonstrated by studying a mixture of magnesium and aluminium crystallites.

It is worth considering at this point some of the advantages[81] of the SCANIIR technique. The equipment is relatively cheap being only an ion gun, spectrometer and recording system. The spectra contain fewer lines than in ordinary spectra chemical analysis by an arc discharge, making identification and analysis a more rapid procedure. Multielement analysis is simple and spatial resolution can be defined easily by optical means. There are certainly problems in depth resolution due to probing beam inhomogenities and ion induced mixing but these are of course also present in SIMS.

3.3.2. Detection of interfaces. During sputter etching of layered materials it is sometimes important to determine when a layer has

Table 1. Absolute photon yield expressed as number of photons emitted per sputtered atom for the prominent lines of 34 elements. The detection limits for these elements are also given.

Element	Line (Å)	Energy of upper level (eV)	Photon per sputtered atom ($\times 10^{-3}$)	Detection limit (ppm by weight)
Ag	3281	3.77	10.14	200
Al	3962	3.14	2.55	50
B	2497	4.96	0.26	100
Ba	5535	2.24	1.44	800
Be	2348	5.27	0.22	50
Ca	4227	2.93	3.00	50
Cd	2288	5.41	0.21	200
Ce	4187	3.51	0.095	2500
Co	3453	4.01	0.41	500
Cr	4254	2.91	1.73	300
Cs	4555	2.72	4.58	100
Cu	3247	3.81	3.83	150
F	6902	14.52	0.007	3000
Fe	3581	4.31	0.75	300
Ge	3039	4.95	0.75	500
H	6563	12.09	0.35	15
In	4511	3.02	2.18	500
K	7665	1.61	2.69	20
Li	6708	1.85	8.37	1
Mg	2852	4.34	6.99	40
Mn	4034	3.07	2.47	200
Mo	3798	3.26	5.33	150
Na	5890	2.10	7.41	1
Ni	3415	3.65	0.71	400
P	2536	7.20	0.003	7500
Pb	4058	4.37	0.082	5000
Re	3460	3.58	0.75	400
Si	2882	5.07	1.28	250
Sr	4607	2.69	4.20	200
Ta	3311	4.43	0.083	3500
Ti	3653	3.44	0.18	700
Tl	3519	4.48	4.65	500
Zn	2138	5.79	0.009	6300
Zr	3601	3.59	0.11	1300

been penetrated as for example in the removal of SiO_2 from an Si substrate. This can be conveniently performed by following the optical signal of one of the constituent elements. Figure 12 shows the record of White *et al*[53] for profiling through an SiO_2 layer on Si; the large change in optical signals is due primarily to a change in the matrix related efficiency for exciting the state. Similar effects are seen also in SIMS spectra. The advantage of the optical emission over SIMS is that no equipment is required to intrude into the vacuum chamber. Optical emissions during plasma etching of surfaces (as in device fabrication) can also provide qualitative indications of erosion rates and detection of interfaces; the arrangement used would be similar to that described by Kelly *et al*[88].

3.3.3. Determination of surface structure. The above discussions have been concerned with composition analysis. There is one case where surface structure has been determined and which could perhaps be developed into a technique of general applicability. Thomas and Efstathiou[89] have studied nitrogen molecular emission induced by ion impact on nitrogen implanted silicon surface. The N_2 emission is in the 0-0 vibrational transition in the $C\ ^3\pi \rightarrow B\ ^3\pi$ band and is found to have an extended rotational structure. At first sight one would expect an N_2 molecule on an Si surface to be in thermal equilibrium with its surroundings and that ejection and excitation should be by a Franck Condon transition that would not alter rotational state population. Thus an N_2 molecule sputtered from a room temperature surface should show a Boltzman distribution of rotational state population with an effective rotational temperature of, say, 300 K. In Figure 13 we show the measured rotational state population as a function of rotational quantum number in a so-called Boltzman plot. In this representation a thermal population should give a straight line of slope related to temperature. The data of Figure 13 are not on a straight line so that no single temperature is appropriate. Similar non-Boltzman distributions are observed for NO scattered[90] at very low energies from Ag. Non-Boltzman distributions with significant high J population are apparently a characteristic feature of molecules that have resided on a surface.

An explanation for this phenomenon has been provided by Gadzuk and co-workers[91] who have pointed out that a molecule residing on a surface cannot have the same quantum mechanical description as a free rotor. They formulate the rotational structure of an N_2 molecule assuming rotation occurs in an infinite conical well of half-angle θ. In effect the molecule is considered as a dumbbell with one atom fixed on the surface and the other rotating about a normal to the surface; rotation occurs only for angles between dumbbell axis and surface normal that are less than the half-angle of the conical potential function. This is called a hindered rotator and it is assumed that the rotational states are populated in a Boltzman distribution appropriate to surface

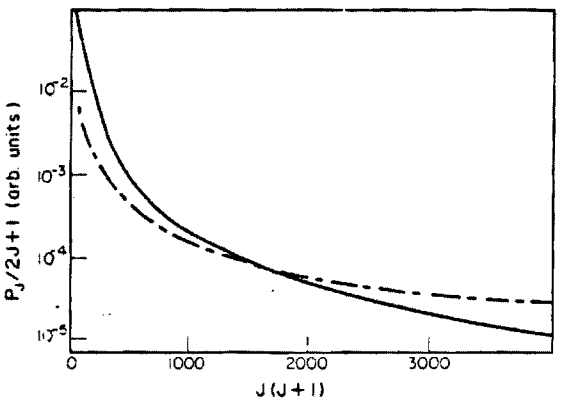

Figure 13. Plot of rotational state population P_J as a functional of rotational quantum number J plotted in the form $\ln P_J/J(J+1)$. The data (solid line) is for the 3371 A band of N_2 excited by 50 keV N^+ (or 100 keV N_2^+) impact on Si. Population is derived by dividing intensity by the Hönl-London factors. Also shown are the predictions for a hindered rotor model with an infinite conical well of half angle 90° (dot-dash line). From Thomas and Efstathiou[89].

temperature. Ejection is simulated by removal of the hindering potential so that a free space rotation results. The population distribution of the free rotor is given by the overlap integral of hindered and free rotor wavefunctions with weightings appropriate to the original population of the hindered rotational states. The result is that the population in the free rotor is non-Boltzman with a significant population of higher rotational quantum number states. In general terms this is similar to the observations in Figure 13. The model has been applied to the case of N_2 and a calculation for a conical potential of half-angle 90° is shown in Figure 13. There is a general qualitative similarity between experiment and simulation suggesting that the N_2 molecule on an Si surface rotates in a well of half-angle 90°. Other angles have been tried and provide less satisfactory agreement. At this stage the theoretical model is quite crude; in particular the use of an infinite conical well is certainly inappropriate and a softer potential function should be employed. It seems possible that by refinement of the model one could obtain a closer agreement with the experiments and thereby determine in detail the form of the potential well in which the bound molecule rotates.

Extension of such studies to other molecules can be envisaged. For example Kelly *et al*[92] have shown the optical spectrum of BH sputtered in an excited state from a boron surface and pronounced irregularities in rotational state population are evident. There is also substantial record[93–95] of CH, OH, AlO and other molecular spectra by bombardment of contaminated metal surfaces which also seem to show rotationally broadened features. These various observations are now being re-examined to ascertain whether they can be used to determine the form of the hindering potentials governing rotation of molecules bound to surfaces.

3.3.4. Fundamental studies of sputtering. The study of ion-induced optical emissions remains an area of active research for the purpose of understanding the basic collision mechanisms leading to excited state formation. Many of the more active areas are reviewed by Kelly[96]. Studies have been made of how signal strength varies with distance from the surface with the expectation that the decay distance is related to the product of ejected particle speed and excited state lifetime. From such data sputtered particle energies of up to 5 keV have been inferred[97] although a range of 10–100 eV is more usual[98–103]. It appears that typical speeds of excited particles represent the most energetic of the total particle flux sputtered from a solid. It is, however, possible that the observations are faulty due to poor spatial resolution and energy distribution derived from Doppler broadened line shapes are far lower than those determined from spatial decay parameters[104]. There is also an active consideration of how the matrix influences emission intensity, particularly the effect of oxygen which almost universally causes an increase in excited state formation. The general question of a theoretical description is a matter of concern. The formulations of Kelly[58] provide a useful statistical theory to relate excitation probability of different levels but do not explain matrix effects nor the influence of surface oxygen.

4. Conclusions

The study of optical and Auger emission remains a subject of current scientific interest. Only recently have the Auger spectra been properly identified and their potential for studying inelastic collisions in solids has not yet been exploited. Optical emissions are fairly unambiguous but the theory of excitation events is not yet formulated. Optical emissions have been proposed as a surface analysis tool and some use made of the technique. The principle problem is that the influence of the matrix on excitation efficiency is quite unpredictable. This problem is, however, common also to the SIMS technique that has been commercially exploited. The potential advantage of the optical technique is its ability to resolve different species quite unambiguously with relatively low cost equipment. Moreover the equipment is external to the vacuum system and requires only the provision of a suitable window. Optical emissions have been used frequently for analytical purposes in the research environment but have not, as yet, been developed into commercial instrumentation suitable for routine analytical use.

References

[1] C W White, E W Thomas, W F Van der Weg and N H Tolk, *Inelastic Ion-Surface Collisions* (Edited by N H Tolk *et al*), Chapter 8, Academic Press, New York (1977).
[2] R A Baragiola, *Ion-Induced Auger Emission from Solids, Inelastic Particle-Surface Collisions*, (Edited by E Taglauer and W Heiland), Springer Series in Chemical Physics, vol 17, p 38. Springer, Berlin (1981).
[3] R A Baragiola, *Rad Effects*, **61**, 47 (1982)
[4] E W Thomas, *Prog Surface Sci*, **10**, 383 (1980).
[5] C Snoek, R Geballe, W F Van der Weg, P K Rol and D J Bierman, *Physica*, **31**, 1553 (1965).
[6] T W Haas, R W Springer, M P Hooker and J T Grant, *Phys Lett*, **47A**, 317 (1974).
[7] W A Metz, K O Legg and E W Thomas, *J Appl Phys*, **51**, 2888 (1980).
[8] D Hasselkamp and A Scharmann, *Vakuum Technik*, **32**, 9 (1983).
[9] M Nègre, J Mischler and N Benazeth, *Surface Sci*, **107**, 562 (1981); J Mischler, M Nègre and N Benazeth, *Rad Effects*, **70**, 117 (1983).
[10] C Benazeth, N Benazeth and L Viel, *Surface Sci*, **78**, 625 (1978).
[11] M Barat and W Lichten, *Phys Rev*, **A6**, 211 (1972).
[12] R Whaley and E W Thomas, *J Appl Phys*, **56**, 1505 (1984).
[13] K Wittmaack, *Surface Sci*, **85**, 69 (1979).
[14a] J J Vrakking and A Kroes, *Surface Sci*, **84**, 153 (1979).
[14b] C Benazeth, N Benazeth and L Viel, *Rad Effects*, **69**, 143 (1983).
[15] D Schneider, G Nolbe, V Wille and N Stolterfoht, *Phys Rev*, **A28**, 161 (1983).
[16] D R Penn, *J Electron Spectrosc Relat Phenom*, **9**, 29 (1976).
[17] N Benazeth, *Nucl Instrum Meth*, **194**, 405 (1982).
[18] K O Legg, W A Metz and E W Thomas, *J Appl Phys*, **51**, 4437 (1980).
[19] P Dahl, M Rodbro, G Hermann, B Fastrup and M E Rudd, *J Phys*, **B9**, 1581 (1976).

[20] E W Thomas and R Whaley, *Nucl Instrum Meth*, **B2**, 516 (1984).
[21] D W Marquardt, *J Soc Ind Appl Math*, **11**, 431 (1963).
[22] J McGuire, *Phys Rev*, **A3**, 587 (1971).
[23] L Viel, C Benazeth and N Benazeth, *Surface Sci*, **54**, 635 (1976).
[24] A A Dorozhkin, A A Petrov and N N Petrov, *Izv Akad Nauk SSSR, Ser Fiz*, **43**, 619 (1979).
[25] A A Dorozhkin, A A Petrov and N N Petrov, *Soviet Phys Solid State*, **20**, 1660 (1978).
[26] A A Dorozhkin, A A Petrov and N N Petrov, *Soviet Phys Solid State*, **21**, 545 (1979).
[27] J D Andreadis, J Fine and J A A Mathew, to be published.
[28] H Dusterhoft, *Phys Stat Sol*, (a) **50**, 503 (1978); Z Jurela, *Int J Mass Spectrom Ion Phys*, **12**, 33 (1973); Z Jurela, *Nucl Instrum Meth*, **194**, 597 (1982).
[29] Z Sroubek, *Phys Rev*, **B25**, 6046 (1982).
[30] V U Kitov and E S Parilis, *Surface Sci*, **107**, 363 (1981).
[31] M Iwami, S C Kim, Y Kataoka, T Imura, A Hirahi and F Fujimoto, *Jpn J Appl Phys*, **19**, 1627 (1980).
[32] A Von Hippel, *Ann Physik*, **80**, 672 (1926).
[33] H Sporn, *Z Physik*, **112**, 278 (1939).
[34] C Snoek, W F Van der Weg and P K Rol, *Physica*, **30**, 341 (1964).
[35] W E Baird, M Zivitz, J Larsen and E W Thomas, *Phys Rev*, **A10**, 2063 (1974).
[36] E W Thomas, *Excitation in Heavy Particle Collisions*, p 57, John Wiley, New York (1972).
[37] C A Andersen and J R Hinthorne, *Science*, **175**, 853 (1972).
[38] C A Andersen and J R Hinthorne, *Analyt Chem*, **45**, 1421 (1973).
[39] C J Good-Zamin, M T Shehata, D B Squires and R Kelly, *Rad Effects*, **35**, 139 (1978).
[40] K J Snowdon, *Rad Effects*, **40**, 9 (1979).
[41] K J Snowdon, G Carter, D G Armour, B Andersen and E Veje, *Surface Sci*, **90**, 429 (1979).
[42] K J Snowdon, B Andersen and E Veje, *Rad Effects*, **40**, 19 (1979).
[43] R J MacDonald and P J Martin, *Surface Sci*, **67**, 237 (1977).
[44] P J Martin and R J MacDonald, *Surface Sci*, **62**, 551 (1977).
[45] R J MacDonald, R F Garrett and P J Martin, *Surface Sci*, **75**, 155 L (1978).
[46] R J MacDonald and P J Martin, *Surface Sci*, **66**, 423 (1977).
[47] T Okutani and R Shimizu, *Surface Sci*, **88**, L51 (1979).
[48] I S T Tsong, *Surface Sci*, **75**, L159 (1978).
[49] A Cobas and W E Lamb, *Phys Rev*, **65**, 327 (1944).
[50] W E Baird, M Zivitz and E W Thomas, *Phys Rev*, **A12**, 876 (1975).
[51] E O Rausch, H Inouye, A J Senol and E W Thomas, *Phys Rev*, **A17**, 473 (1978).
[52] C W White and N H Tolk, *Phys Rev Lett*, **26**, 486 (1971).
[53] C W White, D L Simms, N H Tolk and D K McCaughan, *Surface Sci*, **49**, 657 (1975).
[54] R Hippler, W Kruger, A Scharmann and K H Schartner, *Nucl Instrum Meth*, **132**, 439 (1976).
[55] C B Kerkdijk and R Kelly, *Rad Effects*, **38**, 73 (1978).
[56] R L Erickson and D P Smith, *Phys Rev Lett*, **34**, 297 (1975).
[57] N H Tolk, J C Tully, J Kraus, C W White and S H Neff, *Phys Rev Lett*, **36**, 747 (1976).
[58] R Kelly, *Phys Rev*, **B25**, 700 (1982).
[59] M Szymonski, A Poradzisz and L Gabla, *Surface Sci*, **112**, 254 (1981).
[60] Z Sroubek, K Zdansky and J Zavadil, *Phys Rev Lett*, **45**, 580 (1980).
[61] G Blaize, *Surface Sci*, **60**, 65 (1976).
[62] L W Carlson and N F Lane, *J Phys*, **B12**, L457 (1979).
[63] L Efstathiou and E W Thomas, *Nucl Instrum Meth*, **194**, 589 (1982).
[64] E W Thomas and L Efstathiou, *Nucl Instrum Meth*, **B2**, 479 (1984).
[65] K J Snowdon, W Heiland and E Taglauer, *Phys Rev Lett*, **46**, 284 (1981).
[66] T S Kiyan, V V Gritsyna, Yu E Logachev and Ya M Fogel, *Zh ETF Pis Red*, **21**, 77 (1975); [*Soviet Physics JETP Lett*, **21**, 35 (1975).]
[67] C W White, N H Tolk, J Kraus and W F Van der Weg, *Nucl Instrum Meth*, **132**, 419 (1976).
[68] C B Kerkdijk, K H Schartner, R Kelly and F W Saris, *Nucl Instrum Meth*, **132**, 419 (1976).
[69] C B Kerkdijk, K H Schartner, R Kelly and F W Saris, *Nucl Instrum Meth*, **132**, 427 (1976).
[70] E O Rausch, A I Bazhin and E W Thomas, *J Chem Phys*, **65**, 4447 (1976).
[71] V I Veksler, *Soviet Phys Solid State*, **22**, 1529 (1980).
[72] R Kelly, S Dzioba, N H Tolk and J C Tully, *Surface Sci*, **102**, 486 (1981).
[73] C W White, D L Simms and N H Tolk, *Science*, **177**, 481 (1972).
[74] R S Bhattacharya, J F Van der Veen, C B W Kerkdijk and F W Saris, *Rad Effects*, **32**, 25 (1977).
[75] R J MacDonald, E Taglauer and W Heiland, *Appl Surface Sci*, **5**, 197 (1980).
[76] I S T Tsong and N A Yusuf, *Appl Phys Lett*, **33**, 999 (1978).
[77] A R Knudson, D J Nagel, J Comas, K W Hill, *Nucl Instrum Meth*, **149**, 507 (1978).
[78] P Williams, I S T Tsong and S Tsuji, *Nucl Instrum Meth*, **170**, 591 (1980).
[79] V I Veksler, *Soviet Phys Solid State*, **22**, 1529 (1980).
[80] I S T Tsong and R B Liebert, *Nucl Instrum Meth*, **149**, 523 (1978).
[81] I S T Tsong and A C McLaren, *Nature*, **248**, 43 (1974).
[82] I S T Tsong and A C McLaren, *Spectrochim Acta*, **30B**, 343 (1975).
[83] I S T Tsong and A S Bhalla, *Appl Phys Lett*, **32**, 381 (1978).
[84] H Bach, *Rad Effects*, **28**, 215 (1976).
[85] H Bach, *J Non-Cryst Solids*, **19**, 65 (1975).
[86] H Bach, *Inst J Mass Spectrom Ion Phys*, **9**, 247 (1972).
[87] J P Meriaux, J M Guttierrez, Ch Schneider, R Goutte and Cl Guilland, *Nour Rev d'Optique applique*, **2**, 81 (1971).
[88] A Kelly, S A Shivashankar and J J Cuomo, *J Vac Sci Technol*, **21**, 774 (1982).
[89] E W Thomas and L Efstathiou, *Nucl Instrum Meth*, **B2**, 479 (1984).
[90] A W Kleyn, A L Luntz and D J Auerbach, *Phys Rev Lett*, **47**, 1169 (1981); A C Luntz, A W Kleyn and D J Auerbach, *Phys Rev*, **B25**, 4273 (1982).
[91] J W Gadzuk, U Landman, E J Kuster, C L Cleveland and R N Barnett, *Phys Rev Lett*, **49**, 426 (1982).
[92] R Kelly, S Dzioba, N H Tolk and J C Tully, *Surface Sci*, **102**, 486 (1981).
[93] G E Thomas, E E de Kluizenaar and M Beerlage, *Chem Phys*, **7**, 303 (1975).
[94] G E Thomas and E E de Kluizenaar, *Le Vide*, **167**, 190 (1973).
[95] G E Thomas and E E de Kluizenaar, *Int J Mass Spectrum Ion Phys*, **15**, 165 (1974).
[96] R Kelly, *Inelastic Particle Surface Collisions*, Springer Series in Chemical Physics, Physics, (Edited by E Taglauer and W Heiland), vol 17, p 292, Springer, Berlin (1981).
[97] V V Gritsyna, T S Kijan, A G Koval and Ya M Fogel, *Rad Effects*, **14**, 77 (1972).
[98] S Dzioba, A Auciello and R Kelly, *Rad Effects*, **45**, 235 (1980).
[99] G N Polyakova, A I Ranguk, V I Gerasimenko and O A Opalev, *Soviet Phys Tech Phys*, **27**, 32 (1982).
[100] G L Mladenov and M Braun, *Phys Stat Sol*, **53**, 631 (1979).
[101] M R Morrow, A Auciello, S D Zioba and R Kelly, *Surface Sci*, **97**, 243 (1980).
[102] S Dzioba and R Kelly, *Nucl Instrum Meth*, **182/183**, 207 (1981).
[103] T S Kiyan and V V Gritsyna, *Izvestiya*, **43**, 595 (1979).
[104] C M Loxton, R J MacDonald and E Taglauer, *Surface Sci*, **102**, L76 (1981).

NUCLEAR INSTRUMENTS AND METHODS 168 (1980) 379-382; © NORTH-HOLLAND PUBLISHING CO.

ION INDUCED AUGER SPECTROSCOPY

E. W. THOMAS, K. O. LEGG and W. A. METZ

School of Physics, Georgia Tech, Atlanta, Ga 30332, U.S.A.

Auger electron spectra are induced by impact of heavy ions (e.g. Ar^+) on surfaces; it has been suggested that analysis of such spectra would be a useful technique for surface analysis. We have examined the Auger spectra for various projectile–target combinations and present as representative data the spectra for 100 keV Ar^+ impact on Al, Cr, Mn, Fe and Co. For a projectile incident on a species of higher nuclear charge the spectrum is dominated by Auger lines from the projectile, broadened considerably by the Doppler effect due to the projectile's motion. The spectra are not characteristic of the target and therefore offer no opportunity for surface analysis. For a projectile incident on a target of lower nuclear charge the spectrum is that of the target species but the spectrum is consistent with the source being sputtered excited atoms; the Auger electrons do not come from the surface. We conclude that the ion induced Auger spectra are in general not a convenient method for surface analysis.

1. Introduction

Auger electron spectra induced by electron impact provide an accepted technique for analysing the composition of a surface. Auger electron spectra are also induced by ion impact on a surface. It has been suggested[1]) that surface analysis might conveniently be performed by recording the ion induced Auger spectrum. The purpose of this paper is to examine this suggestion. We present various Auger spectra induced by ion impact, discuss the nature and origin of the ion-induced Auger electron spectrum and conclude that the exitation process is far more complex than for electron induced Augers.

The experimental arrangement employs a conventional Varian Auger electron spectrometer using a cylindrical mirror analyser (CMA) to analyse electrons ejected from metal targets in a uhv environment. The incident ion beam was produced by an Ion Implanter capable of operation from 30 to 200 keV. The angle of ion beam incidence was approximately 60° to the sample surface normal; the CMA axis was at 35° to the surface normal and therefore at 95° to the incident ion beam. Samples were prepared by mechanical polishing and electropolishing. Further in-situ cleaning was possible by sputtering using either 100 keV Ar^+ ions from the accelerator or 3 keV Ar^+ ions from a separate ion gun. Auger electron spectra were produced using energetic ions from the ion implanter; for comparison purposes we could also produce electron induced spectra using the integral electron gun fitted co-axially in the Varian CMA analyser. Spectra were recorded in either the derivative mode (using a 5 eV modulation of the CMA voltage) or in the integral mode by pulse counting using a multichannel analyser (and with no spectrometer modulation). In general we preferred to use the integral mode of operation since this provides the true shape of the Auger spectra lines. However for the low energy LMM lines of heavy metals the Auger peaks are superimposed on a very intense secondary electron background; in such situations the derivative mode of operation was necessary in order to establish the existence and energy of a peak.

2. Results

We shall consider first the spectra induced by Ar^+ impact on aluminium. The spectrum is dominated by Auger lines from the target as are the spectra for other targets (e.g. Be and Si) whose nuclear charge is less than that of the projectile. Fig. 1 shows integral spectra and fig. 2 derivative spectra. The integral spectrum for electron impact (fig. 1a) and that for ion impact (fig. 1b) are similar in that they are dominated by a line at 67 or 61 eV which one may confidently ascribe to the filling of an L-shell vacancy[2]). There are however significant differences in detail. The electron induced spectrum shows a tail towards lower energy which is related to energy loss by the electrons as they traverse the distance from the point of excitation to the surface; electrons excited below the surface are observed at lower energies than those excited at the surface. No such "loss tail" is seen on the ion induced spectrum. Analysis of the derivative spectrum taken with electron impact (fig. 2a) shows subsidiary peaks at 15 eV and 27 eV below the main peak which are consistent with Auger electrons emerging

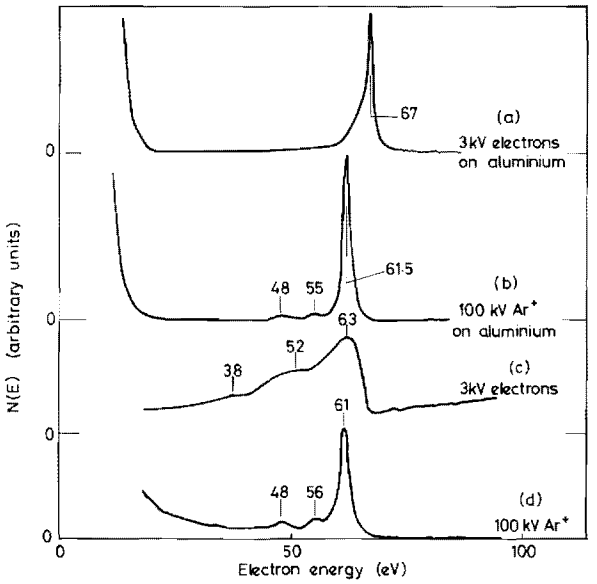

Fig. 1. Auger electron spectra taken in the integral mode. (a) 3 kV electrons on aluminium; (b) 100 kV Ar^+ ions on aluminium, (c) 3 kV electrons on oxidised aluminium; (d) 100 kV Ar^+ ions on oxidised aluminium.

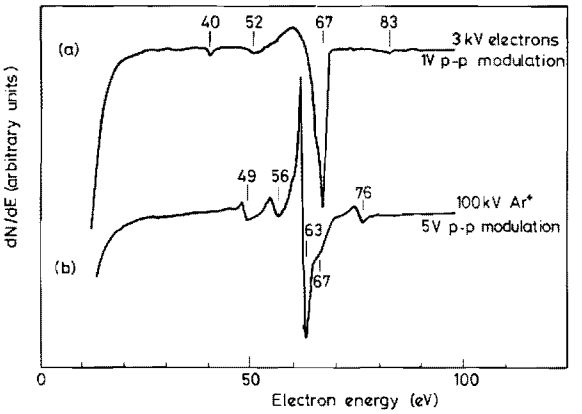

Fig. 2. Auger spectra taken in the derivative mode, (a) 3 kV electrons on aluminium; (b) 100 kV Ar^+ ions on aluminium.

after having excited bulk and surface plasmons[3]). The ion induced spectrum also shows subsidiary peaks (at 48 and 55 eV on the integral spectra) but their position is not consistent with plasmon excitation. In spectrum 1c we show the spectra observed under electron impact for an oxidised surface; the whole spectrum is changed. The electron induced Auger electron is emitted by filling of an L-shell vacancy by an electron from the valence band with the simultaneous ejection of a second valence band electron. The oxide has a different valence band structure from the metal and consequently exhibits this different Auger spectrum. No such change is seen in the ion-induced spectrum (spectrum d) when the surface is oxidised. Thus the ion induced spectra show none of the characteristics expected for the exicted atom being in the solid matrix of the metal; there is no loss tail, no plasmon structure and no matrix effect (as when the oxide is formed). One must conclude that the source of ion induced Auger electrons is not located in the solid.

It is also to be noted that there is a major difference between the energy of the major peak in figs. 1a and 1b; for ion impact it lies 5.5 eV lower than for electron impact. It has sometimes been argued that the width of the ion induced aluminium line is less than that of the electron induced line[4]); this was based on analysis of derivative spectra such as those shown in fig 2. This conclusion is misleading. The integral spectra show that much of the width of the electron induced line is caused by the loss tail. If we discount the loss tail then the electron induced line is about 1.4 eV fwhm while the ion induced line is wider at about 2.3 eV fwhm. It is well known that there is a substantial difference between the nature of the electron and ion impact excitation mechanisms. Electron impact forms an L-shell hole by direct Coulomb excitation. For 100 keV Ar^+ ion impact Coulomb excitation is expected to be small and core hole formation occurs primarily by an electron promotion mechanism during the temporary formation of an $Ar^+ + Al$ molecular system. The mechanism is well discussed by Louchet et al[5]) and is described in a fundamental manner by Barat and Lichten[6]). For the case of Ar^+ on Al the vacancy formation is by promotion of a 2p electron forming an L_{II} or L_{III} hole; promotion does not occur in the inner shells of the argon ion and hence no argon Auger spectrum is seen. Promotion may also occur by Al+Al collisions in the collision cascade; again this will cause L_{II} and L_{III} vacancies of the Al system[6]). It is not clear whether promotion occurs primarily by the $Ar^+ + Al$ event or by the Al+Al collision cascade. Benazeth et al.[7]) show theoretically that the symmetrical Al+Al collisions will produce a negligible fraction of the L-shell vacancies; on the other hand Vrakking and Kroes[8]) show that the Al spectrum is also produced by Ne^+ impact and here the promotion in the $Ne^+ + Al$ collision will occur in the 2p shell of the neon and the only source of 2p vacancies in Al must be the symmetric Al+Al collisions. In any case whether the excitation occurs in $Ar^+ + Al$ or Al+Al, the collision is violent, involv-

ing energy transfer to the Al atoms of at least 300 eV[8]). Taking the product of recoil speed for 300 eV Al atoms and the theoretical lifetime of the 2p vacancy[9]), the decay length for the recoiling Al atoms with 2p vacancies will be 61 Å. By contrast the depth from which 61 eV electrons can escape out of Al is only 4.2 Å [10]). Thus atoms recoiling into the solid will in general emit their Auger electrons at a depth from which the electrons cannot escape. It follows that only excited Al atoms ejected out of the solid (i.e. sputtered) will emit Auger electrons that can be detected. This is consistent with our discussion of line shape which also implies that the Auger spectrum is from ejected particles. If the emerging Al atoms have energies of around 300 eV then the detected line will be Doppler broadened by up to 2.5 eV; this is consistent with the width of the observed lines.

Auger spectra of aluminum induced by gas-phase bi-particle $Ar+Al^+$ collisions show eight or more lines identified as being from ionized states of aluminum[11]). The spectra of the present experiment are much simpler and we are led to examine whether they might be from neutral aluminum. An Al atom with a single 2p vacancy (i.e. $2p^5 3s^2 3p^2$ configuration) decaying to the $2p^6 3s 3p$ or $2p^6 3p^2$ states of Al^+ will produce Auger electrons of energy (estimated from the theoretical binding energies of Shirley et al.[12]), 64 and 57 eV. It is known that Auger electron energies predicted in this way may be too high by as much as 4 eV in some cases[12]). Thus we would argue that the peaks predicted at 64 and 57 eV could be those which are observed at 61.5 and 55 eV. Decay of an Al^+ ions of a $2p^5 3s^2 3p$ configuration to a $2p^6 3s$ or $2p^6 3p$ state will produce electrons at respectively 56 and 49 eV coinciding exactly with the two observed subsidiary peaks. The peak seen at 76 eV in the derivative spectrum has already been identified by Viel et al.[14]) as due to ejected atoms with two 2p vacancies.

Recently Vrakking et al.[8]) have claimed that the ion induced spectrum of Al is from Al atoms deep inside the solid within the disturbed region created by the collision cascade. If this were the case then the emerging electrons would have a very high probability of ionizing other atoms in the cascade and losing an energy equal to the relevant ionization potential. Indeed since ionization cross sections are typically[14]) 10^{-16} cm^2 the probability for such events should be almost unity for all electrons except those from the outermost layer of the surface. Thus we would expect a peak from aluminum 5.98 eV below the main structure; we observe the first subsidiary peak 6.5 eV below the main structure. Furthermore, when the surface is oxidized we should observe an additional peak with a 13.6 eV loss due to ionization of oxygen. While there is a peak at almost this energy it is present when the aluminum is clean and does not increase on oxidation. We conclude that there is no evidence for the electrons coming from Al atoms in a disturbed collision cascade region.

We have also examined the Auger spectra induced by Ar^+ ion impact on various heavy targets; as representative examples we show in fig. 3 spectra induced by 100 keV Ar^+ impact on Cr, Mn, Fe and Co. The spectra are shown only in derivative form; as a result of the large secondary electron background the Auger peaks are not displayed clearly in the integral mode of operation. The spectra are complicated and bear no close resemblance to the well known electron induced spectra of these elements. Hole formation by electron promotion mechanisms for these cases where the target nuclear charge exceeds that of the projectile will lead[6]) to hole formation in the L_{II}, L_{III} shells of the argon

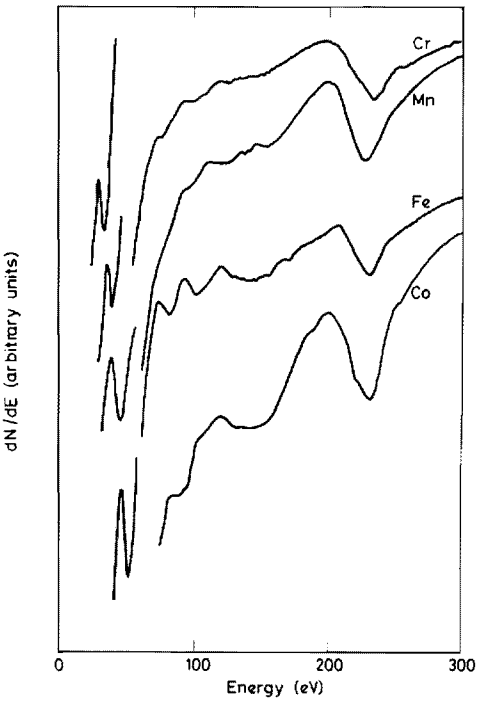

Fig. 3. Auger spectra taken in the derivative mode for 100 kV Ar^+ ions incident on Cr, Mn, Fe and Co. Note that the break in the curves at around 60 eV occurs when the sensitivity was reduced to accommodate the full spectrum on the plotter.

projectile. The broad peak between 210 and 260 eV is indeed the LMM line of Ar. The considerable breadth is consistent with a Doppler broadening effect[16]) due to the source of the electrons (the argon projectile) being in motion when decay occurs. Indeed detailed analysis of line width suggests that the argon Auger electrons arise primarily from backscattered projectiles which have emerged from the target. A variety of additional structure is seen at energies from 80 to 200 eV. We have tentatively ascribed this to LMM transitions involving a vacancy in the $L_{II,III}$ shell of Ar with the decaying and ejected electrons arising from metal atoms in the target; thus these lines are due to decay of an Ar–metal molecular complex. We do also observe the LMM peak of the metal in all cases lying in the region 40–60 eV. According to the electron promotion model[6]) excitation of the metal should not occur by argon–metal collisions; excitation of the metal is probably due to interaction of a recoiling metal atom with a second atom in the matrix. Whatever the precise origin of the structure in these spectra it is clear that the Auger spectra for these cases are dominated by features from the projectile and are not characteristic of the target.

3. Conclusion

The ion-induced Auger spectra fall into two groups which are characterized by the cases displayed here. Excitation is by an electron promotion mechanism following the general scheme detailed by Barat and Lichten[6]). For targets of nuclear charge greater than that of the projectile, hole formation occurs primarily in the projectile leading to a complex spectrum of lines broadened by the Doppler effect. Since such spectra are characteristic of the projectile (rather than the target) they are of little value for the analysis of the target material. For targets of nuclear charge less than that of the projectile the hole formation occurs in the target leading to a spectrum characteristic of the target. All evidence points to the observed Auger spectra being emitted from isolated atoms after their ejection from the solid.The states are complicated involving not only core vacancies but also excited outer electrons. Unlike electron induced Auger spectroscopy the ion induced process provides no information on band structure in the surface and spectra are not influenced by changes to surface chemistry. Ion-induced Auger spectra provide information similar to that of the SIMS technique since they are both related to ejection of atoms; there is little correspondence to the technique of electron induced Auger spectroscopy. We are forced to the general conclusion that ion induced Auger electron spectroscopy offers no general advantages over conventional electron induced Auger spectroscopy or SIMS.

This work was supported in part by the Magnetic Fusion Energy programme of DOE and in part by the Solid State Chemistry programme of the NSF.

References

1) W. Soszka, Surface Sci. **74** (1978) 636.
2) W. A. Coghlan and R. E. Clausing, At. Data **5** (1973) 317.
3) T. Marata and S. Ohtani, J. Vac. Sci. Technol. **9** (1971) 789.
4) R. A. Powell, J. Vac. Sci. Technol. **15** (1978) 125.
5) F. Louchet, L. Viel, C. Benazeth, B. Fagot and N. Colombie, Rad. Effects **14** (1972) 123.
6) M. Barat and W. Lichten, Phys. Rev. **A6** (1972) 211.
7) C. Benazeth, N. Benazeth and L. Viel, Surface Sci. **78** (1978) 625.
8) J. J. Vrakking and A. Kroes, Surface Sci. **84** (1979) 153.
9) E. J. McGuire, Phys. Rev. **A3** (1971) 587.
10) D. R. Penn, J. Electron Spectr. **9** (1976) 29.
11) P. Dahl, M. Rodbro, G. Hermann, B. Fastrup and M. E. Rudd, J. Phys. **B9** (1976) 1581.
12) D. A. Shirley, R. L. Martin, S. P. Kowalczyk, F. R. McFeely and L. Ley, Phys. Rev. **B15** (1977) 544.
13) P. Bisgaard, R. Bruch, P. Dahl, B. Fastrup and M. Rodbro, Phys. Scripta **17** (1978) 49.
14) L. Viel, C. Benazeth and N. Benazeth, Surf Sci. **54** (1976) 635.
15) L. J. Kieffer, At. Data **1** (1969) 19.
16) P. Dahl, M. Rodbro, B. Fastrup and M. E. Rudd, J. Phys. **B9** (1976) 1567.

DATA ON SCIENTIFIC COLLABORATORS

K. O. Legg, Research Assistant	- Recently set up his own company in a field related to this work.
W. A. Metz, Graduate Assistant	- Graduate with Ph.D. Employed by NRC Semiconductor Division.
R. S. Whaley, Graduate Assistant	- Graduated with Ph.D. Now partner in small software company servicing needs of semiconductor industry.
L. Efstathiou, Graduate Assistant	- Did not graduate.
H. R. Turner, Graduate Assistant	- Will finish Ph.D. in spring, 1986.

TECHNICAL SUMMARY

The general objective of the work was to study processes leading to excited state formation (both inner and outer shells) as slow atoms, ejected from a solid by the sputtering mechanism, traverse the discontinuity in potential presented by a solid surface.

A major component of the work was a study of inner shell excited states detected by the Auger spectrum of ejected electrons. For heavy ion (generally Ar^+ at 20 to 200 keV) impact on Mg, Al, and Si, we observed a continuous emission from decay in the matrix, a line spectrum identified as from sputtered neutral atoms and an additional continuum tentatively identified as due to decay of emerging atoms close to the surface (within 5 Å) and therefore distorted by surface potential. The line spectrum of sputtered atoms had never been previously identified and our detailed analysis of the matter brought to a conclusion considerable speculation in the literature. In effect the ejected particle had lost an inner shell electron, probably in the collisional ejection event, but picked up an extra outer electron, probably as it emerged through the surface. For example, the relevant species in Mg had a structure $2p^5 3s^2 3p$. These species cannot be created in a gas phase collision. All significant lines were clearly identified and line intensities shown consistent with theoretical predictions of branching ratios. Lifetimes of such states ar short (37 femfto seconds for Al) so that decay of sputtered atoms may frequently occur within the potential field of the solid. This decay was considered to be responsible for a 5 eV (approximately) continuum that increased in magnitude as lifetime decreased; a definite identification will require a detailed theoretical prediction. The work is all published. The definitive paper is attached as Reprint 1 and earlier intermediate reports as Reprints 2 through 4.

During the course of our Auger studies we discovered that oxygen was desorbed efficiently from Ti and Fe by hydrogen ions (H_2^+, H_3^+) with a mechanism involving electron stimulated desorption by the electrons attached to the projectile. This again was a new discovery and related to inner shell excitation effects; it is fully reported in Reprint 5.

We maintained parallel studies of optical emission spectra related to outer shell excitation concentrating particularly on molecular species. We studied N_2 sputtered from N ion implanted Si and showed a non-thermal distribution of rotational state excitation. This was ascribed to the hindered rotational motion of the N_2 molecule when bound to the surface before ejection. The major report is Reprint 6 with an earlier report being Reprint 7. We showed also that molecules (specifically CN) could be created inside the solid by sequential implantation of its separate components (C and N). With assistance from our theoretical colleagues we suggested that an implanted species causes a localized melting at the end of its range and that recombination occurs in this region. This work is fully published as Reprints 8 and 9.

Throughout the work the PI maintained a considerable interest in review of this general area. A major review of the whole area was written for Progress in Surface Science (Reprint 10) and a minor review for Vacuum (Reprint 11). The question of whether ion-induced Auger spectra could be used for surface analysis was reviewed in Reprint 12.